UNIVERSITAT JAUME·I

Molybdenum sulfide cluster catalysts in hydrogenation and dehydrogenation reactions: a combined theoretical and experimental study

María Gutiérrez Blanco

Supervisors:

Prof. Rosa Mª Llusar Barelles

Prof. Vicente Sixto Safont Villarreal

Castellón de la Plana, January 2024

UNIVERSITAT JAUME·I

Programa de Doctorado en Ciencias

Escuela de doctorado de la Universitat Jaume I

Molybdenum sulfide cluster catalysts in hydrogenation and dehydrogenation reactions: a combined theoretical and experimental study

Memoria presentada por María Gutiérrez Blanco para optar al grado de doctora por la Universitat Jaume I

María Gutiérrez Blanco	Rosa Mª Llusar Barelles	Vicente Sixto Safont Villarreal

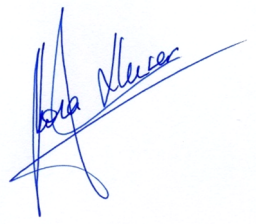

Castellón de la Plana, December 2023

Financiación

La presente tesis doctoral ha sido realizada gracias a la concesión de una beca predoctoral (PRE2019-088511) concedida por el Ministerio de Ciencia e Innovación asociada al proyecto con título "Aproximaciones racionales para el diseño de nuevos materiales mediante la combinación de teoría y experimento" (PGC2018-094417-B-I00) del Ministerio de Ciencia, Innovación y Universidades. Además, dicha ayuda predoctoral ha permitido una estancia breve del 02/05/2022 al 02/08/2022 en el *Leibzniz-Institut für Katalyse* bajo la supervisión del profesor Matthias Beller.

La actividad investigadora durante el periodo predoctoral ha sido financiada gracias a los proyectos concedidos por el Ministerio de Ciencia, Innovación y Universidades (PGC2018-094417-B-I00), por el Ministerio de Ciencia e Innovación (PID2022-141089NB-I00), por la Generalitat Valenciana (CIAICO/2021/122) y por la Universitat Jaume I (UJI-B2019-30, UJI-B2021-29 y UJI-B2022-56).

Licencias

Agradecimientos

Antes de empezar a mostrar el trabajo científico de esta tesis doctoral no podía dejar de lado la parte más humana que ha contribuido casi por igual durante este camino y sin la cual dudo que hubiera sido posible llegar hasta aquí. En primer lugar, me gustaría expresar mi gratitud a mis directores de tesis, *Rosa* y *Sixte*, por apostar por mi desde el principio y hacerme sentir válida dentro de este ámbito. Gracias por todo el tiempo dedicado a enseñarme ciencia, a tener rigor científico, así como también por las palabras de apoyo y reconocimiento cuando han sido necesarias.

También estoy muy agradecida con los miembros del grupo de *Materiales Moleculares* tanto a los actuales como a los anteriores que recuerdo con gran cariño. Gracias *Eva* por enseñarme todo lo que se dentro del laboratorio, pero también muchas cosas que extrapolo a mi vida personal, y sobretodo, por ser una gran amiga dentro y fuera. *Juanjo*, tú has sido mi acompañante en este proceso desde el principio hasta el final, mano a mano entre reacciones, cálculos, estancias, dudas, risas, congresos y un largo etc. Gracias por tu generosidad conmigo, por tu tiempo y por haber sido confidente en muchas ocasiones. Y la última incorporación, *Marcelo*, gracias por estar siempre con una sonrisa para mí y por estar dispuesto a ayudarme cada vez que lo he necesitado.

Gracias al resto de compañeros del departamento *Química Física* y al *Servicio de Instrumentación Científica* , miembros antiguos y actuales, los cuales me han ayudado durante este periodo predoctoral.

Me gustaría agradecer al *Prof. Matthias Beller* así como a *Henrik Junge* y *Kathrin Junge* por su hospitalidad y dedicación durante mi estancia en Rostock. Gracias al grupo de *Sustainable Redox Reactions* por hacerme sentir una más. De esta experiencia me llevo a *Caro* y *Tamara,* gracias por ser casa en Alemania.

Dicen que las situaciones similares unen a las personas y no podía estar más de acuerdo, así he encontrado a los *becarios precarios de Química*. Gracias por todas las comidas de Magdalena, paellas, cenas de San Alberto, y ¡por las que hemos liado

juntos! En especial, gracias *Andrés* porque juntos hemos compartido esto, un máster, muchas historias y algún cumpleaños olvidado. Dentro de la ciencia también he encontrado a dos grandes amigas, *Elena* y *Roser*, gracias por celebrar cada paso juntas, por la compresión y por ser mis personas vitamina.

Pero el apoyo no solo ha estado dentro de este ámbito, gracias a mis amigos *Borja*, *María* y *Patri* por haberme acompañado desde el principio, ya no solo en este camino sino en otros tantos. Gracias por inhibirme de los problemas científicos y por cargarme las pilas y el corazón. *Lorena*, tú tampoco podías faltar aquí, gracias por enseñarme que la amistad no entiende de distancia y por el cariño que siempre me has transmitido.

Gracias *Ferran* porque una parte de esta tesis también es tuya, por ser mi toma a Tierra cuando veía montañas en granos de arena, pero al mismo tiempo por darme alas e impulsarme a volar cuando he soñado alto. Gracias por creer en mi cuando yo no lo he hecho y recordarme que en este equipo cuando yo de 20 tú serás mi 80 y viceversa.

Por último, las personas sin las cuales esto nunca hubiera sido posible: mis padres, *José Luis e Isabel*, y mi hermana, *Ana*. Me habéis inculcado cualidades sin las cuales no estaría aquí: constancia, resiliencia y perseverancia. Gracias por esto, por la paciencia, el cariño y el apoyo inquebrantable. Gracias *Ana* y *Ricardo* por darme el mejor regalo, mi sobrina *Elena*.

A mi familia

"El éxito consiste en hacer cosas ordinarias de manera extraordinaria"

Jim Rohn

Resumen

En la presente tesis doctoral se aborda la síntesis, la caracterización estructural y las aplicaciones catalíticas de sulfuros clúster de molibdeno con ligandos que contienen grupos amino. Este trabajo se lleva a cabo empleando un enfoque integral que combina experimentos y teoría con el fin de esclarecer los mecanismos involucrados en estos procesos catalíticos. En el Capítulo 1 se introducen las bases de estos temas, comenzando por una visión holística de la química de coordinación hasta llegar a la definición de clúster. A continuación, se describen los principios fundamentales de la catálisis con especial énfasis en procesos homogéneos, particularmente en reacciones de hidrogenación y deshidrogenación. En este capítulo también se pone en valor la importancia de la sinergia entre experimentos y cálculos teóricos a la hora de elucidar el mecanismo de procesos catalíticos. Posteriormente, en el Capítulo 2 se enumeran los objetivos principales de esta tesis.

En el Capítulo 3 se describe la síntesis, caracterización estructural y actividad catalítica de clústeres trinucleares con unidad Mo_3S_4 que contienen ligandos imidazolil amino. La actividad catalítica de los nuevos complejos se evalúa en la semihidrogenación de alquinos internos. Todos los compuestos muestran quimio y estereoselectividad hacia la obtención del isómero con configuración *Z*. El análisis de la reacción por espectrometría de masas confirma que se trata de un proceso de catálisis mediada por clústeres, además se sientan las bases sobre el mecanismo de la reacción.

En el Capítulo 4 se presenta un estudio exhaustivo acerca del mecanismo que opera en la semihidrogenación quimio y estereoselectiva del difenilacetileno catalizada por sulfuros de molibdeno funcionalizados con ligandos imidazolil amino. Para ello, se utiliza la combinación de experimentos y cálculos teóricos basados en la Teoría del Funcional de la Densidad (DFT). Los posibles mecanismos que se contemplan difieren en el modo de activación de la molécula de hidrógeno. Por último, se realizan experimentos de marcaje isotópico con deuterio con el fin de respaldar nuestra propuesta.

El Capítulo 5 trata sobre la aplicación catalítica de los sulfuros clúster de molibdeno en la deshidrogenación del ácido fórmico. Para dicho objetivo, se evalúan como posibles catalizadores una serie de clústeres Mo_3S_4 funcionalizados con ligandos de diferente naturaleza. La monitorización de la reacción mediante espectrometría de masas y estudios de resonancia nuclear magnética confirma la integridad del clúster durante el proceso catalítico. También se detallan experimentos estequiométricos y catalíticos destinados a la elucidación mecanística. Con el fin de validar nuestra propuesta, se presenta un estudio teórico basado en cálculos de tipo DFT.

Finalmente, el Capítulo 6 resume todos los resultados obtenidos en esta tesis doctoral en un listado de conclusiones. Todos los procedimientos experimentales y teóricos, junto con la caracterización de los compuestos y los detalles mecanísticos se incluyen en los capítulos correspondientes.

Summary

The present doctoral thesis addresses the synthesis, structural characterization and catalytic applications of molybdenum sulfide cluster catalysts with ligands containing amino groups. This dissertation uses a comprehensive approach that combines experiments and theory to elucidate the mechanisms involved in these catalytic processes. The bases of these topics are introduced in Chapter 1 with a holistic overview starting from coordination chemistry to the definition of cluster. The chapter follows with the fundamental principles of catalysis, with a special focus on homogeneous processes, particularly hydrogenation and dehydrogenation reactions. The importance of the synergy between experiments and computations during the mechanistic elucidation of catalytic processes is also highlighted in this chapter. Then, the general objectives of this thesis are listed in Chapter 2.

Chapter 3 describes the synthesis, structural characterization and catalytic activity of trinuclear clusters of Mo_3S_4 units bearing imidazolyl amino ligands. The catalytic activity of the new complexes is evaluated in the semihydrogenation of internal alkynes. All clusters show chemo- and stereoselectivity towards obtaining the (*Z*)-isomer. A cluster catalysis process is confirmed by analysis of the reaction course by reaction monitoring using mass spectrometry and preliminary experimental results on the mechanism are analyzed.

Chapter 4 provides an in-depth investigation of the mechanism that operates in the chemo- and stereoselective semihydrogenation of diphenylacetylene catalyzed by imidazolyl amino molybdenum sulfide cluster. The investigation combines catalytic experiments and theoretical calculations based on Density Functional Theory (DFT). The mechanistic pathways explored differ in the hydrogen activation mode. In addition, deuterium labeling experiments are performed to support our proposal.

Chapter 5 deals with the catalytic application of molybdenum sulfide clusters in the dehydrogenation of formic acid. For this purpose, a series of Mo_3S_4 complexes

functionalized with ligands of different nature have been evaluated as potential catalysts. Reaction monitoring using mass spectrometry and nuclear magnetic resonance studies confirm the integrity of the cluster during the catalytic process. Stoichiometric and catalytic experiments aimed at mechanistic elucidation are also detailed. To validate the proposal, a theoretical study based on DFT calculations is presented.

Finally, Chapter 6 summarizes all the results obtained in this thesis in a list of concluding remarks. All the experimental and theoretical procedures, along with the characterization of the compounds and mechanistic details are included in the corresponding chapters.

Scientific Divulgation

The results obtained in this doctoral thesis have led to the preparation and publication of several research articles:

1) **Authors:** María Gutiérrez-Blanco, Eva Guillamón, Vicent S. Safont, Andrés G. Algarra, M. Jesús Fernández-Trujillo, Kathrin Junge, Manuel G. Basallote, Rosa Llusar and Matthias Beller.

   Title: Efficient (*Z*)-selective semihydrogenation of alkynes catalyzed by air-stable imidazolyl amino molybdenum cluster sulfides.

   Reference: *Inorg. Chem. Front.*, **2023**, *10*, 1786-1794.

2) **Authors:** María Gutiérrez-Blanco, Carolin A. M. Stein, Carmina Alfonso, Eva Guillamón, Vicent S. Safont, Iván Sorribes, Henrik Junge, Matthias Beller and Rosa Llusar.

   Title: Selective dehydrogenation of formic acid catalyzed by air-stable cuboidal PN molybdenum sulfide clusters.

   Reference: *ChemCatChem.,* **2023**, *15*, e202300740.

3) **Authors:** María Gutiérrez-Blanco, Andrés G. Algarra, Eva Guillamón, M. Jesús Fernández-Trujillo, Mónica Oliva, Manuel G. Basallote, Rosa Llusar and Vicent S. Safont.

   Title: Spin-crossing in the (*Z*)-selective alkyne semihydrogenation mechanism catalyzed by Mo_3S_4 clusters: A DFT exploration.

   Reference: *Inorg. Chem.,* Accepted.

Some of these results have been presented at national and international scientific conferences:

- **Authors**: María Gutiérrez-Blanco, Rosa Llusar, Vicent. S. Safont and Eva Guillamón.
  Title: Semihydrogenation of alkynes catalyzed by imidazolyl-amine Mo_3S_4 clusters: Influence of the alkylation of the N-H functionality.
  Participation: Poster presentation.
  Conference: RSEQ Symposium (Online).
  City: - **Year:** 2021
- **Authors**: María Gutiérrez-Blanco, Eva Guillamón, Rosa Llusar, Vicent S. Safont, Kathrin Junge and Matthias Beller.
  Title: Molybdenum sulfide clusters as alternative for the semihydrogenation of alkynes.
  Participation: Poster presentation.
  Conference: 44th International Conference on Coordination Chemistry.
  City: Rimini, Italy **Year:** 2022
- **Authors**: María Gutiérrez-Blanco, Carolin Stein, Eva Guillamón, Iván Sorribes, Henrik Junge, Rosa Llusar and Matthias Beller.
  Title: Formic acid dehydrogenation catalyzed by Mo_3S_4 clusters.
  Participation: Poster presentation.
  Conference: XVIII Simposio de Jóvenes Investigadores Químicos.
  City: Sevilla, Spain **Year:** 2022
- **Authors**: María Gutiérrez-Blanco, Carolin A. M. Stein, Eva Guillamón, Vicent S. Safont, Henrik Junge, Matthias Beller and Rosa Llusar.
  Title: Selective dehydrogenation of formic acid catalyzed by Mo_3S_4 clusters: catalytic performance and mechanistic insights.
  Participation: Poster presentation.
  Conference: 6th EuChems Inorganic Chemistry Conference.
  City: Vienna, Austria **Year:** 2023

Abbreviations

aq.	Aqueous
au	Atomic units
br	Broad
ca.	*Circa* (approximately)
calcd.	Calculated
CCDC	Cambridge crystallographic data centre
CID	Collision induced dissociation
CSE	Cluster skeletal electrons
CODH	Carbon monoxide dehygrogenase
conv.	Conversion
d	Doublet
ddd	Doublet of doublets of doublets
DFT	Density functional theory
DIP	Dehydroisophytol
dmad	Dimethyl acetylenedicarboxylate
dmen	N,N'-Dimethylethylenediamine
dpa	Diphenylacetylene
DMOA	N,N'-Dimethyloctylamine
dmpe	1,2-bis-(dimethylphosphanyl)ethane
DMSO	Dimethylsulfoxide
edpp	(2-aminoethyl)diphenylphosphine
ed^ip_rp	2-(diisopropylphosphino)ethylamine
ee	Enantiomeric excess
e.g.	*Exempli gratia* (for example)
equiv.	Equivalents
ESI	Electrospray Ionization

Et	Ethyl
et al.	*et alii* (and others)
FA	Formic acid
FAD	Formic acid dehydrogenation
FID	Flame ionization detector
FWHM	Full width at half maximum
G	Graphene
GC	Gas chromatography
GGA	Generalized gradient approximation
h	Hours
HAT	Hydrogen atom transfer
HER	Hydrogen evolution reaction
HO	Harmonic oscillator
HIE	Hydrogen isotope exchange
HF	Hartree Fock
HPLC	High-performance liquid chromatography
HRMS	High-resolution mass spectrometry
HSC	Hydrogen storage content
HSQC	Heteronuclear singlet quantum coherence
IG	Ideal gas
IP	Isophytol
iPr	Isopropyl
i.e.	*Id est* (that is)
$ImNH_2$	(1-methyl-1H-imidazol-2-yl)methanamine
ImNHMe	Methyl[(1-methyl-1H-imidazol-2-yl)methyl)amine
$ImNMe_2$	Dimethyl[(1-methyl-1H-imidazol-2-yl)methyl]amine
IR	Infrared
IRC	Intrinsic reaction coordinate

KS	Kohn Sham
LA	Lewis acid
LDA	Local density approximation
LOHC	Liquid organic hydrogen carrier
m	mass
m/z	mass/charge
M^+	Molecular ion peak
Me	Methyl
MECP	Minimum energy crossing point
MF	Methyl formate
min	Minutes
MLC	Metal ligand cooperativity
MM	Molecular mechanics
MS	Mass spectrometry
NMR	Nuclear magnetic resonance
NPD	Neophytadiene
n.r.	No reaction
ORTEP	Oak ridge thermal ellipsoid plot
P	Pressure
PC	Propylene carbonate
PCM	Polarizable Continuum Model
Ph	Phenyl
PN	Aminophosphine
ppm	Parts per million
q	Quadruplet
QTOF	Quadrupole time of flight
RR	Rigid rotor

r.t.	Room temperature
s	Singlet
SARS-CoV-2	Severe acute respiratory syndrome coronavirus 2
SDG	Sustainable development goals
SI	Supporting information
t	Triplet
T	Temperature
THF	Tetrahydrofuran
TMS	Transition metal sulfides
TOF	Turn over frequency
TON	Turn over number
TS	Transition state
UN	United Nations
u.m.a.	atomic mass unit
UV	Ultraviolet
V	Volume
Vis	Visible
viz.	*Videlicet* (namely)
XRD	X-ray diffraction

Table of contents

Chapter 1

Introduction

"If I have been further, it is by standing on the shoulders of giants."

Isaac Newton

1.1. General Introduction

During the present doctoral thesis, a series of extreme situations have highlighted the importance of our commitment, as chemists, to society. Among them, the SARS-CoV-2 pandemic has demonstrated that science can respond to society's requirements in a short-term way when the scientific community sets the focus and directs their efforts in the same direction.[1–3] In this sense, a number of major issues still need to be addressed as stated in the 2030 Agenda for Sustainable Development proposed by the United Nations.[4] The main objectives are summarized in the 17 Sustainable Development Goals (SDGs), depicted in Figure 1.1, among which climate action (13), affordable and clean energy (7), and responsible consumption and production (12) are the cornerstone of this doctoral thesis.

Figure 1.1. Sustainable Development Goals (SDGs) proposed by the United Nations.[4]

Over the past few decades, the exponential population growth combined with an increasing consumption per capita has intensified the development of industrial processes to fulfill the amenities of society,[5] with the vast majority of such manufacturing sectors causing a high environmental impact.[6] The transition from the use of fossil fuels to other renewable sources is still a problem to tackle in the chemical industry. For instance, the current production of ammonia and methanol

employs *ca.* 70% of non-renewable sources.[7] Moreover, some industrial processes generate high amounts of waste and require the use of harsh conditions (high temperatures and/or pressures).[8] The field of catalysis has contributed to the mitigation of these negative impacts through the design of more effective systems able to outperform current methods. Nevertheless, despite the plethora of developments implemented, there is still room for improvement. Thus, the present doctoral thesis can be framed within the design of efficient catalytic systems based on cluster complexes and the mechanistic elucidation combining experimental and theoretical approaches. In the following sections, we will present a holistic overview of coordination chemistry with special attention to molybdenum sulfide clusters. The basic concepts of catalysis will be reviewed followed by a detailed analysis on homogeneous processes, particularly hydrogenation and dehydrogenation reactions. To conclude, we will emphasize the relevance of computational chemistry to the understanding of homogeneous catalytic processes.

1.2. An overview of Coordination Chemistry

Coordination chemistry falls within the field of inorganic chemistry. This field deals with systems that contain metal atoms surrounded by ligand(s). Albeit coordination compounds are known since antiquity (*e.g.,* Prussian Blue ($KFe_2(CN)_6$) pigment), their chemical composition was a topic under debate for many years. At the end of the 1800s, Werner decided to investigate the properties of some metal halide complexes with ammonia, as for example $CoCl_3 \cdot nNH_3$ (n = 3-6).[9–11] His findings led him to propose two different types of "valence": primary *(Hauptvalenz)* and secondary (*Nebenvalenz*). The former corresponds to the oxidation state while the latter refers to the coordination number. After that, all the pieces of the puzzle were falling in place and the term coordination chemistry blossomed. In 1913, Werner received the first Nobel Prize in inorganic chemistry "*in recognition of his work on the linkage of atoms in molecules which he has thrown new light on earlier investigations and opened up new fields of research especially in inorganic chemistry*".[12]

From that moment on, coordination chemistry has been extended to a wide variety of sophisticated systems. In particular, this doctoral dissertation sets the focus on cluster complexes. The term cluster arose in the mid-1960s during the renaissance of coordination chemistry. It was first defined by Cotton as a complex that contains two or more metal atoms with at least one metal-metal bond.[13] At this point, one should note the conceptual differences between the terms polymetallic and polynuclear cluster. Whereas the former describes the nature of the metal (*i.e.,* different metal atoms), the latter only considers the number of metal ions.[14] For instance, a trimetallic cluster would then be composed of three different metals, while a trinuclear cluster will have three identical metals or, at most, have three different metal atoms.

Cluster complexes can also be classified according to the nature of the metal atom, in main group and transition metal clusters.[15] In this thesis, we have directed our attention towards the study of transition metal clusters. This type of clusters can

also be subdivided depending on the electronic features of the metal in electron rich and electron poor clusters.[16] The first class encompasses complexes built from late transition metals with π-acceptor ligands (*e.g.,* CO, H^-, or PR_3) that partially remove the excess of electron density. In contrast, electron poor clusters are composed of early transition metals with formal oxidation states ranging from +2 to +4 and σ/π-donor ligands such as: O^{2-}, S^{2-}, Cl^- and I^-. In this context, molybdenum sulfide clusters fall into the latter category.

1.2.1. Metal sulfide clusters: between Nature and materials

Metal sulfide clusters are ubiquitous in Nature and play a pivotal role in the reduction of small molecules at the active sites of enzymes.[17] For instance, the biochemical conversion of atmospheric N_2 to ammonia is mediated by Mo-nitrogenase that is composed of two metalloproteins, namely Fe protein and MoFe-protein. These systems contain within their 3D-structures three polynuclear cluster units, depicted in Figure 1.2. According to the most accepted mechanism, the electrons generated in the cellular metabolism are initially transferred from the $[Fe_4S_4]$ cluster (Fe protein, Figure 1.2a) to the $[Fe_8S_7]$ cluster (P-cluster – MoFe-protein, Figure 1.2b).[18] These electrons are then relocated in the FeMo-cofactor active sites (Figure 1.2c) where the N_2 binding and subsequent reduction occurs.[19]

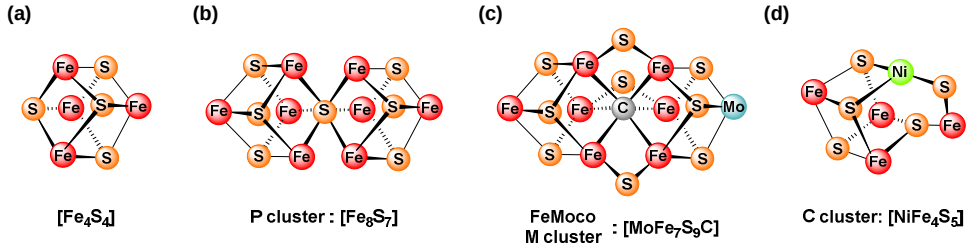

Figure 1.2. Representative examples of metal-sulfur complexes relevant in biological processes. Polynuclear units presented in (a-c) Mo-nitrogenase and (d) carbon monoxide dehydrogenase.

Another interesting example is the carbon monoxide dehydrogenase (CODH), presenting a Ni-Fe cluster. The cuboidal $[NiFe_3S_4]$ core, named C-cluster

in Figure 1.2d, catalyzes the reversible reduction of CO_2 to carbon monoxide (CO) under physiological conditions with excellent selectivity.[20] Understanding the enzymatic mechanism that rules these processes would open new avenues for the design of improved systems. To date, several aspects of high complexity from the mechanistic point of view, such as binding modes or multielectron transformations, remain elusive. These bottlenecks have triggered the development of synthetic analogs able to mimic their activity.[21,22]

Metal sulfide clusters can also be used as models of nanostructured transition metal sulfides (TMS).[23] In the last decade, molybdenum disulfide materials (MoS_2) have received a growing interest due to its numerous applications in optoelectronics[24], biomedical studies,[25] and catalysis.[26] In particular, their implementation in energy conversion processes like the production of green hydrogen ,generated by renewable sources, through the hydrogen evolution reaction (HER, $2H^+ + 2e^- \rightarrow H_2$) is one of the most attractive applications.[27] Despite the many research efforts devoted to unravel the mechanism that rules this transformation, the precise modes of action at the Mo and S sites are still unclear. Thus, the intrinsic drawbacks often found when obtaining relevant mechanistic information on heterogeneous systems have resulted in the development of other approaches to overcome these hurdles. In this context, molybdenum sulfide clusters have been proposed as homogeneous counterparts of MoS_2 due to their structural features resembling the active sites of the material.[28–30] The structure of molybdenum disulfide is characterized by two different structural motifs: basal planes and edge sites (Figure 1.3). The basal planes share structural and activity features with $[Mo_3S_4]^{4+}$ clusters.[31] In contrast, the presence of both S^{2-}/S_2^{2-} in the edge sites of $[Mo_3S_{13}]^{4+}$ and $[Mo_3S_7]^{4+}$ units make them structurally reminiscent of the MoS_2-bonding motifs.[32]

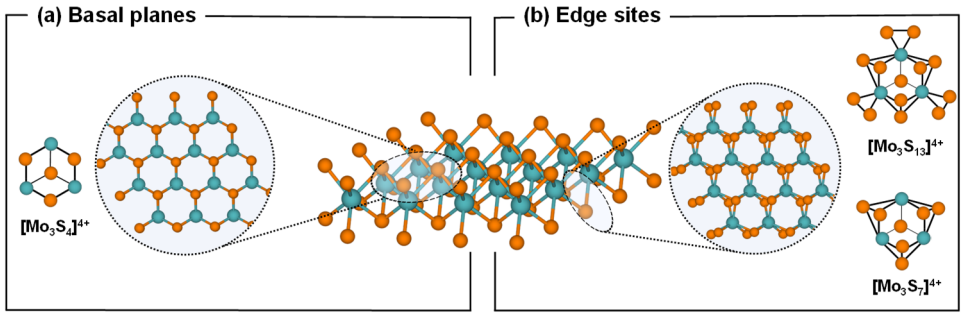

Figure 1.3. Topological relationship between molybdenum sulfide clusters and MoS_2.

The Molecular Materials group at University Jaume I, headed by Llusar, has focused its research on electron deficient molybdenum sulfide clusters and their applications in areas such as molecular electronics, optics, photocatalysis and catalysis. The group has developed a large family of trimetallic clusters containing trinuclear Mo_3S_7 and Mo_3S_4 units which differs in the nature of the S-bridging ligands, disulfides (μ-S_2) and sulfides (μ-S).[33] While Mo_3S_7 clusters show remarkable properties in non-linear optics, photocatalysis and as luminescent materials,[34–36] Mo_3S_4 complexes efficiently catalyze the transformation of several organic substrates.[37–39]

In this PhD thesis, we have focused our attention on $Mo_3(\mu_3\text{-}S)(\mu\text{-}S)_3$ cluster units, known by their interesting electronic properties. The simplified MO diagram for the metal-metal bonding in this trinuclear units was proposed by Cotton and Haas in the early 1960s.[13,40] Based on the idealized C_{3v}, symmetry the MO diagram has three bonding ($1a_1$, 1e), one largely non-bonding ($2a_1$) and five antibonding molecular orbitals.[16] In this MO picture, six cluster skeletal electrons (CSE) - two for each Mo^{IV} atom with a d^2 configuration - occupy the low lying $1a_1$ and 1e orbitals, which formally corresponds to three delocalized metal-metal bonds. The large energy gap between the 1e (HOMO) orbital and the $2a_1$ (LUMO) orbital difficult the formation of clusters with seven or eight CSE with a partially or fully occupied $2a_1$ orbital. In addition, bond analyses of Mo_3S_4 clusters performed by advanced

quantum methods suggest that these systems can be described as a continuous $Mo_3(\mu\text{-}S)_3$ d-pπ system with a strong interaction between the Mo-(μ-S)-Mo bonds.[41,42] In fact, this delocalization has been proposed as a quasi-aromaticity property of the Mo_3S_4 units.[43]

The first example of an isolated trinuclear molybdenum sulfide cluster was reported in 1985 in Cotton's group.[44] They developed a synthetic protocol to obtain the aqua ion, $[Mo_3S_4(H_2O)_9]^{4+}$, by reacting $[Mo(CO)_6]$ with anhydrous Na_2S in acetic acid. The resulting aquo cluster was used to functionalize the Mo_3S_4 cluster units by simply ligand exchange of the water molecules. Since then, a wide number of Mo_3S_4 clusters have been reported in the literature.[45] On this subject, Llusar's group has designed a large family of Mo_3S_4 complexes bearing ligands of diverse nature by simple ligand substitution starting from $[Mo_3S_4(thiourea)_8(H_2O)]Cl_4$ or $Mo_3S_4Cl_4(PPh_3)_3(H_2O)_2$ precursors.[46,47] For instance, they have reported several Mo_3S_4-based clusters decorated with water-soluble phosphines[48] or optically pure diphosphines.[49] The effect of replacing one phosphine moiety for a σ-donor (*i.e.,* amino group) was also investigated by coordination of aminophosphine ligands.[50] Most recently, the research scope has been extended towards the study of diamine or diimine ligands.[51,52] This dissertation contributes to this area by isolating new imidazolyl amino clusters, presented in Chapter 3.

1.3. Catalysis: from concepts to applications

The field of catalysis has played an active role in society since ancient times up to the present day. Some of the first known catalytic processes date back to 1552 when Cordus used sulfuric acid as catalyst in the conversion of an alcohol group to its ether derivative.[53] Nevertheless, three centuries were approximately needed to give a name to the rate acceleration process. The term catalysis was not coined until 1835 when Berzelius was preparing his annual report about the progress of chemistry to the Stockholm Academy of Science.[54] That was the first time this topic was recognized as a promising phenomenon. Later on, at the end of the 19th century,

Ostwald came up with the definition that is used up to date: "*A catalyst is a material that accelerates a chemical reaction without affecting the position of the equilibrium and thermodynamics of the reaction*".[55] In 1909, he was awarded the Nobel Prize in Chemistry for his fundamental work on the topic of catalysis. From that moment on, the investigations on the field experimented a surged in both academia and industry. In fact, the area of catalysis has become one of the most interdisciplinary fields of research with an integrative approach to the scientific disciplines. Such is its importance that over 90% of all chemical products rely on the use of at least one catalytic step.[56]

Apart from the economic advantage in terms of operational costs provided by the rate acceleration, catalysis allows to achieve sustainable industrial processes, shifting from the use of stoichiometric non-reusable reagents to the utilization of efficient catalysts with high selectivity. In fact, it is considered one of the 12 Principles of Green Chemistry proposed by Anastas and Warner in 1988.[57] These principles were created to develop greener chemical process or products, which is closely related to the pursuit of the SDGs (see Section 1.1) towards a sustainable society.

The field of catalysis has been traditionally classified into two categories, namely homogeneous and heterogeneous catalysis, illustrated in Figure 1.4, depending on the phase in which the catalysts interact with the substrate(s). In this case, the word phase refers to the physical state of the species involved. Hence, a homogeneous transformation implies that both catalyst and reactants are in the same phase. On the other hand, when the reaction occurs in different phases the process is categorized as heterogeneous catalysis. Although it might seem quite straightforward, this classification is far from trivial as the boundaries between homogeneous and heterogeneous have become blurry with the consolidation of single atom catalysis (SAC). The concept was raised by Zhang and coworkers only a decade ago, and it comprises the catalytic reactions assisted by single metal atoms on a heterogeneous surface.[58]

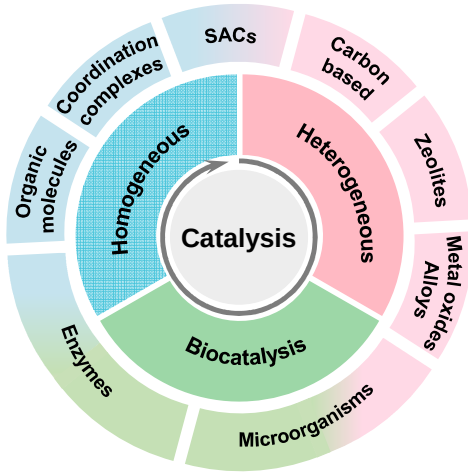

Figure 1.4. Schematic representation of catalysis classification. Examples of homogeneous, heterogeneous and biocatalysts are included.

Conceptually, the structural resemblance of single atoms to molecular complexes has resulted in the postulation of SACs as a "bridge" between homogeneous and heterogeneous catalysis.[59,60] Finally, the biocatalytic transformations rendered by enzymes are considered the highest expression of catalysis. This is the result of the unrivalled specificities attained through shape-specific recognition at the active sites, which preorganizes the substrates in the optimal conformation for their conversion.[61] After providing a holistic vision of the field of catalysis, homogeneous catalysis will be in this thesis's spotlight.

1.3.1. Homogeneous Catalysis

Despite heterogeneous catalysis predominates in industrial processes, homogeneous systems have also demonstrated their feasibility in the industry. For instance, one of the oldest industrial transformations, the so-called lead chamber process (1746), is considered as a homogeneously-catalyzed reaction.[62] In that reaction, Roebuck proposed nitrogen oxides as the catalysts in the oxidation reaction of sulfur dioxide (produced by burning sulfur or roasting sulfur-containing metals) to sulfur trioxide, then NO is re-oxidized by air to NO_2. Since the NO/NO_2 are recovered at the end of the reaction and that all the species involved reside in the gas phase, this system

can be considered as a homogeneous catalytic transformation. This method has been currently replaced by the contact process in which vanadium oxide (V_2O_5) is used as the catalyst. The golden era of homogeneous catalysis arose with the discovery of the well-known Wilkison's catalyst. In 1965, one of his PhD students prepared a new rhodium square planar complex of formula $RhCl(PPh_3)_3$ (PPh_3 = triphenylphosphine). This complex exhibited an outstanding activity in the reduction of alkenes (1 atm H_2 at ambient temperature).[63] Since then, a wide variety of reactions catalyzed by homogeneous systems have been reported, some relevant examples are represented in Figure 1.5. The importance of some of these processes has been recognized by the Nobel Foundation with the following awards in Chemistry: Ziegler-Natta (1963); Knowles, Noyori and Sharpless (2001); Chauvin, Grubbs, and Schrock (2005); Heck, Suzuki, and Negishi (2010); List and MacMillan (2021) and Bertozzi, Medal and Sharpless (2022).[64]

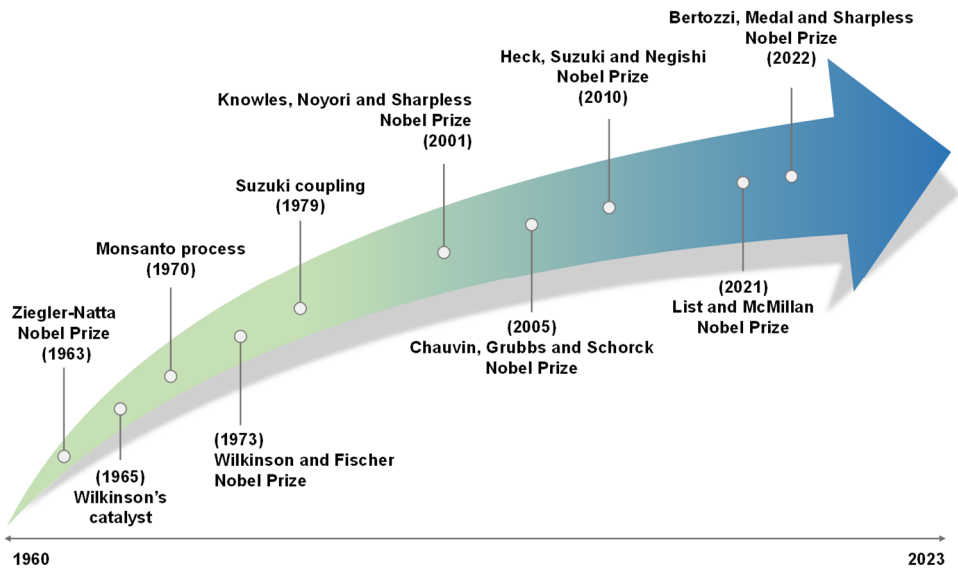

Figure 1.5. Historical overview of homogeneous catalysis.

From an academic point of view, homogeneous systems are among the most studied due to the many advantages that they provide to chemical synthesis.[65] One of the main features of these catalysts is their synthetic flexibility that allows for the simple modulation of the final properties. The metal choice and catalyst design play

a crucial role in the catalytic performance in terms of productivity (turnover number, TON), activity (turnover frequency, TOF), stability and selectivity (chemo-, regio-, stereo-, enantioselectivity). As for the metal site, increasing attention has been drawn to the replacement of noble metals with non-precious ones because of the environmental awareness. The low abundances on the Earth's crust and their high price (*e.g.,* Pd is about 2000 times more expensive than Ni) make noble metals lag behind the current approach of sustainability, mentioned in Section 1.1 of this chapter.

On the other hand, the choice of the optimal ligand that meets the specific catalytic requirements for each reaction can be a daunting task. Ligands can be classified depending on different properties such as denticity, the electronic properties of the binding atom (donor and/or acceptor) or chirality. This large pool of possibilities represents the synthetic playground for the scientific community to build-up an almost infinite number of complexes and consequently, the tunability of the catalytic complexes have basically no limits.

It must be also noted that in the case of cluster complexes, the metal site is replaced by a cluster core adding to the system another variable to consider. In fact, the metal-metal interaction allows for unique reaction pathways compared to traditional mononuclear catalysts.[66] The catalytic activity of these polynuclear units can be defined with the name of cluster catalysis. This term can only be invoked when the cluster core is preserved throughout the reaction.[67] In contrast, when the cluster undergoes fragmentation during the catalytic process it can be referred as a pre-catalyst. For that reason, a combination of characterization techniques is required to ascertain the true nature of the catalytic process.

Regarding homogeneously catalyzed reactions, transformations involving C-C, C-H, C-O or C-N bonds can be highlighted. Hydroformylation, carbonylation or (de)hydrogenation fall within the most popular reactions.[65] Particularly, this thesis has focused its attention on hydrogenation and dehydrogenation transformations, which will be discussed in the following sections.

1.3.1.1. Hydrogenation reactions

The term hydrogenation refers to a chemical reaction in which a dihydrogen molecule is incorporated into an unsaturated bond to generate the corresponding saturated product. At the end of the 19th century, Moissan and Moureu's investigated the fixation of acetylene to some metals (Ni, Fe, and Co) to produce the corresponding coordination complexes. Nevertheless, they obtained unexpected results as the reaction led to coal, hydrogen, and hydrocarbons. The formation of such decomposition products was attributed to a physical phenomenon occurring due to the porosity of the metals.[68] Later on, Sabatier and Senderens decided to take a closer look into that reaction. By subjecting a mixture of ethylene and hydrogen at *ca.* 40 ºC in the presence of disintegrated nickel they were able to produce ethane from its unsaturated analogue for the first time.[69] In 1912, Sabatier was awarded the Nobel Prize in Chemistry for its seminal work on hydrogenation of organic molecules.[70] Since then, we have witnessed the flourishing of hydrogenation reactions.

Homogeneous hydrogenation has helped to tackle the issues related to industrial waste generation by reducing the number of reaction steps and increasing the selectivity towards the desired product (SDG 12-13). An instructive example is the production of Naproxen, an anti-inflammatory drug. While the (*S*)-enantiomer can be used with pharmaceutical purposes, the (*R*)-enantiomer has hepatotoxic properties. The hydrogenation of α-naphthylacrylic acid is the crucial synthetic step since it requires the enantioselective reduction of a double bond (Figure 1.6). When a ruthenium complex with a chiral ligand, the well-known (*S)*-BINAP, is used as catalyst the reaction occurs with a 98% yield towards the desired (*S*)-Naproxen.[71]

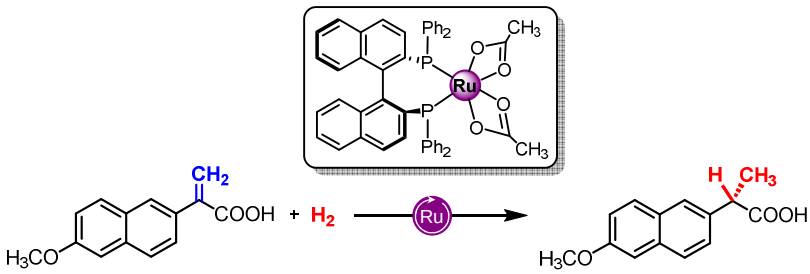

Figure 1.6. Selected example of homogeneous hydrogenation process: synthesis of (*S*)-Naproxen.

Another interesting example that plays a central role in a carbon-neutral economy (SDG 7-13) is the hydrogenation of CO_2 for the production of high value-added C1 products (methanol, formic acid, hydrocarbons, and so on).[72,73] These reactions represent an attractive strategy for reducing greenhouse gas emissions and a possible stepping-stone towards renewable fuels.[74]

During the last decade, the Molecular Materials group has extended its field of research to catalytic hydrogenation of organic substrates using Mo_3S_4 cluster catalysts. In 2012, in collaboration with Beller's group, they reported a cubane-type hydrido Mo_3S_4 cluster functionalized with diphosphane ligands for the selective transfer hydrogenation of nitroarenes applying formates as reducing agents.[38] Lately, the hydrogenation of nitrobenzene derivatives catalyzed by Mo_3S_4 clusters containing diamine and diimine ligands under relatively mild conditions (70 ºC and 20 bar H_2) was reported for the first time.[52] Encouraged by the remarkable activity of these systems, they investigated the reductive amination of aldehydes with nitro compounds using hydrogen as reducing agent.[75] The catalytic hydrogenation of azobenzene was systematically studied from the mechanistic point of view.[76] Besides, they have recently extended the reactivity of these molybdenum sulfide clusters towards the semihydrogenation of C≡C triple bonds.[39] For example, the reduction of diphenylacetylene was assayed, obtaining a moderate stereoselectivity (ratio (*Z*)/(*E*): 6/1) but under extremely harsh reaction conditions (150 ºC and 100 bar H_2). The activity and selectivity are remarkably improved when a family of

imidazolyl amino-based Mo_3S_4 clusters catalyze the semihydrogenation of internal alkynes, as presented in this dissertation (see Chapter 3), towards the (*Z*)-isomer.

1.3.1.2. Dehydrogenation processes as sustainable tools

The current climate situation urgently demands the improvement of our energy technologies to face one of the greatest challenges of the 21st century: climate change (SDG 7-12). Anthropogenic CO_2 emissions and energy supply shortages of fossil fuels have set renewable energies in the spotlight of the scientific community. Despite the promising strides achieved in wind, solar or hydroelectric energy technologies in the last 50 years, their intermittent character result in a non-viable energy supply.[77] Instead, hydrogen gas is a storable form of energy that can be utilized under demand, thereby filling the energy gaps. Thus, the dehydrogenation step to produce hydrogen is receiving increasing attention since it is as important as the hydrogenation reaction. It should be highlighted that the so called hydrogen-based economy was coined as early as 1972 by Bockris.[78] Such is its significance that the global hydrogen market is expected to reach *ca.* US$700 billion by 2050.[79]

The ideal scenario would be based on the production of green hydrogen from the water electrolysis with renewable energies to store, transport or use it depending on the user's necessities. Although hydrogen has a high energy content, its inflammability leads to safety problems. Moreover, the low gravimetric density (0.0899 kg/m^3) under ambient conditions leads to difficulties in the storage systems.[80] Conventionally, hydrogen is physically stored as a compressed gas (100-700 bar) or in its liquified form (at - 253 ºC), hampering the handling and transportation for infrastructures such as on-board H_2 storage systems.[77] In this sense, the development of alternative hydrogen energy carriers has undergone a gold rush.

Liquid organic hydrogen carriers (LOHCs) have received a substantial amount of attention from the field of homogeneous catalysis due to their possibilities to overcome the aforementioned limitations. LOHCs are liquid substances that are

hydrogen-rich (H_n-LOHC) and can release hydrogen through a dehydrogenation process, generating its hydrogen-lean counterpart (H_0-LOHC). This "side-product" (H_0-LOHC) can be activated for use again *via* a hydrogenation reaction to recover its initial state, (H_n-LOHC), an schematic illustration is represented in Figure 1.7.[81]

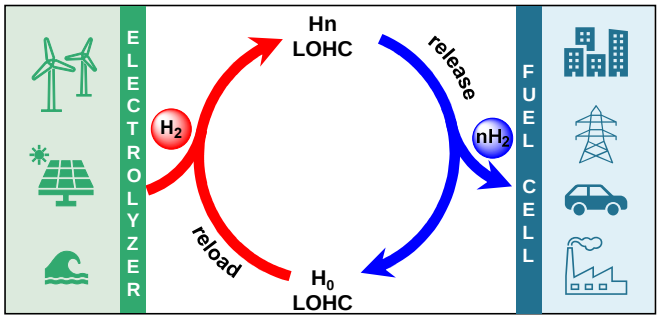

Figure 1.7. Renewable energy storage concept using LOHC technology.

Currently, numerous molecules are considered as LOHCs, Figure 1.8 lists a series of selected dehydrogenation/hydrogenation reactions. The first example describing LOHC as hydrogen carriers dates back to the 1980s. Taube proposed the utilization of a system called MTH (methylcyclohexane, toluene, hydrogen) to efficiently produce hydrogen through hydrogenation/dehydrogenation reactions (Figure 1.8a). In this study, he even evaluated the feasibility of this technology in vehicles.[82] Although the hydrogen storage capacity of the system was competitive (HSC = 6.1%), its thermodynamic requirements were not assumable as temperatures >300 ºC were necessary. Thus, the substitution of carbon atoms in arenes by heteroatoms (nitrogen, oxygen) was investigated, achieving more energetically favored processes.[83] For instance, N-heterocycles have intermediate hydrogen densities (Figure 1.8b; HSC = 5.2%) and can be easily handled.

Regarding aliphatic molecules methanol, formic acid (FA), and methyl formate (MF) are among the most promising alternatives for its hydrogen storage content-abundance trade-off (Figure 1.8c to 1.8e).[84,85] A number of systems have proved successful in methanol reforming (*i.e.,* dehydrogenation of methanol) thanks to the high hydrogen density stored in this widely available solvent (HSC =

12.1%).[86] In contrast, it was not until the last few months that methyl formate (Figure 1.8e; HSC = 8.1%) was proposed as a hydrogen carrier for the first time by Beller.[85] However, these alternatives will not be discussed here, as the focus of our work is formic acid dehydrogenation (FAD).

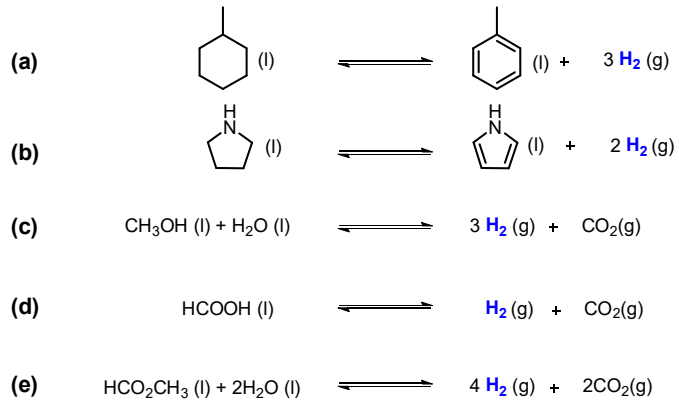

Figure 1.8. Reversible dehydrogenation and hydrogenation of selected LOHC systems: (a-b) heterocyclic and (c-e) aliphatic molecules.

During the 1960s, Coffey reported the first example of the use of homogeneous catalysis for the decomposition of FA (HSC = 4.4%) into hydrogen and carbon dioxide (1:1).[87] However, 40 years were needed for the scientific community to notice the potential application of FA as a liquid organic hydrogen carrier. In 2008, Laurenczy reported the unprecedented activity of Ru-based catalysts decorated with either sulfonated aryl- or arylalkylphosphines in the dehydrogenation of FA in aqueous solution.[88] Notably, the presence of a formate salt (*viz.* NaCOOH) was necessary to initiate the reaction. Almost at the same time, Beller's group demonstrated that hydrogen release from FA:Amine adducts proceeded smoothly in the presence of a $[RuCl_2(PPh_3)_3]$ catalyst.[89] From that moment on, this topic and the reverse reaction (CO_2 hydrogenation) have taken a central role in the roadmap to achieve a net-zero future.

The Molecular Materials group has also contributed to this field by testing the non-noble $[Mo_3S_4H_3(dmpe)_3]^+$ (dmpe = 1,2-bis(dimethylphosphino)ethane) cluster in FAD.[90] This outcome was considered as a proof of concept of the

feasibility of Mo_3S_4 clusters for this transformation. In Chapter 5, the potential of a series of molybdenum sulfide clusters in the hydrogen production from FA will be discussed.

1.4. Beyond experiments through computational chemistry

Once a catalytic system has been designed and its activity has been assessed in a particular reaction, the subsequent step is the mechanistic elucidation. The knowledge gathered in this area can be used to rationalize the results obtained in a reaction, and more importantly, to improve the systems with a tailor-made catalyst design. Many analytical techniques such as nuclear magnetic resonance (NMR), infrared spectroscopy (IR), mass spectrometry (ESI-MS) or X-ray diffraction (XRD) have been employed to unravel the reaction pathways. Despite the discovery of more advanced experimental operando techniques, some steps of complex catalytic reactions cannot be fully understood. In this context, the computational approach has been incorporated into the catalytic toolbox to provide a better understanding of the reaction mechanisms and give reasonable predictions.[91]

Computational chemistry is defined as the study of chemistry through the use of approximate solutions to the electronic Schrödinger equation.[92] There are numerous computational methods available, with their selection depending on the requirements of the process studied. If the object of study is a large system, then molecular mechanics (MM) is the better choice. However, when the system is considered as "small" organic or coordination complex, the use of quantum mechanics (QM) is the best approach. Among the QM methodologies, Hartree Fock (HF) and density functional theory (DFT) can be found, being the latter the most popular method in the mechanistic elucidation on the basis of the efficiency–accuracy trade-off.[93]

1.4.1. Density functional theory

The first investigations that built-up the basis of DFT can be found on a seminal work of Thomas and Fermi, showing that the energy of a system of many electrons could be locally modelled by their uniform electron gas energy densities.[94,95] Although this theory was rejected because it was too simplistic, it inspired Hohenberg and Kohn, whose pioneering work is considered as the milestone of the current DFT methods.[96] In fact, Kohn was awarded in 1998 the Nobel Prize in Chemistry "*for his development of the density-functional theory*" shared with Pople "*for his development of computational methods in quantum chemistry*".[97]

The fundamentals of DFT are based on the two theorems proposed by Hohenberg and Kohn that established the correlation between the total energy of a system and the electron density. The inherent difficulties in the analysis of the resultant solution were addressed by the Kohn-Sham theory (KS).[98] Currently, the KS-DFT is the basis of most of the DFT calculations ruled by equation 1.1, that describes the overall energy functional.

$$E[\rho(r)] = T_{ni}[\rho(r)] + V_{nuc\text{-}e}[\rho(r)] + V_{ee}[\rho(r)] + \Delta T[\rho(r)] + \Delta V_{ee}[\rho(r)] \qquad (1.1)$$

The first three terms are referred to the energy corresponding the non-interacting kinetic energy, the nuclei-electron Coulomb attraction and the electron-electron Coulomb repulsion, respectively. These terms can be calculated in a feasible way, but the problem comes with the two last terms. They represent the corrections to the kinetic energy and the non-classical electron interactions which are collected in a term denoted as $E_{xc}[\rho(r)]$, ($E_{xc}[\rho(r)] = \Delta T[\rho(r)] + \Delta V_{ee}[\rho(r)]$), the exchange-correlation energy functional. This term is the only part of the equation 1.1 for which the exact expression is unknown. In order to address this issue, a variety of approximations have been proposed, *e.g.,* local density approximation (LDA), generalized gradient approximation (GGA) or double hybrid functionals, which differ in the accuracy and computational cost.[99] Thus, the election of the functional

is undoubtedly the main limitation of DFT as there is no rule transferable to a molecular system or a specific reaction.[100]

The use of the density functional theory methodology as an isolated technique can frequently lead to accuracy issues and a disparity in results depending on the functional used. As a matter of fact, a combined approach of computations and experiments can address these problems as one can fill the information gaps of the other.[93,101] This interplay has allowed experimental researchers to understand non-intuitive results, determine short-lived intermediates, or rationalize stereoselectivity and/or chemoselectivity in a mechanistic analysis. In this context, the present dissertation has followed this approach by combining computational and experimental investigation on hydrogenation and dehydrogenation mechanisms (see Chapters 4 and 5). Before delving into them, the following section will briefly discuss the basis of these mechanisms.

1.4.2. Hydrogenation and dehydrogenation mechanisms

Hydrogenation and dehydrogenation reactions represent the opposite process of each other which comprise the activation or release of molecular hydrogen (H_2). The mechanisms that govern both reactions share common features in general terms, although the subtleties of each process trigger a broad landscape of pathways. In general terms, hydrogenation and dehydrogenation mechanisms catalyzed by transition metal complexes can be classified depending on the interaction between the substrate and the coordination complex (metal or ligand). For instance, those mechanisms proceeding with coordination of the substrate to the metal center are labeled as inner-sphere while those with an interaction in the second sphere are named as outer-sphere.[102] Another classification is based on how the ligand influences the H_2 activation and/or release step, *i.e.,* non-cooperative and cooperative mechanisms, represented in Figure 1.9.

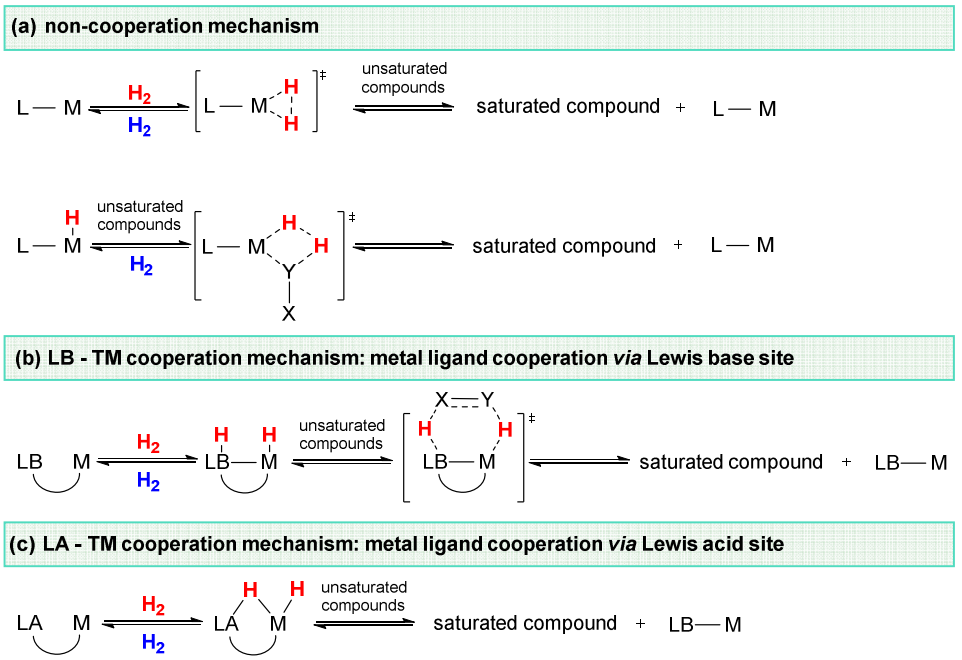

Figure 1.9. Mechanistic classification in hydrogenation and dehydrogenation processes: (a) non-cooperative mechanisms and (b-c) cooperative mechanisms.

Traditionally, hydrogenation and dehydrogenation processes are governed by metal-centered reactivity through oxidative addition/reductive elimination steps or σ-bond metathesis reactions (Figure 1.9a). However, in the past years this classification has been expanded due to the design of catalytic systems featuring a cooperative chemical action between the ligand and the metal, Figure 1.9b and 1.9c.[103] One of the most popular examples of metal-ligand cooperativity (MCL) is the use of a Lewis base (LB) moiety that provides electron density to the transition metal (TM) system to build up an intramolecular Lewis acid-base pair during the cleavage or release of the H_2 molecule (see Figure 1.9b). Another novel strategy is the Lewis acid (LA) - TM-based system that is composed of a LA site (*i.e.,* an electron acceptor moiety) together with a metal center as an electron donor group. Despite the range of these classifications, some compounds defy categorization within these established classes.

Recently, Poli has proposed that the hydrogenation/dehydrogenation transformations can be classified depending on the change in the metal oxidation state upon interaction with the hydrogen molecules as oxidative, neutral, or reductive activation.[104] In the most common hydrogen activation mechanism, named as redox-neutral activation, the metal maintains its initial oxidation state and the hydrogen molecule is transferred as a hydride (H^-) and a proton (H^+).[105] Several reported examples follow an oxidative activation in which the H atoms of molecular hydrogen capture two electrons from the metallic core to form two hydrides ($2H^-$), with the related modification of the metal oxidation state from M^n to M^{n+2}.[106] In contrast, the less common described mechanism, called reductive activation, is based on the transfer of two hydrogen atoms as protons ($2H^+$) which results in the reduction of the metal atom from M^n to M^{n-2}.

Among the few examples that follow a reductive activation pathway, dimolybdenum sulfide compounds reported by DuBois fall within this category.[107] In the mechanism proposed the cyclopentadienyl dinuclear $Mo_2(\mu\text{-}S)_2(\mu\text{-}S_2CH_2)$ complex (Figure 1.10a) activates the hydrogen molecule through the bridging sulfide ligands. This interaction triggers a rearrangement of the electron density that results in a formal two-electron reduction from Mo_2^{IV} to Mo_2^{III} (Figure 1.10b).

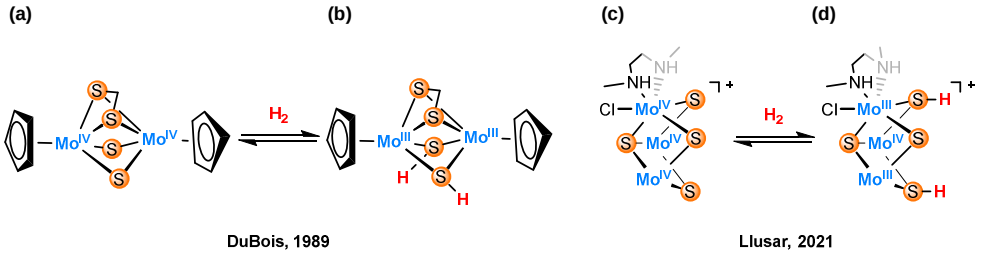

Figure 1.10. Molybdenum sulfide species involved in hydrogen activation. (a-b) DuBois dinuclear $Mo_2(\mu\text{-}S)_2(\mu\text{-}S_2CH_2)$ complexes and (c-d) Llusar's trinuclear $Mo_3(\mu_3\text{-}S)(\mu\text{-}S)_3$ clusters. Ligands on the other Mo centers of the Mo_3S_4 cluster have been omitted for clarity.

Trinuclear Mo_3S_4 complexes activate the H_2 molecule in the sulfur sites through a similar mechanism.[76] Llusar's group has proposed that H_2 delivers two protons and two electrons to the Mo_3S_4 unit (Figure 1.10c) upon interaction with the sulfur moieties. In this process, the trimetallic unit is reduced from Mo_3^{IV} to $Mo^{IV}Mo_2^{III}$ (Figure 1.10d) which allows us to frame these systems into the reductive activation classification.

On the other hand, when Mo_3S_4 cluster units are used in dehydrogenation processes, particularly in formic acid dehydrogenation, they follow a molybdenum-centered mechanism in which the Mo-H bonds are identified as the active species.[90] Analysis of the formal oxidation state of the molybdenum centers during the catalytic cycle reveals a constant Mo_3^{IV} oxidation state, thus suggesting that this mechanism falls into the redox-neutral classification. These difference in the reactivity of Mo_3S_4 clusters emphasizes the versatility of these systems offering conventional metal-centered mechanisms and less common sulfur-based pathways. In this regard, the combination of theoretical and experimental studies is a useful approach to clarify the mechanistic pathways that ruled Mo_3S_4 catalyzed reactions. In Chapters 4 and 5 an in-depth study on the mechanisms of hydrogenation and dehydrogenation reactions will be presented. Further details about the objectives of this dissertation are provided in the following Chapter.

1.5. References

[1] G. Chauhan, M. J. Madou, S. Kalra, V. Chopra, D. Ghosh, S. O. Martinez-Chapa, *ACS Nano* **2020**, *14*, 7760-7782.

[2] X. Huang, E. Kon, X. Han, X. Zhang, N. Kong, M. J. Mitchell, D. Peer, W. Tao, *Nat. Nanotechnol.* **2022**, *17*, 1027-1037.

[3] F. Zhao, X. Zai, Z. Zhang, J. Xu, W. Chen, *npj Vaccines* **2022**, *7*, 167.

[4] United Nations, "https://sdgs.un.org/goals," can be found under https://sdgs.un.org/goals, **2015**.

[5] F. J. Gomes da Silva, R. M. Gouveia, in *Clean. Prod.*, Springer International Publishing, Cham, **2020**, 33-75.

[6] K. Calvin, D. Dasgupta, G. Krinner, A. Mukherji, P. W. Thorne, C. Trisos, J. Romero, P. Aldunce, K. Barrett, G. Blanco, W. W. L. Cheung, S. Connors, F. Denton, A. Diongue-Niang, D. Dodman, M. Garschagen, O. Geden, B. Hayward, C. Jones, F. Jotzo, T. Krug, R. Lasco, Y.-Y. Lee, V. Masson-Delmotte, M. Meinshausen, K. Mintenbeck, A. Mokssit, F. E. L. Otto, M. Pathak, A. Pirani, E. Poloczanska, H.-O. Pörtner, A. Revi, D. C. Roberts, J. Roy, A. C. Ruane, J. Skea, P. R. Shukla, R. Slade, A. Slangen, Y. Sokona, A. A. Sörensson, M. Tignor, D. van Vuuren, Y.-M. Wei, H. Winkler, P. Zhai, Z. Zommers, J.-C. Hourcade, F. X. Johnson, S. Pachauri, N. P. Simpson, C. Singh, A. Thomas, E. Totin, A. Alegría, K. Armour, B. Bednar-Friedl, K. Blok, G. Cissé, F. Dentener, S. Eriksen, E. Fischer, G. Garner, C. Guivarch, M. Haasnoot, G. Hansen, M. Hauser, E. Hawkins, T. Hermans, R. Kopp, N. Leprince-Ringuet, J. Lewis, D. Ley, C. Ludden, L. Niamir, Z. Nicholls, S. Some, S. Szopa, B. Trewin, K.-I. van der Wijst, G. Winter, M. Witting, A. Birt, M. Ha, *IPCC, 2023: Climate Change 2023: Synthesis Report. Contribution of Working Groups I, II and III to the Sixth Assessment Report of the Intergovernmental Panel on Climate Change [Core Writing Team, H. Lee and J. Romero (Eds.)]. IPCC,*

Geneva, Switzerland., **2023**.

[7] A. Nabera, I.-R. Istrate, A. Jose Martin, J. Pérez-Ramírez, G. Guillén-Gosálbez, *Green Chem.* **2023**, *25*, 6603-6611.

[8] R. A. Sheldon, *ACS Sustain. Chem. Eng.* **2018**, *6*, 32-48.

[9] A. Werner, A. Miolati, *Z. Phys. Chem.* **1893**, *12*, 35.

[10] E. C. Constable, C. E. Housecroft, *Chem. Soc. Rev.* **2013**, *42*, 1429-1439.

[11] G. A. Lawrance, *Introduction to Coordination Chemistry*, Wiley, **2010**.

[12] "The Nobel Prize in Chemistry 1913," can be found under https://www.nobelprize.org/prizes/chemistry/1913/summary/.

[13] F. A. Cotton, *Inorg. Chem.* **1964**, *3*, 1217-1220.

[14] F. A. Cotton, R. D. Adams, *Catalysis by Di- and Polynuclear Metal Cluster Complexes*, Wiley-VCH, **1998**.

[15] M. D. Mingos, D. J. Wales, *Introduction to Cluster Chemistry*, Prentice-Hall, **1990**.

[16] A. Müller, R. Jostes, F. A. Cotton, *Angew. Chemie Int. Ed. English* **1980**, *19*, 875-882.

[17] K. Tanifuji, S. Ohta, Y. Ohki, H. Seino, *Coord. Chem. Rev.* **2023**, *475*, 214838.

[18] B. M. Hoffman, D. Lukoyanov, Z.-Y. Yang, D. R. Dean, L. C. Seefeldt, *Chem. Rev.* **2014**, *114*, 4041-4062.

[19] K. Tanifuji, Y. Ohki, *Chem. Rev.* **2020**, *120*, 5194-5251.

[20] A. M. Appel, J. E. Bercaw, A. B. Bocarsly, H. Dobbek, D. L. DuBois, M. Dupuis, J. G. Ferry, E. Fujita, R. Hille, P. J. A. Kenis, C. A. Kerfeld, R. H. Morris, C. H. F. Peden, A. R. Portis, S. W. Ragsdale, T. B. Rauchfuss, J. N. H. Reek, L. C. Seefeldt, R. K. Thauer, G. L. Waldrop, *Chem. Rev.* **2013**, *113*,

6621-6658.

[21] A. Mouchfiq, T. K. Todorova, S. Dey, M. Fontecave, V. Mougel, *Chem. Sci.* **2020**, *11*, 5503-5510.

[22] Y. Ohki, K. Munakata, Y. Matsuoka, R. Hara, M. Kachi, K. Uchida, M. Tada, R. E. Cramer, W. M. C. Sameera, T. Takayama, Y. Sakai, S. Kuriyama, Y. Nishibayashi, K. Tanifuji, *Nature* **2022**, *607*, 86-90.

[23] E. Dornsiepen, F. Pieck, R. Tonner, S. Dehnen, *J. Am. Chem. Soc.* **2019**, *141*, 16494-16500.

[24] M. Timpel, G. Ligorio, A. Ghiami, L. Gavioli, E. Cavaliere, A. Chiappini, F. Rossi, L. Pasquali, F. Gärisch, E. J. W. List-Kratochvil, P. Nozar, A. Quaranta, R. Verucchi, M. V. Nardi, *npj 2D Mater. Appl.* **2021**, *5*, 64.

[25] X. Zhu, X. Ji, N. Kong, Y. Chen, M. Mahmoudi, X. Xu, L. Ding, W. Tao, T. Cai, Y. Li, T. Gan, A. Barrett, Z. Bharwani, H. Chen, O. C. Farokhzad, *ACS Nano* **2018**, *12*, 2922-2938.

[26] J. Hu, L. Yu, J. Deng, Y. Wang, K. Cheng, C. Ma, Q. Zhang, W. Wen, S. Yu, Y. Pan, J. Yang, H. Ma, F. Qi, Y. Wang, Y. Zheng, M. Chen, R. Huang, S. Zhang, Z. Zhao, J. Mao, X. Meng, Q. Ji, G. Hou, X. Han, X. Bao, Y. Wang, D. Deng, *Nat. Catal.* **2021**, *4*, 242-250.

[27] J. Mao, Y. Wang, Z. Zheng, D. Deng, *Front. Phys.* **2018**, *13*, 138118.

[28] H. I. Karunadasa, E. Montalvo, Y. Sun, M. Majda, J. R. Long, C. J. Chang, *Science* **2012**, *335*, 698-702.

[29] J. Kibsgaard, T. F. Jaramillo, F. Besenbacher, *Nat. Chem.* **2014**, *6*, 248-253.

[30] M. L. Grutza, A. Rajagopal, C. Streb, P. Kurz, *Sustain. Energy Fuels* **2018**, *2*, 1893-1904.

[31] J. Al Cheikh, R. Zakari, A. C. Bhosale, A. Villagra, N. Leclerc, S. Floquet, P.

C. Ghosh, A. Ranjbari, E. Cadot, P. Millet, L. Assaud, *Mater. Adv.* **2020**, *1*, 430-440.

[32] S. Batool, S. P. Nandan, S. N. Myakala, A. Rajagopal, J. S. Schubert, P. Ayala, S. Naghdi, H. Saito, J. Bernardi, C. Streb, A. Cherevan, D. Eder, *ACS Catal.* **2022**, *12*, 6641-6650.

[33] R. Llusar, C. Vicent, in *Inorg. Chem. Focus III* (Eds.: G. Meyer, D. Naumann, L. Wesrmann), **2006**.

[34] D. Recatalá, R. Llusar, A. Barlow, G. Wang, M. Samoc, M. G. Humphrey, A. L. Guschin, *Dalt. Trans.* **2015**, *44*, 13163-13172.

[35] D. Recatalá, R. Llusar, F. Galindo, K. A. Brylev, A. L. Gushchin, *Eur. J. Inorg. Chem.* **2015**, 1877-1885.

[36] D. Recatalá, R. Llusar, A. L. Gushchin, E. A. Kozlova, Y. A. Laricheva, P. A. Abramov, M. N. Sokolov, R. Gómez, T. Lana-Villarreal, *ChemSusChem* **2015**, *8*, 148-157.

[37] T. F. Beltrán, M. Feliz, R. Llusar, J. A. Mata, V. S. Safont., *Organometallics* **2011**, *30*, 290-297.

[38] I. Sorribes, G. Wienhöfer, C. Vicent, K. Junge, R. Llusar, M. Beller, *Angew. Chemie - Int. Ed.* **2012**, *51*, 7794-7798.

[39] A. G. Algarra, E. Guillamón, J. Andrés, M. J. Fernández-Trujillo, E. Pedrajas, J. Á. Pino-Chamorro, R. Llusar, M. G. Basallote, *ACS Catal.* **2018**, *8*, 7346-7350.

[40] F. A. Cotton, T. E. Haas, *Inorg. Chem.* **1964**, *3*, 10-17.

[41] M. Feliz, R. Llusar, J. Andrés, S. Berski, B. Silvi, *New J. Chem.* **2002**, *26*, 844-850.

[42] J. Andrés, S. Berski, M. Feliz, R. Llusar, F. Sensato, B. Silvi, *Comptes Rendus*

Chim. **2005**, *8*, 1400-1412.

[43] J. Li, C.-W. Liu, J.-X. Lu, *Polyhedron* **1994**, *13*, 1841-1851.

[44] F. A. Cotton, Z. Dori, R. Llusar, W. Schwotzer, *J. Am. Chem. Soc.* **1985**, *107*, 6734-6735.

[45] A. L. Gushchin, Y. A. Laricheva, M. N. Sokolov, R. Llusar, *Russ. Chem. Rev.* **2018**, *87*, 670-706.

[46] V. P. Fedin, M. N. Sokolov, Y. V. Mironov, B. A. Kolesov, S. V. Tkachev, V. Y. Fedorov, *Inorganica Chim. Acta* **1990**, *167*, 39-45.

[47] A. L. Gushchin, Y. A. Laricheva, P. A. Abramov, A. V. Virovets, C. Vicent, M. N. Sokolov, R. Llusar, *Eur. J. Inorg. Chem.* **2014**, 4093-4100.

[48] T. F. Beltrán, R. Llusar, M. Sokolov, M. G. Basallote, M. J. Fernández-Trujillo, J. Á. Pino-Chamorro, *Inorg. Chem.* **2013**, *52*, 8713-8722.

[49] M. Feliz, E. Guillamón, R. Llusar, C. Vicent, S. E. Stiriba, J. Pérez-Prieto, M. Barberis, *Chem. - A Eur. J.* **2006**, *12*, 1486-1492.

[50] T. F. Beltrán, V. S. Safont, R. Llusar, *Eur. J. Inorg. Chem.* **2016**, 5171-5179.

[51] E. Pedrajas, I. Sorribes, K. Junge, M. Beller, R. Llusar, *ChemCatChem* **2015**, *7*, 2675-2681.

[52] E. Pedrajas, I. Sorribes, A. L. Gushchin, Y. A. Laricheva, K. Junge, M. Beller, R. Llusar, *ChemCatChem* **2017**, *9*, 1128-1134.

[53] V. Cordus, *Le Guidon Des Apotiquaires. C'est à Dire, La Vraye Forme et Maniere de Composer Les Médicamens.*, **1575**.

[54] Jöns Jakob Berzelius, *Jahres-Bericht* **1835**, *14*, 237.

[55] W. Ostwald, *Z. Phys. Chem.* **1894**, *15*, 706.

[56] I. Chorkendorff, J. W. Niemantsverdriet, *Concepts of Modern Catalysis and*

Kinetics, Wiley, **2003**.

[57] P. T. Anastas, J. C. Warner, *Green Chemistry: Theory and Practice*. Oxford University Press, **1998**.

[58] B. Qiao, A. Wang, X. Yang, L. F. Allard, Z. Jiang, Y. Cui, J. Liu, J. Li, T. Zhang, *Nat. Chem.* **2011**, *3*, 634-641.

[59] X. Cui, W. Li, P. Ryabchuk, K. Junge, M. Beller, *Nat. Catal.* **2018**, *1*, 385-397.

[60] S. Mitchell, J. Pérez-Ramírez, *Nat. Commun.* **2020**, *11*, 10-12.

[61] J. B. Pyser, S. Chakrabarty, E. O. Romero, A. R. H. Narayan, *ACS Cent. Sci.* **2021**, *7*, 1105-1116.

[62] P. W. N. M. van Leeuwen, *Homogeneous Catalysis*, Springer Netherlands, Dordrecht, **2004**.

[63] J. A. Osborn, F. H. Jardine, J. F. Young, G. Wilkinson, *J. Chem. Soc. A Inorganic, Phys. Theor.* **1966**, 1711-1732.

[64] "Nobel Prizes in Chemistry," can be found under https://www.nobelprize.org/prizes/lists/all-nobel-prizes-in-chemistry.

[65] A. Behr, P. Neubert, *Applied Homogeneous Catalysis*, Wiley WCH, **2012**.

[66] M. T. Nielsen, R. Padilla, M. Nielsen, *J. Clust. Sci.* **2020**, *31*, 11-61.

[67] R. M. Laine, *J. Mol. Catal.* **1982**, *14*, 137-169.

[68] H. Moissan, C. Moureu, *Comptes Rendus Paris* **1896**, *122*, 1240.

[69] P. Sabatier, J. B. Senderens, *Comptes Rendus Paris* **1897**, *124*, 1358.

[70] "The Nobel Prize in Chemistry 1912," can be found under https://www.nobelprize.org/prizes/chemistry/1912/summary.

[71] T. Ohta, H. Takaya, M. Kitamura, K. Nagai, R. Noyori, *J. Org. Chem.* **1987**,

52, 3174-3176.

[72] S.-T. Bai, G. De Smet, Y. Liao, R. Sun, C. Zhou, M. Beller, B. U. W. Maes, B. F. Sels, *Chem. Soc. Rev.* **2021**, *50*, 4259-4298.

[73] D. Wei, R. Sang, A. Moazezbarabadi, H. Junge, M. Beller, *JACS Au* **2022**, *2*, 1020-1031.

[74] X. F. Wu, M. Beller, *Chemical Transformations of Carbon Dioxide (Topics in Current Chemistry Collections)*, Springer, **2018**.

[75] E. Pedrajas, I. Sorribes, K. Junge, M. Beller, R. Llusar, *Green Chem.* **2017**, *19*, 3764-3768.

[76] E. Guillamón, M. Oliva, J. Andrés, R. Llusar, E. Pedrajas, V. S. Safont, A. G. Algarra, M. G. Basallote, *ACS Catal.* **2021**, *11*, 608-614.

[77] K. Sordakis, C. Tang, L. K. Vogt, H. Junge, P. J. Dyson, M. Beller, G. Laurenczy, *Chem. Rev.* **2018**, *118*, 372-433.

[78] J. O. M. Bockris, *Science* **1972**, *176*, 1323.

[79] European Comission, *A Hydrogen Strategy for a Climate-Neutral Europe*, **2020**.

[80] T. N. Veziroğlu, S. Şahin, *Energy Convers. Manag.* **2008**, *49*, 1820-1831.

[81] P. Preuster, C. Papp, P. Wasserscheid, *Acc. Chem. Res.* **2017**, *50*, 74-85.

[82] M. Taube, D. Rippin, D. Cresswell, W. Knecht, *Int. J. Hydrogen Energy* **1983**, *8*, 213-225.

[83] R. H. Crabtree, *ACS Sustain. Chem. Eng.* **2017**, *5*, 4491-4498.

[84] A. Kumar, P. Daw, D. Milstein, *Chem. Rev.* **2022**, *122*, 385-441.

[85] R. Sang, Z. Wei, Y. Hu, E. Alberico, D. Wei, X. Tian, P. Ryabchuk, A. Spannenberg, R. Razzaq, R. Jackstell, J. Massa, P. Sponholz, H. Jiao, H. Junge, M. Beller, *Nat. Catal.* **2023**, *6*, 543-550.

[86] J. Kothandaraman, S. Kar, A. Goeppert, R. Sen, G. K. S. Prakash, *Top. Catal.* **2018**, *61*, 542-559.

[87] R. S. Coffey, *Chem. Commun.* **1967**, 923b.

[88] C. Fellay, P. J. Dyson, G. Laurenczy, *Angew. Chemie - Int. Ed.* **2008**, *47*, 3966-3968.

[89] B. Loges, A. Boddien, H. Junge, M. Beller, *Angew. Chemie Int. Ed.* **2008**, *47*, 3962-3965.

[90] E. Guillamón, I. Sorribes, V. S. Safont, A. G. Algarra, M. J. Fernández-Trujillo, E. Pedrajas, R. Llusar, M. G. Basallote, *Inorg. Chem.* **2022**, *61*, 16730-16739.

[91] T. Sperger, I. A. Sanhueza, F. Schoenebeck, *Acc. Chem. Res.* **2016**, *49*, 1311-1319.

[92] X. D. Crystallography, *Computational Modeling of Homogeneous Catalysis*, Springer US, Boston, MA, **2002**.

[93] G. J. Cheng, X. Zhang, L. W. Chung, L. Xu, Y. D. Wu, *J. Am. Chem. Soc.* **2015**, *137*, 1706-1725.

[94] L. H. Thomas, *Math. Proc. Cambridge Philos. Soc.* **1927**, *23*, 542-548.

[95] E. Fermi, *Zeitschrift für Phys.* **1928**, *48*, 73-79.

[96] P. Hohenberg, W. Kohn, *Phys. Rev.* **1964**, *136*, B864-B871.

[97] "The Nobel Prize in Chemistry 1998," can be found under https://www.nobelprize.org/prizes/chemistry/1998/summary.

[98] W. Kohn, L. J. Sham, *Phys. Rev.* **1965**, *140*, A1133-A1138.

[99] J. P. Perdew, A. Ruzsinszky, J. Tao, V. N. Staroverov, G. E. Scuseria, G. I. Csonka, *J. Chem. Phys.* **2005**, *123*, 062201.

[100] M. G. Medvedev, I. S. Bushmarinov, J. Sun, J. P. Perdew, K. A. Lyssenko, *Science* **2017**, *355*, 49-52.

[101] K. D. Vogiatzis, M. V. Polynski, J. K. Kirkland, J. Townsend, A. Hashemi, C. Liu, E. A. Pidko, *Chem. Rev.* **2019**, *119*, 2453-2523.

[102] A. Comas-Vives, G. Ujaque, A. Lledós, *Advances in Inorganic Chemistry,* **2010**, 231-260.

[103] L. Alig, M. Fritz, S. Schneider, *Chem. Rev.* **2019**, *119*, 2681-2751.

[104] R. Poli, *Advances in Organometallic Chemistry*, **2023**, 87-133.

[105] R. Kumar, M. K. Pandey, A. Bhandari, J. Choudhury, *ACS Catal.* **2023**, *13*, 4824-4834.

[106] G. R. Morello, H. Zhong, P. J. Chirik, K. H. Hopmann, *Chem. Sci.* **2018**, *9*, 4977-4982.

[107] C. J. Casewit, M. R. DuBois, *J. Am. Chem. Soc.* **1986**, *108*, 5482-5489.

Chapter 2

Objectives

"Humanity also needs dreamers, for whom the disinterested development of an enterprise is so captivating that it becomes impossible for them to devote their care to their own material profit."

Marie Curie

The pivotal role of catalysis in the roadmap of circular economy and sustainable manufacturing has been underscored in Chapter 1. In consequence, developing more efficient and selective catalysts will contribute to fulfill the targets stated in the Sustainable Development Goals (SDGs). Motivated by the current trend to replace noble metal systems with less expensive and environmentally friendly catalysts, the present doctoral thesis is directed towards the design of molecular systems based on Mo_3S_4 homogeneous catalysts for hydrogenation and dehydrogenation of organic substrates combining experimental and theoretical methodologies. Thus, this dissertation integrates concepts from Inorganic, Physical and Sustainable Chemistry to tackle SDGs 7, 12, and 13. This general goal can be divided into the following specific objectives:

i. Synthesis of new Mo_3S_4 clusters containing imidazolyl amino ligands and characterization of the new complexes.
ii. Evaluation of the catalytic activity of the novel cluster complexes in the selective semihydrogenation of alkynes to (*Z*)-alkenes.
iii. Assessment of the catalytic properties of a series of Mo_3S_4 cluster complexes in the dehydrogenation of formic acid for efficient hydrogen storage.
iv. Elucidation of the mechanistic pathways that govern the above studied catalytic transformations through the synergy of computational and experimental methods.

Chapter 3

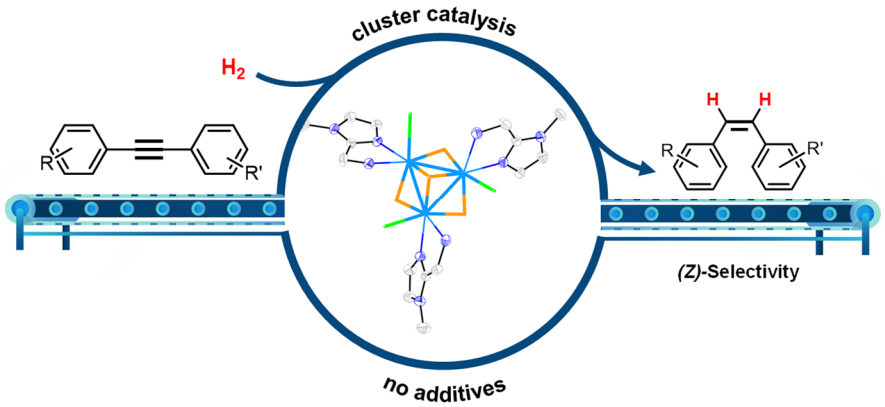

Efficient (*Z*)-selective semihydrogenation of alkynes catalyzed by air-stable imidazolyl amino molybdenum cluster sulfides

The results presented in this section have already been published. Reproduced from *Inorg. Chem. Front.,* **2023**, *10*, 1786-1794 with permission from the Royal Society of Chemistry.

3.1. Main text

3.1.1. Abstract

Imidazolyl amino cuboidal $Mo_3(\mu_3\text{-}S)(\mu\text{-}S)_3$ clusters have been investigated as catalysts for the semihydrogenation of alkynes. For that purpose, three new air-stable cluster salts $[Mo_3S_4Cl_3(ImNH_2)_3]BF_4$ ([**1**]BF_4), $[Mo_3S_4Cl_3(ImNH(CH_3))_3]BF_4$ ([**2**]BF_4) and $[Mo_3S_4Cl_3(ImN(CH_3)_2)_3]BF_4$ ([**3**]BF_4) have been isolated in moderate to high yields and fully characterized. Crystal structures of complexes [**1**]PF_6 and [**2**]Cl confirm the formation of a single isomer in which the nitrogen atoms of the three imidazolyl groups of the ligands are located *trans* to the capping sulfur atom, which leaves the three bridging sulfur centers on one side of the trimetallic plane while the amino groups lie on the opposite side. Kinetic studies show that the cluster bridging sulfurs react with diphenylacetylene (dpa) in a reversible equilibrium to form the corresponding dithiolene adduct. Formation of this adduct is postulated as the first step in the catalytic semihydrogenation of alkynes mediated by molybdenum sulfides clusters. These complexes catalyze the (*Z*)-selective semihydrogenation of dpa under hydrogen in the absence of any additives. The catalytic activity lowers sequentially upon replacement of the hydrogen atoms of the $N\text{-}H_2$ moiety in $\mathbf{1}^+$ without reaching inhibition. Mechanistic experiments support a sulfur-centered mechanism without participation of the amino groups. Different dpa derivatives are selectively hydrogenated using complex $\mathbf{1}^+$ to their corresponding (*Z*)-alkenes in excellent yields. Extension of this protocol to 3,7,11,15-tetramethylhexadec-1-yn-3-ol, an essential intermediate for the production of vitamin E, affords the semihydrogenation product in very good yield.

3.1.2. Introduction

The stereoselective reduction of internal alkynes to disubstituted alkenes by using hydrogen is a highly valuable reaction in the bulk and fine chemical industries.[1] In particular, (*Z*)-alkenes are found in several bioactive compounds, pharmaceuticals and agrochemicals.[2] The selective synthesis of these products has been traditionally

achieved by heterogeneous catalysis where the Pd-based Lindlar's catalyst is still the most common choice.[3] However, for several substrates, drawbacks such as isomerization and overreduction are still unsolved. Although heterogeneous catalysis is frequently preferred by industry, homogeneous catalysis offers some advantages such as a more rational tuning of the catalysts as well as its potential to be used as models capable to emulate the reactivity of its solid analogs. In this regard, homogeneous systems can also provide valuable mechanistic information.

Most of the reported homogeneous catalysts for the (*Z*)-stereoselective hydrogenation of alkynes to alkenes make use of alternative hydrogen donors such as boranes, silanes, alcohols, formic acid or water, while the number of systems which operate using molecular hydrogen as the reductant are surprisingly scarce.[4] Due to economic and environmental reasons, there is a growing interest to replace noble metals by non-precious ones and to optimize the atom economy using hydrogen as reductant. Most examples include mononuclear 3d transition metal complexes based on Mn,[5,6] Fe,[7] Co[8,9] (Figure 3.1) or cubane-type polynuclear Cu[10] compounds functionalized with phosphine ligands. As a very recent example, Milstein and co-workers have evidenced the great potential of Mg pincer complexes as catalysts for the transformation of dpa derivatives to the corresponding (*Z*)-alkenes with good to very good diastereoselectivities.[11]

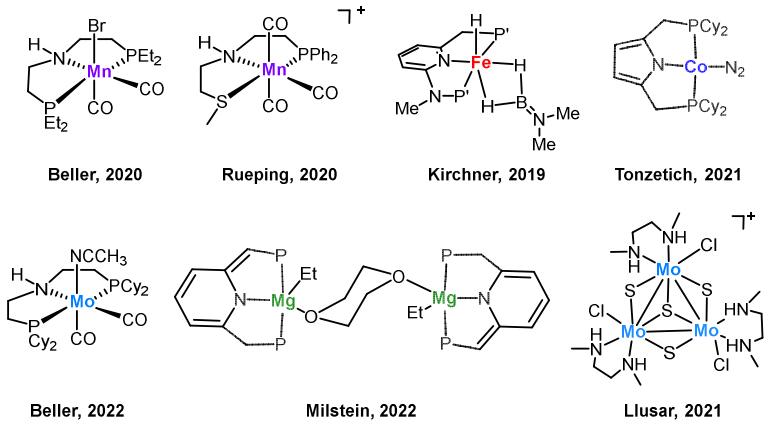

Figure 3.1. Selected examples of homogeneous non-noble metal pre-catalysts for an efficient (*Z*)-selective semihydrogenation of internal alkynes.

Previously, our groups have also shown that low-valent Mo pincer complexes and cuboidal Mo_3S_4 clusters are also efficient homogeneous catalysts for this transformation.[12,13] Notably, pincer complexes utilizing sophisticated phosphine ligands dominate this chemistry and more importantly, mechanistic investigations on these systems have revealed unique reaction pathways. Such studies combining control experiments with DFT calculations showed that hydrogenation by PN(H)P and PN(H)S Mn and Mo pincer complexes proceeds *via* an outer-sphere reaction mechanism utilizing the amino moiety in the ligand backbone for metal-ligand cooperativity (MLC).[5,6,12]

In these cases, a strong base seems to be needed to form the catalytically active species, likely an amido complex, generated by deprotonation of the amine of the ligand backbone. This amido complex presumably activates the hydrogen molecule with the corresponding formation of an $R_2(H)N$-M-H hydrido moiety where the two hydrogen atoms are transferred to the alkyne to produce the (*Z*)-alkene without any direct interaction between the substrate and the metal. On the other hand, pincer PNP complexes of Fe, Co and Mg operate under base-free conditions and H_2 activation generates catalytically active M-H hydrides, which react with the alkyne to form η^2-olefin species.[7,9] In the case of Mg, a metal-ligand cooperation mechanism involving the aromatization/dearomatization of the pincer compound is proposed.[11]

Interestingly, trinuclear Mo_3S_4 clusters containing inexpensive diamino ligands also catalyze the semihydrogenation of diphenylacetylene with an acceptable (*Z*)-stereoselectivity (*Z*/*E* *ca.* 6/1) in the absence of a base, albeit harsh conditions were required (12% mol catalyst, 100 bars of H_2 and 150 °C) to achieve moderate conversion (*ca.* 60%). This complex operates through an unusual cluster catalysis mechanism, depicted in Figure 3.2, where only the three bridging sulfur atoms of the cluster act as the active sites for this transformation.[13]

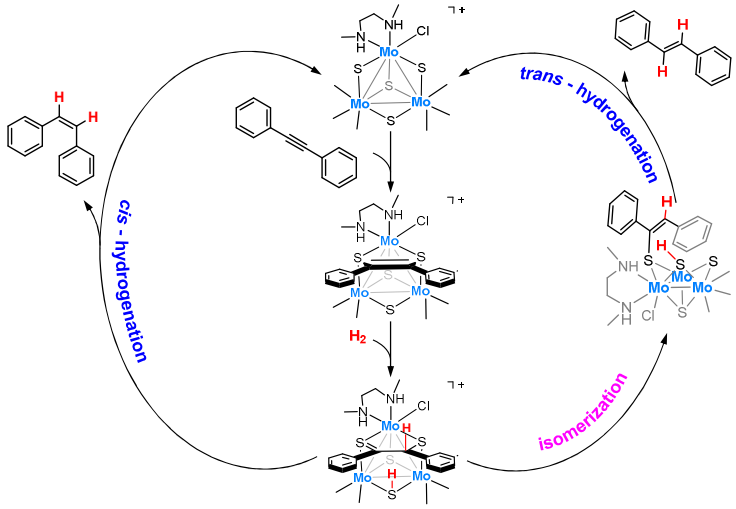

Figure 3.2. Simplified catalytic cycle for the semihydrogenation of dpa in the presence of Mo_3S_4 clusters.

In the first step, the alkyne molecule reacts with two of the bridging sulfides to form a dithiolene adduct. Next, hydrogen activation takes place through the third bridging sulfur atom and one of the dithiolene carbon atoms. Finally, the half-hydrogenated intermediate undergoes a reductive elimination step to produce the desired (*Z*)-alkene or to evolve into an isomerized analogue which after elimination affords the (*E*)-alkene. The relative energy barrier of these two processes (theoretical $\Delta\Delta G^{\ddagger}$ = 1.9 kcal mol^{-1}), *cis*-hydrogenation *vs.* *trans*-isomerization, determines the stereoselectivity of the reaction.

The low cost and low toxicity of molybdenum also makes this metal an attractive substitute to noble metals as hydrogenation catalysts, although this alternative has received little attention in comparison to first-row transition metals.[14,15] Motivated by our earlier results on alkyne semihydrogenation using Mo_3S_4 cluster catalysts, we decided to explore the effect of the outer bidentate ligands. Earlier studies in our group have shown that diphosphino and aminophosphino molybdenum complexes are not efficient catalysts for the direct hydrogenation of organic substrates such as nitroarenes.[16] In this work, we turned our attention to bidentate nitrogen donor ligands containing imidazolyl moieties

inspired by the excellent activity in hydrogenation processes that certain noble and non-noble metal complexes, *i.e.,* Ru[17,18] and Mn[19] exhibit when decorated with such imidazolyl-based ligands.

Herein, we report a novel protocol for the selective (*Z*)-semihydrogenation of a series of alkynes using a Mo_3S_4 cluster catalyst decorated with imidazolyl amino ligands. Three new cluster complexes, which differ in the nature of the amino group: $-NH_2$, $-NH(CH_3)$ and $-N(CH_3)_2$ have been prepared to investigate the influence of the Mo-amino functionality. Mechanistic experiments aimed to understand the reaction mechanism are also presented. The new $[Mo_3S_4Cl_3(ImNH_2)_3]^+$ (**1**$^+$) complex has been applied to the catalytic semihydrogenation of several dpa derivatives affording the (*Z*)-alkenes with excellent yields. Complex **1**$^+$ also catalyzes the semihydrogenation of an industrially relevant terminal alkyne substrate.

3.1.3. Results and discussion

Three new trinuclear cluster salts of formula $[Mo_3S_4Cl_3(ImNH_2)_3]BF_4$ ([**1**]BF_4), $[Mo_3S_4Cl_3(ImNH(CH_3))_3]BF_4$ ([**2**]BF_4) and $[Mo_3S_4Cl_3(ImN(CH_3)_2)_3]BF_4$ ([**3**]BF_4) have been prepared by extending the procedure developed in our group and represented in Scheme 3.1.[20] In this method the outer ligands of the $Mo_3S_4Cl_4(PPh_3)_3(H_2O)_2$ precursor are partially replaced by imidazolyl amino ligands. Acidification of the reaction media avoids formation of hydroxo species which result from the partial replacement of the outer chlorine ligands. As found for the aminophosphine M_3S_4 (Mo or W) derivatives, only one among all possible isomers is formed in moderate to high yields, 67% for [**1**]BF_4, 64% for [**2**]BF_4 and 94% for [**3**]BF_4.[21] All clusters' salts were fully characterized by NMR, elemental analysis, and mass spectrometry.

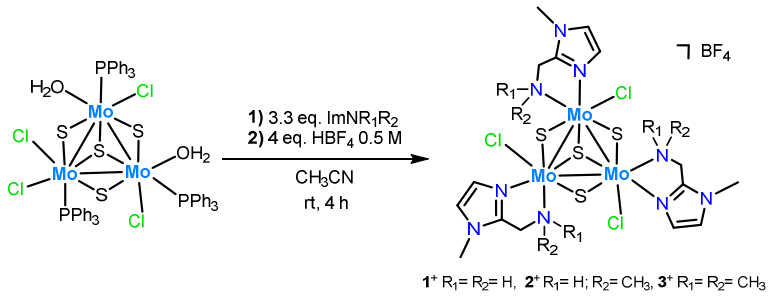

Scheme 3.1. Synthesis of Mo_3S_4 cluster complexes decorated with imidazolyl amino ligands.

The crystal structures of [**1**]PF_6 and [**2**]Cl have been determined by single crystal X-ray diffraction and they share structural features. Figures 3.3 and 3.4 show ORTEP representations of the $\mathbf{1}^+$ and $\mathbf{2}^+$ cations together with relevant bond distances. Both cations contain an incomplete Mo_3S_4 cubane-type structure in which the molybdenum and sulfur atoms occupy adjacent vertices with a missing metal atom. In general, the metal-metal and metal-sulfur bond distances follow the same tendencies observed for other trinuclear Mo_3S_4 species.[20,22] The three outer positions on each metal center are occupied by one chlorine atom and two nitrogen atoms from the imidazolyl amino ligand.

As previously mentioned, only one isomer is formed, wherein all three nitrogen atoms from the imidazolyl group are located *trans* to the capping sulfur while the ones from the amino group are placed *trans* to the bridging sulfur. Therefore, the capping sulfur, the chlorine atoms, and the amino groups of the ligand lie on the same side of the trimetallic plane.

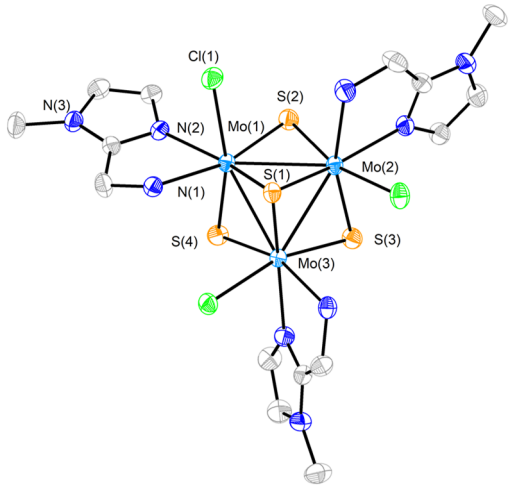

Figure 3.3. ORTEP representation (50% probability ellipsoids) of the cationic cluster $[Mo_3S_4Cl_3(ImNH_2)_3]^+$ (**1**$^+$). Hydrogen atoms have been omitted for clarity. Standard deviations of average distances are given in brackets. Average bond distances: Mo-Mo = 2.737 [7], Mo-(μ_3-S) = 2.328 [2], Mo-(μ-S)$_{\textit{trans}\text{-Cl}}$ = 2.284 [9], Mo-(μ-S)$_{\textit{trans}\text{-NH}_2}$ =2.289 [9] Å. CCDC reference number 2210047.

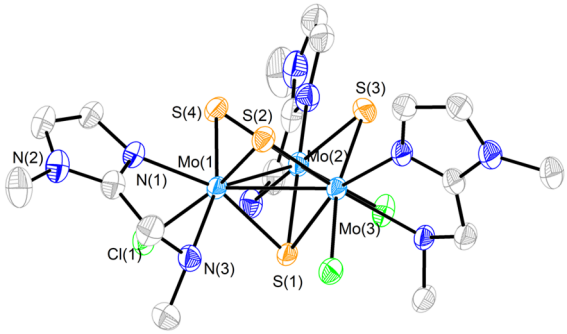

Figure 3.4. ORTEP representation (50% probability ellipsoids) of the cationic cluster $[Mo_3S_4Cl_3(ImNHCH_3)_3]^+$ (**2**$^+$). Standard deviations of average distances are given in brackets. Hydrogen atoms have been omitted for clarity. Average bond distances: Mo-Mo = 2.759 [3], Mo-(μ_3-S) = 2.338 [4], Mo-(μ-S)$_{\textit{trans}\text{-Cl}}$ = 2.288 [6], Mo-(μ-S)$_{\textit{trans}\text{-NHMe}}$ = 2.289 [6] Å. CCDC reference number 2210042.

The short Cl···H(-N) distances in **1**$^+$ (2.458 to 2.802 Å) and **2**$^+$ (2.359 to 2.951 Å) between the chlorine atom and the hydrogen atom of the amino groups of the adjacent metal center evidence the presence of hydrogen bonding interactions. Moreover, in the case of complex **1**$^+$ the above-mentioned values are comparable to

the Cl···H(-N) distances of the chlorine atom and the amino group on the same metal center, with values ranging from 2.747 to 2.938 Å.

The solid-state structures of both cations, **1**$^{+}$ and **2**$^{+}$, are preserved in solution as evidenced by $^{13}C\{^{1}H\}$ NMR and ^{1}H NMR spectroscopy. All attempts to obtain single crystals of **3**$^{+}$ were unfruitful but the product was fully characterized by spectrometric and spectroscopic techniques. The C_3 symmetry of the three complexes has been confirmed in solution (Figures SI3.1-SI3.6). The $^{13}C\{^{1}H\}$ NMR spectra show five characteristic singlets, common for all three compounds, four signals of the imidazole ring and one to the methylene linker group. Nevertheless, the ^{1}H NMR spectrum of **3**$^{+}$ reveals a slightly different solution behavior compared to that of the other two clusters. In clusters **1**$^{+}$ and **2**$^{+}$, the signals for the methylene hydrogen atoms are clearly diastereotopic with resolved multiplets showing both the geminal coupling and the coupling to the amino hydrogen/s in agreement with their crystal structures. In contrast, this multiplet signal appears as a singlet in compound **3**$^{+}$, which suggests the existence of a weak $MoNMe_2$ bond that allows the rapid dissociation-coordination and results in a time-averaged signal for the two methylene protons.

3.1.3.1. Reactivity *versus* alkynes and reaction kinetics

As mentioned in the introduction, the formation of dithiolene adducts upon interaction of alkynes with the bridging sulfur atoms of the cuboidal Mo_3S_4 unit is the first step of the mechanism for the semihydrogenation of alkynes catalyzed by these cluster complexes.[13] It is well established that the [3+2] cycloaddition reaction between the alkynes and these clusters, depends on the alkyne substituents as well as on the nature of the cluster ligands.[23,24] Formation of very stable Mo_3S_4 dithiolene adducts is detrimental for the catalytic semihydrogenation of alkynes. For example, the $[Mo_3S_4Cl_3(dmen)_3]^{+}$ (dmen = N,N'-dimethylethylenediamine) cluster reacts with dimethyl acetylenedicarboxylate (dmad) to form a stable adduct and as a consequence, it is not an active catalyst for alkyne semihydrogenation. On the other

hand, the $[Mo_3S_4Cl_3(dmen)_3]^+$ cluster does not react appreciably with dpa, and thus it catalyzes its semihydrogenation although under harsh conditions. In our case, cluster complexes [**1**]BF_4, [**2**]BF_4 and [**3**]BF_4 react with dpa to form the corresponding dithiolene adduct as evidenced by the appearance of a band in the UV-VIS spectra around 900 nm, characteristic of the formation of the [3+2] cycloaddition product (Figure SI3.7).[25] Adduct formation is also evidenced by ^{1}H NMR spectroscopy where new signals appear due to the loss of symmetry upon adduct formation (Figure SI3.8).[21] However, these new signals coexist with those of $\mathbf{1}^+$, $\mathbf{2}^+$ and $\mathbf{3}^+$ which indicate that formation of the addition dithiolene products occurs under conditions of reversible equilibrium. This assumption is further confirmed by the electrospray ionization mass spectrometry (ESI-MS) of the reaction mixture (Figure SI3.9). The ESI-MS spectrum of $\mathbf{1}^+$ in CH_3CN shows a prominent peak centered at m/z = 856 associated to the $\mathbf{1}^+$ cation according to its m/z value and calculated isotopic pattern. Upon reaction with an excess of dpa (20 eq., room temperature, CH_3CN), the peak at m/z = 856 remains and a new peak of similar intensity emerges at m/z = 1034 identified as the [**1** + dpa]$^+$ cycloaddition product. Incidentally, no evidence exists regarding the addition of a second dithiolene molecule. A similar situation is observed when monitoring the reaction between [**2**]BF_4 and [**3**]BF_4 with dpa in CH_3CN. That is, the cluster cations coexist with the cycloaddition dithiolene adduct even in the presence of a 20-molar excess of dpa.

To obtain additional information on the process, the kinetics of reaction of [**1**]BF_4, [**2**]BF_4 and [**3**]BF_4 with dpa were studied in acetonitrile solution at 25 °C. The reaction was found to occur in a suitable timescale for monitoring the process with a conventional UV-VIS spectrophotometer. The spectral changes observed under pseudo-first order conditions of dpa excess (Figure SI3.7) clearly show the formation of the cycloaddition product with the previously commented band at 900 nm. These changes can be satisfactorily fitted using a kinetic model with a single kinetic step, and the values derived for the observed rate constant (k_{obs}) show a linear dependence

with the alkyne concentration that was fitted using equation 3.1 (Figure 3.5). The values so derived for the slope and the intercept are listed in Table 3.1.

$$k_{obs} = k_0 + k_1 [dpa] \quad (3.1)$$

In agreement with the NMR and ESI-MS results, the existence of a non-zero intercept in Figure 3.5 suggests the possibility that the reaction occurs under conditions of reversible equilibrium, which is confirmed by an increase of the spectral change magnitude with the dpa concentration, so that k_1 corresponds to the formation of the cycloaddition product and k_0 to the reverse process. While the rate of formation (k_1) decreases gradually with the number of the amino methyl groups of the ligand, the rate of the reverse reaction (k_0) shows smaller changes. Therefore, the equilibrium constant decreases upon methylation of the amino groups of the ligand. These results differ from those previously reported for the related diamino cluster, for which we were unable to observe formation of significant amounts of the cycloaddition product.[13]

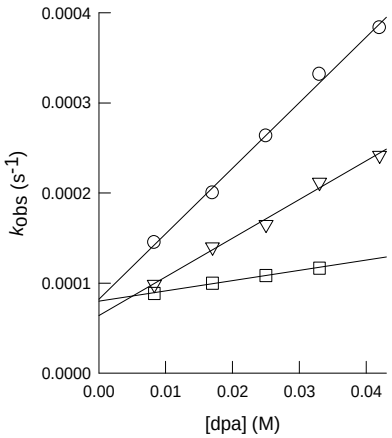

Figure 3.5. Plot of the dependence with the dpa concentration of the observed rate constants for the reaction of clusters [**1**]BF_4 (circles), [**2**]BF_4 (triangles), and [**3**]BF_4 (squares), with an excess of dpa in CH_3CN solution at 25 °C.

Table 3.1. Kinetic data for the reaction of [**1**]BF_4, [**2**]BF_4 and [**3**]BF_4 with an excess of dpa.

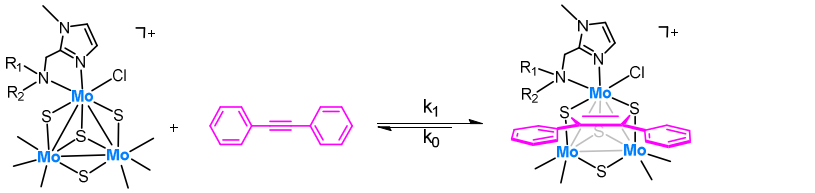

1$^+$ R_1= R_2= H, **2**$^+$ R_1= H; R_2= CH_3, **3**$^+$ R_1= R_2= CH_3

Entry	Cluster	k_1 ($M^{-1}\cdot s^{-1}$)	k_0 (s^{-1})	K_e (M^{-1})
1	1^+	$7.3(3)\times10^{-3}$	$8.2(7)\times10^{-5}$	89(8)
2	2^+	$4.3(2)\times10^{-3}$	$6.4(6)\times10^{-5}$	67(7)
3	3^+	$1.14(4)\times10^{-3}$	$8.0(1)\times10^{-5}$	14.0(5)

Reaction conditions: 25 °C in CH_3CN, pseudo-first order excess of dpa (0.008-0.042 M).

3.1.3.2. Catalytic performance and mechanistic insights

Evaluation of the catalytic activity of [**1**]BF_4, [**2**]BF_4 and [**3**]BF_4 was performed on the semihydrogenation of dpa as model reaction. Reaction conditions for the [**1**]BF_4 cluster salt catalyst was optimized by varying the temperature and H_2 pressure (Table SI3.1). Full conversion and quantitative yield towards the formation of the (*Z*)-isomer was achieved under much milder conditions (70 °C and 20 bar) compared to previously known related molybdenum catalysts. For example, a conversion of 21% (18% of the (*Z*)-isomer and 3% of the (*E*)-isomer) was obtained using the diamino $[Mo_3S_4Cl_3(dmen)_3]^+$ cluster catalyst (18 h at 150 °C, 100 bar H_2 pressure and 5 mol% of the catalyst) in acetonitrile.[13] Further attempts to lower the pressure and/or temperature led to a dramatic decrease of the catalytic activity. Incidentally, our optimized conditions are the typical conditions employed for the hydrogenation of nitroarenes mediated by the diamino $[Mo_3S_4Cl_3(dmen)_3]^+$ catalyst.[16] Then, the solvent influence was investigated. Similar activities are found for CH_3CN and CH_3OH (Table SI3.2), while THF reduced the dpa conversion to 90%. No reaction

is observed in 2-fluoroethanol or hexafluoroisopropanol. Hence at this point, we decided to continue the study in CH_3CN.

Cluster evolution during the catalytic semihydrogenation of dpa using [**1**]BF_4 was monitored from batch experiments at different reaction times (Figure SI3.10). The molecular peak due to $\mathbf{1}^+$ (m/z = 856) coexists with the [**1** + dpa]$^+$ (m/z = 1034) cycloaddition product. As expected, the intensity of the [**1** + dpa]$^+$ peak decreases with time. At the end of our catalytic protocol, the only peak registered, that of $\mathbf{1}^+$, remains intact; therefore, catalysis occurs without degradation of $\mathbf{1}^+$ which is indicative of a cluster catalysis process.

Table 3.2. Evaluation of conditions for diphenylacetylene hydrogenation.[a]

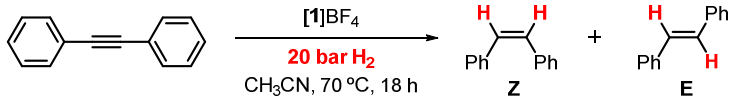

Entry	Deviation	Conversion[b] (%)	Yield[b] (%)	
			Z	*E*
1	None	>99	>99	-
2	[**2**]BF_4	40	40	-
3	[**3**]BF_4	7	7	-
4	[**3**]BF_4[c]	23	23	-
5	$[Mo_3S_4Cl_3(dmen)_3]BF_4$[d]	13	10	3
6	$[Mo_3S_4Cl_3(ImND_2)_3]BF_4$[e]	>99	>99	-
7	addition of CuCl	0	-	-
8	addition of Et_3N (1 eq.)	30	29	-
9	addition of Et_3N (2 eq.)	7	7	-
10	addition of Et_3N (3 eq.)	7	7	-

[a] Standard conditions: Diphenylacetylene (0.1 mmol), H_2 pressure (20 bar), 70 °C, catalyst (5 mol%), CH_3CN, 18 h. [b] Determined by GC analysis using n-hexadecane as an internal standard. [c] Catalyst (12 mol%). [d] Catalyst (12 mol%), H_2 pressure (50 bar), 150 °C. [e] Stoichiometric reaction, 0.01 mmol diphenylacetylene, 0.01 mmol cluster [**1-*d*$_6$**]BF_4, CD_3CN.

Next, we investigated the influence of the structure of the ligand on the catalytic activity for the semihydrogenation of diphenylacetylene at 70 °C and 20 bars of H_2 (Table 3.2, entries 2-4). Substitution of one hydrogen of the N-H moiety in **1**$^+$, leads to a significant decrease in the catalytic activity (Table 3.2, entry 2). The total alkylation of the N-H moiety (Table 3.2, entries 3-4) with methyl substituents does not inhibit the catalytic conversion but drastically lowers the yield. The activity of **3**$^+$ is comparable with that of the diamino $[Mo_3S_4Cl_3(dmen)_3]BF_4$ catalysts (Table 3.2, entry 5).[13]

An extra evidence of the passive role of the N-H moiety is that no deuterated (*Z*)-stilbene (Figure SI3.11) was formed by using the **1-*d*$_6$**$^+$ cluster catalyst (Figure SI3.12) deuterated at the amino positions (Table 3.2, entry 6). These experiments rule out the involvement of the N-H moiety of the ligand backbone in the reaction. In contrast, there are strong evidences on metal-ligand cooperativity when low-valent molybdenum PN(H)P pincer complexes are employed as catalysts for this transformation which give support in this last case to an outer-sphere reaction mechanism.[12]

Then, mechanistic evidence for a sulfur-based reaction mechanism were investigated. For that purpose, CuCl was added to the catalytic reaction mixture in order to block the three bridging sulfur atoms of the cluster. According to ESI-MS formation of the heterometallic $[Mo_3(CuCl)S_4Cl_3(ImNH_2)_3]^+$ (m/z = 956) and $[Mo_3(Cu(dpa))S_4Cl_3(ImNH_2)_3]^+$ (m/z = 1099) cluster cations took place on the basis of their m/z ratios and isotopic pattern (Figure SI3.13). Under these conditions, the catalytic process is inhibited (Table 3.2, entry 7) as previously observed for the semihydrogenation of alkynes and hydrogenation of diazobenzene mediated by the diamino $[Mo_3S_4Cl_3(dmen)_3]^+$ catalysts, which was also attributed to the formation of Mo_3S_4Cu species.[13,26]

In the case of the catalytic diazobenzene hydrogenation, hydrogen activation occurs at the bridging sulfur atoms and results in the formation of a dithiol

$[Mo_3S_2(SH)_2Cl_3(dmen)_3]^+$ adduct from which hydrogen is transferred to form first diphenylhydrazyne and next aniline through two interconnected cycles sharing a common reaction step which involves the above Mo_3S_4 dithiol adduct.[33] Due to the acidic character of this proton S-H groups, addition of a base such as Et_3N inhibits the hydrogenation process by providing an additional reaction pathway which capture these dithiol H atoms. In our case, the same tendency has been observed and addition of Et_3N amine inhibits catalysis (Table 3.2, entries 8-10) suggesting a mechanism for hydrogen activation in which acidic protons are being generated. The above control experiments indicate a sulfur-centered cluster catalysis mechanism without metal-ligand cooperativity. However, details on H_2 activation by the bridging sulfur atoms of the cluster and their subsequent transfer to the alkyne molecule to selectively afford the (*Z*)-alkene remain unclear.

3.1.3.3. Substrate scope

Having in hand the optimal conditions for dpa semihydrogenation mediated by [**1**]BF_4, dpa derivatives featuring different substituents were tested to analyze the tolerance of the system (Table 3.3). Compounds containing a methyl group in the *para* (**2c**) and *meta* (**2b**) positions were successfully reduced with excellent selectivity. However, in the case of the *ortho* derivative (**2b**) there was a drop of the conversion likely due to steric hindrance.[12,27] Alkynes bearing halides as fluorine (**2e**), chlorine (**2f**), bromine (**2g**) or trifluoromethyl (**2h**) groups are smoothly transformed to the respective (*Z*)-alkenes. Remarkably, no dehalogenation products have been detected for any of the halogenated dpa derivatives. Also, substrates containing both trifluoromethyl and methoxy groups (**2i**) afforded good yields and stereoselectivity. Additionally, thioethers (**2j**) or ester groups (**2k**) on the alkynes are well tolerated.

Table 3.3. (*Z*)-selective semihydrogenation of alkynes catalyzed by [**1**]BF_4.[a]

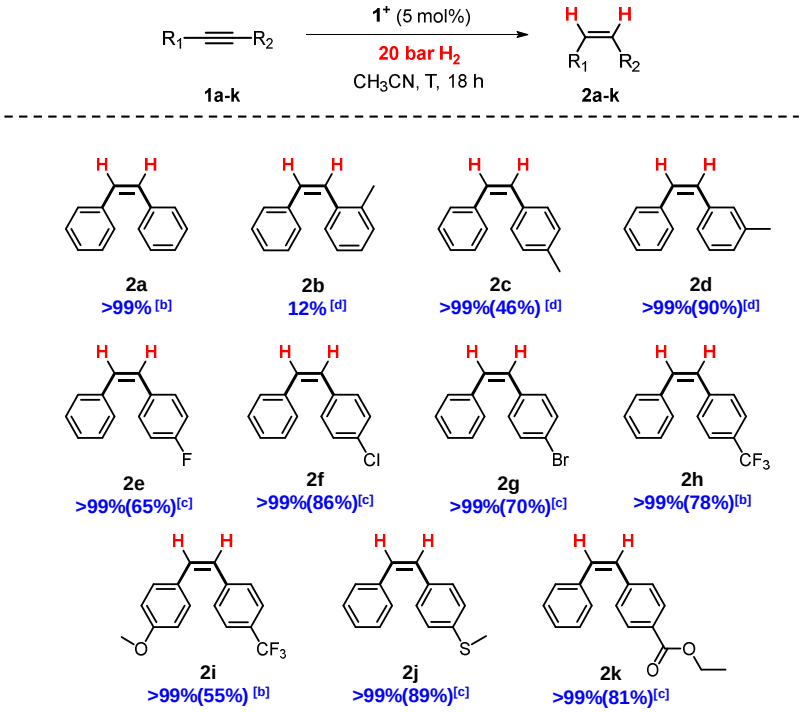

[a] Reaction conditions: 0.1 mmol alkyne, 5 mol% catalyst, 20 bar H_2, CH_3CN (2 mL), 18 h. Yield determined by GC analysis using n-hexadecane as an internal standard (average of two runs). Isolated yields are given in brackets. [b] T = 60 °C. [c] T = 70 °C. [d] T = 80 °C.

Taking into consideration that [**1**]BF_4 is an efficient catalyst for the semihydrogenation of internal alkynes, we decided to extend our study to terminal alkynes. The industrially relevant substrate chosen was 3,7,11,15-tetramethylhexadec-1-yn-3-ol, represented in Figure 3.6, which is an essential intermediate for the production of vitamin E.[28] Application of the optimized catalytic protocol developed for dpa semihydrogenation results in no conversion of the terminal alkyne substrate.

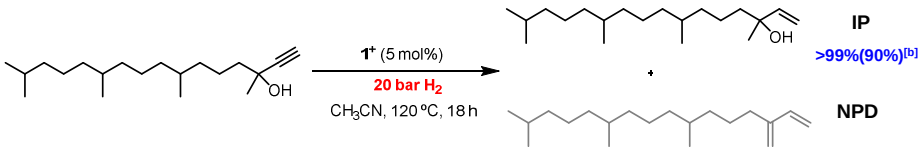

Figure 3.6. Semihydrogenation of DIP. Reaction conditions: 0.1 mmol alkyne, 5 mol% catalyst, 20 bar H_2, 120 °C, CH_3CN (2 mL), 18 h. Conversions and yields determined by GC analysis using n-hexadecane as an internal standard.

Temperature and pressure were then optimized (Table SI3.3) and quantitative conversions were achieved at 120 °C and 20 bar H_2. In terms of chemoselectivity, the major product is the desired isophytol (IP). Notably, no over hydrogenation product was observed during the reaction and the only detected side product corresponds to the dehydration species, neophytadiene (NPD). Then, the influence of the reaction time was investigated to hamper this side-reaction (see Figure SI3.32). While the reaction time can be reduced from 18 h to 8 h maintaining conversion and yield, this has no effect on the final NPD concentration. Unfortunately, all attempts to avoid this side reaction were unfruitful. To the best of our knowledge, it is the first time that a homogeneous molybdenum cluster performs this reaction. Further experiments are under investigation to achieve softer conditions.

3.1.4. Conclusions

In summary, we have synthesized and characterized three new Mo_3S_4 complexes featuring imidazolyl amino ligands with different degrees of methylation in the amino moiety. The bridging sulfur atoms of these $Mo_3(\mu_3\text{-}S)(\mu\text{-}S)_3$ clusters interact with the alkyne, *e.g.,* dpa to form a dithiolene $Mo_3(\mu_3\text{-}S)(\mu\text{-}S)(\mu_3\text{-}SC(Ph)=C(Ph)S)$ adduct under conditions of reversible equilibrium. The $[Mo_3S_4Cl_3(ImNH_2)]BF_4$ cluster salt is an efficient catalyst for the (*Z*)-selective semihydrogenation of dpa under much milder reaction conditions than those previously optimized for related diamino Mo_3S_4 cluster analogues. Mechanistic control experiments support a sulfur-based mechanism and rule out the operation of an outer-sphere reaction mechanism

with participation of the ligand NH group. Extension of our catalytic protocol to other internal alkynes revealed an excellent (*Z*)-selectivity. In addition, the catalytic protocol can also be adapted for the semihydrogenation of alkynols; in particular, to an essential vitamin E precursor. To the best of our knowledge, it is the first time that a homogeneous molybdenum cluster performs this type of reaction.

3.1.5. Experimental section

3.1.5.1. General remarks

Elemental analyses were carried out on a EuroEA3000 Eurovector Analyser. Electrospray mass spectra were recorded with a QuattroLC (quadrupole-hexapole-quadrupole) mass spectrometer with an orthogonal Z-spray electrospray interface (Micromass, Manchester, UK). The cone voltage was set at 20 V unless otherwise stated using CH_3CN as the mobile phase solvent. Sample solutions were infused using a syringe pump directly connected to the ESI source at a flow rate of 10 $mL \cdot min^{-1}$ and a capillary voltage of 3.5 kV was used in the positive scan mode. Nitrogen was employed as drying and nebulizing gas. Isotope experimental patterns were compared with theoretical patterns obtained using the MassLynx 4.1 program.[29] ^{1}H, $^{13}C\{^{1}H\}$ NMR and ^{1}H-^{13}C gradient HSQC spectra were recorded on a Bruker Avance III HD 400 MHz or 300 MHz spectrometers using CD_3CN as solvent. Gas chromatography analyses were performed on an Agilent 7820A GC System equipped with a FID and a capillary column Agilent (HP-5, 30 m x 0.32 mm x 0.25 mm). Mass determination was carried out on a GC-Mass Agilent 5977E network equipped with a mass-selective detector. Kinetic experiments on the cycloaddition of diphenylacetylene to the clusters were carried out using a Cary 50 spectrophotometer provided with a thermostatted multicell holder. All experiments were conducted at 25.0 °C under pseudo-first order conditions of alkyne excess, and the spectral changes were fitted satisfactorily in all cases to a model with a single kinetic step.

3.1.5.2. Catalyst preparation

All reactions were performed under a nitrogen atmosphere using standard Schlenck techniques. The trinuclear precursor $Mo_3S_4Cl_4(PPh_3)_3(H_2O)_2$ was prepared according to the literature procedure.[30]

Synthesis of $[Mo_3S_4Cl_3(ImNH_2)_3]BF_4$ ([1]BF_4): To a green solution of the trinuclear precursor $Mo_3S_4Cl_4(PPh_3)_3(H_2O)_2$ (250 mg, 0.181 mmol) in dry CH_3CN (25 mL) was added a three-fold excess of the ligand (1-methyl-1H-imidazol-2-yl)methanamine (71 mg, 0.609 mmol) under inert atmosphere. The reaction occurred with an immediate colour change from green to brown which gradually turns into a green suspension in 1-2 hours. After stirring the reaction mixture for 4 hours at room temperature, a freshly prepared solution of HBF_4·ether (1.08 mL, 0.540 mmol) 0.5 M in CH_3CN was added and the suspension turned into a dark green solution. The solution was filtrated, taken to dryness, and redissolved in H_2O. Then, the non-soluble PPh_3 was eliminated by filtration. The resulting solution was taken to dryness and dried overnight at the vacuum pump. Finally, the product was washed with a cold mixture of hexane/toluene (1:1, 50 mL), boiling hexane (50 mL) and diethyl ether to afford the green solid that was characterized as $[Mo_3S_4Cl_3(ImNH_2)_3]BF_4$ (112 mg, 67% yield). Elemental analysis (%) calcd. for $Mo_3S_4Cl_3C_{15}H_{27}N_9BF_4$: C: 19.11, H: 2.89, N: 13.37; found: C: 19.80, H: 3.00, N: 13.50; ^{1}H NMR (CD_3CN, 400 MHz): δ = 3.46 (br, 3H, NH, *H*$_A$), 3.81 (s, 9H, N-CH_3, *H*$_C$), 3.95 (ddd, J = 16.3, 6.0 and 1.6 Hz, 3H, CH, *H*$_B$), 4.00 (br, 3H, NH, *H*$_A$), 4.44 (ddd, J = 16.3, 7.7 and 3.4 Hz, 3H, CH, *H*$_B$), 7.48 (d, J = 1.6 Hz, 3H, CH, *H*$_D$), 8.13 (d, J = 1.6 Hz, 3H, CH, *H*$_E$); ^{13}C{^{1}H} NMR (CD_3CN, 101 MHz): δ = 35.28 (s, CH_2, *C*$_C$), 42.50 (s, CH_3, *C*$_B$), 125.78 (s, CH, *C*$_D$), 132.54 (s, CH, *C*$_E$), 151.54 (s, C, *C*$_F$); ESI-MS (MeOH, cone 20 V) *m*/*z* calcd. for $[Mo_3S_4Cl_3C_{15}H_{27}N_9]^+$: 855.9 $[M]^+$; found: 856.0 $[M]^+$

Deuteration of $[Mo_3S_4Cl_3(ImNH_2)_3]BF_4$ ([1-*d*$_6$]BF_4): A solution of 20 mg of **1**$^+$ in 5 mL CD_3OD was kept at 50 °C overnight under continuous stirring. The solution was allowed to cool down and taken to dryness. ^{1}H NMR evidence the complete deuteration of the amino moiety to afford $[Mo_3S_4Cl_3(ImND_2)_3]BF_4$ ([**1**-*d*$_6$]BF_4). ^{1}H

NMR (CD_3CN, 300 MHz): δ = 3.81 (s, 9H, N-CH_3, H_C), 3.91(d, J = 16.3Hz, 3H, CH, H_B), 4.41 (d, J = 16.3 Hz, 3H, CH, H_B), 7.48 (d, J = 1.6 Hz, 3H, CH, H_D), 8.13 (d, J = 1.6 Hz, 3H, CH, H_E).

Synthesis of $[Mo_3S_4Cl_3(ImNHMe)_3]BF_4$ ($[2]BF_4$): A mixture of $Mo_3S_4Cl_4(PPh_3)_3(H_2O)_2$ (210 mg, 0.152 mmol), methyl[(1-methyl-1H-imidazol-2-yl)methyl]amine (65 mg, 0.494 mmol) and CH_3CN (20 mL) was stirred for 4 hours. Then, a 0.5 M solution of HBF_4·ether (1.20 mL, 0.608 mmol) in CH_3CN was added and the mixture was stirred for 30 min. The suspension was taken to dryness, redissolved in H_2O and the non-soluble PPh_3 was eliminated by filtration. The solution was concentrated under reduced pressure and the desired product was precipitated by adding THF. Finally, the resulting solid was dried at 40 °C in a vacuum oven to eliminate the water traces to give (90.8 mg, 64%) of the desired complex. Elemental analysis (%) calcd. for $Mo_3S_4Cl_3C_{18}H_{33}N_9BF_4$: C: 21.95, H: 3.38, N: 12.80; found: C: 20.9 , H: 3.65, N: 12.1; ^{1}H NMR (CD_3CN, 400 MHz): δ = 2.97 (d, 9H, CH_3, H_F), 3.07 (br, 3H, NH, H_A), 3.80 (s, 9H, CH_3, H_C), 3.96 (dd, J = 15.7 and 8.8 Hz, 3H, CH, H_B), 4.33 (dd, J = 15.7 and 6.6 Hz, 3H, CH, H_B), 7.45 (d, J = 1.5 Hz, 3H, CH, H_D), 7.98 (d, J = 1.6 Hz, 3H, CH, H_E); ^{13}C{^{1}H} NMR (CD_3CN, 101 MHz): δ = 35.22 (s, CH_2, C_C), 44.76 (s, CH_3, C_F), 51.59 (s, CH_2, C_B), 125.37 (s, CH, C_D), 132.73 (s, CH, C_E), 150.04 (s, C, C_G); ESI-MS (CH_3CN, cone 20 V): m/z calcd. for $[Mo_3S_4Cl_3C_{18}H_{33}N_9]^+$: 897.9 $[M]^+$; found: 898.0 $[M]^+$.

Synthesis of $[Mo_3S_4Cl_3(ImNMe_2)_3]BF_4$ ($[3]BF_4$): A solution of $Mo_3S_4Cl_4(PPh_3)_3(H_2O)_2$ (100 mg, 0.073 mmol) was reacted with dimethyl[(1-methyl-1H-imidazol-2-yl)methyl]amine (35 mg, 0.240 mmol) in CH_3CN (15 mL). The colour of the solution turned out from green to brown and stirring continued for 5 hours. Next, a 0.5 M solution of HBF_4·ether complex (0.58 mL, 0.291 mmol) in CH_3CN was added dropwise and the solution turned into green. After 30 minutes, the solution was filtrated, taken to dryness, and redissolved in MeOH. The desired product was precipitated by adding diethyl ether (50 mL). Finally, the green solid was separated by filtration and washed with a cold mixture of hexane/toluene (1:1, 50

mL), boiling hexane (50 mL) and diethyl ether to yield an air-stable product characterized as $[Mo_3S_4Cl_3(ImNMe_2)_3]BF_4$ (70.3 mg, 94%). Elemental analysis (%) calcd. for $Mo_3S_4Cl_3C_{21}H_{39}N_9BF_4$: C 24.56, H 3.83, N 12.28; found: C 25.38, H 3.78, N 11.90. ^{1}H NMR (CD_3CN, 400 MHz): δ = 2.96 (s, 18H, CH_3, H_A), 3.91 (s, 9H, CH_3, H_C), 4.61 (s, 6H, CH_2, H_B), 7.53 (d, J = 2.0 Hz, 3H, CH, H_D), 7.56 (d, J = 2.0 Hz, 3H, CH, H_E); ^{13}C{^{1}H} NMR (CD_3CN, 101 MHz): δ = 36.59 (s, CH_3, C_C), 44.85 (s, CH_3, C_A), 49.28 (s, CH_2, C_B), 122.45 (s, CH, C_D), 127.02 (s, CH, C_E), 136.33 (s, C, C_F); ESI-MS (CH_3CN, cone 20 V): m/z calcd. for $[Mo_3S_4Cl_3C_{21}H_{39}N_9]^+$: 940.0 $[M]^+$; found: 940.0 $[M]^+$

3.1.5.3. X-ray data collection and structure refinement

Suitable crystals for X-ray diffraction studies of complex **1**$^+$ were obtained by slow evaporation of a sample of [**1**]BF_4 in CH_3CN in the presence of an excess of NH_4PF_6. Crystals of **2**$^+$ were grown by slow evaporation of a sample solution of **2**$^+$ in CH_3OH acidified with HCl. Diffraction data collection was performed at 200 K on an Agilent Supernova diffractometer equipped with an Atlas CCD detector using Cu-Kα radiation (λ = 1.54184 Å). No instrument or crystal instabilities were observed during data collection. Absorption corrections based on the multiscan method were applied.[31,32] The structure was solved by direct methods and refined by the full-matrix methods based on F2 with the program SHELXL-13 using the Olex2 software package.[33,34] Graphics were performed with the Diamond visual crystal structure information system software.[35]

Crystal data for [1]PF_6·CH_3CN: $C_{17}H_{30}Cl_3F_6Mo_3N_{10}PS_4$, M= 1041.89, triclinic; space group P-1, a = 10.2357(3), b = 12.7929(3), c = 13.9167(4) Å; α = 68.076(3)°, β = 84.513(2)°, γ = 81.883(2)°; V = 1671.76(8) Å^3; T = 200.00(14); Z = 2; μ (Mo-Kα) = 14.717 mm^{-1}; reflections collected/unique = 34375/6824 (R_{int}= 0.0664). The final refinement converged with R_1 = 0.0400 and wR_2 = 0.0881 for all reflections, GOF= 1.0340 a dmax./min residual electron density 0.96/-0.84 e·Å^{-3}.

Crystal data for [2]Cl·CH$_3$OH: $C_{19}H_{37}Cl_4Mo_3N_9OS_4$, M= 965.43, triclinic; space group P-1, a = 9.67045(18), b = 12.8501(2), c = 13.6166(3) Å; α = 79.6676(15)°, β = 86.3570(15)°, γ = 88.6075(14)°; V = 1661.14 Å^3; T = 200.00(14); Z = 2; μ (Cu-kα) = 1.710 mm^{-1}; reflections collected/unique = 30528/6409 (R_{int}= 0.00272). The final refinement converged with R_1 = 0.0302 and wR_2 = 0.0684.

The structures of the complex salts [**1**]PF_6·CH_3CN and [**2**]Cl·CH_3OH were refined in the triclinic P-1 space group. The non-hydrogen atoms of the clusters and the counterions were refined anisotropically, whereas the positions of all hydrogen atoms in the ligands were generated geometrically, assigned isotropic thermal parameters, and allowed to ride on their respective parent carbon atoms. In both cases the solvent molecules in the crystal were refined anisotropically and their hydrogen atoms were included at their idealized positions.

CCDC 2210047 and 2210042 contain the supplementary crystallographic data for this chapter. The data can be obtained free of charge from The Cambridge Crystallographic Data Centre via www.ccdc.cam.ac.uk/structures.

3.1.5.4. Catalytic activity tests

General procedure for hydrogenation experiments: A 4 mL glass vial containing a stirring bar was sequentially charged with the corresponding molybdenum catalyst, alkyne (0.1 mmol), n-hexadecane (15 μL; added as an internal standard) and 2 mL of dry CH_3CN. Afterwards, the reaction vial was capped with a screw cap containing a septum with a needle and set in the alloy plate, which was then placed into a 300 mL autoclave. The sealed autoclave was purged three times with 30 bar of hydrogen before the desired pressure was set. Then, it was placed into an aluminum block which was preheated with the desired temperature. After 18 h, the autoclave was cooled to room temperature and the hydrogen was released. Ethyl acetate (2 mL) was then added, and a sample was analyzed by GC. To determine the isolated yield of alkenes, the reaction was scaled up by the factor of three, and no internal standard was added. After completion of the reaction, the mixture was taken to dryness,

solved in pentane, and filtered through silica. The solvent was removed *via* rotary evaporation and dried under vacuum.

3.1.6. References

[1] M. Crespo-Quesada, F. Cárdenas-Lizana, A. L. Dessimoz, L. Kiwi-Minsker, *ACS Catal.* **2012**, *2*, 1773-1786.

[2] B. Chen, U. Dingerdissen, J. G. E. Krauter, H. G. J. Lansink Rotgerink, K. Möbus, D. J. Ostgard, P. Panster, T. H. Riermeier, S. Seebald, T. Tacke, H. Trauthwein, *Appl. Catal. A Gen.* **2005**, *280*, 17-46.

[3] H. Lindlar, Ein neuer Katalysator für selektive Hydrierungen, *Helv. Chim. Acta* **1952**, *35*, 446-450.

[4] D. Decker, H. J. Drexler, D. Heller, T. Beweries, *Catal. Sci. Technol.* **2020**, *10*, 6449-6463.

[5] M. Garbe, S. Budweg, V. Papa, Z. Wei, H. Hornke, S. Bachmann, M. Scalone, A. Spannenberg, H. Jiao, K. Junge, M. Beller, *Catal. Sci. Technol.* **2020**, *10*, 3994-4001.

[6] V. Zubar, J. Sklyaruk, A. Brzozowska, M. Rueping, *Org. Lett.* **2020**, *22*, 5423-5428.

[7] N. Gorgas, J. Brünig, B. Stöger, S. Vanicek, M. Tilset, L. F. Veiros, K. Kirchner, *J. Am. Chem. Soc.* **2019**, *141*, 17452-17458.

[8] C. Chen, Y. Huang, Z. Zhang, X. Q. Dong, X. Zhang, *Chem. Commun.* **2017**, *53*, 4612-4615.

[9] H. Alawisi, H. D. Arman, Z. J. Tonzetich, *Organometallics* **2021**, *40*, 1062-1070.

[10] K. Semba, R. Kameyama, Y. Nakao, *Synlett* **2015**, *26*, 318-322.

[11] Y. Liang, U. K. Das, J. Luo, Y. Diskin-Posner, L. Avram, D. Milstein, *J. Am. Chem. Soc*, **2022**, *144*, 19115-19126.

[12] N. F. Both, A. Spannenberg, K. Junge, M. Beller, *Organometallics* **2022**, *41*, 1797-1805.

[13] A. G. Algarra, E. Guillamón, J. Andrés, M. J. Fernández-Trujillo, E. Pedrajas, J. Á. Pino-Chamorro, R. Llusar, M. G. Basallote, *ACS Catal.* **2018**, *8*, 7346-7350.

[14] M. V. Joannou, M. J. Bezdek, P. J. Chirik, *ACS Catal.* **2018**, *8*, 5276-5285.

[15] T. Vielhaber, K. Faust, C. Topf, *Organometallics* **2020**, *39*, 4535-4543.

[16] E. Pedrajas, I. Sorribes, A. L. Gushchin, Y. A. Laricheva, K. Junge, M. Beller, R. Llusar, *ChemCatChem* **2017**, *9*, 1128-1134.

[17] J. R. Cabrero-Antonino, E. Alberico, H.-J. Drexler, W. Baumann, K. Junge, H. Junge, M. Beller, *ACS Catal.* **2016**, *6*, 47-54.

[18] R. Adam, E. Alberico, W. Baumann, H. J. Drexler, R. Jackstell, H. Junge, M. Beller, *Chem. Eur. J.* **2016**, *22*, 4991-5002.

[19] V. Papa, J. R. Cabrero-Antonino, E. Alberico, A. Spanneberg, K. Junge, H. Junge, M. Beller, *Chem. Sci.* **2017**, *8*, 3576-3585.

[20] E. Pedrajas, I. Sorribes, K. Junge, M. Beller, R. Llusar, *ChemCatChem* **2015**, *7*, 2675-2681.

[21] T. F. Beltrán, J. Á. Pino-Chamorro, M. J. Fernández-Trujillo, V. S. Safont, M. G. Basallote, R. Llusar, *Inorg. Chem.* **2015**, *54*, 607-618.

[22] A. L. Gushchin, Y. A. Laricheva, P. A. Abramov, A. V. Virovets, C. Vicent, M. N. Sokolov, R. Llusar, *Eur. J. Inorg. Chem.* **2014**, 4093-4100.

[23] J. A. Pino-Chamorro, Y. A. Laricheva, E. Guillamón, M. J. Fernández-Trujillo, E. Bustelo, A. L. Gushchin, N. Y. Shmelev, P. A. Abramov, M. N. Sokolov, R. Llusar, M. G. Basallote, A. G. Algarra, *New J. Chem.* **2016**, *40*, 7872-7880.

[24] A. G. Algarra, M. G. Basallote, in *Advances in Inorganic Chemistry*, eds. C. D. Hubbard and R. van Eldik, Academic Press, **2017**, *8*, 311-342.

[25] Y. Ide, M. Sasaki, M. Maeyama, T. Shibahara, *Inorg. Chem.* **2004**, *43*, 602-612.

[26] E. Guillamón, M. Oliva, J. Andrés, R. Llusar, E. Pedrajas, V. S. Safont, A. G. Algarra, M. G. Basallote, *ACS Catal.* **2021**, *11*, 608-614.

[27] R. Kusy, M. Lindner, J. Wagner, K. Grela, *Chem Catal.* **2022**, *2*, 1346-1361.

[28] K. Baldenius, L. von dem Bussche-Hünnefeld, E. Hilgemann, P. Hoppe, R. Stürmer, in *Ullmann's Encyclopedia of Industrial Chemistry*, Wiley-VCH Verlag GmbH & Co. KGaA, Weinheim, Germany, **2021**, 1-21.

[29] MassLynx, 4.1.; Waters Corporation: Milford, MA, **2005**.

[30] V. P. Fedin, M. N. Sokolov, Y. V. Mironov, B. A. Kolesov, S. V. Tkachev, V. Y. Fedorov, *Inorg. Chim. Acta* **1990**, *167*, 39-45.

[31] CrysAlis, version 171.36.24, Agilent Technologies: Santa Clara, CA, **2012**.

[32] R. C. Clark, J. S. Reid, *Acta Crystallogr. A.* **1995**, *51*, 887-897.

[33] G. M. Sheldrick, *Acta Crystallogr. A.* **2008**, *64*, 112-122.

[34] O. V. Dolomanov, L. J. Bourhis, R. J. Gildea, J. A. K. Howard, H. Puschmann, *J. Appl. Crystallogr.* **2009**, *42*, 339-341.

[35] K. Brandenburg, H. Putz, Diamond; Crystal Impact GbR: Bonn, Germany, **2005**.

3.2. Supporting information

3.2.1. Catalyst characterization

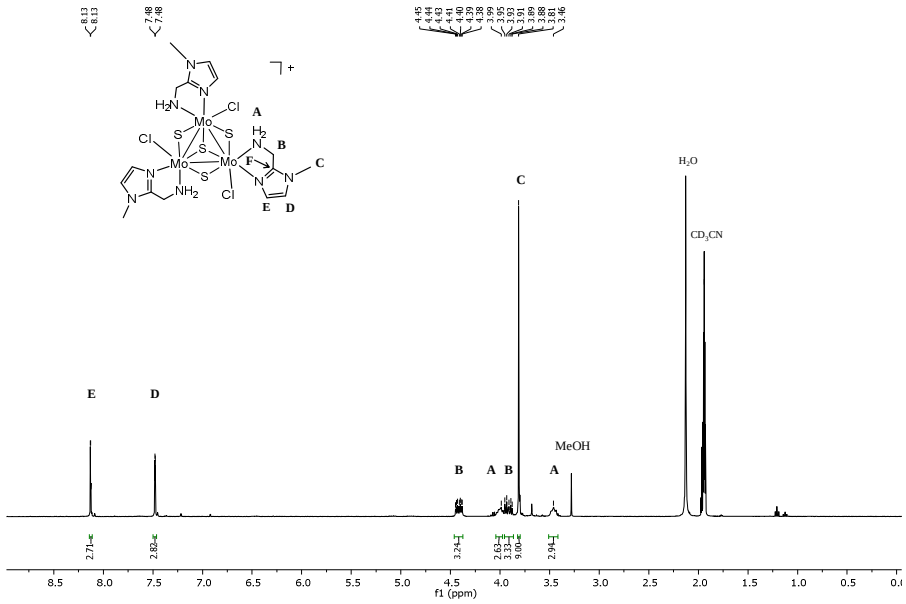

Figure SI3.1. ^{1}H NMR (400 MHz, CD_3CN, 298 K) spectrum of the [**1**]BF_4 complex.

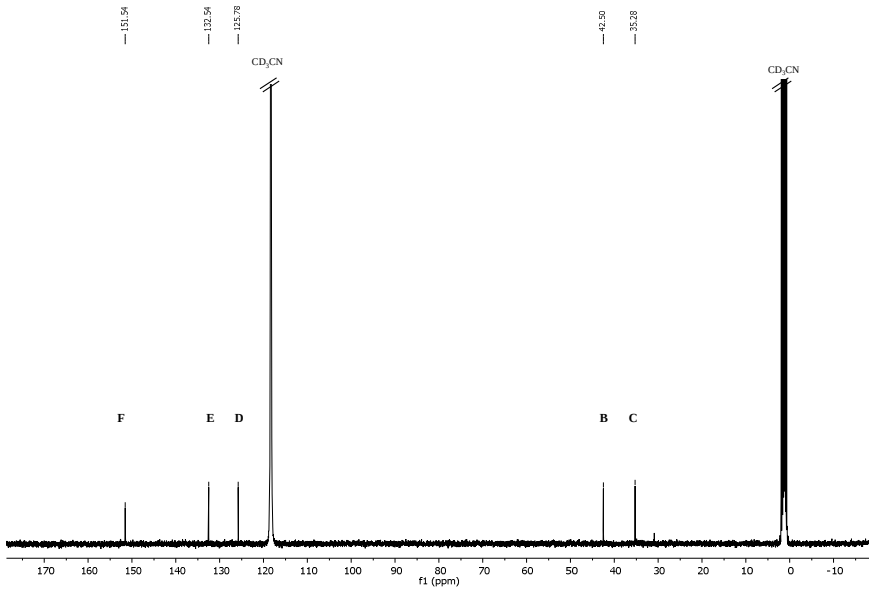

Figure SI3.2. $^{13}C\{^{1}H\}$ NMR (101 MHz, CD_3CN, 298 K) spectrum of the [**1**]BF_4 complex.

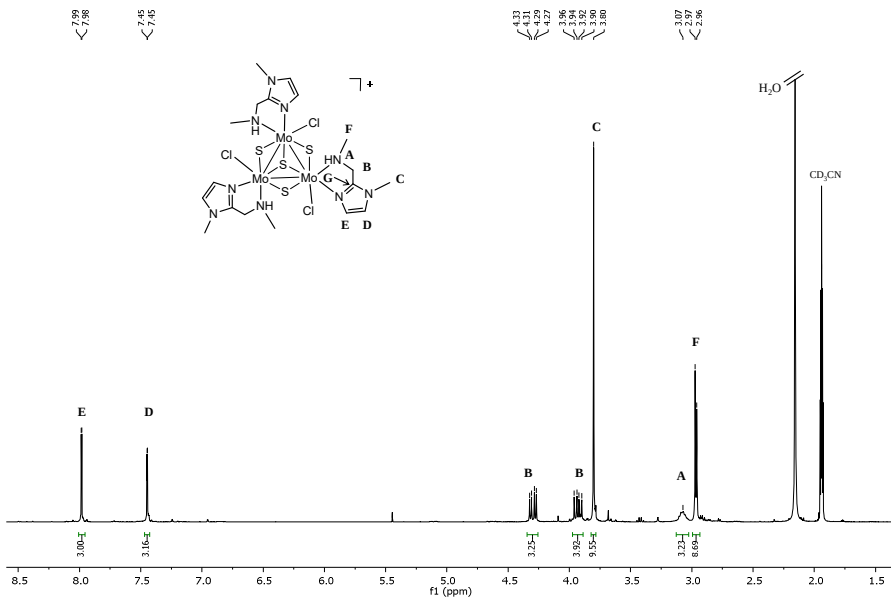

Figure SI3.3 ^{1}H NMR (400 MHz, CD_3CN, 298 K) spectrum of the [**2**]BF_4 complex.

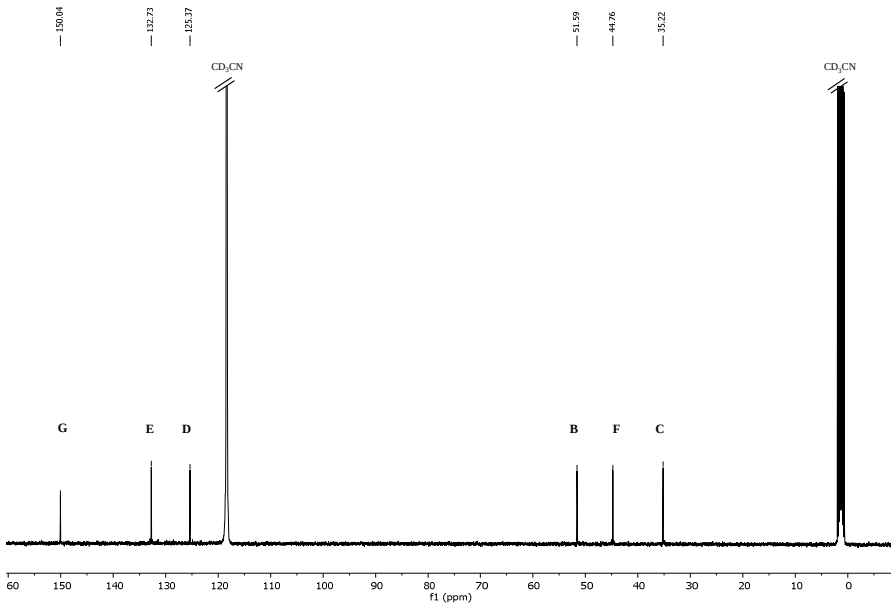

Figure SI3.4. $^{13}C\{^{1}H\}$ NMR (101 MHz, CD_3CN, 298 K) spectrum of the [**2**]BF_4 complex.

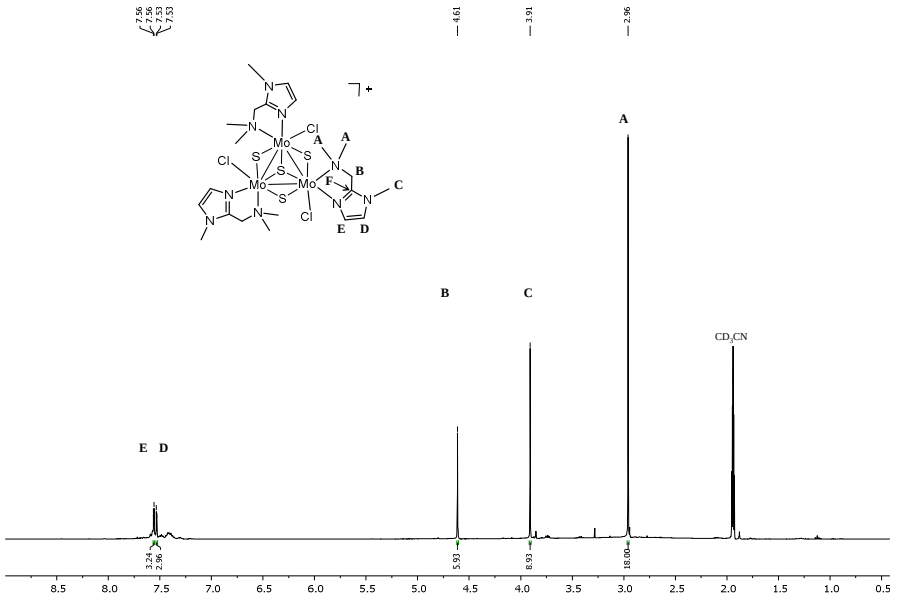

Figure SI3.5. ^{1}H NMR (400 MHz, CD_3CN, 298 K) spectrum of the [**3**]BF_4 complex.

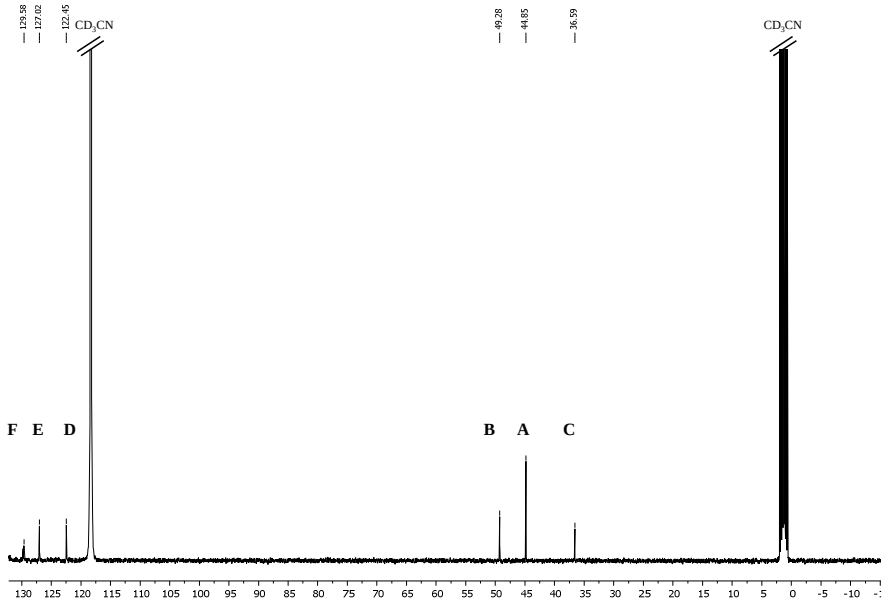

Figure SI3.6. $^{13}C\{^{1}H\}$ NMR (101 MHz, CD_3CN, 298 K) spectrum of the [**3**]BF_4 complex.

3.2.2. Mo_3S_4 cluster reactivity towards diphenylacetylene (dpa)

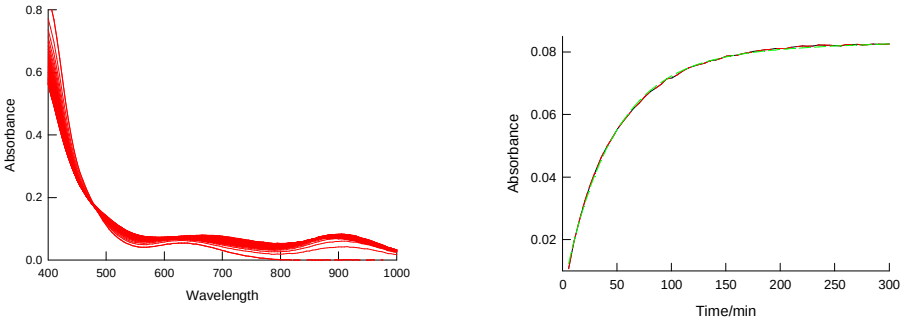

Figure SI3.7. Left: typical spectral changes in UV-Vis spectrum of $[Mo_3S_4Cl_3(ImNH_2)_3]^+$ (**1**$^+$) upon reaction with an excess of dpa ([**1**$^+$]= 2.5×10^{-4} M, [dpa]= 0.042 M, acetonitrile solution at 298 K). Right: trace at 900 nm: red (experimental) and green (fit to a single exponential).

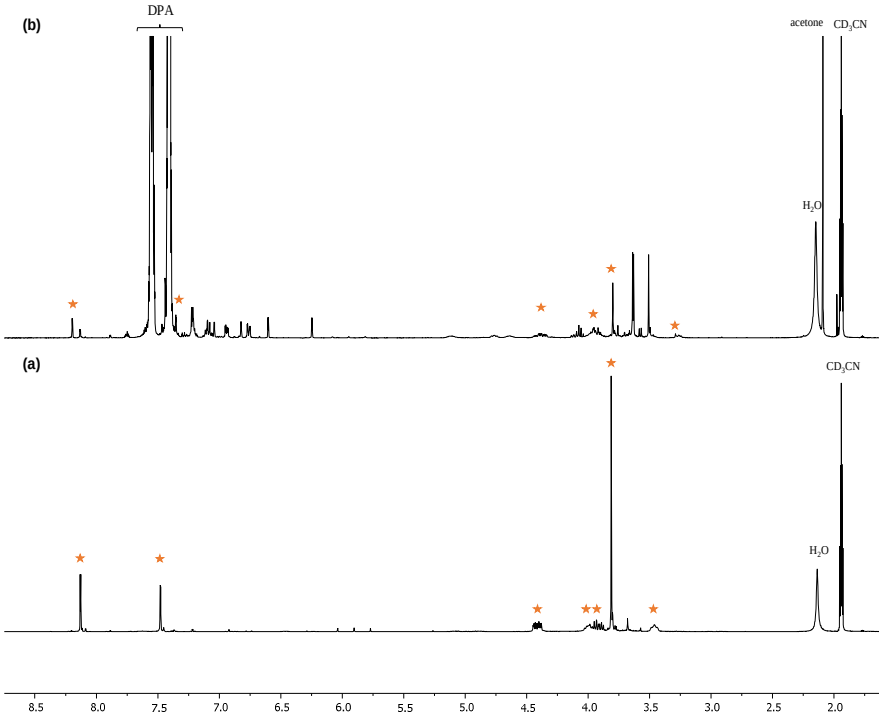

Figure SI3.8. ^{1}H NMR (400 MHz, CD_3CN, 298 K) spectra of (a) complex **1**$^+$ and (b) complex **1**$^+$ with an excess of diphenylacetylene (20 eq.) after 18 h of reaction. Signals marked with a star in both spectra correspond to the **1**$^+$ cluster.

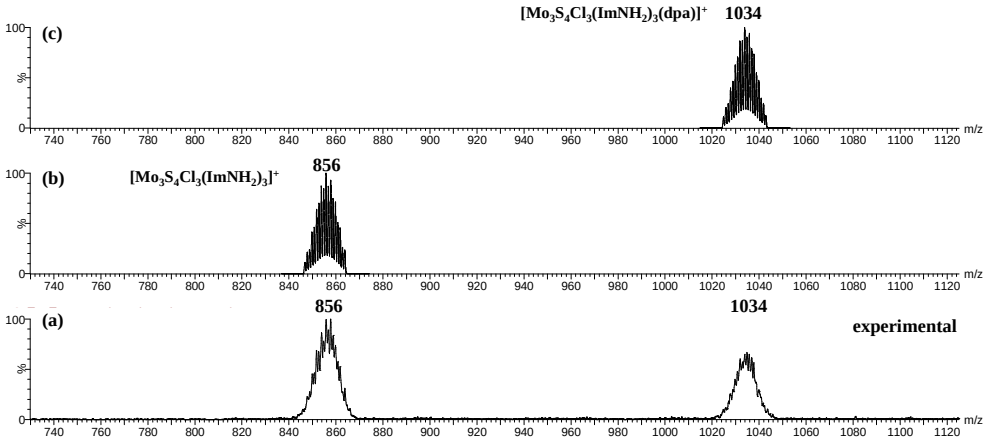

Figure SI3.9. ESI-MS spectrum of a solution 1 M of $[Mo_3S_4Cl_3(ImNH_2)_3]^+$ (**1**$^+$) in acetonitrile after addition of (a) a 20-molar excess of dpa together with (b) the simulated spectra of **1**$^+$ and (c) [**1** + dpa]$^+$. Experiment recorded at 20 V.

3.2.3. Conditions optimization for the semihydrogenation of diphenylacetylene (1a) to *cis*-stilbene (2a)

Table SI3.1. Influence of the pressure and temperature on the catalytic reduction of **1a** to **2a**.[a]

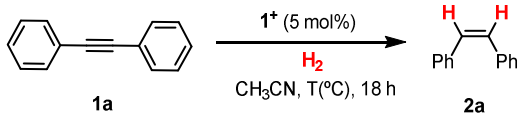

1a **2a**

Entry	T (ºC)	H_2 (bar)	Conversion[b] (%)	Yield 2a [b] (%)
1	150	-	0	0
2	150	50	>99	99
3	100	50	>99	99
4	100	30	>99	99
5	100	20	>99	99
6	70	20	>99	99
7	70	10	16	16
8	60	20	80	79
9	50	20	42	42

[a] Reaction conditions: diphenylacetylene (0.1 mmol), catalyst (5 mol%), 18 h. [b]Determined by GC analysis using n-hexadecane as an internal standard.

Table SI3.2. Influence of the solvent on the catalytic reduction of **1a** to **2a**.[a]

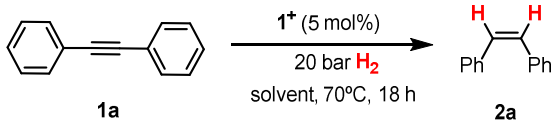

Entry	Solvent	Conversion[b] (%)	Yield 2a[b] (%)
1	CH_3CN	>99	99
2	CH_3OH	>99	99
3	2-Fluoroethanol	n.r	-
4	Hexafluoroisopropanol	n.r	-
5	THF	90	90

[a] Reaction conditions: diphenylacetylene (0.1 mmol), H_2 (20 bar), catalyst (5 mol%), 18 h, 70 ºC. [b] Determined by GC analysis using n-hexadecane as an internal standard.

3.2.4. Cluster monitoring during catalysis

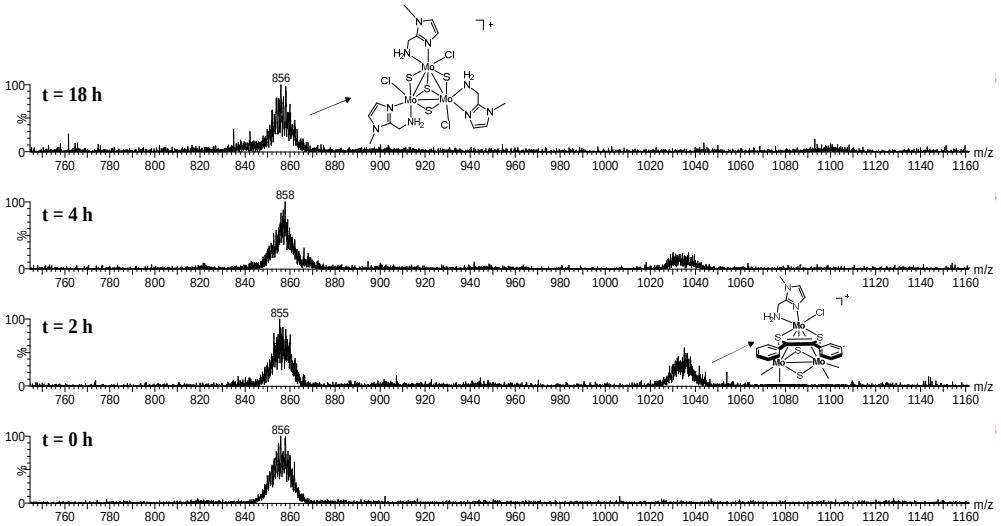

Figure SI3.10. ESI-MS spectra for the dpa semihydrogenation reaction monitoring at (a) t = 0 , (b) t = 2 h, (c) t = 4 h and (d) t = 18 h. All the experiments were recorded at 20 V.

3.2.5. Mechanism control experiments

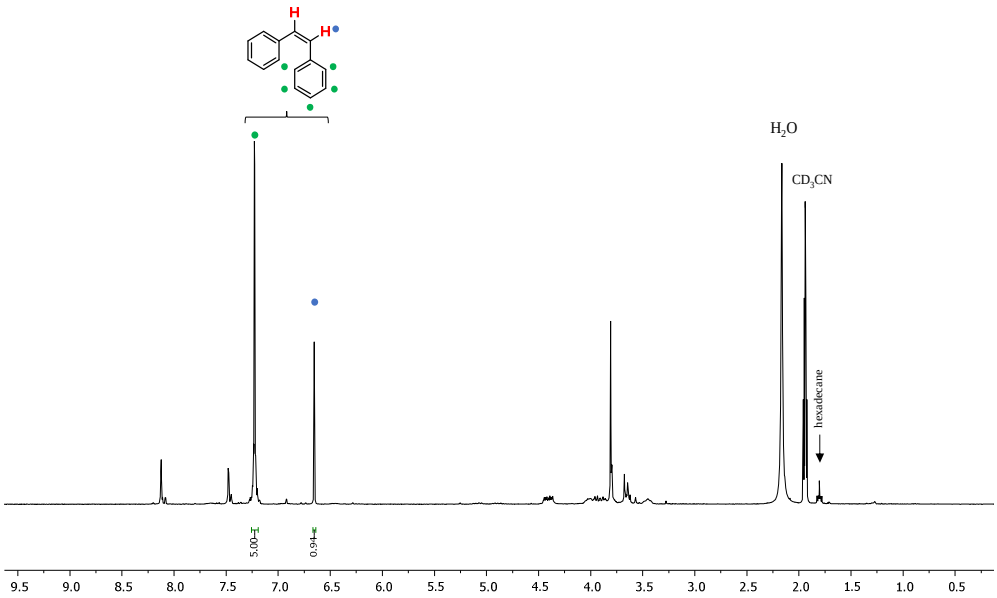

Figure SI3.11. ^{1}H NMR (400 MHz, CD_3CN, 298 K) spectrum of the catalytic reaction mixture (diphenylacetylene and the $[Mo_3S_4Cl_3(ImND_2)_3)]^+$ complex) at 70 ºC and 20 bar H_2 after 18 hours of reaction.

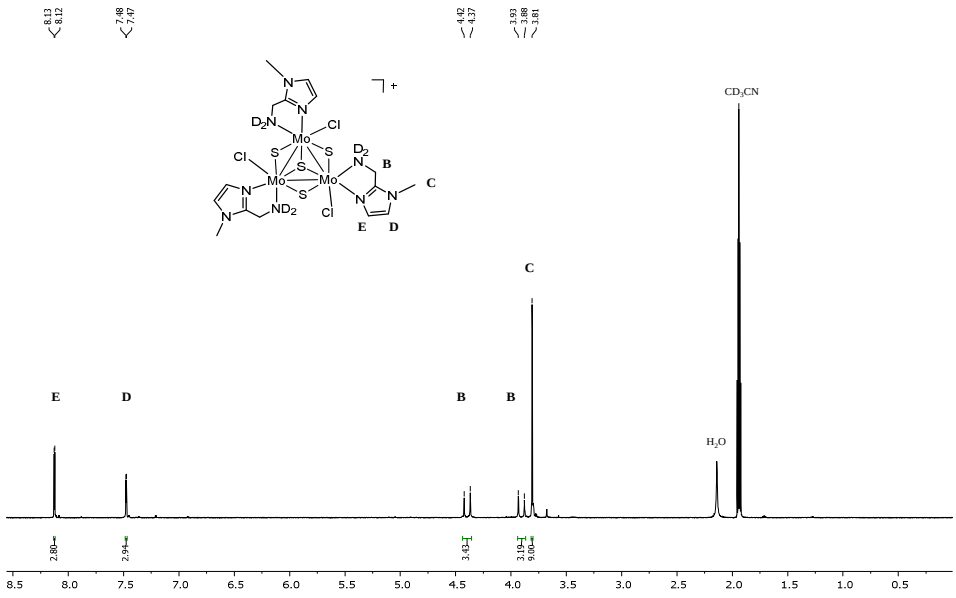

Figure SI3.12. ^{1}H NMR (300 MHz, CD_3CN, 298 K) spectrum of the $[Mo_3S_4Cl_3(ImND_2)_3]PF_6$ complex.

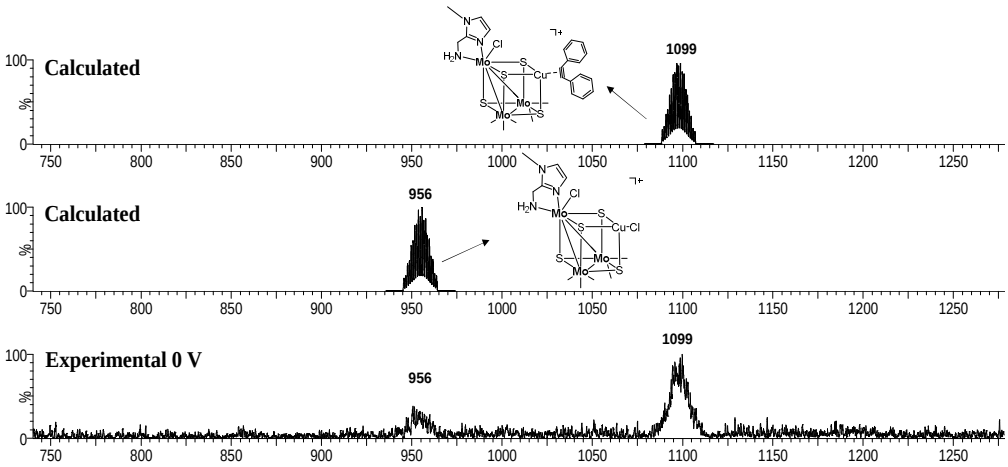

Figure SI3.13. ESI spectrum of the catalytic reaction mixture (diphenylacetylene, $[Mo_3S_4Cl_3(ImNH_2)_3)]^+$ complex and CuCl) at 70 ºC and 20 bar H_2 after 18 hours of reaction. The experiment was recorded at 0 V.

3.2.6. Characterization data of isolated alkenes prepared from diphenylacetylene derivatives

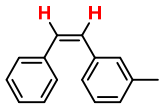

(*Z*)-1-methyl-2-styrylbenzene.[1] 51 mg, 90%, colorless oil (pentane). ^{1}H NMR (300 MHz, $CDCl_3$): δ 7.28 - 7.19 (m, 5H), 7.14 - 7.01 (m, 4H), 6.58 (s, 2H), 2.27 (s, 3H); $^{13}C\{^1H\}$ NMR (101 MHz, $CDCl_3$): δ 137.91, 137.49, 137.35, 130.52, 130.22, 129.74, 129.02, 128.29, 128.21, 127.98, 127.18, 126.01, 21.47.

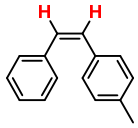

(*Z*)-1-methyl-4-styrylbenzene.[1] 26.6 mg, yield 46%, colorless oil (pentane). ^{1}H NMR (300 MHz, $CDCl_3$): δ 7.30 - 7.19 (m, 5H), 7.18 - 7.14 (m, 2H), 7.04 (d, 2H), 6.55 (s, 2H), 2.32 (s, 3H); $^{13}C\{^1H\}$ NMR (75 MHz, $CDCl_3$): δ 137.62, 136.99, 134.39, 130.33, 129.68, 129.04, 128.97, 128.92, 128.32, 127.10, 21.37.

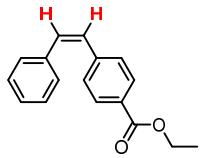

Ethyl-(*Z*)-4-styrylbenzoate.[1] 62 mg, 81%, colorless liquid (pentane). ^{1}H NMR (300 MHz, $CDCl_3$): δ 7.89 (m, 2H), 7.29 (m, 2H), 7.23 (m, 5H), 6.66 (q, 2H), 4.36 (q, 2H), 1.38 (s, 3H); ^{13}C{^{1}H} NMR (75 MHz, $CDCl_3$): δ 166.57, 142.10, 136.82, 132.29, 129.61, 129.39, 128.99, 128.95, 128.47, 127.62, 61.02, 14.46.

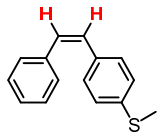

(*Z*)-methyl(4-styrylphenyl)sulfane.[1] 60 mg, 89%, white solid (pentane). ^{1}H NMR (300 MHz, $CDCl_3$): δ 7.43-7.32 (m, 4H), 7.24 - 7.29 (m, 2H), 7.16 - 7.14 (m, 3H), 6.97 (s, 2H), 2.41 (s, 3H); ^{13}C{^{1}H} NMR (75 MHz, $CDCl_3$): δ 137.98. 137.44. 134.40. 128.81. 128.19. 128.15. 127.68. 127.02. 126.81. 126.56. 15.93.

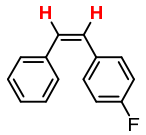

(*Z*)-1-fluoro-4-styrylbenzene.[1] 50 mg, 86%, colorless liquid (pentane). ^{1}H NMR (400 MHz, $CDCl_3$): δ 7.30 - 7.21 (m, 6H), 6.94 (t, J = 8.8 Hz, 1H), 6.63 (d, J = 12.2 Hz, 1H), 6.58 (d, J = 12.2 Hz, 1H); ^{13}C{^{1}H} NMR (101 MHz, $CDCl_3$): δ 163.21, 160.76, 137.20, 133.33, 130.71, 130.63, 130.41, 129.23, 128.97, 128.45, 127.34, 115.39, 115.18.

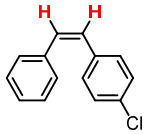

(*Z*)-1-chloro-4-styrylbenzene.[1] 41.4 mg, 65%, colorless liquid (pentane). ^{1}H NMR (400 MHz, $CDCl_3$): δ 7.25-7.14 (m, 9 H), 6.63 (d, J = 12.2 Hz, 1H), 6.53 (d, 12.2 Hz. 1H); $^{13}C\{^{1}H\}$ NMR (101 MHz, $CDCl_3$): δ 136.72, 135.50, 132.60, 130.80, 130.05, 128.76, 128.64, 128.24, 128.17, 127.15.

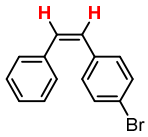

(*Z*)-1-bromo-4-styrylbenzene.[1] 53.9 mg, 70%, colorless liquid (pentane). ^{1}H NMR (400 MHz, $CDCl_3$): δ 7.37 - 7.32 (m, 2H), 7.25 - 7.19 (m, 5H), 7.14 - 7.08 (m, 2H), 6.64 (d, *J* = 12.2 Hz, 1H), 6.51 (d, *J* = 12.2 Hz, 1H); $^{13}C\{^{1}H\}$ NMR (101 MHz, $CDCl_3$): δ 137.01, 136.28, 131.52, 131.20, 130.69, 129.10, 128.94, 128.50, 127.49, 121.09.

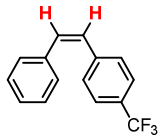

(*Z*)-1-styryl-4-(trifluoromethyl)benzene.[1] 58 mg, 78%, colorless liquid (pentane). ^{1}H NMR (400 MHz, $CDCl_3$): δ 7.47 (d, *J* = 8.2 Hz, 3H), 7.34 (d, *J* = 8.1 Hz, 3H), 7.28 - 7.19 (m, 5H), 6.73 (d, *J* = 12.2 Hz, 1H), 6.60 (d, *J* = 12.2 Hz, 1H). $^{13}C\{^{1}H\}$ NMR (101 MHz, $CDCl_3$): δ 141.08, 136.72, 132.49, 129.29, 128.97, 128.90, 128.57, 127.72, 125.36, 125.32, 125.28, 125.24.

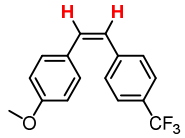

(*Z*)-1-methoxy-4-(4-(trifluoromethyl)styryl)benzene.[2] 45 mg, 55%, colorless liquid (pentane). ^{1}H NMR (400 MHz, $CDCl_3$): δ 7.48 (d, *J* = 8.2 Hz, 2H), 7.37 (d, *J*

= 8.5 Hz, 2H), 7.16 (d, *J* = 8.4 Hz, 1H), 6.78 (d, 2H), 6.65 (d, *J* = 12.2 Hz, 1H), 6.50 (d, *J* = 12.2 Hz, 1H); $^{13}C\{^{1}H\}$ NMR (101 MHz, $CDCl_3$): δ 159.23, 141.51, 131.98, 130.32, 129.22, 129.09, 128.77, 127.37, 125.3, 123.02, (q, *J* = 3.8 Hz), 113.96, 55.36.

3.2.7. ^{1}H NMR and ^{13}C{^{1}H} NMR spectra of isolated products

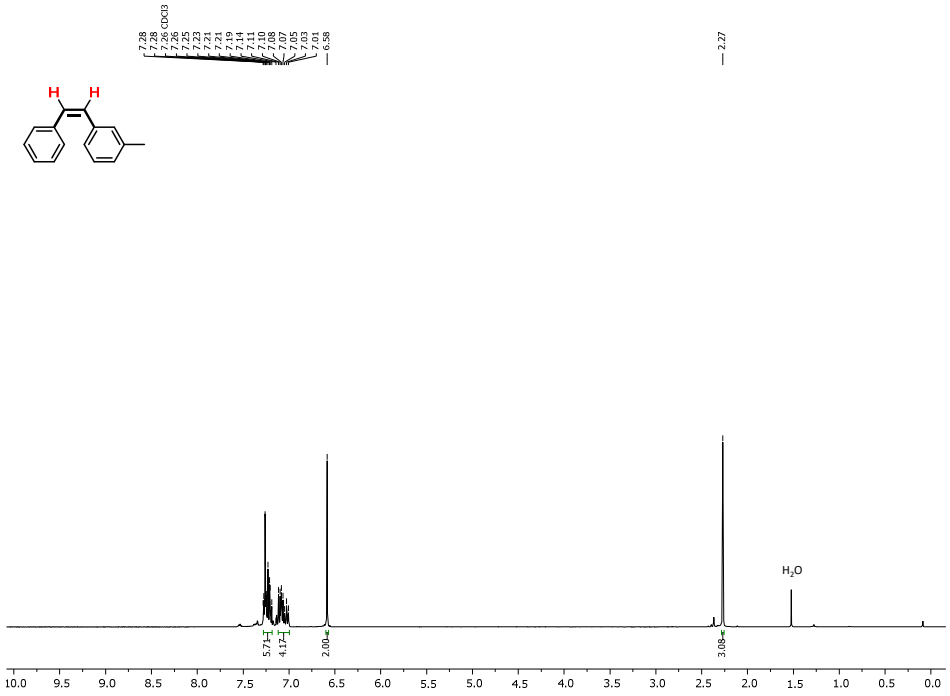

Figure SI3.14. ^{1}H NMR (300 MHz, $CDCl_3$, 298 K) spectrum of (*Z*)-1-methyl-2-styrylbenzene.

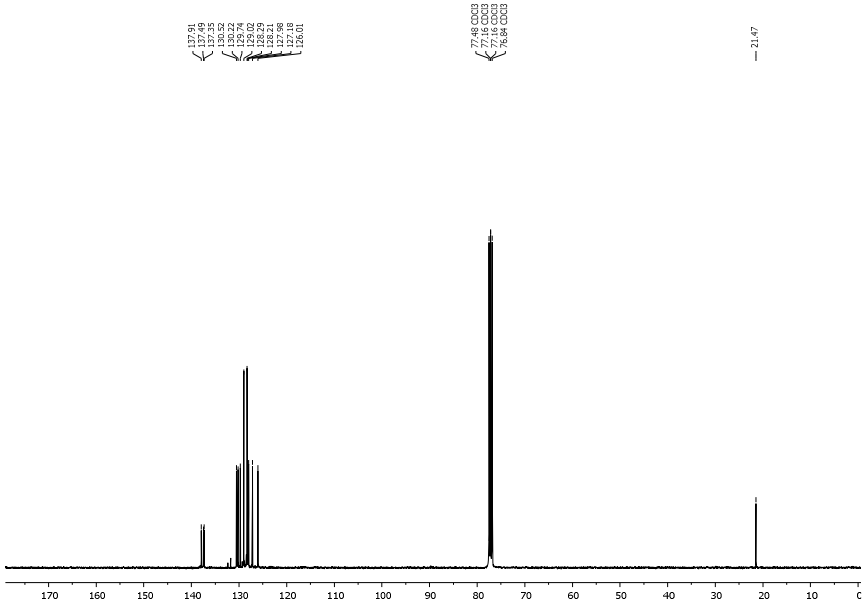

Figure SI3.15. ^{13}C{^{1}H} NMR (75 MHz, $CDCl_3$, 298 K) spectrum of (*Z*)-1-methyl-2-styrylbenzene**.**

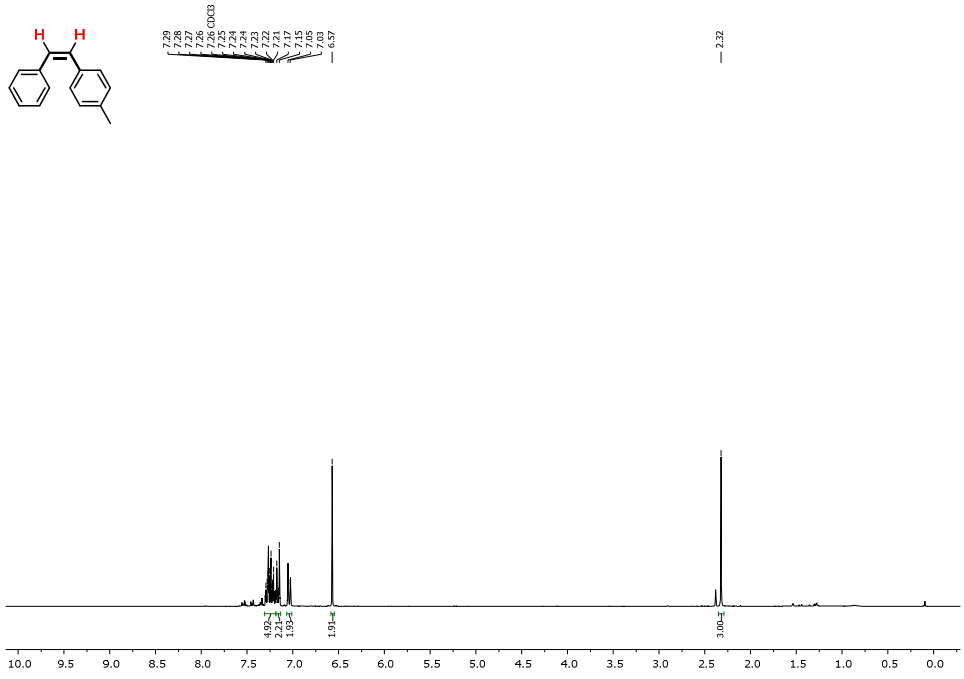

Figure SI3.16. ^{1}H NMR (300 MHz, $CDCl_3$, 298 K) spectrum of (*Z*)-1-methyl-4-styrylbenzene.

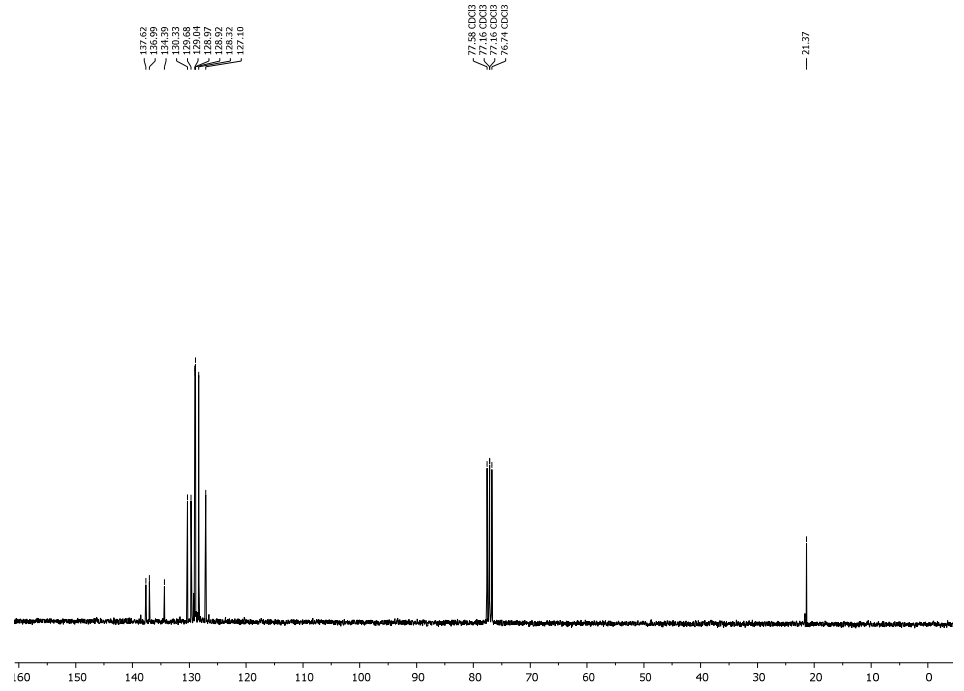

Figure SI3.17. $^{13}C\{^{1}H\}$ NMR (75 MHz, $CDCl_3$, 298 K) spectrum of (*Z*)-1-methyl-4-styrylbenzene.

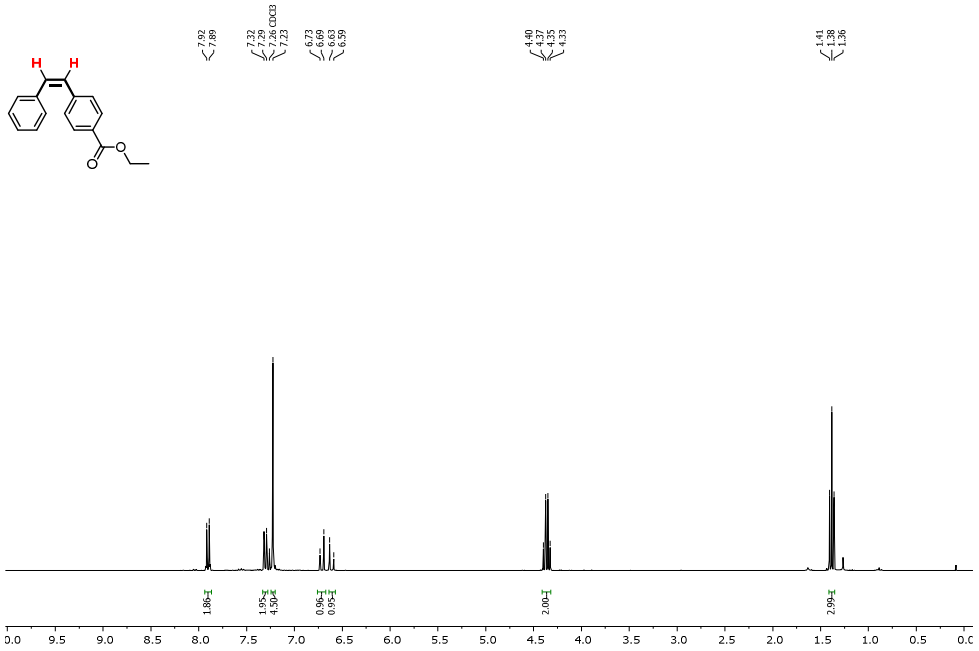

Figure SI3.18. ^{1}H NMR (300 MHz, $CDCl_3$, 298 K) spectrum of ethyl-(*Z*)-4-styrylbenzoate.

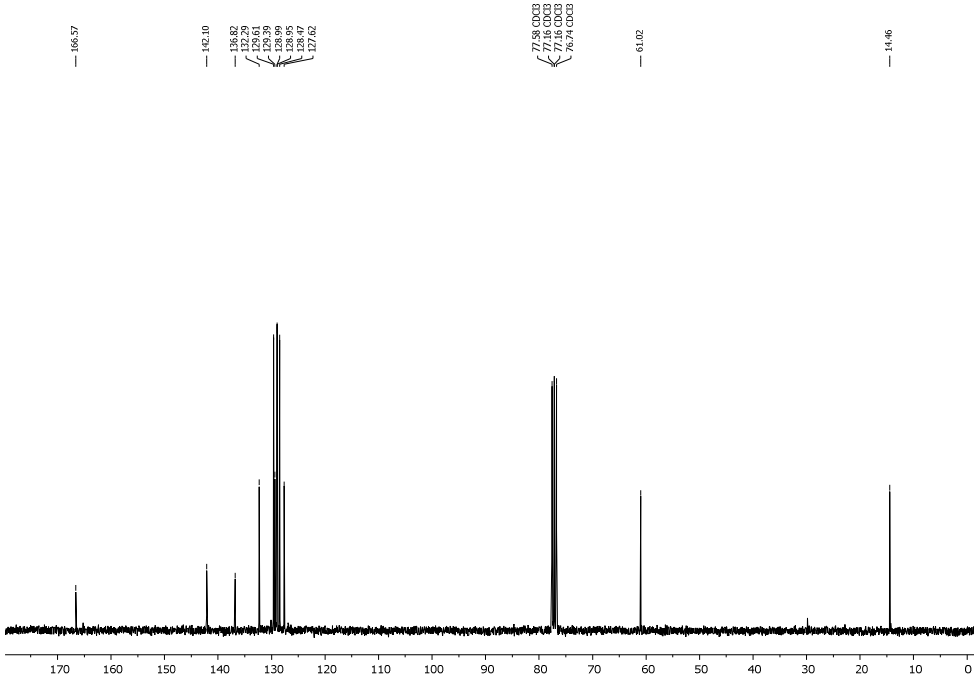

Figure SI3.19. $^{13}C\{^{1}H\}$ NMR (75 MHz, $CDCl_3$, 298 K) spectrum of ethyl-(*Z*)-4-styrylbenzoate.

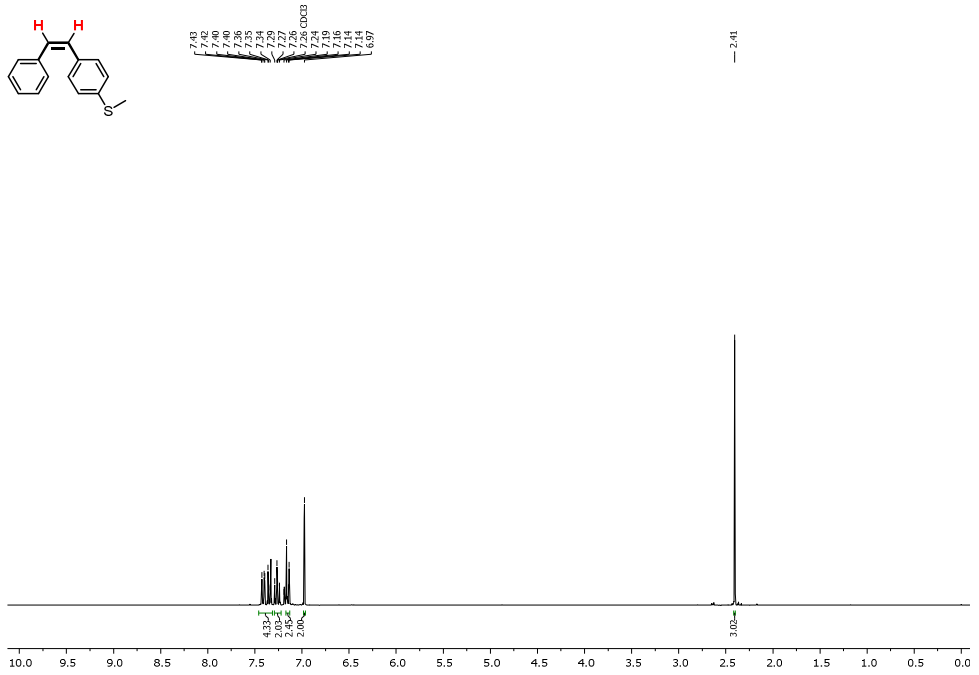

Figure SI3.20. ^{1}H NMR (300 MHz, $CDCl_3$, 298 K) spectrum of (*Z*)-methyl(4-styrylphenyl)sulfane.

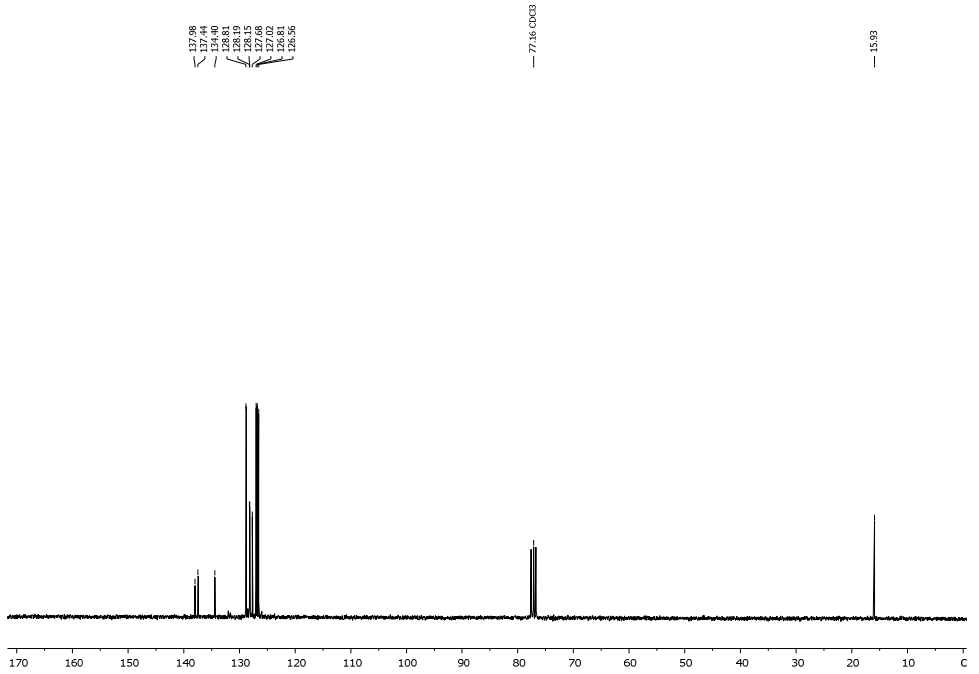

Figure SI3.21. $^{13}C\{^{1}H\}$ NMR (75 MHz, $CDCl_3$, 298 K) spectrum of (*Z*)-methyl(4-styrylphenyl)sulfane.

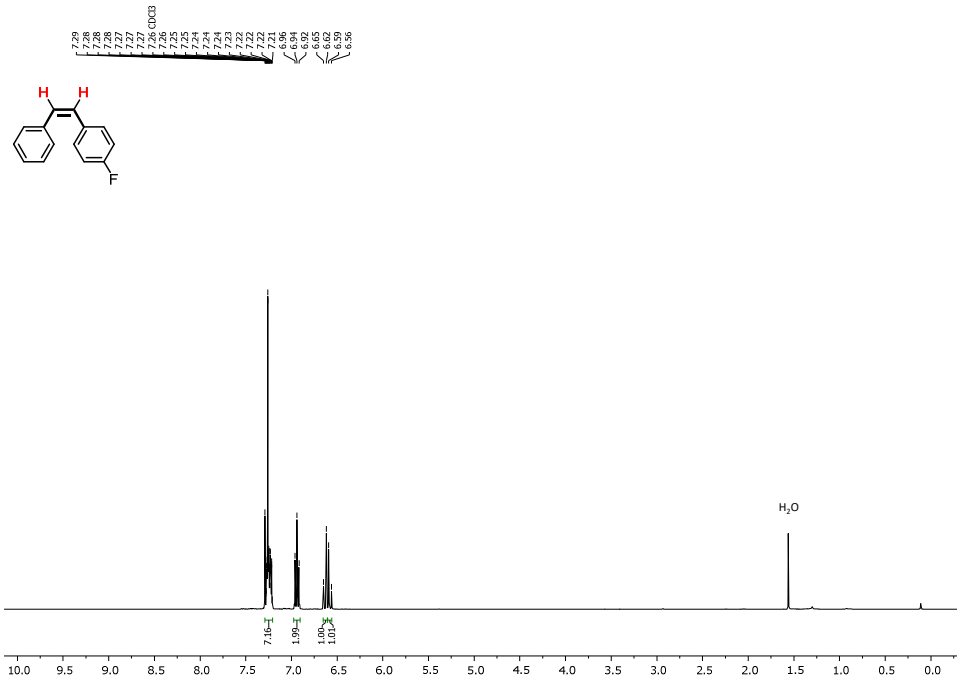

Figure SI3.22. ^{1}H NMR (400 MHz, $CDCl_3$, 298 K) spectrum of (*Z*)-1-fluoro-4-styrylbenzene.

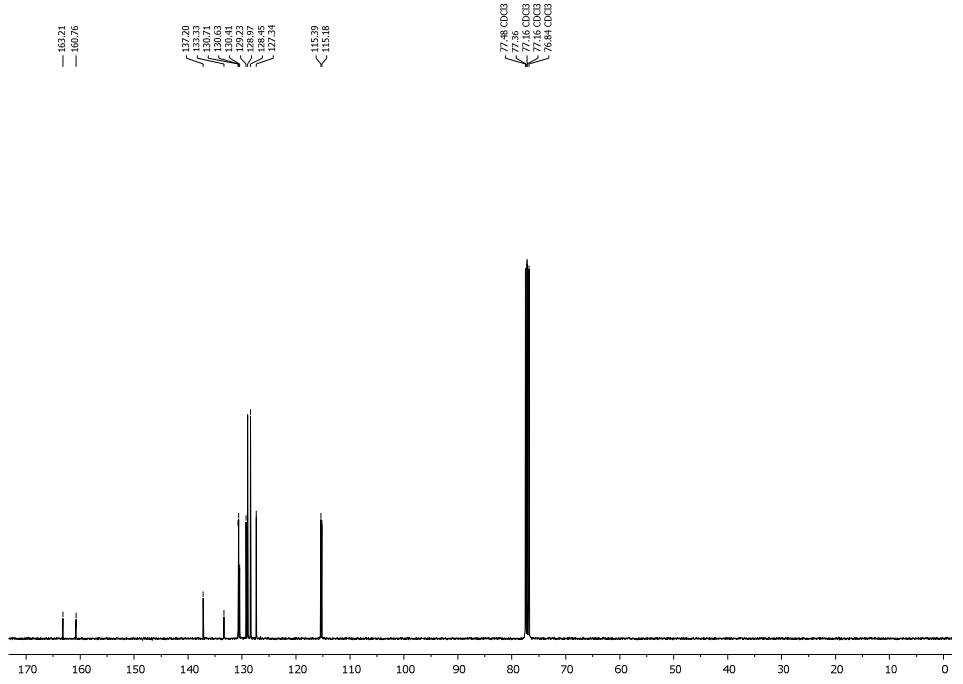

Figure SI3.23. $^{13}C\{^{1}H\}$ NMR (101 MHz, $CDCl_3$, 298 K) spectrum of (*Z*)-1-fluoro-4-styrylbenzene.

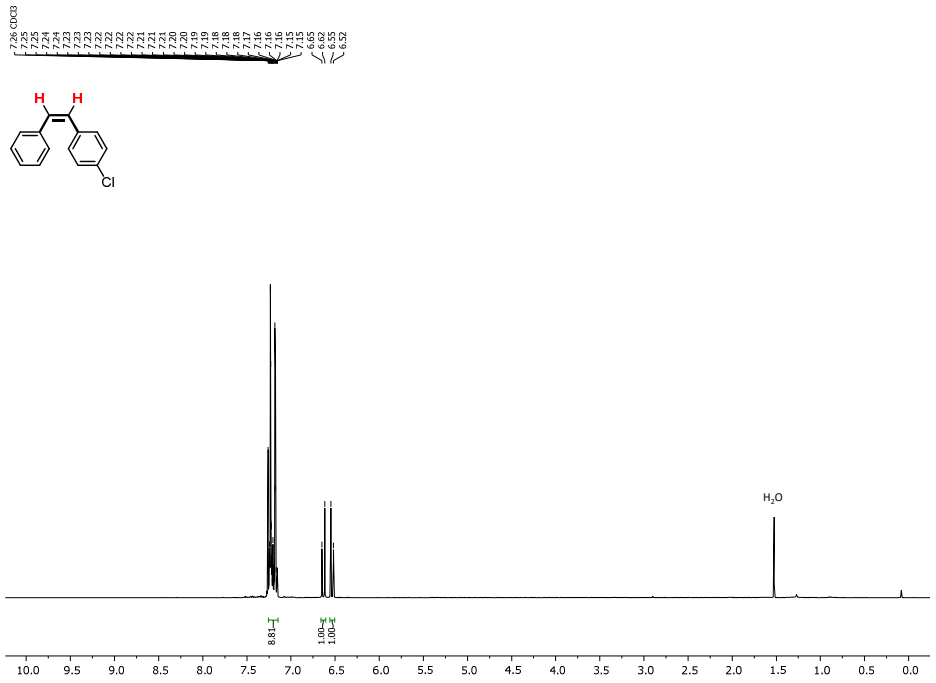

Figure SI3.24. ^{1}H NMR (400 MHz, $CDCl_3$, 298 K) spectrum of (*Z*)-1-chloro-4-styrylbenzene.

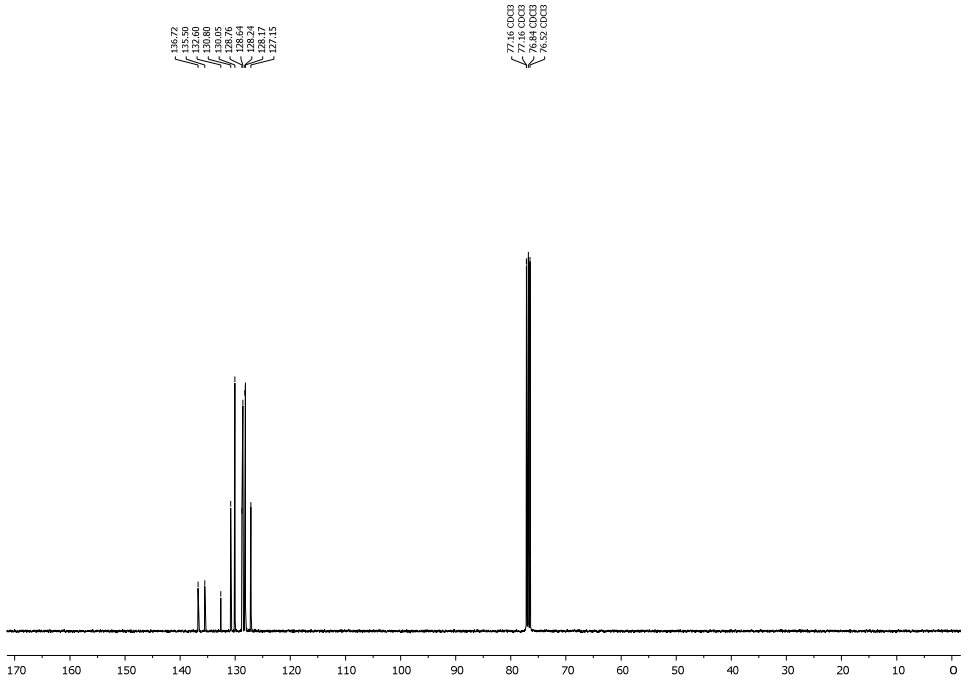

Figure SI3.25. $^{13}C\{^{1}H\}$ NMR (101 MHz, $CDCl_3$, 298 K) spectrum of (*Z*)-1-chloro-4-styrylbenzene.

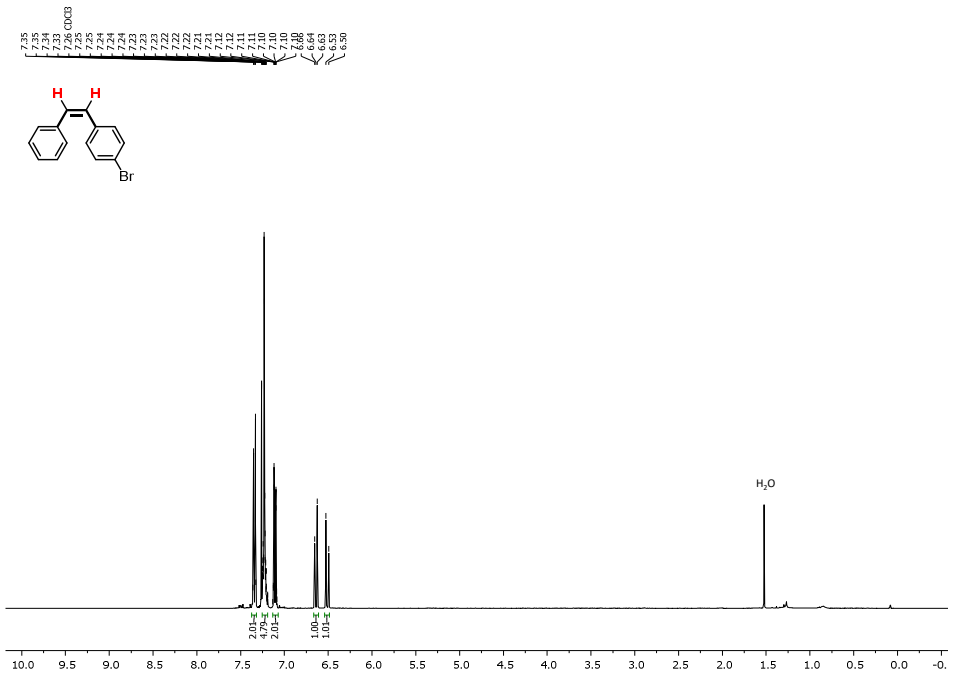

Figure SI3.26. ^{1}H NMR (400 MHz, $CDCl_3$, 298 K) spectrum of (*Z*)-1-bromo-4-styrylbenzene.

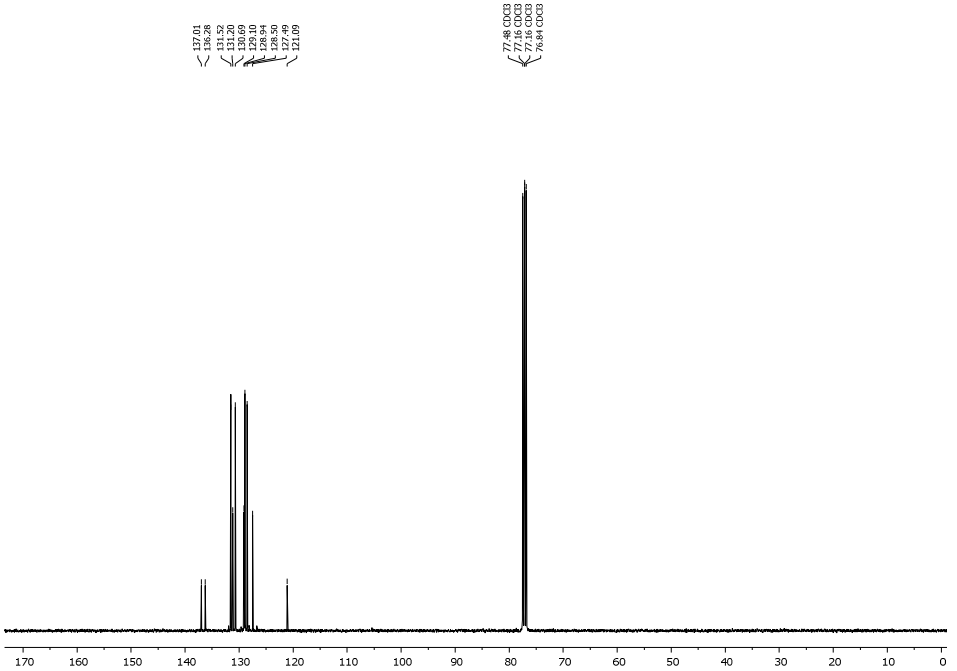

Figure SI3.27. ^{13}C{^{1}H} NMR (101 MHz, $CDCl_3$, 298 K) spectrum of (*Z*)-1-bromo-4-styrylbenzene.

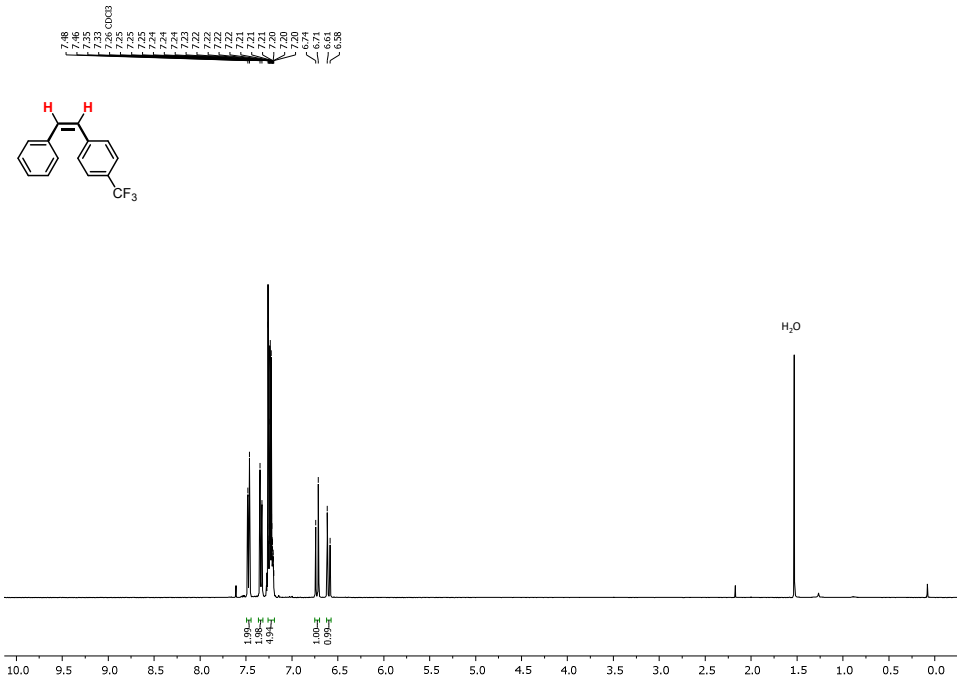

Figure SI3.28. ^{1}H NMR (400 MHz, $CDCl_3$, 298 K) spectrum of (*Z*)-1-styryl-4-(trifluoromethyl)benzene.

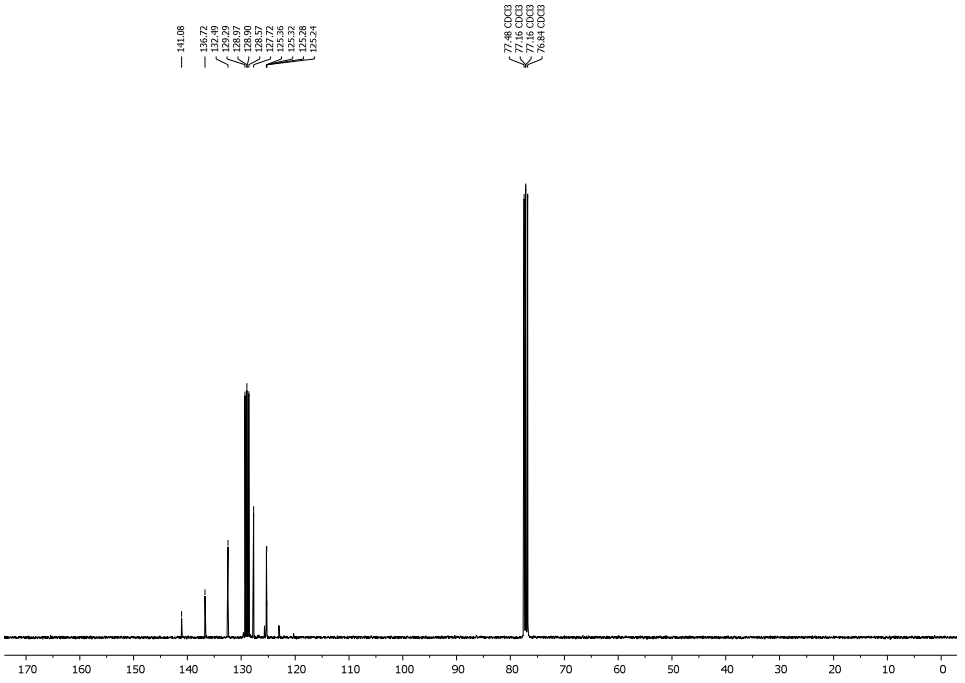

Figure SI3.29. $^{13}C\{^{1}H\}$ NMR (101 MHz, $CDCl_3$, 298 K) spectrum of (*Z*)-1-styryl-4-(trifluoromethyl)benzene.

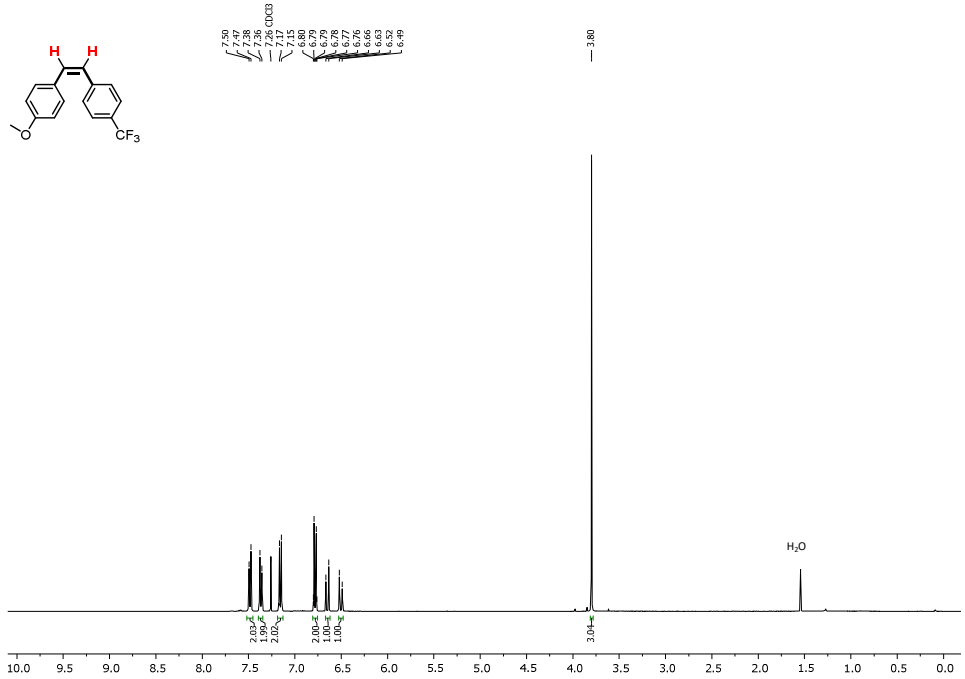

Figure SI3.30. ^{1}H NMR (400 MHz, $CDCl_3$, 298 K) spectrum of (*Z*)-1-methoxy-4-(4-(trifluoromethyl)styryl)benzene.

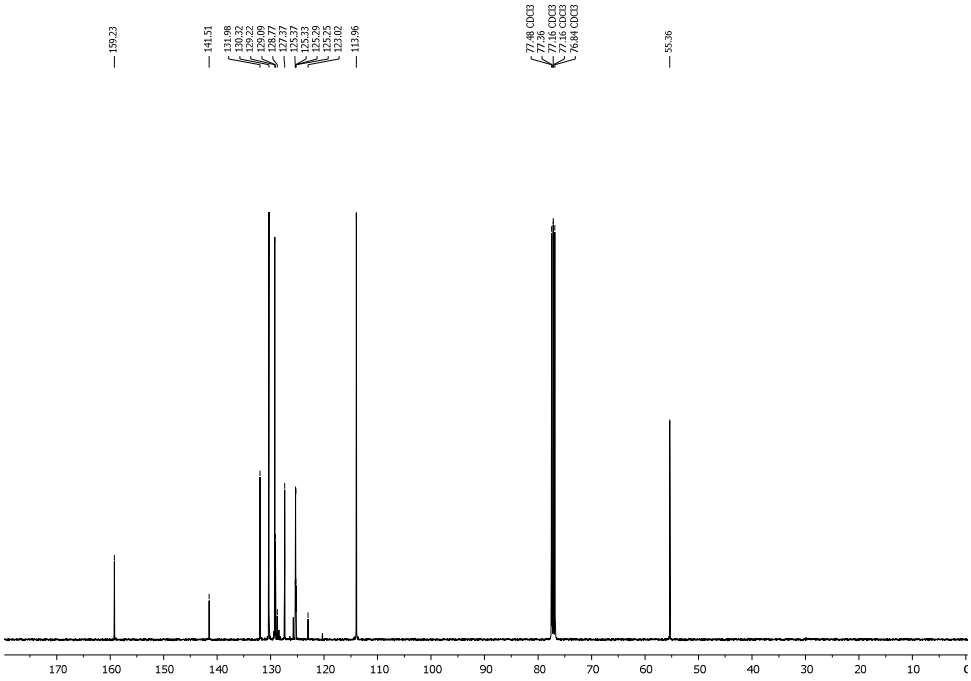

Figure SI3.31. ^{13}C{^{1}H} NMR (101 MHz, $CDCl_3$, 298 K) spectrum of (*Z*)-1-methoxy-4-(4-(trifluoromethyl)styryl)benzene.

3.2.8. Conditions optimization for the semihydrogenation of 3,7,11,15-tetramethylhexadec-1-yn-3-ol (1b) and reaction monitoring

Table SI3.3. Optimization of the pressure and temperature on the catalytic reduction of **1b** to **2b**.[a]

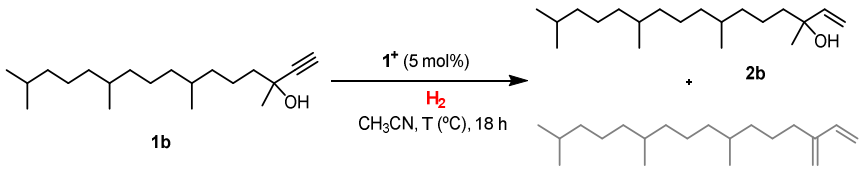

Entry	T (ºC)	H_2 (bar)	Conversion[b] (%)	Yield 2b[b] (%)
1	60	20	n.r	n.r
2	100	20	22	22
3	120	20	>99	90
4	120	40	>99	82

[a] Reaction conditions: 3,7,11,15-tetramethylhexadec-1-yn-3-ol (0.1 mmol), catalyst (5 mol%), 18 h. [b] Determined by GC analysis using n-hexadecane as an internal standard.

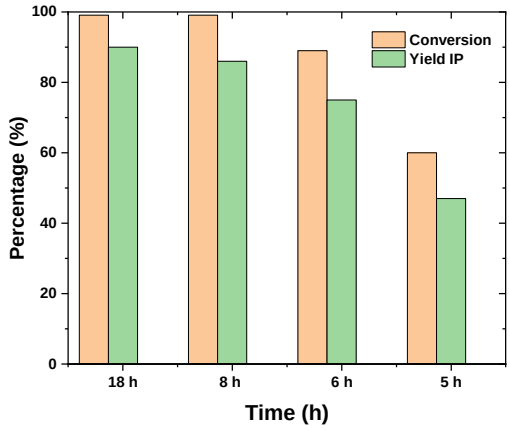

Figure SI3.32 Influence of the time on the catalytic reduction of **1b** to **2b**. Reaction conditions: 3,7,11,15- tetramethylhexadec-1-yn-3-ol (0.1 mmol), catalyst (5 mol%), 120 ºC, 20 bar H_2, 18 h. Conversion and yield determined by GC analysis using n-hexadecane as an internal standard.

3.2.9. References

[1] Z. Huang, Z. Huang, X. Leng, Y. Wang, *J. Am. Chem. Soc.* **2021**, *143*, 4824-4836.

[2] M. K. Armstrong, M. B. Goodstein, G. Lalic, *J. Am. Chem. Soc.* **2018**, *140*, 10233-10241.

Chapter 4

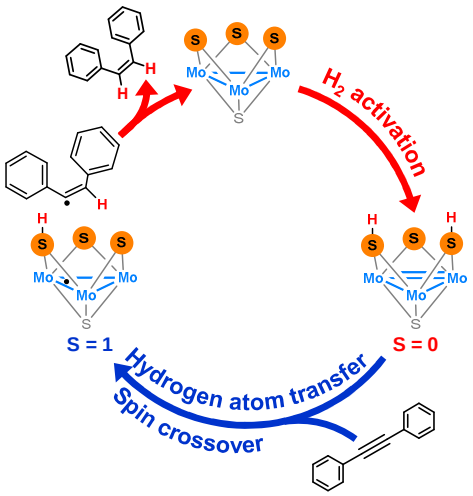

Spin-crossing in the (*Z*)-selective alkyne semihydrogenation mechanism catalyzed by Mo_3S_4 clusters: A DFT exploration

The results presented in this section have already been accepted. Reproduced from *Inorg. Chem.* with permission from the American Chemical Society of Chemistry.

4.1. Main text

4.1.1. Abstract

Semihydrogenation of internal alkynes catalyzed by the air-stable imidazolyl amino $[Mo_3S_4Cl_3(ImNH_2)_3]^+$ cluster selectively affords the (*Z*)-alkene under soft conditions with excellent yields. Experimental results suggest a sulfur-based mechanism with the formation of a dithiolene adduct through interaction of the alkyne with the bridging sulfur atoms. However, computational studies indicate that this mechanism is unable to explain the experimental outcome: mild reaction conditions, excellent selectivity towards the (*Z*)-isomer and complete deuteration of the vinylic positions in the presence of CD_3OD and CH_3OD. An alternative mechanism that explains the experimental results is proposed. The reaction begins with the hydrogenation of two of the $Mo_3(\mu_3\text{-}S)(\mu\text{-}S)_3$ bridging sulfurs to yield a bis(hydrosulfide) intermediate that carries out two sequential hydrogen atom transfers (HAT) from the S-H groups to the alkyne. The first HAT occurs with a spin change from singlet to triplet. After the second HAT, the singlet state is recovered. Although the dithiolene adduct is more stable than the hydrosulfide species, the large energy required for the subsequent H_2 addition makes the system evolve *via* the second alternative pathway to selectively render the (*Z*)-alkene with a lower overall activation barrier.

4.1.2. Introduction

The stereoselective catalytic semihydrogenation of internal alkynes into (*E*)- or (*Z*)-alkene isomers is among the most relevant processes in synthetic organic chemistry.[1] To date, a plethora of heterogeneous and homogeneous metal-based catalysts for internal alkyne semihydrogenation have been reported.[2-5] In spite of the many advances in the field, there are still some unsolved problems such as overreduction and isomerization.[6,7] For that reason, most of the current efforts are devoted to render selective catalysts working under mild conditions, with these ideally being also inexpensive, atom-economic and environmentally benign. Thus, the interest to replace noble metals by non-precious ones together with using

hydrogen as reducing agent is notably increasing. Heterogeneous catalysts are usually preferred by industry, but due to the inherent difficulties to obtain mechanistic information from solid-state catalysts, the use of molecular models capable of mimicking their behavior has become a widespread approach. Homogeneous catalysts also offer a more rational tuning of the catalyst through metal election and ligand design, enabling to achieve high stereoselectivity under mild conditions and broad functional group tolerance. In this context, mechanistic understanding is essential for the development of better catalysts. There are many examples in the literature supporting this statement.[8-10]

Noble metal coordination complexes have been extensively studied and excellent selectivities towards the (*Z*)-isomer were obtained in alkyne hydrogenation and transfer hydrogenation processes.[11,12] However, the number of base-metal catalysts for the hydrogenation of alkynes into (*Z*)-alkenes using dihydrogen is still very limited. Some recent representative examples include pincer complexes of Mg, Mn, Fe, Co and Mo containing PN(H)P, PN(H)S, or PNP ligands.[13-17] Interestingly, mechanistic investigations revealed unique reaction pathways for those pincer complexes containing M-N bonds in which ligand participation in the mechanism was crucial. In general terms, their reaction mechanisms can be classified according to the interaction of the hydrogen molecule with the substrate as inner-sphere when the substrate is activated by metal coordination or as outer-sphere when the substrate is activated in the second coordination sphere rather than by direct interaction with the metal.[18]

Despite the variety of known transition metal-sulfur complexes, only a few have been applied to catalytic hydrogenation reactions.[19] This is somewhat surprising taking into consideration the key role of metal-sulfur compounds in biologically relevant hydrogenation processes. For instance, the heterolysis of dihydrogen catalyzed by [NiFe] hydrogenase is likely to proceed through a cooperative H-H bond splitting at the Ni-S bond.[20] In a seminal work by DuBois and coworkers, the catalytic semihydrogenation of alkynes into (*Z*)-alkene using

cyclopentadienyl dinuclear $Mo_2(\mu\text{-}S)_2(\mu\text{-}S_2CH_2)$ complexes in the presence of a Brønsted acid cocatalysts was reported.[21] These dinuclear complexes react with alkynes to afford dithiolene adducts that upon hydrogenation selectively generate the (*Z*)-alkene. Unfortunately, the efficiency of these systems is limited because alkyne excess inhibits the hydrogenation.

Recent work by us in collaboration with Beller's group has shown that cuboidal $Mo_3(\mu_3\text{-}S)(\mu\text{-}S)_3$ clusters are active catalysts for the hydrogenation of various organic substrates.[22-25] Compounds containing the $Mo_3(\mu_3\text{-}S)(\mu\text{-}S)_3$ cluster unit have been widely studied and their chemistry has been recently reviewed.[26] With a handful of exceptions, Mo_3S_4 complexes are electron precise with six cluster skeletal electrons (CSE) for the formation of three metal-metal bonds and a formal oxidation state of IV for the metal atoms. Electrochemical studies show the presence of three sequential one-electron reduction processes ($Mo_3^{IV} \leftrightarrow Mo_2^{IV}Mo^{III} \leftrightarrow Mo^{IV}Mo_2^{III} \leftrightarrow Mo_3^{III}$) or two successive two- and one-electron reductions ($Mo_3^{IV} \leftrightarrow Mo^{IV}Mo_2^{III} \leftrightarrow Mo_3^{III}$) depending on the nature of the terminal ligands.[26] The three metal atoms in the six CSE Mo_3^{IV} clusters define an equilateral triangle. Reduction to the $Mo_2^{IV}Mo^{III}$ seven CSE cluster causes a substantial elongation (*ca.* 0.038 Å) of one of the Mo-Mo distances while the other two remain practically unchanged. DFT studies prove that the origin of this distortion and expansion obeys to electronic factors and localize the unpaired electron in one of the Mo atoms.[27]

Our recent work on alkyne semihydrogenation using Mo_3S_4 cluster catalysts has proved that the selectivity towards the (*Z*)-isomer is strongly dependent on the nature of the outer ligand. While the diamino $[Mo_3S_4Cl_3(dmen)_3]^+$ (dmen = $Me_2NCH_2CH_2NMe_2$) cluster catalyzes the semihydrogenation of diphenylacetylene (dpa) to produce mixtures of (*Z*)- and (*E*)-alkenes (*Z*/*E* *ca.* 6/1) under harsh conditions with moderate yields,[28] the imidazolyl amino $[Mo_3S_4Cl_3(ImNH_2)_3]^+$ cluster performs the selective transformation towards the (*Z*)-alkene under softer conditions with quantitative yields.[29] Based on catalytic and stoichiometric experiments we were able to propose a reaction mechanism for the

$[Mo_3S_4Cl_3(dmen)_3]^+$ cluster, depicted in Figure 4.1a, which starts with the formation of a dithiolene adduct by interaction between the bridging sulfides of the molybdenum cluster complex and the alkyne substrate.

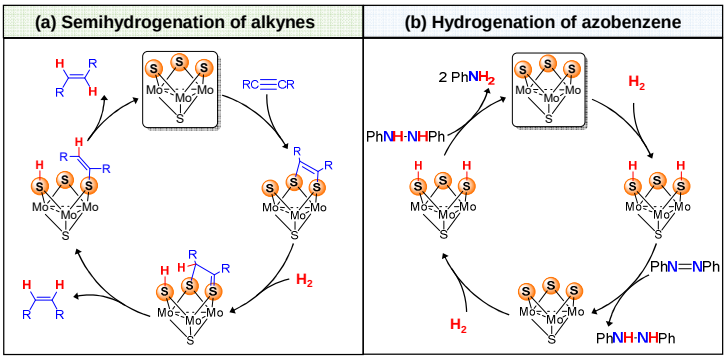

Figure 4.1. Simplified catalytic cycles for (a) alkyne semihydrogenation and (b) azobenzene hydrogenation in the presence of Mo_3S_4 clusters.

Activation of the alkyne by the trinuclear $Mo^{IV}_3(\mu_3\text{-}S)(\mu\text{-}S)_3$ cluster unit occurs without participation of the metal (see Figure 4.1a). During the course of this [3+2] cycloaddition reaction, *i.e.,* alkyne addition to the cluster, the trimetallic unit undergoes a formal two-electron reduction from Mo_3^{IV} to $Mo^{IV}Mo_2^{III}$. This internal electron transfer causes the shortening of one of the Mo-Mo bonds from 2.759 Å, characteristic of a single bond, to 2.653 Å, typical of a double bond. Therefore, the resulting Mo_3S_4 dithiolene cluster contains eight CSE for the formation of two single and one double Mo-Mo bonds.[28] In the next step, H_2 activation occurs at the third bridging sulfur and one of the dithiolene carbon atoms, as shown in Figure 4.1a. This mechanism cannot be categorized as an inner or outer-sphere mechanism, and it is better framed within the category of reductive activation as opposed to oxidative and redox neutral activation.[30] This last classification was recently proposed by Poli based on how the H_2 molecule is activated and transferred to the catalysts and how they alter (or not) the metal formal oxidation state. Although formally speaking a reductive activation mechanism entails the transfer of both hydrogens as protons thus resulting in a two-electron reduction of the metal catalysts, in this case, reduction occurs upon alkyne cycloaddition and hydrogens are formally transferred

as a proton and a hydride. After H_2 activation, the half-hydrogenated intermediate renders the desired (*Z*)-alkene or isomerizes into an analogue from which (*E*)-alkene is released. The relative energies of these two processes, (*Z*)-hydrogenation *vs.* (*E*)-isomerization determine the stereoselectivity of the process.

Cubane-type $Mo^{IV}_3(\mu_3\text{-}S)(\mu\text{-}S)_3$ clusters can also activate H_2 *via* direct interaction of the hydrogen atoms with two of the bridging sulfurs to form a $Mo^{IV}Mo_2^{III}(\mu_3\text{-}S)(\mu\text{-}S\text{-}H)_2(\mu\text{-}S)$ intermediate containing two hydrosulfide groups. We have postulated this mechanism for the catalyzed hydrogenation of azobenzene by the diamino $[Mo_3S_4Cl_3(dmen)_3]^+$ cluster cation (see Figure 4.1b) on the basis of kinetic, stoichiometric and catalytic experiments combined with DFT calculations.[31] In our proposal, H_2 delivers two protons to two of the bridging Mo_3S_4 sulfur atoms while the trimetallic unit gets reduced by two electrons from Mo_3^{IV} to $Mo^{IV}Mo_2^{III}$ so a dihydrogen reductive activation mechanism, according to Poli's classifications, operates in this case. Next, the bis(hydrosulfido) intermediate is able to transfer both hydrogen atoms to azobenzene and to 1,2-diphenylhydrazine to finally afford aniline through two interconnected cycles with similar rate constants. Incidentally, a similar H_2 activation mechanism has been suggested for the hydrogenation of azo compounds using cyclopentadienyl dinuclear $Mo_2(\mu\text{-}S)_2(\mu\text{-}S_2CH_2)$ complexes, although the intimate mechanism of the hydrogen transfer to the azo substrate remains unclarified.[32]

Motivated by the excellent performance of the imidazolyl amino $[Mo_3S_4Cl_3(ImNH_2)_3]^+$ cluster catalyst for the (*Z*)-selective semihydrogenation of diphenylacetylene under mild conditions, we decided to undertake a full mechanistic investigation considering the two potential catalytic cycles represented in Figure 4.1. Despite the relevant differences between both mechanisms, the direct participation of the bridging sulfide ligands in the hydrogenation of unsaturated moieties represents a common feature. Nevertheless, while the sulfur sites act as a platform for the unsaturated bond activation during the hydrogenation of alkynes, they are responsible for the H-H bond cleavage during the hydrogenation of

azobenzene.[28,31] To our surprise, the results point to a mechanism involving the initial activation of H_2 at the μ-S ligands of the cluster to yield an intermediate capable of undergoing two sequential hydrogen atom transfers to the alkyne that entails a spin crossover between singlet and triplet electronic states. This finding reveals the subtle aspects that control the reactivity of the bridging sulfide ligands in these molybdenum sulfide clusters.

4.1.3. Results and discussion

4.1.3.1. Mechanism *via* alkyne addition to the cluster

As starting point, we assume that a mechanism analogous to the one previously reported by our group for the semihydrogenation of diphenylacetylene (dpa),[28] represented in Figure 4.1a, using a diamino Mo_3S_4 cluster catalyst, also operates for the remarkably more active and selective $[Mo_3S_4Cl_3(ImNH_2)_3]^+$ (**1**$^+$) complex.[29] The computed free energy profile is represented in Figure 4.2.

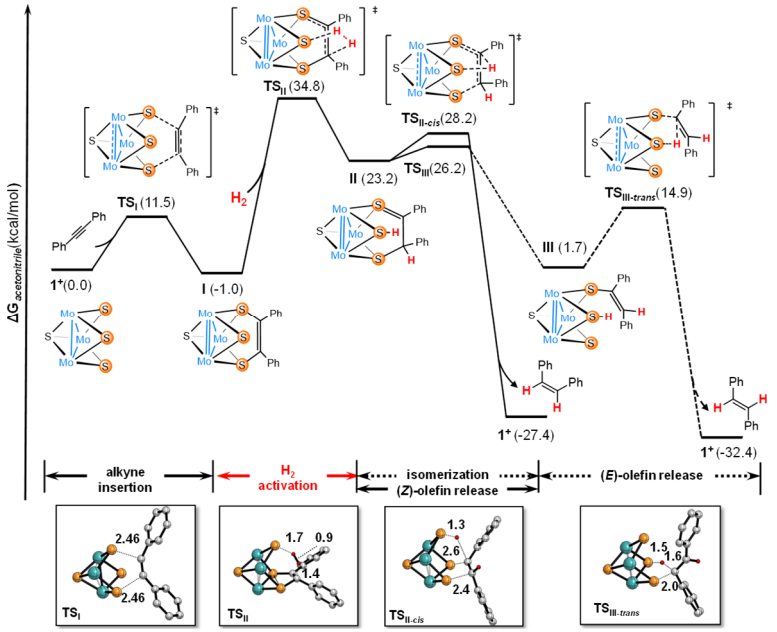

Figure 4.2. Gibbs energy profile for the semihydrogenation of dpa through the dithiolene-mediated mechanism. Free energy values are given in kcal·mol^{-1}, quoted relative to **1**$^+$+ dpa + H_2. Ligands and hydrogen atoms have been omitted for clarity (except vinylic hydrogens). Selected bond distances are given in Å.

The process starts with the [3+2] cycloaddition reaction between the two *sp* C atoms of dpa and two of the three bridging sulfide ligands of the cluster. This reaction has been thoroughly described in the literature, and it is known to proceed with relatively low barriers, as shown in Figure 4.2.[33] At this point, interaction between intermediate **I** and H_2 results in the cleavage of the latter, together with the formation of an S-H and a C-H bonds. With a free energy barrier of 35.8 kcal·mol^{-1}, transition state $\mathbf{TS_{II}}$ represents the computed rate-determining step of the whole process. Unfortunately, such barrier does not agree with the mild experimental conditions required for the catalytic process, and therefore suggests that it is not the operating mechanism. Further comparison of experimental and computed selectivities points towards the same conclusion. From **II**, the (*Z*)-isomer can be released *via* $\mathbf{TS_{II\text{-}}}_{\boldsymbol{cis}}$. Alternatively, **II** can rearrange into **III** through $\mathbf{TS_{III}}$ and afford (*E*)-isomer. Alkene selectivity according to this mechanism is determined by the energy difference between $\mathbf{TS_{II\text{-}}}_{\boldsymbol{cis}}$ and $\mathbf{TS_{III}}$, which feature free energy barriers of 5.0 and 3.0 kcal·mol^{-1}, respectively. Based on these values, (*E*)-stilbene should be the major product (computed enantiomeric excess (*ee*): 89.9), while experimentally this isomer is not observed. Hence, in light of these results this mechanism can be discarded.

4.1.3.2. Mechanism *via* H_2 addition to the cluster

At this point we moved into the computational analysis of an alternative sulfur-mediated pathway reminiscent to that proposed for the hydrogenation of azobenzene.[31,34] This involves (i) hydrogen activation by the sulfide centers of the cluster; (ii) direct interaction with the substrate and (iii) release of the hydrogenated molecule, represented in Figure 4.3.

The initial step of the catalytic cycle entails the homolytic cleavage of H_2 to generate a bis(hydrosulfido) species (see Figure 4.3, H_2 activation). This step is computed to take place *via* $^1\mathbf{TS_1}$ with a free energy barrier of 19.2 kcal·mol^{-1}, leading to intermediate $[Mo_3(\mu_3\text{-}S)(\mu\text{-}S\text{-}H)_2(\mu\text{-}S)(ImNH_2)_3]^+$ ($^1\mathbf{I1}$). The formation of this

species is endergonic by 16.6 kcal·mol^{-1}, and inspection of its structure shows two identical S-H bonds resulting from the homolytic H_2 activation. This addition triggers the shortening of one Mo-Mo bond - from 2.787 to 2.677 Å - indicative of an electronic rearrangement within the system whereby the Mo centers undergo a redox process from Mo_3^{IV} to $Mo^{IV}Mo_2^{III}$.[28,31] The structural parameters of **^{1}I1** suggest the presence of eight cluster skeletal electrons (CSE) in the Mo_3S_4 unit, which prompted us to corroborate the assigned closed-shell singlet configuration. For that purpose, we optimized the **I_1** intermediate as an open-shell singlet and as a triplet (see Table SI4.3). While the open-shell singlet converged to the closed-shell singlet, the triplet state lied 8.3 kcal·mol^{-1} above the singlet state. Incidentally, this mechanism shares common features with the reductive activation pathway whereby H_2 dissociation results in $2H^+$ and $2e^-$.[30]

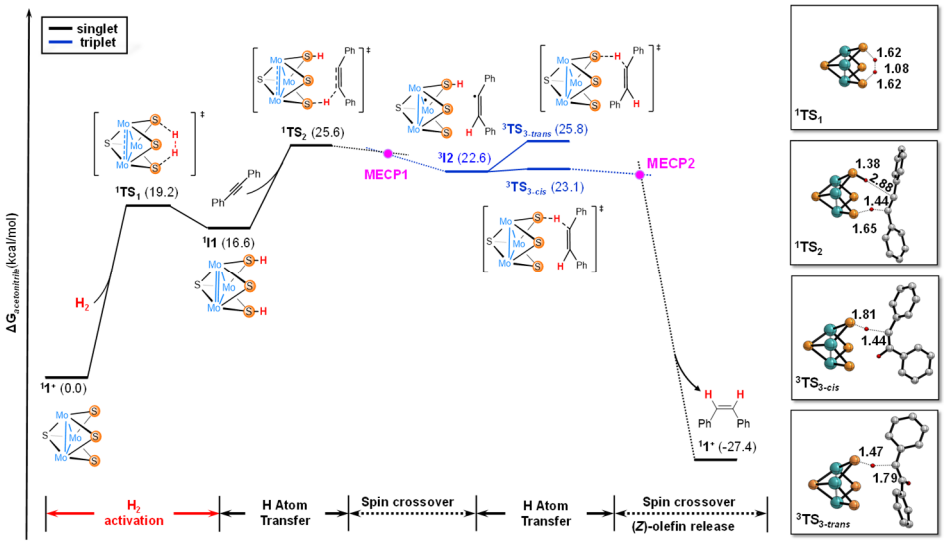

Figure 4.3. Gibbs energy profile for the semihydrogenation of dpa through the bis(hydrosulfido)-mediated mechanism. Free energy profiles for the singlet and triplet states are given in kcal mol^{-1}, quoted relative to **1**$^+$ + dpa + H_2. Ligands and hydrogen atoms have been omitted for clarity (except vinylic hydrogens). Selected bond distances are given in Å.

The subsequent step involves the transfer of the H atoms to dpa to afford the corresponding alkene. All attempts to transfer both H atoms *via* a synchronous transition step were unsuccessful and therefore alternative pathways based on

stepwise processes were considered. As shown in Figure 4.3, the transfer of the first H atom into dpa (^{1}**TS$_2$**) features a relative free energy of 25.6 kcal·mol^{-1}, being the rate-determining step of the whole process. This value is in good agreement with the experimental requirements of moderate pressure (20 bar) and temperature (70 °C) to obtain the product. In fact, a similar tendency was observed in earlier studies on the hydrogenation of unsaturated N=N bonds catalyzed by Mo_3S_4 clusters, whereby the hydrogen transfer also represented the rate-determining step.[31]

From a structural perspective, ^{1}**TS$_2$** features the expected H atom that is being transferred halfway between the sulfide ligand to which it was bound and the alkyne C atom to which it will bind. The product of ^{1}**TS$_2$**, labelled as ^{1}**I2**, features a relative free energy of 24.8 kcal mol^{-1} (see Table SI4.6) and consists of a weakly bound adduct between the half-hydrogenated dpa molecule and the cluster with a single S-H group. A key question at this point is whether this process is best described as the transfer of a proton, a hydrogen atom, or a hydride ligand. For that purpose, the two moieties within **I2** were computed separately considering each of the three possibilities (Table SI4.2). The relative free energy (to the reactants) of these two species when a hydrogen atom transfer (HAT) process occurs is 23.2 kcal mol^{-1}. In contrast, the calculated free energies for these species show significantly higher values, 43.2 and 61.6 kcal·mol^{-1}, for proton and hydride transfers respectively. These findings claim that this process is better framed within a hydrogen atom transfer, not a proton or a hydride transfer.[35]

Considering the above results, we decided to take a closer look at the electronic structure of **I2**.Computation of this adduct in the triplet state (^{3}**I2**) shows a stabilization of 2.2 kcal·mol^{-1} with respect to ^{1}**I2** (22.6 *vs.* 24.8 kcal·mol^{-1}), suggesting the formation of species with unpaired electrons. Single point calculation of the ^{3}**I2** structure as an open-shell singlet results in a value of 3.8 kcal·mol^{-1} above ^{3}**I2** (in terms of electronic energies), confirming its nature as a triplet state (Table SI4.3). Analysis of the distances in the optimized ^{3}**I2** reveals a slight elongation (*ca.* 0.059 Å) of one of the Mo-Mo bonds while the others recovered its initial distances

(Figure SI4.12). As we mentioned before, a similar tendency in the intermetallic distances is found in the $Mo_2^{IV}Mo^{III}$ seven CSE species.[27] Based on these structural parameters, we envisage that one unpaired electron is located in the Mo_3S_4 unit while the other lies in the organic substrate. This assumption is confirmed by the spin density map of **^{3}I2** depicted in Figure 4.4.

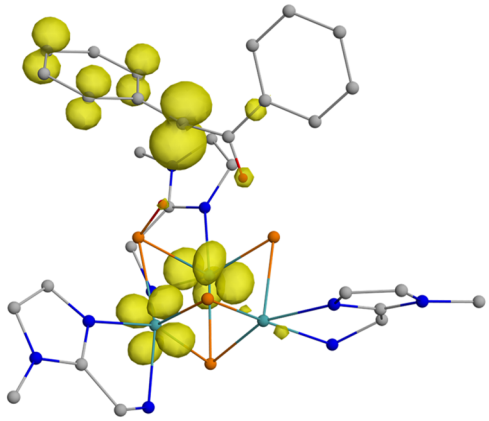

Figure 4.4. Spin density map of intermediate **^{3}I2** calculated at UBP86/6-31G(d,p) level. The isovalue was arbitrarily chosen to be 0.008 au. Hydrogen atoms were omitted for clarity except those contained in the substrate and in the S-H moieties. Color code: Mo (cyan), S (orange), N (blue), C (grey), H (red).

The spin density in the organic moiety is mostly localized on the non-hydrogenated carbon atom, with a minor portion being distributed across the adjacent benzene ring. The rest of the spin density is found on the two Mo-centers bridged by the remaining S-H group (Table SI4.4).

A minimum energy crossing point (MECP1) was computed between **^{1}TS2** and **^{3}I2**, confirming that the first transfer occurs with a spin change. This structure (MECP1) at the BS2 level appears in the potential energy surface 4.6 kcal mol^{-1} below **^{1}TS2**, so the spin crossover is expected to be barrierless. Then, intermediate **^{3}I2** releases either (*Z*) or (*E*)-stilbene through a second H atom transfer and regenerates the initial **1**$^+$ species. The transition states for these processes, namely **^{3}TS$_{3\text{-}cis}$** and **^{3}TS$_{3\text{-}trans}$**, have relative free energies of 23.1 and 25.8 kcal mol^{-1}, respectively. Note that, based on the previous computations, we expect that their counterparts in the

singlet potential energy surface could not be optimized. Comparison of both structures indicate that the higher relative free energy of $^{3'}$**TS3-*trans*** is likely due to the steric hindrance as a result of the interaction between the phenyl rings of the alkyne and the cluster. The energy difference between the two transition states is computed to lead to an enantiomeric excess of 96.3 in favor to the (*Z*)-stilbene in line with the experimental observation.[29] Moreover, $^{3'}$**TS3-*cis*** is only 0.5 kcal mol^{-1} above the adduct ^{3}**I2**, so this second HAT is expected to occur immediately after the formation of the latter species, releasing (*Z*)-stilbene. A minimum energy crossing point (MECP2) was located after $^{3'}$**TS3-*cis*** in order to recover the singlet state and regenerate catalyst **1**$^{+}$.

According to the DFT studies, the bis(hydrosulfido)-mediated mechanism is therefore consistent with the thermodynamic preference and the selectivity control. However, the experimental results confirmed the existence of an equilibrium with the cycloaddition product $[Mo_3S_4Cl_3(ImNH_2)_3(dpa)]^+$ along the reaction course. In order to get a better understanding of the plausible mechanism, both catalytic cycles are summarized in Scheme 4.1.

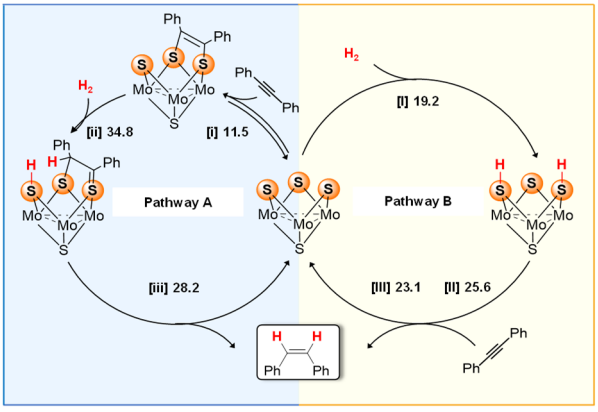

Scheme 4.1. Schematic representation of the proposed catalytic cycles for the semihydrogenation of dpa catalyzed by **1**$^{+}$. Relative free energies for the TSs are given in kcal mol^{-1}.

The first step of the catalytic cycles entails the formation of the dithiolene (pathway A) *vs.* bis(hydrosulfido) (pathway B) species. It should be noted that the formation of the dithiolene adduct (pathway A) was computed to feature a relatively

low free energy barrier (11.5 kcal·mol^{-1}, pathway A), with the step being slightly exergonic by -1.0 kcal mol^{-1}. This supports the experimentally observed equilibrium between the trinuclear cluster and the dithiolene adduct.[29] The dynamic character of the system plays a critical role in the mechanism since both species, the cluster and the dithiolene complex, are in solution leading to the interconnection of the two catalytic cycles. From this situation, the formation of the hydrosulfido S-H bonds ([I], pathway B) on **1**$^{+}$ has the lowest computed barrier for the H_2 activation ($\Delta G^{\ddagger}$ = 19.2 kcal·mol^{-1}). In contrast, the cleavage of the hydrogen molecule *via* interaction with the cycloaddition product ([ii], pathway A) is too energy-demanding to take place under these reaction conditions ($\Delta G^{\ddagger}$ = 34.8 kcal·mol^{-1}). Considering all the gathered information, we believe that an equilibrium between the cluster and the dithiolene complex is initially established, which supports the initial detection of the aforementioned complex. However, hydrogenation of the dithiolene adduct is too energy-demanding in comparison with the activation of H_2 at **1**$^{+}$, and therefore the system is forced to continue through pathway B (Scheme 4.1).

4.1.3.3. Experimental investigations

To further verify the proposed mechanism, a series of experiments aimed to obtain additional mechanistic evidences were conducted (see 4.1.5. Experimental Section for more details on the procedure). The proposed mechanism involves the participation of hydrosulfido moieties in the catalytic cycle, which possess an acidic character,[36] as revealed by the measured pK_a values of some bimetallic hydrosulfide complexes.[37] Regarding trinuclear molybdenum sulfide clusters, a value of 4.1 (calculated pK_a)[31] was obtained which follows the same tendency as its dinuclear analogues. Based on these considerations, we envisaged that the introduction of a solvent with an acidic deuterium (D) atom with a higher pK_a could result in the exchange of the S-H groups to S-D at a faster rate than the H transfer to the alkyne, thus labeling the vinylic positions. The results of deuterium labeling experiments are shown in Scheme 4.2, where the deuterium content has been obtained by integration

of the vinylic and the aromatic CH signals in the ^{1}H-NMR spectra (see 4.2. Supporting Information: Figures SI4.1-SI4.11).

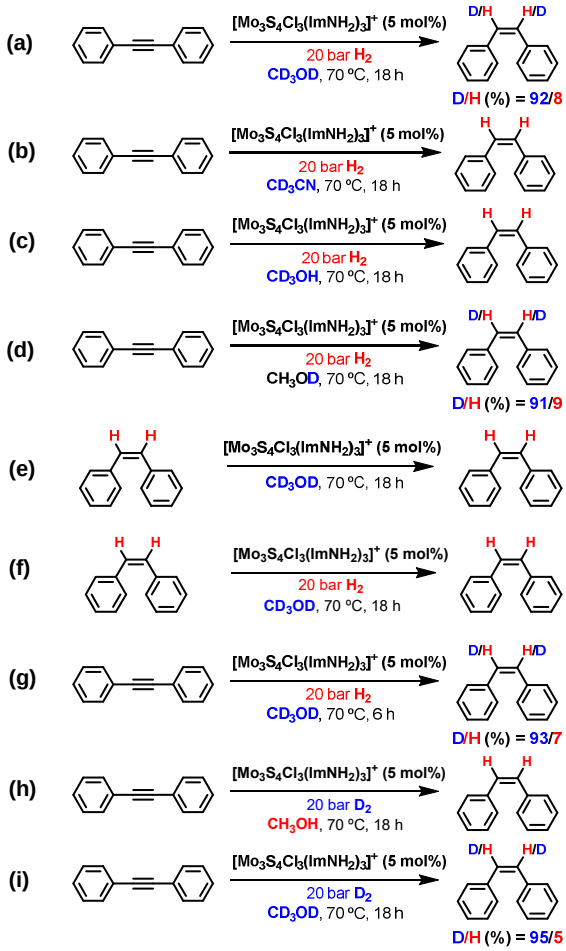

Scheme 4.2. Deuterium labeling experiments upon (a-b) different deuterated solvents, (c-d) deuteration position (CH_3OD and CD_3OH), (g) lower reaction time and (h-i) using D_2 as reducing agent. (e-f) Deuteration of (*Z*)-stilbene was also assessed.

The results clearly indicate that deuterium was highly incorporated (deuteration degree: >90%) into both olefinic positions when CD_3OD or CH_3OD were used as solvent (Scheme 4.2: [a] and [d], Figure SI4.2 and SI4.4). The deuteration degree was not quantitative due to water traces in the solvent which also exchange with the S-H/D moieties. In contrast, no signal of deuteration was observed when using CD_3CN or CD_3OH as solvent (Scheme 4.2: [b] and [c], Figure

SI4.1 and SI4.3), thus showing that the source of deuterium atoms in (*Z*)-stilbene are those in the alcoholic group of methanol.

Additional experiments ruled out the possibility that the deuterium atoms in (*Z*)-stilbene were result of a hydrogen isotope exchange (HIE) or reductive deuteration processes of the alkyne.[38] Direct C-H activation through a HIE process rendering H/D exchange [39] can be discarded by the absence of deuterated product when (*Z*)-stilbene is dissolved in CD_3OD (Scheme 4.2[e], Figure SI4.5). The same tendency was observed including H_2 gas during the catalytic reaction (Scheme 4.2[f], Figure SI4.6). These results preclude a HIE reaction after releasing (*Z*)-stilbene from the semihydrogenation reaction.[38] In fact, when the reaction was performed at shorter times, comparative deuterium contents to those obtained after 18 hours were observed (Scheme 4.2[g], Figure SI4.7). The possibility of deuterium atoms being incorporated into dpa by interaction with deuterated or semideuterated hydrogen, either added as D_2 or resulting from H_2 exchange with S-D groups, can be also ruled out on the basis of entries [f], [g], [h] and [i] of Scheme 4.2 (Figures SI4.6-SI4.9). The absence of deuterated (*Z*)-stilbene in the entry [h] can be rationalized considering the very rapid exchange between the S-D moieties just formed and the O-H groups of the methanol, that would take place before the alkyne approach to the hydrogenated cluster. Incidentally, the presence of water traces in CD_3OD was confirmed when deuterium gas is used as reductant (Scheme 4.2[i], Figure SI4.9) because a 5% of the hydrogenated product was observed.

Thus, deuterium labeling experiments provide support to the formation of intermediates containing S-H groups. In addition, an important difference between the computed mechanisms above is that only one S-H group is formed in the mechanism involving initial cycloaddition of the alkyne (Scheme 4.1, pathway A) whereas two S-H groups are formed in the mechanism involving initial H_2 activation (Scheme 4.1, pathway B). Thus, both mechanisms are expected to differ in the number of C-H bonds of (*Z*)-stilbene that will be deuterated, one in the dithiolene mechanism and two in the mechanism involving initial H_2 activation. The

experimental results showing that both C-H groups in (*Z*)-stilbene are deuterated clearly favor the mechanism involving the initial addition of H_2 to the cluster to form an intermediate with two S-H groups.

As pointed out above, we have previously reported that the related $[Mo_3S_4Cl_3(dmen)_3]^+$ cluster also catalyzes the semihydrogenation of dpa,[28] although with a lower efficiency and selectivity, and proposed a mechanism similar to that depicted in Figure 4.2 for $\mathbf{1}^+$. Given the present results, which clearly point towards a different reaction mechanism, we decided to carry out deuteration experiments also for the $[Mo_3S_4Cl_3(dmen)_3]^+$ cluster. Experiments in CH_3OH indicate that hydrogenation occurs with a yield of 24% using 90 °C, 40 bar H_2, 12 mol% of catalyst and 65 hours, thus confirming the lower catalytic activity of this cluster (Figure SI4.10). As observed in CH_3CN, a mixture of (*Z*) and (*E*)-isomers in *ca.* 6:1 ratio is formed. When the experiments with $[Mo_3S_4Cl_3(dmen)_3]^+$ are carried out in CD_3OD, significant deuteration (78%) of (*Z*)-stilbene is observed (Figure SI4.11). Unfortunately, the deuteration degree of the (*E*)-isomer could not be determined because the signal for its vinylic protons overlaps with those for the aromatic protons of the (*Z*)-isomer, which is the major product. Yet, the 78% deuteration degree for (*Z*)-stilbene is halfway between those expected for the previously reported mechanism and the one proposed here for $\mathbf{1}^+$, thus suggesting that both mechanisms are competitive in the case of the $[Mo_3S_4Cl_3(dmen)_3]^+$ cluster. At this point, we calculated the energy of the rate-determining transition state with the new mechanistic proposal ($^1\mathbf{TS_2}$, Figure 4.3) for the $[Mo_3S_4Cl_3(dmen)_3]^+$ cluster (Table SI4.7). The free energy value of $^1\mathbf{TS_{2dmen}}$ is 33.1 kcal mol^{-1}, that is 7.5 kcal mol^{-1} above the calculated $^1\mathbf{TS_2}$ (25.6 kcal·mol^{-1}) for $\mathbf{1}^+$. The energy of $\mathbf{TS_{IIdmen}}$ was previously reported to be of 42.0 kcal mol^{-1},[28] also significantly larger than for $\mathbf{1}^+$ (see $\mathbf{TS_{II}}$, Figure 4.2) , thus showing that independently of the actual reaction mechanism operating for the dmen cluster, its reaction is much slower than that of $\mathbf{1}^+$. However, the difference between the energies corresponding to both mechanisms for $[Mo_3S_4Cl_3(dmen)_3]^+$ is of 8.9 kcal mol^{-1}, very close to the

corresponding value for **1**$^{+}$ (9.2 kcal mol^{-1}), which indicates that the mechanism in Figure 4.3 should be also preferred in the case of $[Mo_3S_4Cl_3(dmen)_3]^+$. With these results, we cannot give a satisfactory explanation to the reasons leading to the operation of both mechanisms in the case of this dmen cluster, which are probably related to subtle aspects not captured by the present calculations.

4.1.4. Conclusions

Computational and experimental studies on the selective semihydrogenation of dpa catalyzed by cluster $[Mo_3S_4Cl_3(ImNH_2)_3]^+$ (**1**$^{+}$) reveals that the previously proposed mechanism for the related $[Mo_3S_4Cl_3(dmen)_3]^+$ cluster, in which there is initial cycloaddition of the alkyne to two bridging S, is unable to explain the major experimental findings for **1**$^{+}$: milder reaction conditions; higher selectivity towards the (*Z*)-isomer; and complete deuteration of the reaction product. In contrast, a thorough exploration allowed us to propose a novel mechanism reminiscent of that recently reported for the hydrogenation of azobenzene that accounts for the experimental results. The first step entails the H_2 activation in the sulfur units that generates the $[Mo_3(\mu_3\text{-}S)(\mu\text{-}S\text{-}H)_2(\mu\text{-}S)]^+$ intermediate, followed by two consecutive hydrogen atom transfers (HAT) from the bis(hydrosulfido) species to the alkyne. The product of the first HAT can be formally described as a radical pair with one of the unpaired electrons in the Mo_3S_4 moiety and the other in the semihydrogenated alkyne. As a result of the unpaired electrons that the system features, a spin crossover process between the singlet and the triplet spin states is necessary along the first HAT. In the final step, the radical pair species undergo a quasi-barrierless second HAT with another concomitant spin crossover - from triplet to singlet state - to release the (*Z*)-stilbene and to regenerate the **1**$^{+}$ cluster. The computations indicate that the unobserved (*E*)-stilbene could also be formed from this radical pair, however, steric effects result in an energy barrier 2.7 kcal mol^{-1} higher, which is in line with the exclusive formation of (*Z*)-stilbene. Remarkably, the deuteration of the vinylic positions in the (*Z*)-stilbene was achieved using H_2 and non-expensive

CD_3OD, thus opening new avenues for the synthesis of labelled molecules using molybdenum sulfide clusters as catalysts in reductive deuteration reactions.

4.1.5. Experimental section

4.1.5.1. General remarks

The $[Mo_3S_4Cl_3(ImNH_2)_3]BF_4$ and $[Mo_3S_4Cl_3(dmen)_3]BF_4$ catalysts were prepared according to the published procedure.[24,29] All other reagents were obtained from commercial sources and used as received. ^1H NMR spectra were recorded on a Bruker Avance III HD 400 MHz spectrometer using *d*$_6$-dimethylsulfoxide (DMSO) as solvent. Gas chromatography analysis was performed on an Agilent 7820A GC System equipped with a FID and a capillary column Agilent (HP-5, 30 m x 0.32 mm x 0.25 mm).

4.1.5.2. Catalytic activity tests

General procedure for the catalytic semihydrogenation of diphenylacetylene: A 4 mL glass vial containing a stirring bar was sequentially charged with the corresponding molybdenum catalyst (4.5 mg, 0.005 mmol of $[Mo_3S_4Cl_3(ImNH_2)_3]BF_4$]), diphenylacetylene (18.0 mg, 0.1 mmol), n-hexadecane (15 μL; added as an internal standard) and 2 mL of the corresponding solvent (CH_3CN, CD_3CN, CD_3OD, CH_3OD, CD_3OH). Afterwards, the reaction vial was capped with a screw cap containing a septum with a needle and set in the alloy plate, which was then placed into a 300 mL autoclave. The sealed autoclave was purged three times with 30 bar of hydrogen before setting the pressure at 20 bar. Then, it was placed into an aluminum block which was preheated with at 70 °C. After 18 h, the autoclave was cooled to room temperature and the hydrogen was released. Ethyl acetate (2 mL) was then added, and a sample was analyzed by GC. To determine the deuterium content, the reaction mixture was taken to dryness *via* rotatory evaporation and solved in a deuterated solvent (*d*$_6$-DMSO).

4.1.5.3. Computational details

All the density functional theory (DFT) calculations were performed with Gaussian 09 (Revision D.01).[40] Geometry optimizations were carried out at the BP86/BS1 level,[41,42] where Mo and S atoms were described using the SDD relativistic ECP and associated basis set,[43] added polarization functions for the latter (ζ = 0.503),[44] and the remaining atoms were described with the 6-31G(d,p) basis set.[45,46] Solvent effects (acetonitrile, ε = 35.688) were included self-consistently in these optimizations through the PCM method.[47,48] All stationary points were characterized at this level of theory by analytical frequency calculations as either minima (all positive eigenvalues) or transition states (one imaginary eigenvalue), while intrinsic reaction coordinate (IRC) calculations and subsequent geometry optimizations were used to confirm the minima linked by each transition state. The frequency calculations were also used to obtain the thermochemistry corrections (zero-point, thermal and entropic energies) at the experimental temperature (343.15 K) and at the standard 1 atm pressure, based on the IGRRHO (ideal gas/rigid rotor/harmonic oscillator) approach. However, this pressure and temperature do not correspond to the 1 M concentration of the standard state used for species reacting in solution. Therefore, corrections (2.275 kcal·mol^{-1}) were applied to all Gibbs values to change the standard state to 1M at 343.15 K. This correction has been calculated using the formula $RTlnV_m$= 2.275 kcal·mol^{-1}, where V_m = 28.1 L·mol^{-1} and corresponds to the molar volume of an ideal gas at 1 atm and 343.15 K.

Improved energetic values were obtained by performing single-point energy calculations with a larger basis set system (BS2), also including solvent effects through the PCM method.[47,48] BS2 differs from BS1 in the employment of the 6-311+G(2d,2p) to describe Cl, C, N, O and H atoms. In addition, single-point dispersion corrections were computed using Grimme's D3 (zero damping) parameter set.[49] Thus, the Gibbs energies in acetonitrile($G_{acetonitrile}$) shown in the text were obtained adding to the potential energies in acetonitrile calculated at BP86/BS2, the Gibbs contribution at the BP86/BS1 level, the dispersion correction

and the standard state correction. All the above energetic values are provided in Table SI4.6.

The minimum energy crossing points (MECPs) were located using Harvey's algorithm combined with Gaussian 09.[50] The three-dimensional (3D) structures were depicted using CYLview software and VESTA for the spin density map.[51,52]

4.1.6. References

[1] K. C. K. Swamy, A. S. Reddy, K. Sandeep, A. Kalyani, *Tetrahedron Lett.* **2018**, *59*, 419-429.

[2] H. U. Blaser, C. Malan, B. Pugin, F. Spindler, H. Steiner, M. Studer, *Adv. Synth. Catal.* **2003**, *345*, 103-151.

[3] G. J. Kubas, *J. Organomet. Chem.* **2014**, *751*, 33-49.

[4] M. Garbe, S. Budweg, V. Papa, Z. Wei, H. Hornke, S. Bachmann, M. Scalone, A. Spannenberg, H. Jiao, K. Junge, M. Beller, *Catal. Sci. Technol.* **2020**, *10*, 3994-4001.

[5] R. Kumar, M. K. Pandey, A. Bhandari, J. Choudhury, *ACS Catal.* **2023**, *13*, 4824-4834.

[6] J. Luo, Y. Liang, M. Montag, Y. Diskin-Posner, L. Avram, D. Milstein, *J. Am. Chem. Soc.* **2022**, *144*, 13266-13275.

[7] Y. Wu, Y. Ao, Z. Li, C. Liu, J. Zhao, W. Gao, X. Li, H. Wang, Y. Liu, Y. Liu, *Nat. Commun.* **2023**, *14*, 1655.

[8] S. Shekhar, T. S. Ahmed, A. R. Ickes, M. C. Haibach, *Org. Process Res. Dev.* **2022**, *26*, 14-42.

[9] J. Loup, U. Dhawa, F. Pesciaioli, J. Wencel-Delord, L. Ackermann, *Angew. Chemie - Int. Ed.* **2019**, *58*, 12803-12818.

[10] K. D. Vogiatzis, M. V. Polynski, J. K. Kirkland, J. Townsend, A. Hashemi, C. Liu, E. A. Pidko, *Chem. Rev.* **2019**, *119*, 2453-2523.

[11] D. Decker, H. J. Drexler, D. Heller, T. Beweries, *Catal. Sci. Technol.* **2020**, *10*, 6449-6463.

[12] B. J. Gregori, M. O. W. S. Schmotz, A. Jacobi von Wangelin, *ChemCatChem* **2022**, *14*, e202200886.

[13] Y. Liang, U. K. Das, J. Luo, Y. Diskin-Posner, L. Avram, D. Milstein, *J. Am. Chem. Soc.* **2022**, *144*, 19115-19126.

[14] V. Zubar, J. Sklyaruk, A. Brzozowska, M. Rueping, *Org. Lett.* **2020**, *22*, 5423-5428.

[15] N. Gorgas, J. Brünig, B. Stöger, S. Vanicek, M. Tilset, L. F. Veiros, K. Kirchner, *J. Am. Chem. Soc.* **2019**, *141*, 17452-17458.

[16] C. Chen, Y. Huang, Z. Zhang, X. Q. Dong, X. Zhang, *Chem. Commun.* **2017**, *53*, 4612-4615.

[17] N. F. Both, A. Spannenberg, K. Junge, M. Beller, *Organometallics* **2022**, *41*, 1797-1805.

[18] A. Comas-Vives, G. Ujaque, A. Lledós, in *Adv. in Inorg. Chem.*, **2010**, 231-260.

[19] L. Omann, C. D. F. Königs, H. F. T. Klare, M. Oestreich, *Acc. Chem. Res.* **2017**, *50*, 1258-1269.

[20] W. Lubitz, H. Ogata, O. Rüdiger, E. Reijerse, *Chem. Rev.* **2014**, *114*, 4081-4148.

[21] M. R. Dubois, *Chem. Rev.* **1989**, *89*, 1-9.

[22] I. Sorribes, G. Wienhöfer, C. Vicent, K. Junge, R. Llusar, M. Beller, *Angew. Chemie - Int. Ed.* **2012**, *51*, 7794-7798.

[23] E. Pedrajas, I. Sorribes, A. L. Gushchin, Y. A. Laricheva, K. Junge, M. Beller, R. Llusar, *ChemCatChem* **2017**, *9*, 1128-1134.

[24] E. Pedrajas, I. Sorribes, K. Junge, M. Beller, R. Llusar, *Green Chem.* **2017**, *19*, 3764-3768.

[25] V. S. Safont, I. Sorribes, J. Andrés, R. Llusar, M. Oliva, M. R. Ryzhikov, *Phys. Chem. Chem. Phys.* **2019**, *21*, 17221-17231.

[26] A. L. Gushchin, Y. A. Laricheva, M. N. Sokolov, R. Llusar, *Russ. Chem. Rev.* **2018**, *87*, 670-706.

[27] P. A. Petrov, D. Y. Naumov, R. Llusar, C. J. Gómez-García, V. Polo, S. N. Konchenko, *Dalt. Trans.* **2012**, *41*, 14031-14034.

[28] A. G. Algarra, E. Guillamón, J. Andrés, M. J. Fernández-Trujillo, E. Pedrajas, J. Á. Pino-Chamorro, R. Llusar, M. G. Basallote, *ACS Catal.* **2018**, *8*, 7346-7350.

[29] M. Gutiérrez-Blanco, E. Guillamón, V. S. Safont, A. G. Algarra, M. J. Fernández-Trujillo, K. Junge, M. G. Basallote, R. Llusar, M. Beller, *Inorg. Chem. Front.* **2023**, *10*, 1786-1794.

[30] R. Poli, *Advances in Organometallic Chemistry*, **2023**, 87-133.

[31] E. Guillamón, M. Oliva, J. Andrés, R. Llusar, E. Pedrajas, V. S. Safont, A. G. Algarra, M. G. Basallote, *ACS Catal.* **2021**, *11*, 608-614.

[32] M. McKenna, L. L. Wright, D. J. Miller, L. Tanner, R. C. Haltiwanger, M. R. DuBois, *J. Am. Chem. Soc.* **1983**, *105*, 5329-5337.

[33] A. G. Algarra, M. G. Basallote, R. van Eldik, in *Adv. Inorg. Chem.*, **2017**, 311-342.

[34] C. J. Casewit, D. E. Coons, L. L. Wright, W. K. Miller, M. R. DuBois, *Organometallics* **1986**, *5*, 951-955.

[35] R. G. Agarwal, S. C. Coste, B. D. Groff, A. M. Heuer, H. Noh, G. A. Parada, C. F. Wise, E. M. Nichols, J. J. Warren, J. M. Mayer, *Chem. Rev.* **2022**, *122*, 1-49.

[36] S. Kuwata, M. Hidai, *Coord. Chem. Rev.* **2001**, *213*, 211-305.

[37] J. Birnbaum, G. Godziela, M. Maciejewski, T. L. Tonker, R. C. Haltiwanger, M. R. DuBois, *Organometallics* **1990**, *9*, 394-401.

[38] S. Kopf, F. Bourriquen, W. Li, H. Neumann, K. Junge, M. Beller, *Chem. Rev.* **2022**, *122*, 6634-6718.

[39] G. Prakash, N. Paul, G. A. Oliver, D. B. Werz, D. Maiti, *Chem. Soc. Rev.* **2022**, *51*, 3123-3163.

[40] M. J. Frisch. G. W. Trucks. H. B. Schlegel. G. E. Scuseria. M. A. Robb. J. R. Cheeseman. G. Scalmani. V. Barone. B. Mennucci. G. A. Petersson. H. Nakatsuji. M. Caricato. X. Li. H. P. Hratchian. A. F. Izmaylov. J. Bloino. G. Zheng. J. L. Sonnenberg. M. Had, **2013**.

[41] J. P. Perdew, *Phys. Rev. B* **1986**, *33*, 8822-8824.

[42] A. D. Becke, *Phys. Rev. A* **1988**, *38*, 3098-3100.

[43] D. Andrae, U. Häubermann, M. Dolg, H. Stoll, H. Preub, *Theor. Chim. Acta* **1990**, *77*, 123-141.

[44] A. Hollwarth, M. Bohme, S. Dapprich, A. W. Ehlers, A. Gobbi, V. Jonas, K. F. Kohler, R. Stegmann, A. Veldkamp, G. Frenking, Chem. Phys. Letters **1993**, *208*, 237-240.

[45] W. J. Hehre, R. Ditchfield, J. A. Pople, *J. Chem. Phys* **1972**, *56*, 2257-2261.

[46] P. C. Harihanan, J. A. Pople, *Theor. Chim. Acta* **1973**, *28*, 213-222.

[47] M. Cossi, G. Scalmani, N. Rega, V. Barone, *J. Chem. Phys* **2002**, *117*, 43-54.

[48] J. Tomasi, B. Mennucci, R. Cammi, *Chem. Rev.* **2005**, *105*, 2999-3093.

[49] S. Grimme, J. Antony, S. Ehrlich, H. Krieg, *J. Chem. Phys.* **2010**, *132*, 154104.

[50] J. Harvey, *Coord. Chem. Rev.* **2003**, *238-239*, 347-361.

[51] C. Y. Legault, CYLview 1.0b. Université de Sherbrooke, **2009**.

[52] K. Momma, F. Izumi, *J. Appl. Crystallogr.* **2011**, *44*, 1272-1276.

4.2. Supporting information

4.2.1. Mechanistic experiments

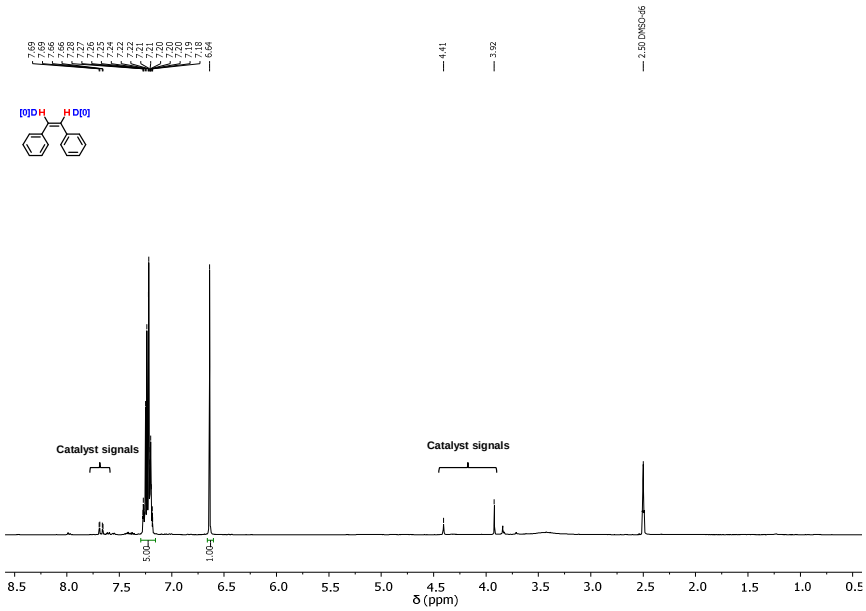

Figure SI4.1. ^{1}H NMR (400 MHz, DMSO, 298 K) spectrum of the reaction mixture after the standard catalytic conditions.

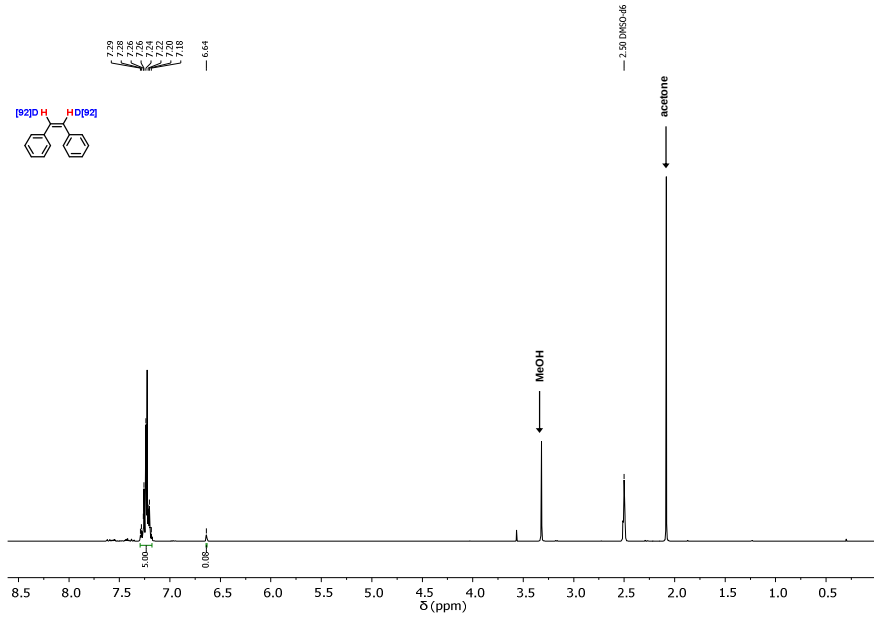

Figure SI4.2. ^{1}H NMR (400 MHz, DMSO, 298 K) spectrum of the reaction mixture after the catalytic protocol using *d*$_4$-methanol as solvent.

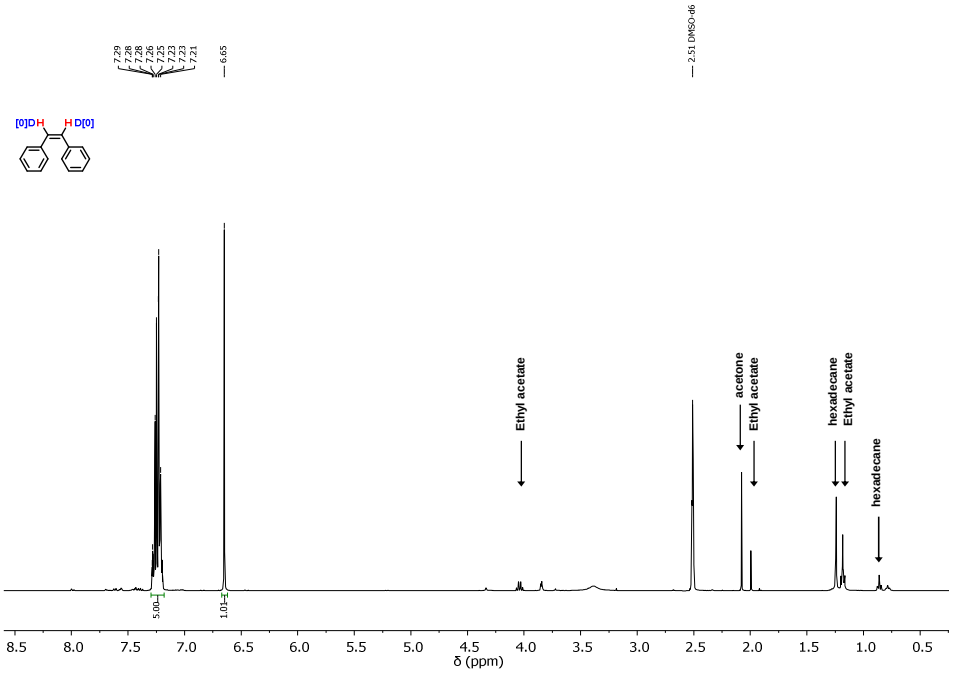

Figure SI4.3. ^{1}H NMR (400 MHz, DMSO, 298 K) spectrum of the reaction mixture after the catalytic protocol using d_3-methanol as solvent.

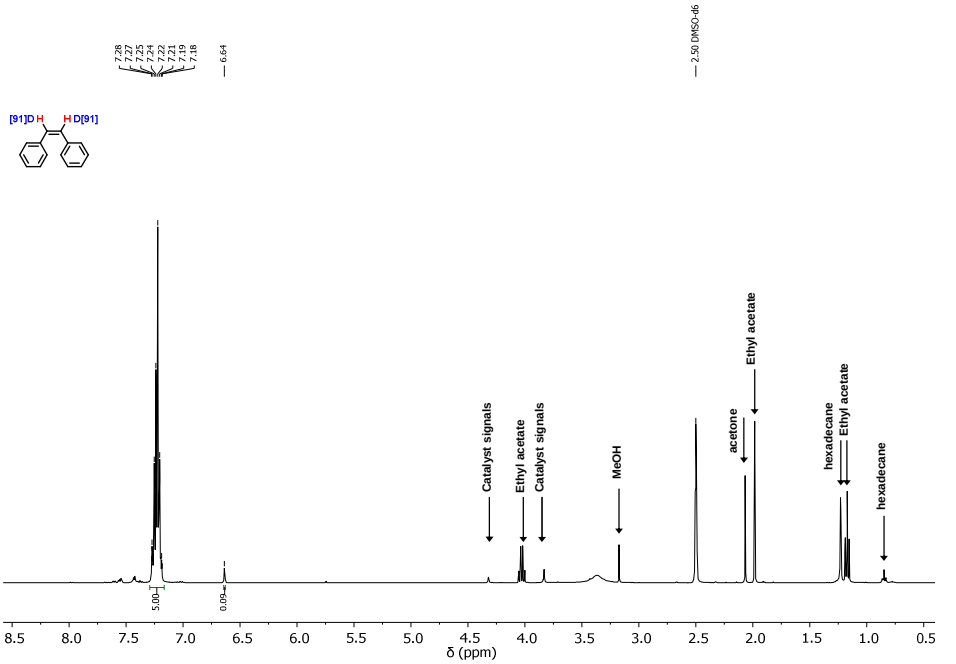

Figure SI4.4. ^{1}H NMR (400 MHz, DMSO, 298 K) spectrum of the reaction mixture after the catalytic protocol using d_1-methanol as solvent.

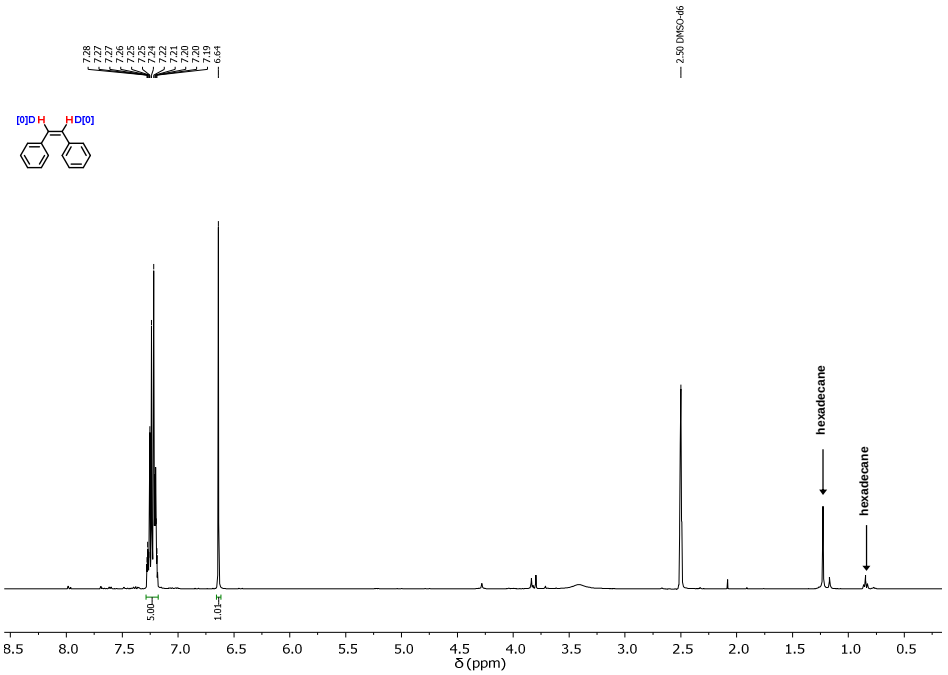

Figure SI4.5. ^{1}H NMR (400 MHz, DMSO, 298 K) spectrum after reacting (*Z*)-stilbene in the standard catalytic conditions in the absence of H_2 using *d*$_4$-methanol as solvent.

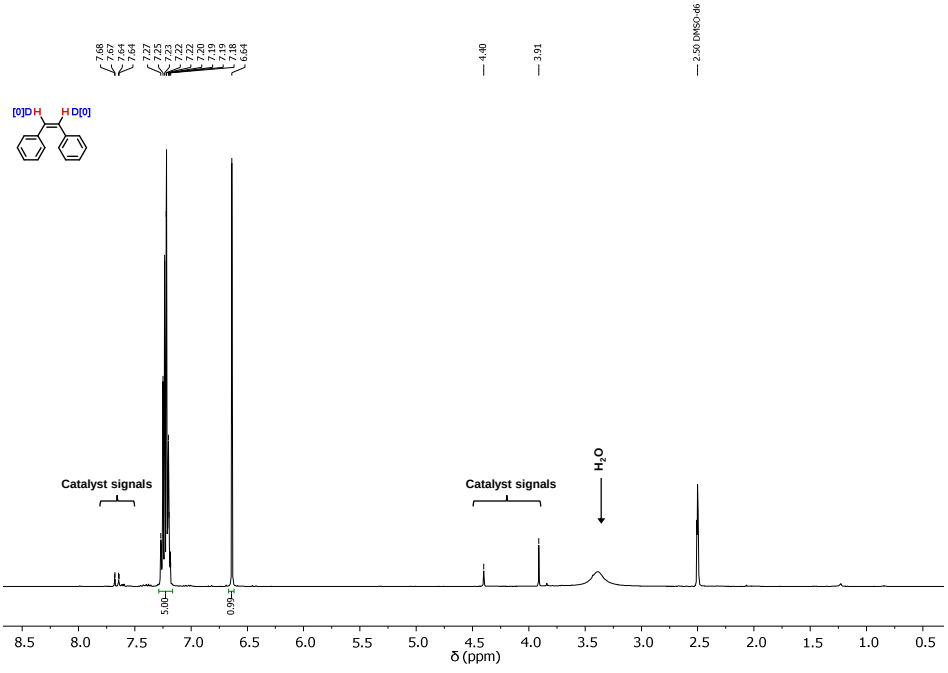

Figure SI4.6. ^{1}H NMR (400 MHz, DMSO, 298 K) spectrum after reacting (*Z*)-stilbene in the standard catalytic conditions using *d*$_4$-methanol as solvent.

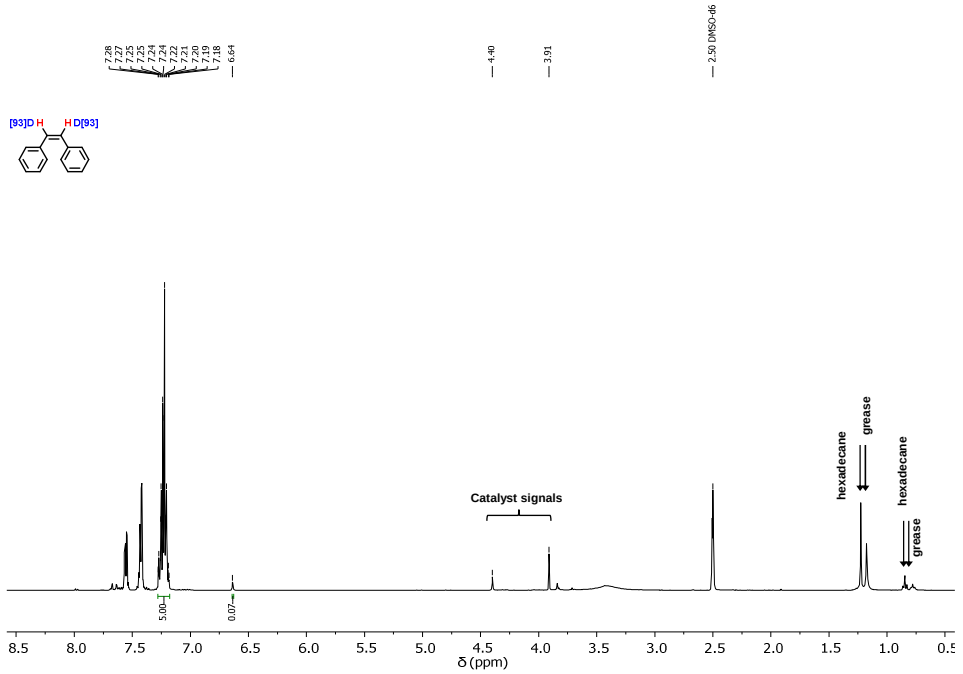

Figure SI4.7. ^{1}H NMR (400 MHz, DMSO, 298 K) spectrum of the reaction mixture after standard catalytic conditions at t = 6 hours.

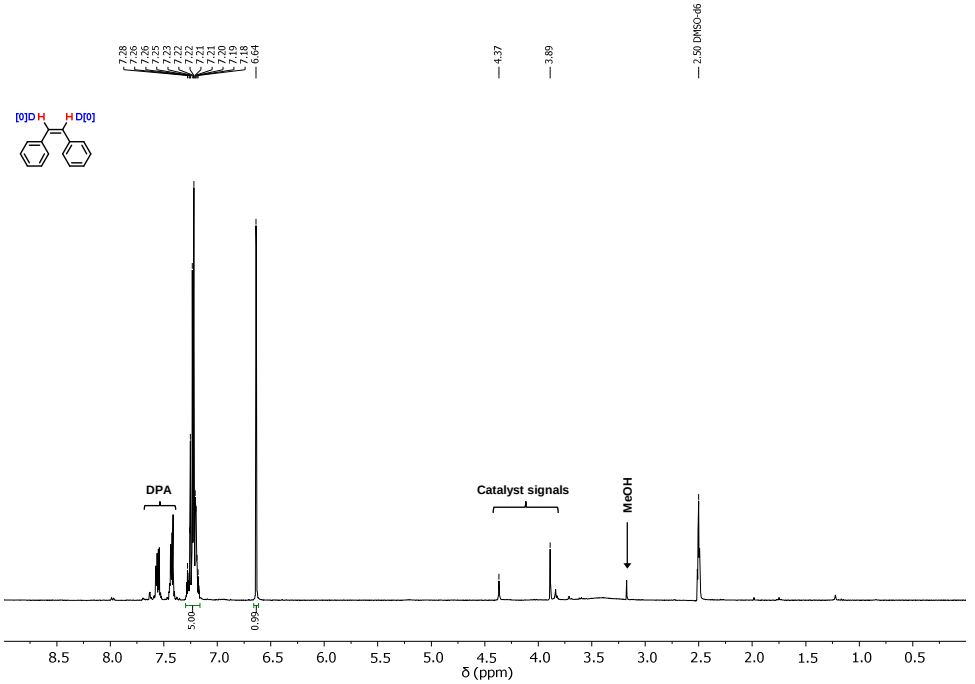

Figure SI4.8. ^{1}H NMR (400 MHz, DMSO, 298 K) spectrum of the reaction mixture after standard catalytic conditions using D_2 gas as reductant.

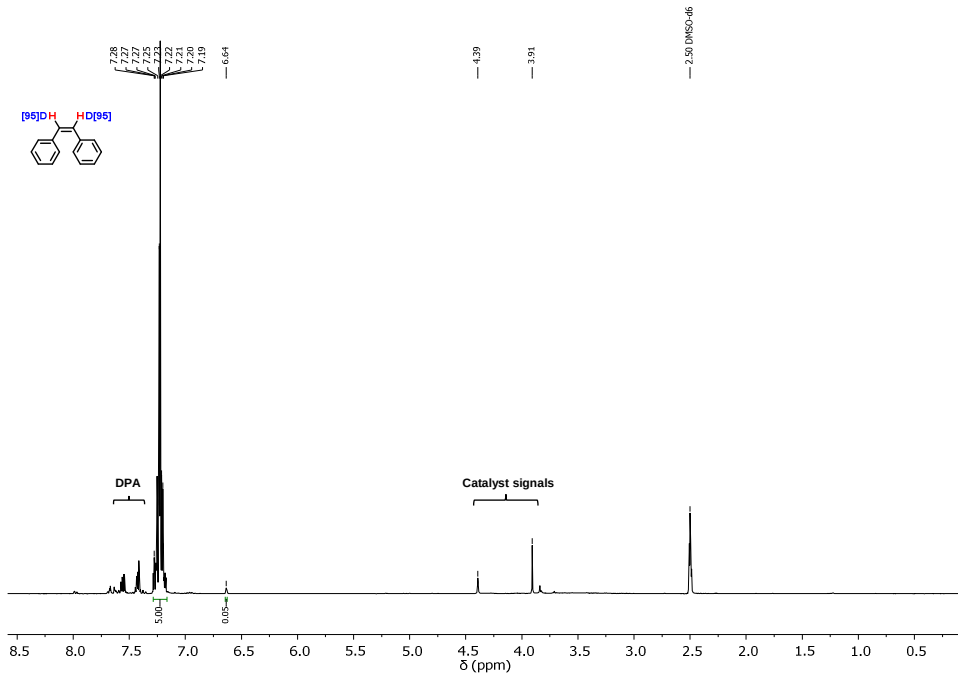

Figure SI4.9. ^{1}H NMR (400 MHz, DMSO, 298 K) spectrum of the reaction mixture after standard catalytic conditions using D_2 gas as reductant and d_4-methanol as solvent.

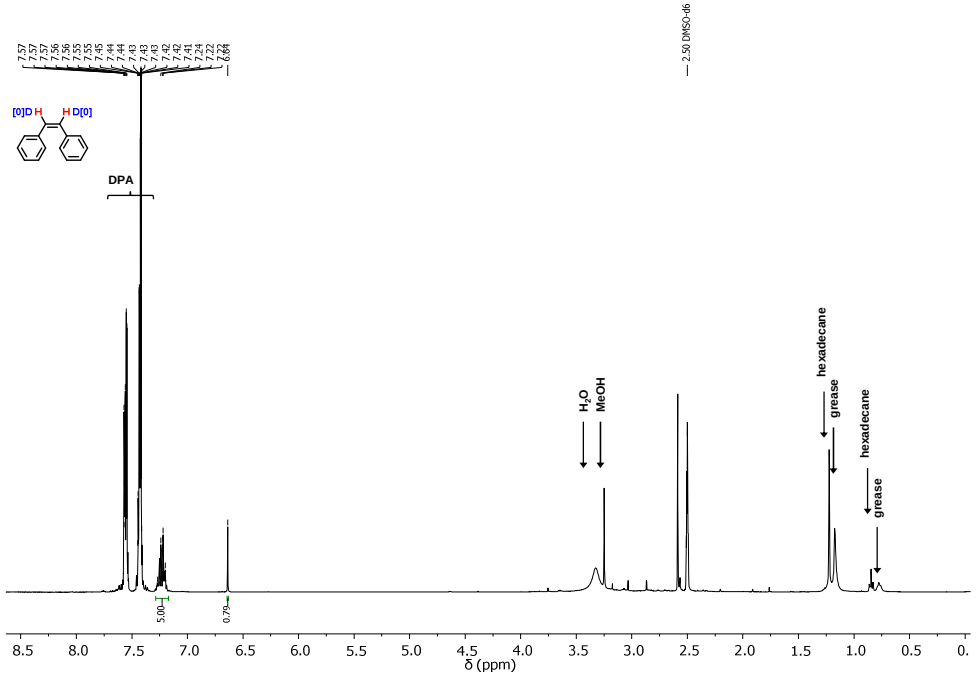

Figure SI4.10. ^{1}H NMR (400 MHz, DMSO, 298 K) spectrum of the reaction mixture catalyzed by $[Mo_3S_4Cl_3(dmen)_3]^+$ complex under the catalytic conditions.

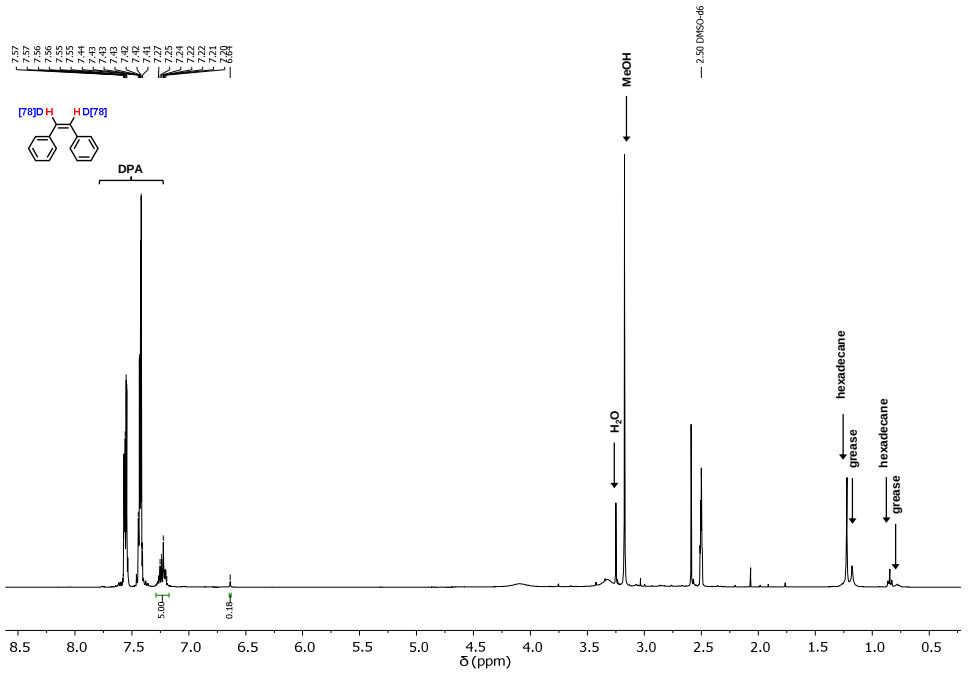

Figure SI4.11. ^{1}H NMR (400 MHz, DMSO, 298 K) spectrum of the reaction mixture catalyzed by $[Mo_3S_4Cl_3(dmen)_3]^+$ complex under the catalytic conditions using.*d*$_4$-methanol as solvent.

4.2.2. DFT benchmarking study of computed species

Geometry optimizations were carried out at the BP86/BS1 level and solvent effects (acetonitrile, ε = 35.688) were included self-consistently in these optimizations through the PCM method. In addition, single point calculations with an extended basis set system (BS2), the Gibbs contribution at the BP86/BS1(PCM) level, single-point dispersion corrections using Grimme's D3 parameter set, and the standard state correction, were added to obtain the Gibbs energies reported in the manuscript.

Functional test calculations were carried out via single point energy calculations on the BP86/BS1 optimized geometries using other functionals which are commonly employed (PBE0, B3LYP and M06). These calculations were performed with the appropriate functional using the BS2 basis set and the solvent effects through the PCM method. Moreover, the corrections to go from electronic to free energies were taken from the BP86/BS1(PCM) calculations. Dispersion and standard state corrections were also added.

The results show that the main features of the computed Gibbs energy values remain similar for all the functionals. Despite in all cases the formation of the (*Z*)-stilbene is preferred, the determining step barrier is always significantly higher than for the BP86 functional. Thus, we consider that the selected functional (BP86) is the one that better describes the system in terms of thermodynamics and kinetics. Furthermore, this functional allows us to compare with our previous work on semihydrogenation of alkynes catalyzed by Mo_3S_4 clusters.[28]

Table SI4.1. Free energy values of the proposed mechanism (Figure 4.3) calculated with different functionals. All values are given in kcal·mol^{-1}.

Stationary point	BP86 [a]	B3LYP	PBE0	M06
TS_1	19.2	26.8	19.0	24.7
I1	16.6	18.3	12.6	16.1
$^1TS_2$	25.6	32.8	30.2	33.6
$^3I2$	22.7	21.5	17.1	21.5
$TS_{3\text{-}cis}$	23.1	24.6	20.7	27.2
$TS_{3\text{-}trans}$	25.8	27.5	24.9	28.8

[a] Values used in the main text.

4.2.3. Analysis of the electronic properties of the system - Figure 4.3

Table SI4.2. Investigation of the character of the transferred hydrogens to the diphenylacetylene in intermediate **I_2**. BP86 Electronic energies (E) computed with BS1 and including solvent effects; correction to Gibbs Free energies (G corr.) at the same level of theory; Grimme's D3 dispersion correction; BP86 Electronic energies (E) computed with BS2 and including solvent effects; and final Gibbs Free energies obtained as the sum of the three previous columns. All values are given in Hartrees.

Species	E_{solv} (BS1/PCM)	G corr (BS1/PCM)	D3 corr (0)	E_{solv} (BS2/PCM)	G_{solv} (BS2)
Proton transfer					
Mo_3S_4 unit	-2.708.4447	0.3630	-0.1348	-2708.8441	-2708.6159
Substrate	-539.8609	0.1484	-0.0186	-540.0015	-539.8717
Hydrogen atom transfer					
Mo_3S_4 unit	-2708.2988	0.3642	-0.1354	-2708.6958	-2708.4670
Substrate	-540.0317	0.1463	-0.0185	-540.1803	-540.0525
Hydride transfer					
Mo_3S_4 unit	-2708.1171	0.3674	-0.1356	-2708.5129	-2708.2810
Substrate	-540.1367	0.1467	-0.0211	-540.3029	-540.1773

Table SI4.3. Energies of the **I1** and **I2** intermediates in different electronic spin states. BP86 Electronic energies (E) computed with BS1 and including solvent effects; correction to Gibbs Free energies (G corr.) at the same level of theory; Grimme's D3 dispersion correction; BP86 Electronic energies (E) computed with BS2 and including solvent effects; and final Gibbs Free energies obtained as the sum of the three previous columns. All values are given in Hartrees.

Configuration	**E_{solv} (BS1/PCM)**	**G corr (BS1/PCM)**	**D3 corr (0)**	**E_{solv} (BS2/PCM)**	**G_{solv} (BS2)**
Intermediate: I1					
Closed-shell singlet	-2.708.8842	0.3725	-0.1388	-2709.2824	-2709.0487
Open-shell singlet	-2708.8842	0.3725	-0.1388	-2709.2824	-2709.0487
Triplet	-2708.4965	0.3694	-0.1377	-2709.2670	-2709.0353
Intermediate: I2					
Open-shell singlet	-3248.3316	-	-	-3248.8685	-
Triplet	-3248.3343	-	-	-3.248.8746	-

4.2.4. 3D views of Mo_3S_4 species along the reaction pathway

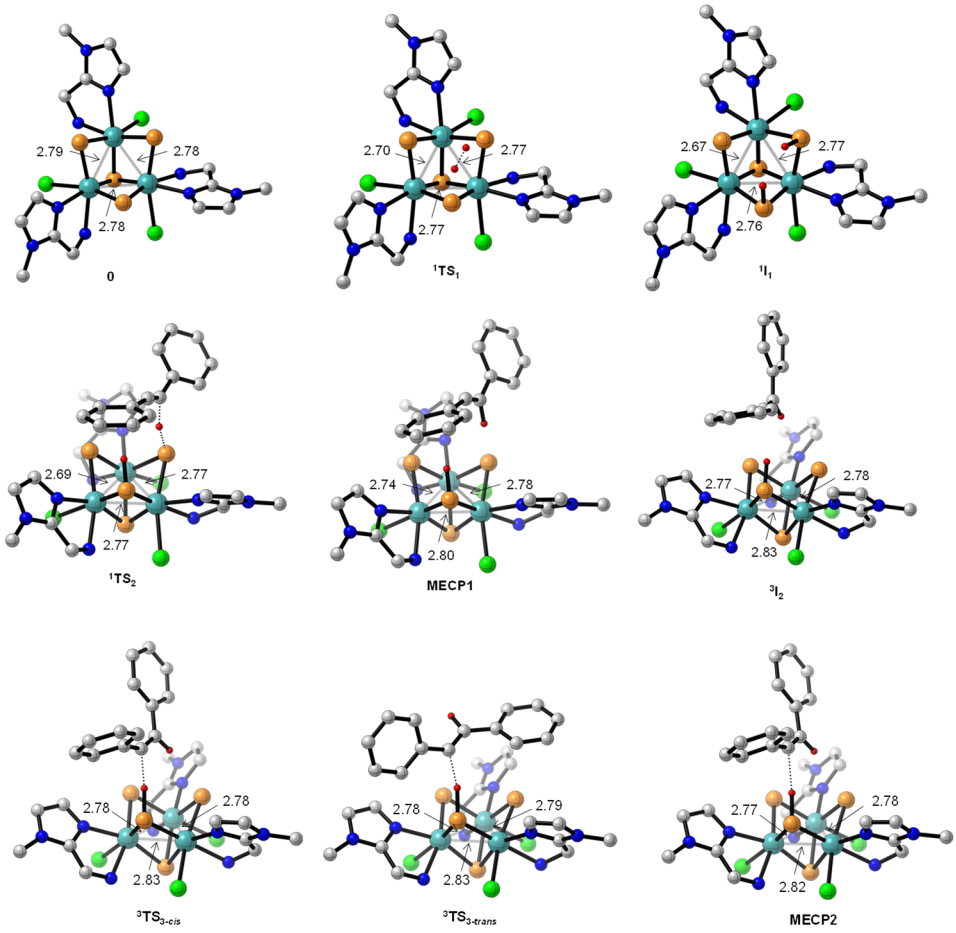

Figure SI4.12. Optimized structures of intermediates and transition states of Gibbs energy profile of Figure 4.3. Selected distances are given in Å. H atoms (except the vinilyc ones) have been omitted for clarity. Color code: Mo (cyan), S (orange), N (blue), Cl (green), H (red) and C (grey).

4.2.5. Spin densities

Table SI4.4. Mulliken spin density of all the species in the bis(hydrosulfido)-mediated mechanism - Figure 4.3.

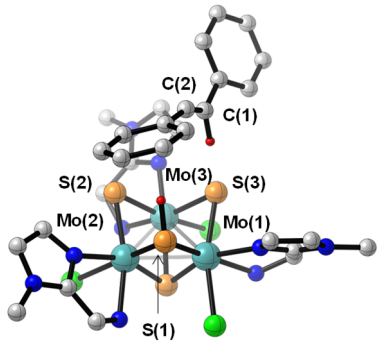

Species	Mo_3S_4 unit							DPA	
	Mo(1)	Mo(2)	Mo(3)	(μ_3-S)	S(1)	S(2)	S(3)	C(1)	C(2)
1^+	0	0	0	0	0	0	0	0	0
TS_1	0	0	0	0	0	0	0	0	0
I1	0	0	0	0	0	0	0	0	0
$^1TS_2$	0	0	0	0	0	0	0	0	0
MECP1	0.64	0.45	0.07	-0.01	0.02	-0.02	0.02	-0.10	0.61
$^3I2$	0.43	0.54	-0.05	-0.04	0.02	0.02	-0.01	-0.10	0.65
$^1TS_{3\text{-cis}}$	0.53	0.46	0.00	-0.01	0.02	0.01	0.09	-0.07	0.60
MECP2	0.50	0.48	0.00	-0.01	0.02	0.01	0.03	-0.09	0.65

Table SI4.5. Mulliken charges of all the species in the bis(hydrosulfido)-mediated mechanism - Figure 4.3.

Species	**Mo_3S_4 unit**						
	Mo(1)	**Mo(2)**	**Mo(3)**	**(μ_3-S)**	**S(1)**	**S(2)**	**S(3)**
1^+	0.01	0.01	0.01	0.23	-0.08	-0.08	-0.08
TS_1	-0.01	-0.03	-0.02	0.19	-0.01	-0.10	0.00
I1	0.01	-0.05	-0.04	0.18	-0.04	-0.15	-0.04
$^1TS_2$	0.08	-0.06	0.02	0.19	-0.15	-0.20	-0.18
MECP1	0.04	-0.02	0.01	0.19	-0.15	-0.13	-0.17
$^3I2$	0.01	0.02	-0.01	0.19	-0.15	-0.13	-0.12
$^3TS_{3\text{-}cis}$	0.05	0.04	0.04	0.19	-0.14	-0.13	-0.14
MECP2	0.04	0.03	-0.05	0.20	-0.13	-0.13	-0.13

4.2.6. Absolute energies of the computed species

Table SI4.6. BP86 Electronic energies (E) computed with BS1 and including solvent effects; correction to Gibbs Free energies (G corr.) at the same level of theory; Grimme's D3 dispersion correction; BP86 Electronic energies (E) computed with BS2 and including solvent effects; and final Gibbs Free energies obtained as the sum of the three previous columns. All values are given in Hartrees.

Species	E_{solv} (BS2/PCM)	G corr (BS1/PCM)	D3 corr (0)	E_{solv} (BS2/PCM)	G_{solv} (BS2)
Reagents and products					
dpa	-539.4537	0.1382	-0.0166	-539.6031	-539.4815
(*Z*)-stilbene	-540.6940	0.1619	-0.0231	-540.8421	-540.7033
(*E*)-stilbene	-540.7031	0.1606	-0.0204	-540.8513	-540.7111
H_2	-1.1766	-0.0039	-0.0001	-1.1780	-1.1819
Pathway A : Dithiolene-mediated mechanism					
1^+	-2707.7245	0.3570	-0.1327	-2708.1210	-2707.8968
TS_I	-3247.1555	0.5203	-0.1824	-3247.6942	-3247.3563
I	-3247.1803	0.5264	-0.1854	-3247.7173	-3247.3762
TS_{II}	-3248.3060	0.5380	-0.1914	-3248.8441	-3248.4975
II	-3.248.3669	0.5449	-0.1911	-3248.8697	-3248.5159
$TS_{II\text{-}cis}$	-3248.3196	0.5439	-0.1936	-3248.8581	-3248.5079
TS_{III}	-3248.3238	0.5470	-0.1963	-3248.8618	-3248.5111
III	-3248.3608	0.5433	-0.1951	-3248.8983	-3248.5501
$TS_{III\text{-}trans}$	-3248.3439	0.5422	-0.1954	-3248.8759	-3248.5291
Pathway B : Bis(hydrosulfido)-mediated mechanism					
1^+	-2707.7245	0.3570	-0.1327	-2708.1210	-2707.8968
TS_1	-2708.8762	0.3681	-0.1375	-2709.2751	-2709.0445
^{1}I1	-2708.8842	0.3725	-0.1388	-2709.2824	-2709.0487
$^1TS_2$	-3248.3204	0.5291	-0.1810	-3248.8601	-3248.5121
$^3TS_2$	-3248.3122	0.5304	-0.1774	-3248.8520	-3248.4990
MECP1	-3248.3272	-	-	-3248.8675	-
^{3}I2	-3248.3317	0.5315	-0.1739	-3248.8709	-3248.5133
^{1}I2	-3248.3343	0.5286	-0.1708	-3248.8746	-3248.5168
$TS_{3\text{-}cis}$	-3248.3333	0.5328	-0.1761	-3248.8727	-3248.5161

$TS_{3\text{-}trans}$	-3248.3257	0.5348	-0.1828	-3248.8637	-3248.5117
MECP2	-3248.3336	-	-	-3248.8734	-

Table SI4.7. Absolute energies of selected intermediates and transition states for the semihydrogenation of dpa catalyzed by $[Mo_3S_4Cl_3(dmen)_3]^+$ cluster.

Species	E_{solv} (BS1/PCM)	G corr (BS1/PCM)	D3 corr (0)	E_{solv} (BS2/PCM)	G_{solv}(BS2)
Pathway B : Bis(hydrosulfido)-mediated mechanism					
Mo_3S_4-dmen	-2434.5020	0.4358	-0.1576	-2434.8227	-2434.5445
$^1TS_{2dmen}$	-2975.0885	0.6116	-0.2071	-2975.5523	-2975.1479
$^3I2_{dmen}$	-2975.1021	0.6075	-0.1933	-2975.5676	-2975.1534

4.2.7. Cartesian coordinates of the DFT optimized species

Stationary point: diphenylacetylene (dpa)

	x	y	z
C	-4.7547	1.3973	-0.8662
C	-3.6460	1.2042	0.0014
C	-3.2594	2.2628	0.8669
C	-3.9629	3.4738	0.8597
C	-5.0587	3.6545	-0.0035
C	-5.4501	2.6129	-0.8640
H	-5.0571	0.5857	-1.5348
H	-2.4065	2.1198	1.5373
H	-3.6547	4.2815	1.5314
H	-5.6053	4.6028	-0.0055
H	-6.3025	2.7488	-1.5375
C	-2.9335	-0.0306	0.0027
C	-2.3187	-1.0974	0.0026
C	-1.6062	-2.3322	0.0042
C	-1.9956	-3.3927	-0.8577
C	-0.4948	-2.5235	0.8687
C	-1.2922	-4.6036	-0.8501
H	-2.8507	-3.2511	-1.5256
C	0.2005	-3.7392	0.8670

H	-0.1901	-1.7104	1.5345
C	-0.1937	-4.7825	0.0100
H	-1.6026	-5.4129	-1.5190
H	1.0551	-3.8736	1.5380
H	0.3529	-5.7309	0.0124

Stationary point: hydrogen (H_2)

	x	y	z
H	0.7135	1.2738	0.0000
H	-0.0374	1.2738	0.0000

Stationary point: (*Z*)-stilbene

	x	y	z
C	-0.7999	0.6596	0.3952
H	-0.1773	-0.2423	0.3122
C	-0.1369	1.7833	0.7915
H	0.9520	1.6698	0.8888
C	-0.6152	3.1333	1.1466
C	0.2785	4.2247	1.0043
C	-1.8921	3.3909	1.7065
C	-0.1000	5.5263	1.3641
H	1.2806	4.0418	0.5993
C	-2.2663	4.6897	2.0757
H	-2.5861	2.5608	1.8656
C	-1.3770	5.7658	1.8993
H	0.6062	6.3531	1.2341
H	-3.2555	4.8630	2.5130
H	-1.6736	6.7794	2.1883
C	-2.2111	0.4298	0.0285
C	-2.7558	-0.8660	0.2132
C	-3.0304	1.4124	-0.5825
C	-4.0770	-1.1588	-0.1547
H	-2.1291	-1.6471	0.6590
C	-4.3470	1.1164	-0.9604
H	-2.6221	2.4087	-0.7749
C	-4.8810	-0.1669	-0.7416

H	-4.4764	-2.1652	0.0094
H	-4.9585	1.8896	-1.4378
H	-5.9104	-0.3935	-1.0375

Stationary point: (*E*)-stilbene

	x	y	z
C	-1.5779	1.5852	0.7381
H	-1.1412	0.5773	0.7402
C	-0.7434	2.6614	0.7381
H	-1.1800	3.6692	0.7402
C	0.7239	2.6399	0.7378
C	1.4204	3.8757	0.7524
C	1.4939	1.4471	0.7232
C	2.8215	3.9227	0.7537
H	0.8443	4.8084	0.7633
C	2.8929	1.4950	0.7247
H	0.9942	0.4729	0.7095
C	3.5663	2.7315	0.7400
H	3.3326	4.8912	0.7654
H	3.4648	0.5610	0.7130
H	4.6606	2.7633	0.7408
C	-3.0452	1.6066	0.7378
C	-3.7417	0.3708	0.7524
C	-3.8152	2.7994	0.7232
C	-5.1428	0.3238	0.7537
H	-3.1656	-0.5618	0.7633
C	-5.2141	2.7516	0.7247
H	-3.3155	3.7736	0.7095
C	-5.8876	1.5150	0.7400
H	-5.6538	-0.6447	0.7654
H	-5.7861	3.6855	0.7130
H	-6.9819	1.4833	0.7408

Stationary point: 1^+ cluster

	x	y	z
Mo	0.4357	1.5279	0.8999

Mo	1.2480	-1.1358	0.7824
S	-0.3403	-2.0610	2.2218
S	2.0632	0.5012	2.2233
S	-1.3594	1.3019	2.3649
S	0.0142	0.0198	-0.8882
Cl	1.0222	-3.1359	-0.8102
Cl	2.2391	2.4637	-0.6672
Mo	-1.4619	-0.5128	0.8954
Cl	-3.2058	0.7058	-0.5403
N	-3.2920	-1.2594	1.8836
C	-3.8071	-2.4023	1.3953
C	0.0231	4.4910	1.5148
N	0.7918	3.4606	1.9123
C	4.0607	-2.2700	1.1364
N	2.8230	-2.4251	1.6404
C	2.8866	-3.4541	2.5654
H	2.0094	-3.7895	3.1126
N	3.0933	-0.8054	-0.5237
H	3.1160	0.1943	-0.7963
H	2.9531	-1.3612	-1.3776
C	4.3735	-1.1970	0.1393
H	4.7782	-0.3062	0.6526
H	5.1246	-1.5236	-0.5993
N	4.9143	-3.1650	1.7056
C	6.3529	-3.2863	1.4412
H	6.7162	-4.2077	1.9139
H	6.5324	-3.3472	0.3577
H	6.8953	-2.4244	1.8589
C	4.1837	-3.9189	2.6166
H	4.6478	-4.7085	3.2018
N	-0.8061	3.0644	-0.2498
H	-1.6878	2.6074	-0.5469
H	-0.2745	3.3015	-1.0979
C	-1.0968	4.2997	0.5386
H	-2.0485	4.1423	1.0777
H	-1.2294	5.1745	-0.1194
N	0.3932	5.6291	2.1642
C	-0.2316	6.9512	2.0391

H	-0.4339	7.1703	0.9808
H	-1.1717	6.9894	2.6107
H	0.4647	7.7043	2.4301
C	1.6830	3.9552	2.8497
H	2.4313	3.3228	3.3203
C	1.4407	5.3020	3.0178
H	1.9136	6.0499	3.6488
N	-2.1944	-2.2510	-0.3963
H	-1.3665	-2.7592	-0.7582
H	-2.6826	-1.8327	-1.1993
C	-3.1037	-3.1867	0.3310
H	-3.8107	-3.6786	-0.3577
H	-2.4815	-3.9767	0.7888
N	-4.9646	-2.7096	2.0429
C	-5.8012	-3.8947	1.8179
H	-5.9807	-4.0277	0.7410
H	-5.3137	-4.7934	2.2258
H	-6.7639	-3.7422	2.3225
C	-5.1896	-1.7177	2.9905
C	-4.1481	-0.8207	2.8800
H	-3.9650	0.0977	3.4320
H	-6.0616	-1.7384	3.6387

Stationary point: TS_I

	x	y	z
Mo	0.6031	1.5892	0.8336
Mo	1.3329	-1.0353	0.8624
S	2.1965	0.6322	2.2365
S	0.0680	0.0083	-0.8648
Cl	0.9837	-3.1713	-0.5332
Cl	2.3602	2.4027	-0.8371
Mo	-1.3644	-0.3722	0.9911
Cl	-3.1375	0.8369	-0.4452
N	-3.1955	-1.0110	2.0627
C	-3.7310	-2.1855	1.6842
C	0.2500	4.5888	1.3020
N	1.0340	3.5754	1.7131

C	4.1325	-2.2187	1.1825
N	2.9150	-2.3123	1.7465
C	2.9866	-3.3097	2.7041
H	2.1268	-3.5864	3.3092
N	3.1294	-0.8389	-0.5233
H	3.1554	0.1396	-0.8665
H	2.9525	-1.4508	-1.3304
C	4.4261	-1.2021	0.1230
H	4.8464	-0.2870	0.5781
H	5.1560	-1.5711	-0.6168
N	4.9825	-3.1214	1.7463
C	6.4027	-3.3022	1.4245
H	6.7545	-4.2214	1.9101
H	6.5329	-3.4022	0.3368
H	6.9932	-2.4485	1.7909
C	4.2694	-3.8161	2.7164
H	4.7343	-4.5977	3.3116
N	-0.6966	3.0778	-0.3254
H	-1.5968	2.6117	-0.5501
H	-0.2122	3.2682	-1.2122
C	-0.9336	4.3526	0.4147
H	-1.8468	4.2279	1.0242
H	-1.1093	5.1957	-0.2741
N	0.6831	5.7643	1.8371
C	0.0722	7.0862	1.6542
H	-0.1458	7.2542	0.5894
H	-0.8569	7.1662	2.2391
H	0.7846	7.8486	1.9949
C	2.0022	4.1208	2.5398
H	2.7784	3.5094	2.9929
C	1.7901	5.4807	2.6286
H	2.3186	6.2633	3.1666
N	-2.1657	-2.1833	-0.1489
H	-1.3502	-2.7228	-0.4938
H	-2.6743	-1.8201	-0.9659
C	-3.0585	-3.0564	0.6679
H	-3.7866	-3.5959	0.0389
H	-2.4285	-3.8133	1.1689

N	-4.8820	-2.4207	2.3734
C	-5.7303	-3.6142	2.2780
H	-5.8112	-3.9296	1.2281
H	-5.3096	-4.4361	2.8777
H	-6.7318	-3.3639	2.6517
C	-5.0810	-1.3465	3.2335
C	-4.0318	-0.4759	3.0281
H	-3.8316	0.4874	3.4895
H	-5.9426	-1.3002	3.8945
S	-1.1302	1.4286	2.4385
S	-0.2405	-1.7466	2.4776
C	0.0635	-0.5636	4.6242
C	-0.4493	0.6007	4.6502
C	0.8341	-1.5464	5.3605
C	0.3573	-2.8657	5.5683
C	2.0759	-1.1668	5.9336
C	1.0945	-3.7697	6.3464
H	-0.5975	-3.1679	5.1275
C	2.8086	-2.0811	6.7033
H	2.4508	-0.1522	5.7685
C	2.3227	-3.3840	6.9129
H	0.7068	-4.7800	6.5122
H	3.7627	-1.7727	7.1431
H	2.8971	-4.0946	7.5154
C	-0.9732	1.6593	5.4893
C	-1.9132	1.3318	6.5019
C	-0.5494	3.0059	5.3578
C	-2.4004	2.3246	7.3636
H	-2.2487	0.2953	6.6043
C	-1.0363	3.9884	6.2308
H	0.1681	3.2715	4.5753
C	-1.9650	3.6549	7.2334
H	-3.1227	2.0557	8.1412
H	-0.6894	5.0217	6.1268
H	-2.3475	4.4275	7.9077

Stationary point: I

	x	y	z
Mo	0.6030	1.5059	0.6715
Mo	1.3294	-1.0585	0.6840
S	2.1985	0.5776	2.1150
S	0.0540	-0.0403	-1.0668
Cl	0.9337	-3.2510	-0.5823
Cl	2.3313	2.3447	-0.9712
Mo	-1.3911	-0.4279	0.7713
Cl	-3.1462	0.8508	-0.5806
N	-3.2392	-1.1123	1.7927
C	-3.7429	-2.2922	1.3894
C	0.1975	4.4904	1.2290
N	1.0115	3.4816	1.5927
C	4.1407	-2.2065	0.9919
N	2.9309	-2.3148	1.5669
C	3.0277	-3.2986	2.5362
H	2.1760	-3.5894	3.1459
N	3.0891	-0.8627	-0.7156
H	3.0952	0.1164	-1.0616
H	2.9205	-1.4788	-1.5212
C	4.4016	-1.1940	-0.0794
H	4.8045	-0.2655	0.3642
H	5.1296	-1.5529	-0.8258
N	5.0129	-3.0849	1.5610
C	6.4347	-3.2401	1.2332
H	6.8031	-4.1585	1.7080
H	6.5624	-3.3269	0.1441
H	7.0127	-2.3805	1.6059
C	4.3206	-3.7797	2.5459
H	4.8042	-4.5448	3.1476
N	-0.7496	3.0046	-0.4174
H	-1.6471	2.5320	-0.6472
H	-0.2791	3.2264	-1.3041
C	-0.9967	4.2572	0.3559
H	-1.9003	4.1065	0.9736
H	-1.1938	5.1144	-0.3097
N	0.6232	5.6604	1.7810

C	-0.0183	6.9738	1.6469
H	-0.2315	7.1815	0.5880
H	-0.9538	7.0064	2.2260
H	0.6718	7.7380	2.0268
C	1.9950	4.0271	2.4019
H	2.7956	3.4191	2.8156
C	1.7599	5.3796	2.5310
H	2.2894	6.1592	3.0725
N	-2.1411	-2.2199	-0.4073
H	-1.3080	-2.7415	-0.7402
H	-2.6416	-1.8581	-1.2301
C	-3.0299	-3.1297	0.3738
H	-3.7311	-3.6749	-0.2804
H	-2.3930	-3.8808	0.8749
N	-4.9019	-2.5603	2.0522
C	-5.7230	-3.7698	1.9262
H	-5.7708	-4.0780	0.8721
H	-5.3006	-4.5880	2.5299
H	-6.7385	-3.5429	2.2764
C	-5.1406	-1.5010	2.9211
C	-4.1063	-0.6062	2.7473
H	-3.9383	0.3568	3.2225
H	-6.0158	-1.4805	3.5652
S	-1.1799	1.2925	2.3932
S	-0.2924	-1.7961	2.3706
C	-0.1766	-0.8104	3.9493
C	-0.6161	0.4700	3.9761
C	0.4477	-1.5613	5.0640
C	0.0624	-2.8924	5.3560
C	1.4779	-0.9677	5.8339
C	0.6769	-3.5999	6.4018
H	-0.7335	-3.3660	4.7718
C	2.0927	-1.6808	6.8723
H	1.7975	0.0525	5.6018
C	1.6938	-2.9982	7.1620
H	0.3564	-4.6231	6.6236
H	2.8903	-1.2078	7.4544
H	2.1745	-3.5525	7.9744

C	-0.7653	1.3286	5.1718
C	-1.3935	0.8283	6.3395
C	-0.3272	2.6749	5.1621
C	-1.5596	1.6463	7.4657
H	-1.7568	-0.2038	6.3530
C	-0.4891	3.4869	6.2956
H	0.1593	3.0767	4.2673
C	-1.1060	2.9775	7.4507
H	-2.0517	1.2436	8.3571
H	-0.1310	4.5214	6.2743
H	-1.2374	3.6139	8.3316

Stationary point: TS_{II}

	x	y	z
Mo	0.6453	1.6251	0.4161
Mo	1.1803	-0.9357	0.8887
S	2.3098	0.8624	1.9345
S	0.0434	-0.1296	-1.0733
Cl	0.5547	-3.2672	-0.0345
Cl	2.5329	2.0164	-1.2743
Mo	-1.5368	-0.0327	0.6782
Cl	-3.0850	1.1927	-0.9311
N	-3.4895	-0.3630	1.6812
C	-4.1119	-1.5217	1.3994
C	0.4551	4.6824	0.4622
N	1.1690	3.6951	1.0332
C	3.8320	-2.3388	1.4548
N	2.6324	-2.1618	2.0359
C	2.6357	-2.9055	3.2045
H	1.7731	-2.9442	3.8657
N	2.9202	-1.2524	-0.4972
H	3.0427	-0.3681	-1.0252
H	2.6499	-1.9870	-1.1648
C	4.1953	-1.6236	0.1913
H	4.7399	-0.6906	0.4234
H	4.8405	-2.2312	-0.4648
N	4.6037	-3.1705	2.2085

C	5.9896	-3.5661	1.9336
H	6.2194	-4.4656	2.5193
H	6.1064	-3.7989	0.8654
H	6.6845	-2.7591	2.2132
C	3.8582	-3.5331	3.3239
H	4.2582	-4.2014	4.0820
N	-0.4647	3.0115	-1.0144
H	-1.3817	2.5810	-1.2489
H	0.1015	3.0436	-1.8724
C	-0.6677	4.3913	-0.4842
H	-1.6364	4.4166	0.0467
H	-0.7224	5.1338	-1.2987
N	0.8911	5.8959	0.9012
C	0.3403	7.2061	0.5356
H	0.2243	7.2732	-0.5561
H	-0.6352	7.3635	1.0211
H	1.0408	7.9834	0.8672
C	2.0959	4.2999	1.8670
H	2.8170	3.7214	2.4387
C	1.9291	5.6667	1.7972
H	2.4498	6.4865	2.2852
N	-2.4190	-1.9018	-0.2774
H	-1.6358	-2.5555	-0.4623
H	-2.8241	-1.6230	-1.1808
C	-3.4561	-2.5739	0.5606
H	-4.1849	-3.1241	-0.0580
H	-2.9464	-3.3126	1.2053
N	-5.3325	-1.5591	2.0026
C	-6.2942	-2.6670	1.9593
H	-6.4611	-2.9806	0.9181
H	-5.9256	-3.5208	2.5483
H	-7.2451	-2.3188	2.3823
C	-5.4892	-0.3674	2.7022
C	-4.3425	0.3685	2.4912
H	-4.0810	1.3616	2.8474
H	-6.3922	-0.1558	3.2690
S	-1.1216	1.8273	2.1338
S	-0.6686	-1.3570	2.4358

C	-0.5046	-0.3254	3.9131
C	-0.6047	1.0814	3.8210
C	-0.0804	-1.0296	5.1263
C	-0.4054	-2.4012	5.3370
C	0.6878	-0.3696	6.1282
C	0.0203	-3.0749	6.4886
H	-1.0173	-2.9289	4.5987
C	1.1228	-1.0565	7.2683
H	0.9536	0.6834	6.0029
C	0.7918	-2.4102	7.4591
H	-0.2577	-4.1241	6.6316
H	1.7228	-0.5281	8.0163
H	1.1239	-2.9389	8.3578
C	-1.1619	1.9475	4.9136
C	-2.2381	1.4905	5.7090
C	-0.6666	3.2548	5.1232
C	-2.7965	2.3208	6.6935
H	-2.6354	0.4837	5.5478
C	-1.2274	4.0807	6.1086
H	0.1699	3.6185	4.5158
C	-2.2947	3.6173	6.8981
H	-3.6281	1.9505	7.3019
H	-0.8251	5.0871	6.2641
H	-2.7301	4.2615	7.6686
H	1.5917	1.3892	3.4054
H	0.7895	1.4527	3.8652

Stationary point: II

	x	y	z
Mo	0.7976	1.6222	0.4784
Mo	1.2265	-0.9536	0.9077
S	2.6267	0.8186	1.8815
S	0.0440	-0.0994	-0.9824
Cl	0.4149	-3.2644	0.1185
Cl	2.6726	1.9177	-1.2569
Mo	-1.4681	0.0573	0.8334
Cl	-2.9989	1.3306	-0.7564

N	-3.4209	-0.1743	1.8675
C	-4.0789	-1.3254	1.6347
C	0.7449	4.6853	0.4653
N	1.4340	3.6821	1.0385
C	3.8561	-2.4937	1.2567
N	2.7237	-2.2529	1.9407
C	2.8033	-2.9849	3.1146
H	2.0132	-2.9672	3.8609
N	2.8458	-1.3534	-0.6095
H	2.9794	-0.4736	-1.1430
H	2.4769	-2.0632	-1.2559
C	4.1498	-1.8068	-0.0381
H	4.7750	-0.9130	0.1381
H	4.6944	-2.4573	-0.7429
N	4.6557	-3.3531	1.9471
C	5.9803	-3.8306	1.5348
H	6.2955	-4.6221	2.2269
H	5.9316	-4.2457	0.5171
H	6.7129	-3.0095	1.5645
C	4.0006	-3.6695	3.1306
H	4.4372	-4.3483	3.8586
N	-0.3042	3.0216	-0.9331
H	-1.2473	2.6324	-1.1340
H	0.2388	3.0077	-1.8067
C	-0.4242	4.4219	-0.4316
H	-1.3693	4.5036	0.1352
H	-0.4776	5.1453	-1.2633
N	1.2425	5.8892	0.8641
C	0.7383	7.2122	0.4782
H	0.6601	7.2812	-0.6171
H	-0.2477	7.3957	0.9320
H	1.4469	7.9715	0.8330
C	2.4081	4.2658	1.8325
H	3.1187	3.6696	2.3990
C	2.2960	5.6367	1.7353
H	2.8640	6.4447	2.1888
N	-2.4265	-1.8075	-0.0434
H	-1.6664	-2.4867	-0.2424

H	-2.8622	-1.5391	-0.9358
C	-3.4426	-2.4311	0.8535
H	-4.1844	-3.0175	0.2857
H	-2.9142	-3.1286	1.5288
N	-5.3237	-1.2767	2.1848
C	-6.3262	-2.3482	2.1803
H	-6.4180	-2.7733	1.1701
H	-6.0473	-3.1417	2.8905
H	-7.2936	-1.9205	2.4738
C	-5.4614	-0.0344	2.7950
C	-4.2792	0.6427	2.5845
H	-3.9933	1.6458	2.8874
H	-6.3759	0.2462	3.3111
S	-0.9086	1.9661	2.1708
S	-0.5217	-1.2076	2.6072
C	-0.1646	-0.1575	3.9881
C	-0.4065	1.3159	3.9414
C	0.3714	-0.7687	5.1869
C	0.2702	-2.1763	5.4353
C	1.0130	0.0203	6.1963
C	0.8010	-2.7519	6.5931
H	-0.2697	-2.8062	4.7206
C	1.5596	-0.5710	7.3401
H	1.0889	1.1044	6.0764
C	1.4616	-1.9587	7.5518
H	0.6885	-3.8289	6.7562
H	2.0569	0.0622	8.0823
H	1.8741	-2.4125	8.4579
C	-1.4689	1.8642	4.8844
C	-2.4848	1.0508	5.4268
C	-1.4329	3.2327	5.2356
C	-3.4449	1.5945	6.2967
H	-2.5159	-0.0138	5.1748
C	-2.3924	3.7753	6.1033
H	-0.6415	3.8734	4.8290
C	-3.4043	2.9567	6.6366
H	-4.2235	0.9476	6.7140
H	-2.3440	4.8359	6.3712

H	-4.1491	3.3766	7.3203
H	2.2259	0.8639	3.1920
H	0.5388	1.8610	4.1538

Stationary point: $TS_{II\text{-}cis}$

	x	y	z
Mo	0.7775	1.6983	0.4727
Mo	1.0697	-1.0820	0.9575
S	2.3946	0.7192	1.9739
S	0.0799	-0.0833	-0.9591
Cl	0.3502	-3.3031	-0.0563
Cl	2.7143	1.9420	-1.1898
Mo	-1.3759	0.0466	0.9062
Cl	-2.8934	1.3242	-0.7101
N	-3.3613	-0.1103	1.9246
C	-4.0655	-1.2285	1.6712
C	0.8017	4.7536	0.4665
N	1.4435	3.7275	1.0530
C	3.6960	-2.6090	1.3849
N	2.4819	-2.5052	1.9608
C	2.4128	-3.5059	2.9159
H	1.5197	-3.6730	3.5070
N	2.8472	-1.2948	-0.4381
H	2.9966	-0.3909	-0.9255
H	2.5850	-1.9935	-1.1460
C	4.1014	-1.7207	0.2527
H	4.6096	-0.8138	0.6256
H	4.7938	-2.2267	-0.4410
N	4.4058	-3.6254	1.9490
C	5.7805	-4.0211	1.6232
H	5.9715	-5.0087	2.0623
H	5.9040	-4.0875	0.5324
H	6.4993	-3.2944	2.0320
C	3.6035	-4.1994	2.9274
H	3.9480	-5.0387	3.5259
N	-0.2611	3.1131	-0.9408
H	-1.2073	2.7265	-1.1345

H	0.2743	3.0926	-1.8195
C	-0.3665	4.5153	-0.4389
H	-1.3130	4.6064	0.1241
H	-0.4056	5.2400	-1.2696
N	1.3436	5.9381	0.8650
C	0.8976	7.2804	0.4736
H	0.7337	7.3186	-0.6131
H	-0.0334	7.5461	0.9976
H	1.6830	7.9998	0.7391
C	2.4302	4.2740	1.8576
H	3.1087	3.6527	2.4366
C	2.3741	5.6479	1.7521
H	2.9677	6.4348	2.2100
N	-2.4138	-1.7692	0.0136
H	-1.6833	-2.4795	-0.1986
H	-2.8298	-1.4658	-0.8765
C	-3.4665	-2.3572	0.8940
H	-4.2255	-2.9050	0.3108
H	-2.9798	-3.0837	1.5689
N	-5.3266	-1.1179	2.1725
C	-6.3800	-2.1380	2.1257
H	-6.4691	-2.5402	1.1056
H	-6.1577	-2.9567	2.8272
H	-7.3317	-1.6679	2.4054
C	-5.4274	0.1336	2.7707
C	-4.2070	0.7516	2.6027
H	-3.8840	1.7395	2.9192
H	-6.3448	0.4592	3.2541
S	-0.8824	2.0063	2.1746
S	-0.5651	-1.3020	2.8010
C	-0.0267	-0.0867	4.0578
C	-0.4473	1.3330	3.9931
C	0.7481	-0.5613	5.1876
C	0.8166	-1.9540	5.5137
C	1.4032	0.3373	6.0957
C	1.4941	-2.4129	6.6466
H	0.2824	-2.6693	4.8824
C	2.0993	-0.1344	7.2122

H	1.3672	1.4170	5.9237
C	2.1574	-1.5118	7.5008
H	1.5031	-3.4858	6.8670
H	2.5955	0.5844	7.8729
H	2.6976	-1.8735	8.3807
C	-1.6677	1.7108	4.8261
C	-2.4781	0.7397	5.4483
C	-1.9618	3.0777	5.0368
C	-3.5631	1.1251	6.2538
H	-2.2490	-0.3213	5.3091
C	-3.0457	3.4613	5.8401
H	-1.3303	3.8448	4.5735
C	-3.8532	2.4846	6.4511
H	-4.1793	0.3567	6.7323
H	-3.2525	4.5248	5.9991
H	-4.6940	2.7835	7.0852
H	1.8379	0.7612	3.2296
H	0.3773	2.0098	4.2911

Stationary point: TS_{III}

	x	y	z
Mo	0.8521	1.6096	0.634
Mo	1.1807	-0.9976	1.135
S	2.6428	0.7447	2.0564
S	0.0317	-0.1481	-0.7531
Cl	0.2703	-3.2843	0.3892
Cl	2.7312	1.8047	-1.1217
Mo	-1.4633	0.1808	1.0522
Cl	-2.8744	1.3332	-0.7466
N	-3.4793	0.1819	1.9665
C	-4.2034	-0.9458	1.8212
C	0.9395	4.6687	0.5326
N	1.5806	3.6536	1.1392
C	3.8033	-2.5966	1.3709
N	2.6675	-2.4084	2.068
C	2.6764	-3.3393	3.0932
H	1.8627	-3.4168	3.805

N	2.7756	-1.3884	-0.4207
H	2.89	-0.5177	-0.9749
H	2.4202	-2.1231	-1.0474
C	4.0957	-1.7933	0.1469
H	4.6496	-0.8726	0.4029
H	4.6991	-2.3544	-0.5862
N	4.5415	-3.6002	1.9206
C	5.8564	-4.0702	1.4707
H	6.0648	-5.0335	1.9541
H	5.8518	-4.2137	0.3803
H	6.6402	-3.3472	1.7442
C	3.8391	-4.0759	3.0207
H	4.225	-4.8848	3.6354
N	-0.1675	3.0157	-0.8307
H	-1.118	2.6562	-1.0486
H	0.3944	2.9695	-1.6913
C	-0.2465	4.4252	-0.3484
H	-1.1816	4.5339	0.2307
H	-0.2943	5.1386	-1.1888
N	1.4992	5.8599	0.8868
C	1.0579	7.1947	0.4662
H	0.8717	7.2037	-0.6175
H	0.1404	7.4848	1.0011
H	1.8554	7.9137	0.6944
C	2.5857	4.2147	1.9093
H	3.2685	3.6035	2.4938
C	2.5414	5.5855	1.7649
H	3.1506	6.3794	2.1888
N	-2.49	-1.7394	0.3543
H	-1.7645	-2.4772	0.2422
H	-2.8797	-1.5363	-0.5758
C	-3.5764	-2.1878	1.2718
H	-4.3093	-2.8324	0.7584
H	-3.1131	-2.7847	2.0783
N	-5.5032	-0.7165	2.1542
C	-6.5943	-1.6969	2.1656
H	-6.5418	-2.3268	1.2658
H	-6.5361	-2.3318	3.063

H	-7.5495	-1.1557	2.1626
C	-5.6077	0.6199	2.5278
C	-4.3505	1.1664	2.3993
H	-4.0129	2.1786	2.6023
H	-6.5523	1.0441	2.8572
S	-0.8593	2.0908	2.2393
S	-0.5524	-1.1131	2.9103
C	-0.0844	-0.0413	4.2928
C	-0.6637	1.2351	4.4836
C	0.9616	-0.5324	5.2042
C	0.9902	-1.8979	5.597
C	1.9107	0.3451	5.8046
C	1.9225	-2.3645	6.5338
H	0.2359	-2.5825	5.1944
C	2.8598	-0.1357	6.7167
H	1.908	1.413	5.5623
C	2.8731	-1.4913	7.0901
H	1.8996	-3.4169	6.8354
H	3.585	0.5609	7.1501
H	3.6031	-1.8577	7.8182
C	-2.0744	1.471	4.8918
C	-2.9216	0.4026	5.2704
C	-2.5342	2.7979	5.0851
C	-4.1882	0.6547	5.8189
H	-2.5672	-0.6277	5.1643
C	-3.8013	3.0461	5.629
H	-1.881	3.6356	4.8157
C	-4.6347	1.9745	5.9997
H	-4.8225	-0.1855	6.12
H	-4.135	4.0784	5.7776
H	-5.6182	2.1686	6.4394
H	2.2671	0.873	3.3705
H	0.0092	1.9598	4.9683

Stationary point: III

	x	y	z
Mo	0.5720	1.4321	-1.3088
Mo	1.1189	-1.2157	-0.5998
S	2.1343	0.7246	0.4421
S	-0.0098	-0.5152	-2.5531
Cl	0.5292	-3.5727	-1.4170
Cl	2.5584	1.6636	-2.9206
Mo	-1.4792	-0.1790	-0.7158
Cl	-3.0303	0.6763	-2.5524
N	-3.4684	-0.3096	0.2766
C	-4.0832	-1.5076	0.2360
C	0.4536	4.4617	-1.6898
N	1.1249	3.5569	-0.9580
C	3.9097	-2.4390	-0.1859
N	2.6998	-2.4494	0.4078
C	2.7513	-3.4212	1.3943
H	1.8939	-3.6548	2.0176
N	2.8579	-1.3783	-2.0458
H	2.8864	-0.5127	-2.6201
H	2.6660	-2.1744	-2.6696
C	4.1726	-1.5673	-1.3687
H	4.5400	-0.5725	-1.0589
H	4.9245	-2.0036	-2.0478
N	4.7323	-3.3553	0.3930
C	6.1348	-3.6167	0.0512
H	6.4329	-4.5671	0.5125
H	6.2472	-3.7015	-1.0397
H	6.7820	-2.8095	0.4269
C	4.0100	-3.9812	1.4024
H	4.4541	-4.7553	2.0224
N	-0.4810	2.6088	-2.9211
H	-1.4006	2.1490	-3.0793
H	0.0708	2.5175	-3.7839
C	-0.6755	4.0512	-2.5830
H	-1.6371	4.1435	-2.0460
H	-0.7378	4.6727	-3.4918
N	0.9199	5.7160	-1.4334

C	0.4213	6.9673	-2.0158
H	1.0965	7.7809	-1.7216
H	0.4084	6.8946	-3.1135
H	-0.5928	7.1859	-1.6476
C	2.0568	4.2528	-0.2076
H	2.7453	3.7472	0.4647
C	1.9346	5.5978	-0.4907
H	2.4712	6.4681	-0.1218
N	-2.3764	-2.2201	-1.2903
H	-1.6016	-2.9058	-1.4024
H	-2.8135	-2.0963	-2.2127
C	-3.3896	-2.7145	-0.3134
H	-4.0987	-3.4186	-0.7802
H	-2.8569	-3.2592	0.4857
N	-5.3655	-1.3947	0.6807
C	-6.3401	-2.4804	0.8358
H	-6.1439	-3.0473	1.7589
H	-7.3458	-2.0428	0.8823
H	-6.2874	-3.1571	-0.0292
C	-5.5759	-0.0605	1.0131
C	-4.3979	0.6025	0.7456
H	-4.1565	1.6563	0.8477
H	-6.5309	0.2845	1.4008
S	-1.1032	1.9238	0.2497
S	-0.5377	-1.4236	1.1941
C	-0.0718	-0.8505	2.9159
C	-0.3202	0.2607	3.6643
C	0.6683	-1.9606	3.6019
C	0.0921	-3.2480	3.7227
C	1.9180	-1.7167	4.2159
C	0.7470	-4.2577	4.4459
H	-0.8810	-3.4500	3.2635
C	2.5700	-2.7288	4.9378
H	2.3781	-0.7276	4.1201
C	1.9889	-4.0026	5.0545
H	0.2804	-5.2436	4.5409
H	3.5381	-2.5211	5.4051
H	2.4979	-4.7912	5.6175

C	-1.1147	1.4987	3.5360
C	-0.5102	2.7344	3.8755
C	-2.5035	1.4727	3.2855
C	-1.2636	3.9160	3.9111
H	0.5593	2.7615	4.1120
C	-3.2622	2.6527	3.3510
H	-2.9886	0.5182	3.0628
C	-2.6462	3.8788	3.6531
H	-0.7767	4.8635	4.1649
H	-4.3428	2.6119	3.1786
H	-3.2421	4.7955	3.7099
H	1.3990	0.9022	1.5994
H	0.1611	0.1954	4.6537

Stationary point: TS III-*trans*

	x	y	z
Mo	0.6152	1.3825	-1.9090
Mo	1.1200	-1.3197	-1.3308
S	2.0222	0.5209	-0.1187
S	0.1265	-0.4916	-3.3050
Cl	0.6071	-3.6286	-2.3550
Cl	2.6986	1.6879	-3.3772
Mo	-1.4473	-0.2962	-1.5372
Cl	-2.9037	0.6581	-3.4123
N	-3.4951	-0.5158	-0.6829
C	-4.0582	-1.7352	-0.7851
C	0.5372	4.4310	-2.1159
N	1.1507	3.4760	-1.3966
C	3.8204	-2.6600	-0.7678
N	2.5664	-2.6464	-0.2757
C	2.4839	-3.6848	0.6355
H	1.5710	-3.8980	1.1823
N	2.9846	-1.4231	-2.6321
H	3.0851	-0.5179	-3.1314
H	2.8248	-2.1610	-3.3314
C	4.2225	-1.7164	-1.8539
H	4.5901	-0.7631	-1.4334

H	5.0211	-2.1309	-2.4920
N	4.5431	-3.6610	-0.1950
C	5.9532	-3.9806	-0.4430
H	6.1534	-4.9886	-0.0569
H	6.1570	-3.9681	-1.5236
H	6.6104	-3.2576	0.0642
C	3.7070	-4.3143	0.7041
H	4.0590	-5.1505	1.3019
N	-0.3268	2.6639	-3.5141
H	-1.2353	2.2213	-3.7573
H	0.2774	2.6189	-4.3448
C	-0.5352	4.0853	-3.1021
H	-1.5284	4.1530	-2.6221
H	-0.5379	4.7602	-3.9742
N	0.9996	5.6613	-1.7558
C	0.5451	6.9555	-2.2766
H	0.4226	6.8974	-3.3676
H	-0.4108	7.2445	-1.8130
H	1.3064	7.7120	-2.0459
C	2.0362	4.1134	-0.5451
H	2.6732	3.5591	0.1397
C	1.9469	5.4738	-0.7557
H	2.4658	6.3134	-0.3007
N	-2.2731	-2.3079	-2.2657
H	-1.4790	-2.9660	-2.4094
H	-2.7088	-2.1396	-3.1822
C	-3.2775	-2.8899	-1.3282
H	-3.9270	-3.6276	-1.8285
H	-2.7313	-3.4164	-0.5258
N	-5.3771	-1.6759	-0.4516
C	-6.3204	-2.7984	-0.3917
H	-6.1904	-3.4446	-1.2718
H	-6.1622	-3.3872	0.5248
H	-7.3414	-2.3952	-0.3955
C	-5.6669	-0.3538	-0.1315
C	-4.4973	0.3563	-0.2941
H	-4.3105	1.4199	-0.1796
H	-6.6646	-0.0493	0.1741

S	-1.1744	1.7847	-0.4763
S	-0.5167	-1.4459	0.4262
C	0.1845	-0.4948	2.0858
C	-0.3930	0.3897	2.9750
C	1.1453	-1.4512	2.7501
C	0.6446	-2.6514	3.3082
C	2.4981	-1.1145	2.9695
C	1.4760	-3.4903	4.0663
H	-0.4098	-2.9103	3.1620
C	3.3289	-1.9555	3.7293
H	2.8976	-0.1785	2.5660
C	2.8222	-3.1451	4.2779
H	1.0674	-4.4075	4.5034
H	4.3726	-1.6724	3.9008
H	3.4692	-3.7946	4.8763
C	-1.4528	1.3974	2.9598
C	-2.7173	1.2031	2.3576
C	-1.2395	2.5826	3.7151
C	-3.7318	2.1615	2.5114
H	-2.9112	0.2786	1.8080
C	-2.2376	3.5575	3.8265
H	-0.2741	2.7305	4.2122
C	-3.4950	3.3451	3.2307
H	-4.7198	1.9784	2.0778
H	-2.0463	4.4704	4.3996
H	-4.2913	4.0876	3.3447
H	1.0799	0.3670	1.0552
H	0.1268	0.3732	3.9469

Stationary point: $^1TS_1$ (s = 0)

	x	y	z
Mo	0.6379	1.7155	0.2267
Mo	1.3162	-0.9425	0.6450
S	0.1137	-0.1037	-1.2272
Cl	0.8814	-3.2480	-0.3848
Cl	2.5570	2.1733	-1.4031
Mo	-1.3192	-0.0839	0.6788

Cl	-3.0340	0.8985	-0.9161
N	-3.1476	-0.4802	1.8665
C	-3.7078	-1.6936	1.7112
C	0.3818	4.7605	0.1889
N	1.1081	3.8063	0.7967
C	4.0900	-2.1114	1.1840
N	2.8565	-2.1149	1.7205
C	2.8973	-2.9454	2.8282
H	2.0164	-3.1348	3.4361
N	3.1328	-0.9885	-0.7217
H	3.1859	-0.0730	-1.2073
H	2.9522	-1.7133	-1.4290
C	4.4153	-1.2721	-0.0122
H	4.8506	-0.3073	0.3051
H	5.1467	-1.7619	-0.6769
N	4.9195	-2.9113	1.9089
C	6.3493	-3.1355	1.6652
H	6.6640	-4.0232	2.2289
H	6.5228	-3.3143	0.5942
H	6.9374	-2.2650	1.9943
C	4.1769	-3.4421	2.9579
H	4.6207	-4.1200	3.6822
N	-0.5225	3.0206	-1.2179
H	-1.4283	2.5477	-1.4022
H	0.0047	3.0421	-2.1005
C	-0.7545	4.4110	-0.7216
H	-1.7082	4.4172	-0.1635
H	-0.8545	5.1237	-1.5572
N	0.8113	5.9946	0.5730
C	0.2447	7.2841	0.1608
H	0.0871	7.2934	-0.9275
H	-0.7117	7.4671	0.6745
H	0.9565	8.0774	0.4227
C	2.0356	4.4500	1.5982
H	2.7611	3.9008	2.1929
C	1.8562	5.8116	1.4713
H	2.3720	6.6552	1.9226
N	-2.1549	-2.0652	-0.0991

H	-1.3526	-2.6796	-0.3417
H	-2.6587	-1.8520	-0.9695
C	-3.0673	-2.7499	0.8644
H	-3.8137	-3.3717	0.3421
H	-2.4581	-3.4252	1.4922
N	-4.8469	-1.7828	2.4521
C	-5.7187	-2.9571	2.5747
H	-5.9626	-3.3503	1.5769
H	-5.2272	-3.7407	3.1716
H	-6.6472	-2.6497	3.0726
C	-5.0135	-0.5694	3.1102
C	-3.9564	0.2325	2.7357
H	-3.7299	1.2576	3.0177
H	-5.8611	-0.3920	3.7670
S	-1.0191	1.9104	1.8635
S	-0.1846	-1.2708	2.4245
H	0.3058	0.0199	3.2712
S	2.1547	0.8820	1.8744
H	1.0959	0.7349	3.0944

Stationary point: ^{1}I1 (s = 0)

	x	y	z
Mo	0.6532	1.6960	0.2291
Mo	1.3307	-0.9551	0.6545
S	0.1428	-0.1245	-1.2311
Cl	0.8597	-3.2655	-0.3233
Cl	2.6054	2.1471	-1.3633
Mo	-1.2919	-0.0851	0.6731
Cl	-2.9896	0.9167	-0.9216
N	-3.1378	-0.4632	1.8466
C	-3.7126	-1.6686	1.6844
C	0.3620	4.7381	0.1833
N	1.1065	3.7966	0.7880
C	4.1088	-2.1319	1.1605
N	2.8835	-2.1289	1.7155
C	2.9394	-2.9544	2.8264
H	2.0674	-3.1384	3.4486

N	3.1248	-1.0037	-0.7282
H	3.1787	-0.0865	-1.2117
H	2.9299	-1.7247	-1.4358
C	4.4186	-1.2992	-0.0437
H	4.8730	-0.3392	0.2611
H	5.1302	-1.7992	-0.7223
N	4.9475	-2.9301	1.8765
C	6.3725	-3.1591	1.6107
H	6.6991	-4.0325	2.1896
H	6.5261	-3.3635	0.5411
H	6.9658	-2.2805	1.9077
C	4.2194	-3.4540	2.9391
H	4.6724	-4.1299	3.6597
N	-0.5056	2.9799	-1.2221
H	-1.4042	2.4918	-1.4094
H	0.0251	3.0107	-2.1022
C	-0.7663	4.3658	-0.7271
H	-1.7197	4.3509	-0.1687
H	-0.8807	5.0753	-1.5636
N	0.7675	5.9797	0.5703
C	0.1713	7.2592	0.1697
H	-0.0478	7.2486	-0.9077
H	-0.7563	7.4462	0.7328
H	0.8920	8.0609	0.3768
C	2.0222	4.4562	1.5902
H	2.7597	3.9193	2.1814
C	1.8163	5.8145	1.4677
H	2.3161	6.6666	1.9210
N	-2.1399	-2.0637	-0.1046
H	-1.3419	-2.6899	-0.3324
H	-2.6256	-1.8469	-0.9841
C	-3.0784	-2.7335	0.8440
H	-3.8284	-3.3408	0.3097
H	-2.4917	-3.4215	1.4793
N	-4.8607	-1.7437	2.4133
C	-5.7480	-2.9071	2.5261
H	-5.9787	-3.3024	1.5259
H	-5.2765	-3.6939	3.1351

H	-6.6819	-2.5870	3.0056
C	-5.0181	-0.5286	3.0707
C	-3.9465	0.2594	2.7075
H	-3.7085	1.2814	2.9913
H	-5.8701	-0.3404	3.7189
S	-0.9750	1.8870	1.9170
S	-0.2021	-1.3499	2.4591
H	0.0483	-0.3019	3.3557
S	2.2510	0.9056	1.8785
H	1.4682	0.9477	3.0406

Stationary point: ^{3}I1 (s = 1)

	x	y	z
Mo	0.4048	1.5258	0.8614
Mo	1.1909	-1.2136	0.8035
S	1.9468	0.4573	2.2511
S	-0.0268	-0.0426	-0.8995
Cl	0.8547	-3.3298	-0.5661
Cl	2.2322	2.3753	-0.7172
Mo	-1.5265	-0.5303	0.8750
Cl	-3.2171	0.8270	-0.4388
N	-3.3945	-1.2795	1.8091
C	-3.8794	-2.4354	1.3231
C	0.0415	4.4967	1.5141
N	0.8152	3.4538	1.8651
C	4.0325	-2.2497	1.1621
N	2.8053	-2.4417	1.6782
C	2.9143	-3.4525	2.6189
H	2.0527	-3.8124	3.1752
N	2.9944	-0.8640	-0.5226
H	2.9848	0.1286	-0.8236
H	2.8746	-1.4474	-1.3609
C	4.2935	-1.1856	0.1414
H	4.6571	-0.2662	0.6351
H	5.0574	-1.4932	-0.5925
N	4.9240	-3.1020	1.7397
C	6.3634	-3.1748	1.4639

H	6.7673	-4.0680	1.9573
H	6.5353	-3.2576	0.3805
H	6.8754	-2.2811	1.8524
C	4.2286	-3.8672	2.6691
H	4.7265	-4.6285	3.2639
N	-0.8684	3.0837	-0.2120
H	-1.7643	2.6425	-0.4931
H	-0.3492	3.3091	-1.0716
C	-1.1143	4.3270	0.5765
H	-2.0513	4.1923	1.1464
H	-1.2509	5.2040	-0.0784
N	0.4476	5.6232	2.1632
C	-0.1696	6.9518	2.0789
H	-0.3970	7.1927	1.0304
H	-1.0950	6.9866	2.6745
H	0.5420	7.6924	2.4664
C	1.7493	3.9293	2.7709
H	2.5094	3.2817	3.2006
C	1.5270	5.2756	2.9679
H	2.0319	6.0110	3.5889
N	-2.2031	-2.2725	-0.4056
H	-1.3645	-2.7869	-0.7395
H	-2.6630	-1.8587	-1.2272
C	-3.1393	-3.2138	0.2811
H	-3.8208	-3.6990	-0.4378
H	-2.5364	-4.0104	0.7535
N	-5.0472	-2.7563	1.9464
C	-5.8571	-3.9584	1.7165
H	-6.0146	-4.1045	0.6377
H	-5.3608	-4.8447	2.1408
H	-6.8315	-3.8198	2.2024
C	-5.3121	-1.7565	2.8753
C	-4.2838	-0.8428	2.7775
H	-4.1302	0.0870	3.3193
H	-6.1989	-1.7851	3.5030
S	-0.4493	-2.1338	2.3811
H	-0.2745	-1.4095	3.5335
S	-1.4728	1.3203	2.4598

H	-0.8536	0.8245	3.5800

Stationary point: $^1TS_2$ (s = 0)

	x	y	z
Mo	0.6457	1.5425	0.5023
Mo	1.3167	-1.1388	0.6272
S	0.1811	-0.0900	-1.1787
Cl	0.8676	-3.3225	-0.6435
Cl	2.5796	2.2023	-1.0912
Mo	-1.3175	-0.2922	0.6519
Cl	-2.9664	0.9062	-0.8748
N	-3.2154	-0.7851	1.6997
C	-3.7892	-1.9566	1.3719
C	0.3710	4.5774	0.7680
N	1.1025	3.5749	1.2854
C	4.0747	-2.3914	1.0434
N	2.8390	-2.4467	1.5711
C	2.8633	-3.4151	2.5610
H	1.9759	-3.6700	3.1346
N	3.1421	-1.0345	-0.7174
H	3.2098	-0.0703	-1.0944
H	2.9692	-1.6717	-1.5061
C	4.4153	-1.4080	-0.0323
H	4.8422	-0.4912	0.4128
H	5.1566	-1.8090	-0.7439
N	4.8907	-3.2901	1.6614
C	6.3168	-3.5062	1.3905
H	6.6287	-4.4324	1.8900
H	6.4820	-3.6129	0.3082
H	6.9147	-2.6655	1.7746
C	4.1356	-3.9423	2.6298
H	4.5673	-4.7148	3.2610
N	-0.4933	2.9898	-0.8212
H	-1.3860	2.5290	-1.0876
H	0.0635	3.1253	-1.6751
C	-0.7649	4.3036	-0.1662
H	-1.7101	4.2079	0.3982

H	-0.8980	5.1078	-0.9091
N	0.8100	5.7764	1.2425
C	0.2482	7.0967	0.9357
H	0.1170	7.2058	-0.1510
H	-0.7210	7.2315	1.4402
H	0.9502	7.8639	1.2872
C	2.0454	4.1511	2.1196
H	2.7779	3.5546	2.6581
C	1.8686	5.5190	2.1060
H	2.3934	6.3229	2.6152
N	-2.1449	-2.1573	-0.3837
H	-1.3395	-2.7580	-0.6503
H	-2.5946	-1.8373	-1.2509
C	-3.1226	-2.9242	0.4435
H	-3.8525	-3.4617	-0.1851
H	-2.5636	-3.6835	1.0197
N	-4.9777	-2.0979	2.0227
C	-5.8812	-3.2516	1.9466
H	-6.0720	-3.5110	0.8947
H	-5.4455	-4.1180	2.4678
H	-6.8321	-2.9816	2.4236
C	-5.1635	-0.9618	2.8026
C	-4.0668	-0.1533	2.5901
H	-3.8384	0.8268	3.0009
H	-6.0485	-0.8361	3.4211
S	-1.0531	1.5414	2.1206
S	-0.3107	-1.7924	2.2984
S	2.2860	0.5802	1.9679
H	-0.1774	-0.9178	3.3616
H	1.9276	0.6196	3.5744
C	1.2268	0.1800	5.6269
C	2.0241	0.9185	4.9787
C	0.2426	-0.7339	6.0374
C	0.5956	-2.0521	6.4606
C	-1.1354	-0.3540	6.0218
C	-0.3998	-2.9516	6.8484
H	1.6504	-2.3405	6.4807
C	-2.1181	-1.2694	6.4144

H	-1.4048	0.6580	5.7066
C	-1.7560	-2.5653	6.8271
H	-0.1233	-3.9588	7.1750
H	-3.1710	-0.9720	6.4024
H	-2.5291	-3.2742	7.1393
C	2.9795	2.0183	5.1370
C	2.6465	3.1280	5.9517
C	4.2396	1.9858	4.4945
C	3.5608	4.1769	6.1203
H	1.6715	3.1541	6.4475
C	5.1508	3.0387	4.6733
H	4.5068	1.1281	3.8702
C	4.8138	4.1374	5.4820
H	3.2940	5.0280	6.7549
H	6.1282	2.9968	4.1820
H	5.5249	4.9582	5.6177

Stationary point: $^3TS_2$ (s = 1)

	x	y	z
Mo	0.5890	1.5871	0.4778
Mo	1.4681	-1.0664	0.5376
S	0.1819	-0.0791	-1.2015
Cl	1.1449	-3.2540	-0.7317
Cl	2.4383	2.4268	-1.1157
Mo	-1.3135	-0.5002	0.6106
Cl	-3.0446	0.6051	-0.9320
N	-3.1479	-1.1485	1.6686
C	-3.6146	-2.3733	1.3664
C	0.0359	4.5650	0.8257
N	0.8481	3.6157	1.3239
C	4.3349	-2.0694	0.8744
N	3.1222	-2.2459	1.4257
C	3.2600	-3.2156	2.4052
H	2.4136	-3.5567	2.9957
N	3.2450	-0.7582	-0.8359
H	3.2184	0.2263	-1.1662
H	3.1034	-1.3661	-1.6531

C	4.5659	-1.0547	-0.2018
H	4.9518	-0.1164	0.2359
H	5.3028	-1.4018	-0.9460
N	5.2475	-2.8868	1.4697
C	6.6782	-2.9620	1.1522
H	7.1346	-3.7303	1.7886
H	6.8199	-3.2402	0.0966
H	7.1647	-1.9946	1.3480
C	4.5789	-3.6186	2.4443
H	5.0961	-4.3496	3.0606
N	-0.6929	2.9484	-0.8155
H	-1.5499	2.4246	-1.0749
H	-0.1587	3.1303	-1.6755
C	-1.0521	4.2346	-0.1493
H	-2.0066	4.0822	0.3868
H	-1.2093	5.0428	-0.8835
N	0.3281	5.7746	1.3809
C	-0.3487	7.0465	1.1007
H	-0.3383	7.2503	0.0192
H	-1.3884	7.0172	1.4615
H	0.1917	7.8487	1.6192
C	1.6887	4.2387	2.2313
H	2.4492	3.6886	2.7784
C	1.3726	5.5806	2.2774
H	1.7906	6.4051	2.8490
N	-1.9930	-2.4216	-0.4116
H	-1.1526	-2.9480	-0.7162
H	-2.4978	-2.1218	-1.2566
C	-2.8769	-3.2800	0.4299
H	-3.5655	-3.8854	-0.1843
H	-2.2370	-3.9809	0.9957
N	-4.7723	-2.6169	2.0414
C	-5.5541	-3.8577	2.0078
H	-5.7262	-4.1657	0.9661
H	-5.0289	-4.6610	2.5477
H	-6.5237	-3.6711	2.4867
C	-5.0525	-1.4916	2.8087
C	-4.0408	-0.5865	2.5659

H	-3.8998	0.4171	2.9582
H	-5.9337	-1.4421	3.4432
S	-1.1760	1.3923	1.9874
S	-0.0899	-1.9577	2.1901
S	2.3457	0.7179	1.8765
H	0.0532	-1.1485	3.2867
H	1.9355	0.6536	3.4014
C	0.9000	0.4563	5.4115
C	1.9771	0.8263	4.8680
C	-0.3304	0.0047	5.9264
C	-0.5262	-1.3746	6.2437
C	-1.3809	0.9330	6.1990
C	-1.7320	-1.8000	6.8084
H	0.2818	-2.0870	6.0529
C	-2.5757	0.4902	6.7724
H	-1.2322	1.9913	5.9674
C	-2.7578	-0.8732	7.0766
H	-1.8702	-2.8574	7.0542
H	-3.3708	1.2101	6.9894
H	-3.6955	-1.2121	7.5274
C	3.2802	1.4393	5.1355
C	3.3468	2.6326	5.8959
C	4.4764	0.8542	4.6590
C	4.5891	3.2128	6.1876
H	2.4211	3.0881	6.2597
C	5.7158	1.4380	4.9639
H	4.4305	-0.0653	4.0682
C	5.7764	2.6178	5.7250
H	4.6291	4.1310	6.7823
H	6.6372	0.9674	4.6062
H	6.7448	3.0721	5.9568

MECP1

	x	y	z
Mo	0.1976	1.3710	-1.1896
Mo	0.8636	-1.3211	-1.0630
S	-0.3405	-0.2864	-2.8346

Cl	0.3800	-3.5248	-2.2649
Cl	2.0401	2.0431	-2.8818
Mo	-1.8113	-0.4880	-0.9846
Cl	-3.4708	0.7098	-2.5054
N	-3.6920	-0.9613	0.0895
C	-4.2753	-2.1332	-0.2195
C	-0.0645	4.4011	-0.8858
N	0.6720	3.3887	-0.3931
C	3.6314	-2.5474	-0.6824
N	2.4099	-2.5985	-0.1234
C	2.4630	-3.5463	0.8848
H	1.5913	-3.7953	1.4851
N	2.6475	-1.2319	-2.4538
H	2.6976	-0.2720	-2.8439
H	2.4649	-1.8802	-3.2311
C	3.9380	-1.5816	-1.7849
H	4.3618	-0.6509	-1.3659
H	4.6683	-1.9876	-2.5043
N	4.4674	-3.4294	-0.0663
C	5.8892	-3.6393	-0.3630
H	6.2183	-4.5563	0.1425
H	6.0330	-3.7596	-1.4468
H	6.4880	-2.7890	-0.0021
C	3.7393	-4.0655	0.9328
H	4.1896	-4.8233	1.5694
N	-0.9824	2.8352	-2.4712
H	-1.8856	2.3828	-2.7108
H	-0.4489	2.9639	-3.3410
C	-1.2171	4.1509	-1.8075
H	-2.1568	4.0748	-1.2307
H	-1.3434	4.9606	-2.5456
N	0.3750	5.5900	-0.3875
C	-0.1897	6.9150	-0.6668
H	-0.3107	7.0505	-1.7516
H	-1.1644	7.0324	-0.1686
H	0.5052	7.6763	-0.2895
C	1.6155	3.9493	0.4511
H	2.3448	3.3438	0.9842

C	1.4370	5.3166	0.4664
H	1.9631	6.1106	0.9902
N	-2.6494	-2.3560	-1.9859
H	-1.8517	-2.9616	-2.2606
H	-3.1082	-2.0355	-2.8487
C	-3.6200	-3.1137	-1.1425
H	-4.3550	-3.6572	-1.7597
H	-3.0550	-3.8656	-0.5624
N	-5.4566	-2.2607	0.4458
C	-6.3642	-3.4126	0.3938
H	-6.5689	-3.6819	-0.6529
H	-5.9236	-4.2746	0.9179
H	-7.3080	-3.1351	0.8803
C	-5.6287	-1.1150	1.2147
C	-4.5306	-0.3138	0.9810
H	-4.2939	0.6704	1.3770
H	-6.5064	-0.9774	1.8405
S	-1.5095	1.3808	0.4061
S	-0.7552	-1.9959	0.6394
S	1.8426	0.3956	0.1810
H	-0.5779	-1.1607	1.7257
H	1.7297	0.4408	2.4386
C	0.8553	0.1505	4.2789
C	1.6979	0.8022	3.5157
C	-0.1462	-0.7591	4.5820
C	0.1570	-2.0493	5.1465
C	-1.5236	-0.4394	4.3062
C	-0.8647	-2.9602	5.4027
H	1.1993	-2.2993	5.3643
C	-2.5294	-1.3706	4.5747
H	-1.7637	0.5437	3.8915
C	-2.2106	-2.6292	5.1229
H	-0.6226	-3.9390	5.8288
H	-3.5711	-1.1169	4.3557
H	-3.0058	-3.3492	5.3389
C	2.6095	1.9307	3.7943
C	2.3866	2.8271	4.8646
C	3.7340	2.1272	2.9581

C	3.2684	3.8931	5.0882
H	1.5106	2.6847	5.5063
C	4.6198	3.1905	3.1916
H	3.9127	1.4343	2.1285
C	4.3872	4.0792	4.2547
H	3.0801	4.5866	5.9142
H	5.4904	3.3239	2.5409
H	5.0722	4.9143	4.4323

Stationary point: ^{1}I2 (s = 0)

	x	y	z
Mo	-0.0697	1.2960	-1.2734
Mo	1.3107	-1.0751	-1.4864
S	-0.2943	-0.2914	-3.0533
Cl	1.3496	-3.2231	-2.8877
Cl	1.3605	2.6006	-2.9944
Mo	-1.4560	-1.0556	-1.1281
Cl	-3.5325	-0.2702	-2.3908
N	-3.0031	-2.1440	0.0343
C	-3.2498	-3.4117	-0.3412
C	-1.0789	4.1065	-0.6190
N	-0.0609	3.2883	-0.2991
C	4.3410	-1.4647	-1.4455
N	3.2464	-1.9307	-0.8199
C	3.6667	-2.9294	0.0423
H	2.9666	-3.4887	0.6576
N	2.8536	-0.3384	-2.9728
H	2.5837	0.6258	-3.2482
H	2.7885	-0.9358	-3.8074
C	4.2490	-0.3498	-2.4404
H	4.4287	0.6210	-1.9439
H	4.9912	-0.4529	-3.2496
N	5.4501	-2.1261	-1.0111
C	6.8342	-1.8786	-1.4311
H	7.4651	-2.6897	-1.0456
H	6.8987	-1.8691	-2.5291
H	7.1919	-0.9173	-1.0313

C	5.0366	-3.0554	-0.0636
H	5.7442	-3.7155	0.4313
N	-1.7259	2.4918	-2.2907
H	-2.4976	1.8311	-2.5034
H	-1.3472	2.8348	-3.1827
C	-2.2212	3.6325	-1.4650
H	-3.0373	3.2537	-0.8231
H	-2.6366	4.4387	-2.0925
N	-0.9009	5.3272	-0.0395
C	-1.8070	6.4782	-0.1267
H	-2.0791	6.6645	-1.1761
H	-2.7176	6.2991	0.4653
H	-1.2862	7.3611	0.2659
C	0.7994	4.0080	0.5118
H	1.7183	3.5740	0.8976
C	0.2849	5.2762	0.6842
H	0.6480	6.1368	1.2398
N	-1.8328	-3.0088	-2.2502
H	-0.9293	-3.3281	-2.6516
H	-2.4588	-2.7772	-3.0326
C	-2.4417	-4.0808	-1.4094
H	-3.0482	-4.7767	-2.0134
H	-1.6218	-4.6675	-0.9564
N	-4.2582	-3.9374	0.4089
C	-4.7961	-5.2996	0.3164
H	-5.0381	-5.5386	-0.7299
H	-4.0684	-6.0292	0.7037
H	-5.7151	-5.3518	0.9143
C	-4.6662	-2.9562	1.3056
C	-3.8840	-1.8473	1.0609
H	-3.8994	-0.8700	1.5365
H	-5.4684	-3.1356	2.0167
S	-1.5498	0.6904	0.4335
S	0.1410	-2.2370	0.2921
S	1.8241	0.6828	-0.0246
H	0.2563	-1.3429	1.3603
H	0.7204	0.4023	2.4265
C	0.0149	1.3066	4.1553

C	0.8544	0.5107	3.5527
C	-0.9628	2.1512	4.6360
C	-2.2282	1.6253	5.0863
C	-0.7405	3.5737	4.7127
C	-3.2094	2.4863	5.5709
H	-2.3959	0.5456	5.0446
C	-1.7400	4.4110	5.2006
H	0.2197	3.9767	4.3796
C	-2.9747	3.8773	5.6304
H	-4.1669	2.0798	5.9102
H	-1.5647	5.4898	5.2533
H	-3.7517	4.5445	6.0150
C	1.9779	-0.2678	4.1282
C	2.2050	-0.3008	5.5249
C	2.8429	-0.9891	3.2768
C	3.2724	-1.0382	6.0508
H	1.5353	0.2549	6.1901
C	3.9130	-1.7266	3.8086
H	2.6795	-0.9607	2.1938
C	4.1317	-1.7543	5.1958
H	3.4358	-1.0563	7.1332
H	4.5745	-2.2782	3.1325
H	4.9654	-2.3298	5.6105

Stationary point: ^{3}I2 (s = 1)

	x	y	z
Mo	0.1643	1.6146	-2.2016
Mo	0.9885	-1.0913	-2.1622
S	-0.2056	-0.0027	-3.9031
Cl	0.7517	-3.1392	-3.6524
Cl	2.1336	2.4006	-3.6063
Mo	-1.7101	-0.4276	-2.0788
Cl	-3.4512	0.6982	-3.6100
N	-3.5494	-1.0911	-1.0499
C	-4.0643	-2.2669	-1.4527
C	-0.3587	4.6016	-1.8464
N	0.4356	3.6386	-1.3464

C	3.7847	-2.2275	-1.6459
N	2.5202	-2.3758	-1.2116
C	2.5302	-3.4008	-0.2794
H	1.6227	-3.7313	0.2193
N	2.9042	-0.7720	-3.3548
H	2.9483	0.2223	-3.6494
H	2.7975	-1.3422	-4.2044
C	4.1519	-1.1645	-2.6342
H	4.5421	-0.2736	-2.1103
H	4.9333	-1.5019	-3.3356
N	4.6036	-3.1212	-1.0256
C	6.0550	-3.2442	-1.2041
H	6.3820	-4.1913	-0.7562
H	6.3017	-3.2539	-2.2759
H	6.5762	-2.4087	-0.7121
C	3.8208	-3.8685	-0.1526
H	4.2493	-4.6560	0.4619
N	-1.0620	2.9976	-3.5061
H	-1.9167	2.4837	-3.7944
H	-0.5122	3.1916	-4.3536
C	-1.4376	4.2781	-2.8325
H	-2.3963	4.1131	-2.3082
H	-1.5927	5.0880	-3.5646
N	-0.0484	5.8041	-1.2867
C	-0.7164	7.0865	-1.5387
H	-0.8492	7.2344	-2.6202
H	-1.6966	7.1155	-1.0383
H	-0.0828	7.8921	-1.1455
C	1.2850	4.2435	-0.4354
H	2.0444	3.6819	0.1024
C	0.9888	5.5894	-0.3861
H	1.4185	6.4049	0.1896
N	-2.4467	-2.2514	-3.2449
H	-1.6178	-2.7820	-3.5707
H	-2.9381	-1.8942	-4.0748
C	-3.3520	-3.1315	-2.4478
H	-4.0547	-3.6828	-3.0948
H	-2.7257	-3.8767	-1.9253

N	-5.2375	-2.5121	-0.8048
C	-6.0776	-3.7078	-0.9397
H	-6.1575	-3.9892	-1.9995
H	-5.6515	-4.5460	-0.3670
H	-7.0801	-3.4759	-0.5574
C	-5.4726	-1.4437	0.0527
C	-4.4219	-0.5654	-0.1120
H	-4.2446	0.3980	0.3590
H	-6.3568	-1.4055	0.6835
S	-1.6044	1.4569	-0.6954
S	-0.5942	-1.8855	-0.6364
S	1.8246	0.6759	-0.6546
H	-1.1367	-0.1952	1.9582
H	1.1433	0.4413	0.5223
C	-0.6040	-0.1966	2.9266
C	0.6636	0.1853	2.9508
C	-1.4222	-0.6503	4.0812
C	-0.9092	-0.6971	5.3991
C	-2.7603	-1.0502	3.8586
C	-1.7134	-1.1323	6.4598
H	0.1254	-0.3880	5.5832
C	-3.5638	-1.4870	4.9236
H	-3.1688	-1.0155	2.8417
C	-3.0439	-1.5299	6.2279
H	-1.3021	-1.1622	7.4743
H	-4.5979	-1.7931	4.7333
H	-3.6694	-1.8696	7.0596
C	1.9650	0.5243	3.2940
C	2.3109	1.8749	3.6634
C	3.0245	-0.4538	3.2510
C	3.6288	2.2083	3.9724
H	1.5192	2.6288	3.7063
C	4.3336	-0.0933	3.5669
H	2.7802	-1.4839	2.9754
C	4.6505	1.2348	3.9268
H	3.8692	3.2374	4.2594
H	5.1215	-0.8534	3.5401
H	5.6812	1.5070	4.1731

Stationary point: $^{3'}TS_{3\text{-}cis}$ (s = 1)

	x	y	z
Mo	0.5152	1.7322	0.3608
Mo	1.3701	-0.9627	0.4651
S	0.2097	0.0843	-1.3239
Cl	1.2053	-3.0424	-1.0018
Cl	2.4960	2.5317	-1.0296
Mo	-1.3379	-0.3429	0.4624
Cl	-3.0544	0.7313	-1.1405
N	-3.1981	-1.0247	1.4416
C	-3.6804	-2.2144	1.0395
C	-0.0604	4.7166	0.6471
N	0.7308	3.7735	1.1881
C	4.1673	-2.0555	1.0602
N	2.8968	-2.2101	1.4740
C	2.9012	-3.2155	2.4274
H	1.9880	-3.5493	2.9135
N	3.3059	-0.6448	-0.6975
H	3.3423	0.3460	-1.0043
H	3.2248	-1.2286	-1.5404
C	4.5417	-1.0083	0.0575
H	4.9083	-0.1024	0.5725
H	5.3422	-1.3500	-0.6198
N	4.9850	-2.9267	1.7142
C	6.4413	-3.0351	1.5664
H	6.7698	-3.9740	2.0302
H	6.7096	-3.0523	0.4999
H	6.9431	-2.1888	2.0603
C	4.1950	-3.6650	2.5880
H	4.6205	-4.4351	3.2261
N	-0.7086	3.0722	-0.9948
H	-1.5496	2.5409	-1.2915
H	-0.1420	3.2567	-1.8333
C	-1.1141	4.3600	-0.3547
H	-2.0810	4.1930	0.1535
H	-1.2650	5.1541	-1.1049
N	0.2270	5.9355	1.1833
C	-0.4412	7.2061	0.8777

H	-0.5355	7.3279	-0.2114
H	-1.4390	7.2390	1.3414
H	0.1720	8.0256	1.2743
C	1.5535	4.4087	2.1032
H	2.3062	3.8676	2.6708
C	1.2449	5.7527	2.1124
H	1.6544	6.5860	2.6774
N	-2.0090	-2.1937	-0.7019
H	-1.1619	-2.7139	-0.9966
H	-2.4822	-1.8541	-1.5498
C	-2.9219	-3.0796	0.0795
H	-3.5940	-3.6530	-0.5806
H	-2.2985	-3.8058	0.6313
N	-4.8715	-2.4686	1.6503
C	-5.6887	-3.6788	1.5054
H	-5.7490	-3.9644	0.4452
H	-5.2572	-4.5082	2.0868
H	-6.7004	-3.4629	1.8725
C	-5.1531	-1.3909	2.4819
C	-4.1113	-0.4986	2.3395
H	-3.9651	0.4754	2.7996
H	-6.0588	-1.3579	3.0817
S	-1.3032	1.5606	1.8163
S	-0.2393	-1.7618	1.9520
S	2.1857	0.8394	1.9213
H	-0.6577	0.5230	4.2282
H	1.6217	0.6254	3.2327
C	-0.0291	0.2970	5.1081
C	1.2871	0.4875	5.0018
C	-0.7721	-0.2303	6.2787
C	-0.1378	-0.5964	7.4902
C	-2.1776	-0.3682	6.1810
C	-0.8908	-1.0762	8.5694
H	0.9486	-0.5008	7.5818
C	-2.9291	-0.8486	7.2642
H	-2.6788	-0.0933	5.2460
C	-2.2886	-1.2042	8.4629
H	-0.3852	-1.3536	9.5003

H	-4.0159	-0.9445	7.1709
H	-2.8724	-1.5803	9.3091
C	2.5526	0.5810	5.6254
C	2.8898	1.7285	6.4175
C	3.5553	-0.4233	5.4236
C	4.1562	1.8422	6.9946
H	2.1348	2.5054	6.5708
C	4.8140	-0.2941	6.0148
H	3.3159	-1.2992	4.8121
C	5.1245	0.8360	6.7989
H	4.3942	2.7185	7.6060
H	5.5635	-1.0782	5.8666
H	6.1150	0.9324	7.2539

Stationary point: $^3TS_{3\text{-}trans}$ (s = 1)

	x	y	z
Mo	0.5637	1.1947	0.0690
Mo	1.9885	-1.2030	0.5316
S	0.8938	-0.5773	-1.4774
Cl	2.4907	-3.3532	-0.7748
Cl	2.4843	2.3492	-1.1668
Mo	-0.7614	-1.2549	0.1210
Cl	-2.4276	-0.7307	-1.7835
N	-2.5277	-2.3129	0.9322
C	-2.6593	-3.6056	0.5849
C	-0.7008	3.9712	-0.0194
N	0.2056	3.2864	0.6997
C	4.8584	-1.6693	1.4877
N	3.6024	-2.0440	1.7941
C	3.6993	-3.0351	2.7570
H	2.8183	-3.5190	3.1707
N	3.9455	-0.5215	-0.4252
H	3.8174	0.4408	-0.7918
H	4.0899	-1.1421	-1.2328
C	5.1275	-0.5908	0.4846
H	5.2285	0.3862	0.9900
H	6.0599	-0.7714	-0.0759

N	5.7550	-2.3852	2.2220
C	7.2167	-2.2545	2.1828
H	7.6555	-3.0858	2.7494
H	7.5705	-2.3066	1.1426
H	7.5315	-1.3007	2.6327
C	5.0320	-3.2519	3.0343
H	5.5274	-3.9327	3.7214
N	-0.7202	2.1154	-1.5571
H	-1.3607	1.3820	-1.9165
H	-0.0929	2.3908	-2.3246
C	-1.5056	3.2966	-1.0862
H	-2.4561	2.9200	-0.6668
H	-1.7516	3.9769	-1.9184
N	-0.7527	5.2664	0.3998
C	-1.6448	6.3167	-0.1046
H	-1.7001	6.2648	-1.2014
H	-2.6539	6.2044	0.3211
H	-1.2329	7.2926	0.1837
C	0.7565	4.1728	1.6095
H	1.5409	3.8724	2.2995
C	0.1623	5.4057	1.4373
H	0.3089	6.3576	1.9407
N	-0.8151	-3.2807	-0.9386
H	0.1663	-3.5914	-1.0678
H	-1.2205	-3.1153	-1.8692
C	-1.6044	-4.3150	-0.2085
H	-2.0360	-5.0584	-0.8997
H	-0.9167	-4.8527	0.4692
N	-3.8127	-4.1157	1.1001
C	-4.2845	-5.4998	0.9785
H	-4.1690	-5.8438	-0.0597
H	-3.7173	-6.1613	1.6516
H	-5.3484	-5.5318	1.2468
C	-4.4379	-3.0985	1.8123
C	-3.6339	-1.9839	1.6973
H	-3.7758	-0.9830	2.0970
H	-5.3859	-3.2597	2.3189
S	-1.3720	0.6826	1.2585

S	0.4043	-2.2657	1.8691
S	2.1583	0.8319	1.8949
H	-0.1676	-0.7070	5.8593
H	1.5425	0.6224	3.2113
C	0.0340	0.2261	5.2997
C	1.3247	0.4859	4.9840
C	-1.1538	1.0224	4.9849
C	-1.0590	2.3338	4.4527
C	-2.4372	0.5095	5.2991
C	-2.2094	3.1008	4.2408
H	-0.0716	2.7430	4.2149
C	-3.5892	1.2793	5.0829
H	-2.5219	-0.4963	5.7262
C	-3.4797	2.5776	4.5540
H	-2.1179	4.1143	3.8368
H	-4.5725	0.8709	5.3379
H	-4.3774	3.1843	4.3968
C	2.5837	0.3147	5.6281
C	2.6611	0.5287	7.0455
C	3.7959	0.0085	4.9346
C	3.8775	0.4207	7.7218
H	1.7438	0.7799	7.5867
C	5.0064	-0.0965	5.6246
H	3.7685	-0.1539	3.8539
C	5.0577	0.1096	7.0177
H	3.9107	0.5803	8.8044
H	5.9213	-0.3406	5.0760
H	6.0110	0.0322	7.5495

MECP2

	x	y	z
Mo	0.0915	1.6143	-2.1898
Mo	0.9433	-1.0758	-2.0880
S	-0.2303	-0.0351	-3.8694
Cl	0.7627	-3.1589	-3.5437
Cl	2.0684	2.4085	-3.5858
Mo	-1.7603	-0.4586	-2.0703
Cl	-3.4856	0.6230	-3.6531
N	-3.6161	-1.1383	-1.0760

C	-4.1015	-2.3284	-1.4734
C	-0.4865	4.5975	-1.8927
N	0.3117	3.6544	-1.3622
C	3.7402	-2.1718	-1.4911
N	2.4695	-2.3270	-1.0782
C	2.4746	-3.3272	-0.1194
H	1.5626	-3.6614	0.3683
N	2.8789	-0.7662	-3.2553
H	2.9180	0.2222	-3.5699
H	2.7971	-1.3543	-4.0951
C	4.1144	-1.1276	-2.4979
H	4.4788	-0.2198	-1.9843
H	4.9168	-1.4708	-3.1726
N	4.5591	-3.0362	-0.8299
C	6.0161	-3.1426	-0.9706
H	6.3424	-4.0831	-0.5079
H	6.2902	-3.1566	-2.0355
H	6.5141	-2.2972	-0.4714
C	3.7697	-3.7717	0.0469
H	4.1969	-4.5359	0.6907
N	-1.1443	2.9540	-3.5316
H	-1.9873	2.4231	-3.8244
H	-0.5840	3.1401	-4.3736
C	-1.5453	4.2427	-2.8898
H	-2.5103	4.0782	-2.3766
H	-1.6973	5.0370	-3.6396
N	-0.2055	5.8129	-1.3461
C	-0.8847	7.0806	-1.6385
H	-0.9878	7.2080	-2.7259
H	-1.8798	7.1028	-1.1681
H	-0.2751	7.9024	-1.2409
C	1.1318	4.2862	-0.4423
H	1.8865	3.7439	0.1212
C	0.8151	5.6281	-0.4204
H	1.2211	6.4593	0.1508
N	-2.4395	-2.3124	-3.2231
H	-1.5928	-2.8323	-3.5203
H	-2.9151	-1.9751	-4.0701

C	-3.3500	-3.1959	-2.4362
H	-4.0261	-3.7678	-3.0941
H	-2.7268	-3.9250	-1.8879
N	-5.2907	-2.5798	-0.8584
C	-6.1104	-3.7890	-0.9991
H	-6.1786	-4.0741	-2.0589
H	-5.6770	-4.6192	-0.4203
H	-7.1192	-3.5709	-0.6257
C	-5.5685	-1.4997	-0.0285
C	-4.5259	-0.6092	-0.1761
H	-4.3787	0.3666	0.2798
H	-6.4728	-1.4645	0.5737
S	-1.7029	1.4379	-0.7098
S	-0.6455	-1.8543	-0.5774
S	1.7779	0.7277	-0.6389
H	-1.0872	0.4207	1.8021
H	1.1707	0.5062	0.6015
C	-0.4804	0.1773	2.6937
C	0.8312	0.3859	2.6465
C	-1.2492	-0.3744	3.8385
C	-0.6304	-0.7482	5.0553
C	-2.6511	-0.5185	3.7178
C	-1.3950	-1.2424	6.1193
H	0.4542	-0.6441	5.1603
C	-3.4152	-1.0126	4.7867
H	-3.1411	-0.2377	2.7784
C	-2.7905	-1.3753	5.9917
H	-0.9006	-1.5249	7.0546
H	-4.5002	-1.1115	4.6789
H	-3.3850	-1.7593	6.8269
C	2.1208	0.4877	3.1893
C	2.5039	1.6480	3.9471
C	3.1105	-0.5293	2.9626
C	3.7942	1.7595	4.4656
H	1.7623	2.4335	4.1209
C	4.3943	-0.3975	3.4939
H	2.8379	-1.4135	2.3780
C	4.7468	0.7421	4.2472

H	4.0651	2.6438	5.0515
H	5.1315	-1.1892	3.3253
H	5.7552	0.8360	4.6613

Stationary point: $[Mo_3S_4Cl_3(dmen)_3]^+$

	x	y	z
S	-0.1981	-2.0645	-0.1981
Mo	-1.3812	-0.4173	0.9655
S	0.3388	1.1371	1.1042
Mo	-0.9242	1.7297	-0.7705
S	-2.9345	0.4677	-0.6011
Mo	-1.3479	-0.8348	-1.8024
Cl	-2.5618	-0.1931	-3.9256
N	0.5197	3.4924	-1.1184
C	0.2565	4.0870	-2.4657
C	-1.2413	4.2302	-2.6889
N	-1.9391	2.9200	-2.4993
C	-3.4182	3.1181	-2.5194
C	1.9843	3.3405	-0.8859
Cl	-2.0509	3.5502	0.5826
S	0.3806	0.6391	-2.3525
N	-0.4590	-2.3540	-3.2939
C	1.0156	-2.5181	-3.4383
N	-2.9476	-2.5395	-1.8593
C	-4.4043	-2.2161	-1.8705
C	-1.1208	-3.6814	-3.1008
C	-2.6236	-3.4976	-2.9621
N	-0.5015	-1.2292	2.9392
C	-0.7833	-0.2556	4.0390
C	-2.2268	0.2148	3.9568
N	-2.5246	0.7898	2.6081
C	-3.9867	1.0568	2.4750
Cl	-3.1284	-2.1355	1.5999
C	0.9073	-1.7110	3.0084
H	-0.8180	-1.9569	-4.1770
H	-2.7611	-3.0026	-0.9548
H	-1.1190	-2.0446	3.0840

H	-2.0540	1.7063	2.5266
H	0.1567	4.1529	-0.4122
H	-1.7178	2.3082	-3.3020
H	1.4648	-1.5541	-3.7133
H	1.2430	-3.2644	-4.2196
H	1.4405	-2.8530	-2.4804
H	-0.6871	-4.1411	-2.1967
H	-0.9017	-4.3454	-3.9571
H	-3.0453	-3.0753	-3.8896
H	-3.1127	-4.4712	-2.7788
H	-4.6616	-1.6894	-0.9418
H	-4.9988	-3.1444	-1.9386
H	-4.6204	-1.5735	-2.7362
H	1.0569	-2.5067	2.2660
H	1.1295	-2.1022	4.0167
H	1.5889	-0.8771	2.7838
H	-0.5948	-0.7245	5.0223
H	-0.0822	0.5883	3.9249
H	-2.4326	0.9615	4.7446
H	-2.9163	-0.6334	4.1038
H	-4.1583	1.6739	1.5829
H	-4.3564	1.5953	3.3655
H	-4.5162	0.0983	2.3743
H	2.1575	3.0145	0.1488
H	2.5020	4.3000	-1.0604
H	2.3850	2.5807	-1.5730
H	0.7106	3.4201	-3.2183
H	0.7448	5.0753	-2.5494
H	-1.6733	4.9329	-1.9566
H	-1.4410	4.6270	-3.7004
H	-3.9093	2.1395	-2.6042
H	-3.7052	3.7453	-3.3818
H	-3.7242	3.6091	-1.5845

Stationary point: $^1TS_2$ - $[Mo_3S_4Cl_3(dmen)_3]^+$ (s = 0)

	x	y	z
Mo	0.8271	1.3719	0.3240
Mo	1.4242	-1.3341	0.6498
S	0.4270	-0.3595	-1.2727
Cl	0.9546	-3.6239	-0.3767
Cl	2.9475	1.8872	-1.0346
Mo	-1.1908	-0.4221	0.4625
Cl	-2.7407	0.7919	-1.1324
N	-3.2878	-0.6792	1.4613
N	1.4418	3.4906	1.0912
N	2.8106	-2.7740	1.8509
N	3.3860	-1.2995	-0.5561
C	4.4902	-1.7910	0.3288
H	4.7132	-1.0016	1.0648
H	5.4063	-1.9772	-0.2611
N	-0.2308	2.7826	-1.1374
C	-0.3217	4.1397	-0.5074
H	-1.0796	4.0927	0.2918
H	-0.6522	4.8880	-1.2503
N	-1.9977	-2.3758	-0.4780
C	-3.0891	-2.9039	0.4021
H	-3.6305	-3.7259	-0.1012
H	-2.6243	-3.3130	1.3142
S	-0.9539	1.4928	1.8416
S	-0.3092	-1.8016	2.2736
S	2.3287	0.4376	1.9644
H	-0.1839	-0.8069	3.2293
H	1.8967	0.5509	3.5496
C	1.1837	0.1617	5.6340
C	1.9758	0.8877	4.9664
C	0.2305	-0.7360	6.1438
C	0.6130	-2.0468	6.5647
C	-1.1376	-0.3397	6.2599
C	-0.3473	-2.9277	7.0672
H	1.6633	-2.3444	6.4963
C	-2.0837	-1.2341	6.7702
H	-1.4272	0.6699	5.9553

C	-1.6947	-2.5266	7.1707
H	-0.0485	-3.9300	7.3886
H	-3.1289	-0.9235	6.8618
H	-2.4399	-3.2201	7.5724
C	2.9218	1.9980	5.1239
C	2.6082	3.0558	6.0142
C	4.1498	2.0293	4.4228
C	3.5079	4.1144	6.1956
H	1.6586	3.0337	6.5571
C	5.0479	3.0907	4.6165
H	4.4053	1.2163	3.7376
C	4.7295	4.1369	5.4983
H	3.2546	4.9241	6.8874
H	6.0010	3.0959	4.0781
H	5.4301	4.9649	5.6449
C	4.0351	-3.0644	1.0276
H	3.7676	-3.8346	0.2871
H	4.8374	-3.4725	1.6674
C	-4.0416	-1.7676	0.7489
H	-4.4713	-1.3356	-0.1687
H	-4.8751	-2.1298	1.3762
C	1.0414	4.5091	0.0602
H	1.8024	4.5040	-0.7358
H	1.0224	5.5186	0.5076
C	3.4323	-1.9414	-1.9018
H	2.6625	-1.4865	-2.5403
H	4.4263	-1.7937	-2.3604
H	3.2191	-3.0159	-1.8155
H	3.5207	-0.2803	-0.7107
C	3.1614	-2.4859	3.2696
H	3.8017	-1.5937	3.3193
H	2.2425	-2.2963	3.8410
H	3.6994	-3.3417	3.7140
H	2.2358	-3.6281	1.8433
C	-2.3816	-2.4116	-1.9190
H	-3.2488	-1.7604	-2.0945
H	-1.5406	-2.0413	-2.5222
H	-2.6281	-3.4452	-2.2203

C	-3.4045	-0.8095	2.9411
H	-2.9825	-1.7730	3.2618
H	-2.8409	0.0026	3.4221
H	-4.4636	-0.7582	3.2498
H	-3.7234	0.2144	1.1960
H	-1.1703	-3.0015	-0.3904
C	1.0718	3.9416	2.4619
H	-0.0186	4.0680	2.5254
H	1.3824	3.1860	3.1949
H	1.5643	4.9026	2.6930
C	0.1850	2.8631	-2.5672
H	1.1926	3.2944	-2.6409
H	0.2072	1.8498	-2.9913
H	-0.5297	3.4869	-3.1320
H	-1.1804	2.3545	-1.1352
H	2.4675	3.4103	1.0556

Stationary point: $^3I_2$ - $[Mo_3S_4Cl_3(dmen)_3]^+$ (s = 1)

	x	y	z
Mo	0.6158	2.2210	-2.1422
Mo	1.2912	-0.5189	-2.5155
S	0.3998	0.9597	-4.1463
Cl	1.1100	-2.2967	-4.3026
Cl	2.8400	3.0832	-2.9810
Mo	-1.3662	0.3305	-2.6451
Cl	-2.8694	1.8835	-3.9996
N	-3.4788	-0.2666	-1.9013
N	1.0086	4.0640	-0.7765
N	2.5413	-2.2588	-1.6184
N	3.4259	-0.0933	-3.2921
H	3.5392	0.9170	-3.0795
C	4.4032	-0.8712	-2.4632
H	4.5009	-0.3697	-1.4865
H	5.3990	-0.8761	-2.9419
N	-0.4031	3.9181	-3.2849
H	-1.3184	3.4844	-3.5229
C	-0.6538	5.0437	-2.3260

H	-1.4815	4.7447	-1.6618
H	-0.9648	5.9521	-2.8724
N	-2.0181	-1.2758	-4.1811
H	-1.1630	-1.8638	-4.2096
C	-3.1255	-2.0738	-3.5612
H	-3.6073	-2.7198	-4.3173
H	-2.6823	-2.7242	-2.7894
S	-1.3269	1.9059	-0.9145
S	-0.5212	-1.4170	-1.3503
S	1.9754	0.8706	-0.5952
H	-1.1912	-0.3974	2.1476
H	1.1042	0.4852	0.3970
C	-0.6509	-0.3513	3.1095
C	0.6199	0.0204	3.1090
C	-1.4653	-0.7268	4.2948
C	-0.9371	-0.7131	5.6075
C	-2.8136	-1.1098	4.1108
C	-1.7368	-1.0714	6.6998
H	0.1063	-0.4179	5.7628
C	-3.6134	-1.4688	5.2068
H	-3.2336	-1.1244	3.0985
C	-3.0786	-1.4510	6.5056
H	-1.3131	-1.0550	7.7095
H	-4.6558	-1.7627	5.0448
H	-3.7009	-1.7302	7.3619
C	1.9246	0.3660	3.4272
C	2.2825	1.7306	3.7298
C	2.9766	-0.6215	3.4362
C	3.6037	2.0693	4.0181
H	1.4960	2.4909	3.7438
C	4.2896	-0.2552	3.7282
H	2.7220	-1.6641	3.2240
C	4.6186	1.0874	4.0169
H	3.8518	3.1091	4.2559
H	5.0710	-1.0223	3.7404
H	5.6520	1.3637	4.2464
C	-4.1431	-1.1219	-2.9472
H	-4.5502	-0.4500	-3.7190

H	-4.9853	-1.6804	-2.5027
C	0.6167	5.3063	-1.5288
H	1.4461	5.5617	-2.2071
H	0.4774	6.1493	-0.8299
C	3.8851	-2.2926	-2.2913
H	3.7523	-2.7728	-3.2736
H	4.5929	-2.9033	-1.7038
H	2.0127	-3.0712	-1.9646
H	2.0372	4.0510	-0.7365
H	-3.9536	0.6462	-1.9183
C	0.1808	4.4050	-4.5701
H	0.2897	3.5558	-5.2589
H	-0.4827	5.1637	-5.0202
H	1.1733	4.8408	-4.3920
C	3.7058	-0.2267	-4.7535
H	3.0073	0.4135	-5.3106
H	4.7432	0.0840	-4.9691
H	3.5569	-1.2672	-5.0717
C	-2.3140	-0.9138	-5.5977
H	-3.2078	-0.2775	-5.6454
H	-1.4630	-0.3528	-6.0090
H	-2.4771	-1.8292	-6.1932
C	0.5117	4.0902	0.6290
H	0.9282	4.9617	1.1636
H	-0.5856	4.1539	0.6351
H	0.8151	3.1668	1.1417
C	-3.6552	-0.8311	-0.5325
H	-3.2032	-1.8321	-0.4827
H	-3.1510	-0.1789	0.1940
H	-4.7285	-0.9041	-0.2842
C	2.6567	-2.3990	-0.1384
H	3.1473	-3.3536	0.1202
H	3.2494	-1.5670	0.2689
H	1.6520	-2.3695	0.3068

Proton transfer

Stationary point: semihydrogenated dpa (dpaH)

	x	y	z
H	-0.2495	0.5513	4.6643
C	0.1197	0.2345	5.6567
C	1.4021	0.4240	5.8165
C	-0.8776	-0.3275	6.5895
C	-0.5213	-0.7604	7.8888
C	-2.2190	-0.4289	6.1577
C	-1.5005	-1.2864	8.7382
H	0.5167	-0.6838	8.2275
C	-3.1926	-0.9577	7.0169
H	-2.4935	-0.0940	5.1525
C	-2.8366	-1.3866	8.3061
H	-1.2215	-1.6201	9.7423
H	-4.2298	-1.0337	6.6769
H	-3.5977	-1.7989	8.9756
C	2.7472	0.6354	5.9447
C	3.2331	1.8920	6.4660
C	3.6786	-0.4018	5.5654
C	4.6005	2.0889	6.5975
H	2.5115	2.6629	6.7471
C	5.0405	-0.1764	5.7083
H	3.2900	-1.3446	5.1727
C	5.4957	1.0608	6.2205
H	4.9875	3.0325	6.9899
H	5.7606	-0.9485	5.4269
H	6.5720	1.2275	6.3281

Stationary point: hydrosulfido cluster

	x	y	z
Mo	0.5255	1.6636	0.3333
Mo	1.3337	-0.9434	0.4638
S	0.1925	0.0411	-1.3741
Cl	1.1397	-3.1309	-0.9562
Cl	2.5129	2.4866	-1.1503
Mo	-1.3272	-0.3377	0.4371
Cl	-3.0730	0.7695	-1.1829
N	-3.2082	-1.0144	1.4211
C	-3.6913	-2.2010	1.0163
C	0.0127	4.6668	0.6499
N	0.7982	3.7116	1.1741
C	4.1564	-1.9955	1.0482
N	2.8971	-2.1648	1.4841
C	2.9398	-3.1336	2.4719
H	2.0388	-3.4645	2.9827
N	3.2436	-0.6884	-0.7611
H	3.2496	0.2889	-1.1113
H	3.1690	-1.3202	-1.5690
C	4.4905	-0.9754	0.0027
H	4.8206	-0.0359	0.4823
H	5.3100	-1.3129	-0.6553
N	5.0064	-2.8226	1.7219
C	6.4611	-2.9032	1.5544
H	6.8225	-3.8037	2.0678
H	6.7134	-2.9784	0.4862
H	6.9509	-2.0166	1.9864
C	4.2459	-3.5475	2.6331
H	4.6996	-4.2832	3.2923
N	-0.6832	3.0528	-1.0047
H	-1.5333	2.5349	-1.2966
H	-0.1156	3.2398	-1.8415
C	-1.0608	4.3328	-0.3402
H	-2.0169	4.1652	0.1886
H	-1.2211	5.1448	-1.0701
N	0.3100	5.8793	1.2009
C	-0.3559	7.1557	0.9209

H	-0.4718	7.2892	-0.1647
H	-1.3450	7.1920	1.4036
H	0.2689	7.9691	1.3127
C	1.6276	4.3304	2.0932
H	2.3754	3.7733	2.6524
C	1.3306	5.6775	2.1233
H	1.7479	6.5009	2.6971
N	-2.0072	-2.1973	-0.7141
H	-1.1435	-2.7110	-0.9773
H	-2.4654	-1.8716	-1.5743
C	-2.9262	-3.0726	0.0673
H	-3.5933	-3.6580	-0.5883
H	-2.3049	-3.7887	0.6356
N	-4.8787	-2.4640	1.6350
C	-5.6923	-3.6751	1.4883
H	-5.7803	-3.9415	0.4248
H	-5.2429	-4.5147	2.0413
H	-6.6954	-3.4732	1.8864
C	-5.1554	-1.3926	2.4770
C	-4.1142	-0.4988	2.3312
H	-3.9587	0.4691	2.8016
H	-6.0572	-1.3656	3.0832
S	-1.2661	1.5221	1.8792
S	-0.2692	-1.6912	2.0438
S	1.9520	0.7658	2.0584
H	1.0015	0.5217	3.0809

Hydrogen atom transfer

Stationary point: semihydrogenated dpa (dpaH)

	x	y	z
H	-0.3244	0.5308	4.6265
C	0.0945	0.2360	5.6070
C	1.3868	0.4093	5.8183
C	-0.8984	-0.3242	6.5564
C	-0.5372	-0.7547	7.8553
C	-2.2501	-0.4342	6.1578
C	-1.5011	-1.2780	8.7257
H	0.5086	-0.6729	8.1720
C	-3.2152	-0.9590	7.0315
H	-2.5406	-0.1038	5.1538
C	-2.8451	-1.3830	8.3186
H	-1.2054	-1.6067	9.7278
H	-4.2578	-1.0365	6.7055
H	-3.5965	-1.7926	9.0014
C	2.7424	0.6254	5.9517
C	3.2532	1.8758	6.4644
C	3.7014	-0.3929	5.5907
C	4.6247	2.0778	6.5990
H	2.5427	2.6595	6.7433
C	5.0672	-0.1620	5.7363
H	3.3342	-1.3468	5.2005
C	5.5448	1.0683	6.2394
H	4.9903	3.0339	6.9886
H	5.7769	-0.9475	5.4551
H	6.6200	1.2382	6.3498

Stationary point: hydrosulfido cluster

	x	y	z
Mo	0.5143	1.7224	0.3450
Mo	1.3694	-0.9746	0.4326
S	0.2043	0.0820	-1.3461
Cl	1.1997	-3.0373	-1.0358
Cl	2.5176	2.5124	-1.0048

Mo	-1.3350	-0.3385	0.4503
Cl	-3.0562	0.7537	-1.1240
N	-3.1841	-1.0222	1.4502
C	-3.6794	-2.2040	1.0401
C	-0.0493	4.7093	0.6325
N	0.7330	3.7620	1.1789
C	4.1700	-2.0519	1.0490
N	2.8945	-2.2233	1.4410
C	2.8951	-3.2307	2.3921
H	1.9778	-3.5745	2.8631
N	3.3148	-0.6382	-0.7088
H	3.3511	0.3530	-1.0152
H	3.2438	-1.2199	-1.5543
C	4.5471	-0.9979	0.0545
H	4.9065	-0.0919	0.5746
H	5.3548	-1.3325	-0.6179
N	4.9870	-2.9130	1.7161
C	6.4474	-2.9997	1.5975
H	6.7800	-3.9360	2.0637
H	6.7379	-3.0079	0.5367
H	6.9263	-2.1484	2.1053
C	4.1912	-3.6633	2.5746
H	4.6156	-4.4287	3.2192
N	-0.6893	3.0676	-1.0162
H	-1.5322	2.5405	-1.3159
H	-0.1192	3.2481	-1.8533
C	-1.0932	4.3593	-0.3816
H	-2.0678	4.2000	0.1143
H	-1.2288	5.1526	-1.1353
N	0.2333	5.9248	1.1783
C	-0.4289	7.1980	0.8702
H	-0.5079	7.3258	-0.2193
H	-1.4330	7.2298	1.3204
H	0.1797	8.0146	1.2796
C	1.5449	4.3907	2.1080
H	2.2878	3.8451	2.6838
C	1.2386	5.7353	2.1196
H	1.6419	6.5648	2.6945

N	-2.0242	-2.1792	-0.7182
H	-1.1813	-2.7018	-1.0200
H	-2.4993	-1.8330	-1.5621
C	-2.9394	-3.0645	0.0620
H	-3.6225	-3.6232	-0.5993
H	-2.3194	-3.8040	0.6001
N	-4.8563	-2.4647	1.6745
C	-5.6800	-3.6705	1.5293
H	-5.7698	-3.9360	0.4660
H	-5.2349	-4.5114	2.0833
H	-6.6808	-3.4596	1.9278
C	-5.1142	-1.4006	2.5311
C	-4.0730	-0.5094	2.3798
H	-3.9100	0.4528	2.8585
H	-6.0058	-1.3747	3.1520
S	-1.2826	1.5599	1.8161
S	-0.2358	-1.7723	1.9324
S	2.1364	0.8188	1.9575
H	1.3821	0.5707	3.0764

Hydride transfer

Stationary point: semihydrogenated dpa

	x	y	z
H	-0.7851	0.5658	4.1735
C	-0.0464	0.4108	4.9893
C	1.2471	0.7482	4.7712
C	-0.7041	-0.1618	6.1933
C	-0.0097	-0.4785	7.3915
C	-2.1015	-0.4141	6.1717
C	-0.6795	-1.0147	8.5003
H	1.0683	-0.2948	7.4350
C	-2.7738	-0.9503	7.2801
H	-2.6619	-0.1787	5.2570
C	-2.0665	-1.2555	8.4566
H	-0.1153	-1.2485	9.4112
H	-3.8541	-1.1310	7.2270
H	-2.5859	-1.6740	9.3255

C	2.4173	0.6884	5.5736
C	2.8727	1.8119	6.3626
C	3.3331	-0.4299	5.5238
C	4.1056	1.8079	7.0212
H	2.2209	2.6915	6.4382
C	4.5617	-0.4159	6.1901
H	3.0435	-1.3126	4.9395
C	4.9787	0.6996	6.9503
H	4.3934	2.6891	7.6107
H	5.2116	-1.2989	6.1202
H	5.9460	0.7063	7.4632

Stationary point: hydrosulfido cluster

	x	y	z
Mo	0.4841	1.7545	0.2917
Mo	1.3580	-1.0277	0.3511
S	0.2149	0.1061	-1.4002
Cl	1.3258	-2.9368	-1.1636
Cl	2.4917	2.5388	-0.9547
Mo	-1.3186	-0.3272	0.4108
Cl	-3.0360	0.7537	-1.0812
N	-3.1258	-1.0098	1.4599
C	-3.6333	-2.1962	1.0710
C	-0.0875	4.7350	0.5856
N	0.6782	3.7762	1.1379
C	4.1454	-2.0822	1.0668
N	2.8499	-2.2881	1.3760
C	2.8068	-3.3609	2.2532
H	1.8716	-3.7477	2.6490
N	3.3727	-0.5603	-0.6350
H	3.4235	0.4427	-0.8973
H	3.3600	-1.0930	-1.5158
C	4.5659	-0.9596	0.1728
H	4.8850	-0.0890	0.7726
H	5.4090	-1.2379	-0.4806
N	4.9296	-2.9824	1.7162
C	6.3963	-3.0540	1.6739
H	6.7082	-4.0259	2.0768
H	6.7450	-2.9706	0.6346

H	6.8364	-2.2471	2.2794
C	4.0952	-3.7951	2.4748
H	4.4897	-4.6007	3.0884
N	-0.6883	3.0939	-1.0782
H	-1.5327	2.5661	-1.3765
H	-0.1228	3.2630	-1.9213
C	-1.0979	4.3993	-0.4646
H	-2.0965	4.2629	-0.0128
H	-1.1845	5.1832	-1.2341
N	0.1807	5.9360	1.1633
C	-0.4724	7.2173	0.8639
H	-0.5281	7.3641	-0.2244
H	-1.4847	7.2411	1.2952
H	0.1305	8.0236	1.3008
C	1.4647	4.3830	2.1039
H	2.1903	3.8274	2.6918
C	1.1577	5.7264	2.1298
H	1.5445	6.5431	2.7333
N	-2.0384	-2.1665	-0.7430
H	-1.2344	-2.7080	-1.1006
H	-2.5462	-1.8093	-1.5637
C	-2.9355	-3.0548	0.0614
H	-3.6454	-3.5934	-0.5875
H	-2.3076	-3.8106	0.5655
N	-4.7819	-2.4565	1.7504
C	-5.6053	-3.6681	1.6468
H	-5.6627	-3.9887	0.5972
H	-5.1757	-4.4767	2.2577
H	-6.6168	-3.4348	2.0037
C	-5.0100	-1.3907	2.6132
C	-3.9801	-0.4955	2.4215
H	-3.8061	0.4675	2.8938
H	-5.8767	-1.3650	3.2682
S	-1.2615	1.5901	1.7650
S	-0.1942	-1.8008	1.8624
S	2.1832	0.8192	1.8353
H	1.4829	0.5519	2.9724

Chapter 5

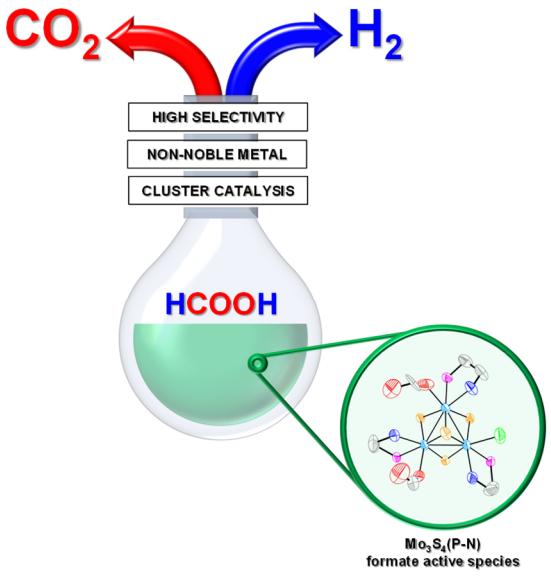

Selective dehydrogenation of formic acid catalyzed by air-stable cuboidal PN molybdenum sulfide clusters

The results presented in this section have already been published. Reproduced from *ChemCatChem,* **2023**, *15*, e202300740 with permission from Wiley-VCH GmbH.

5.1. Main text

5.1.1. Abstract

Formic acid is considered as a promising hydrogen storage material in the context of a green hydrogen economy. In this work, we present a series of aminophosphino and imidazolylamino Mo_3S_4 cuboidal clusters which are active and selective for formic acid dehydrogenation (FAD). Best results are obtained with the new $[Mo_3S_4Cl_3(ed^ipr_rp)_3](BPh_4)$ (**4**(BPh_4)) (ed^ipr_rp = (2-(diisopropylphosphino)ethylamine)) cluster, which is prepared through a simple ligand exchange process from the $Mo_3S_4Cl_4(PPh_3)_3(H_2O)_2$ precursor. Under the conditions investigated, complex **4**$^+$ showed significantly improved performance (TOF = 4048 h^{-1} and 3743 h^{-1} at 120 °C in propylene carbonate using N,N-dimethyloctylamine as base after 10 and 15 min, respectively) compared to the other reported molybdenum compounds. Mechanistic investigations based on stoichiometric and catalytic experiments show that cluster **4**$^+$ reacts with formic acid in the presence of a base to form formate substituted species $[Mo_3S_4Cl_{3-x}(OCOH)_x(ed^ipr_rp)_3]^+$ (x = 1-3) from which the catalytic cycle starts. Subsequently, formate decarboxylation of the partially substituted $[Mo_3S_4Cl_{3-x}(OCOH)_x(ed^ipr_rp)_3]^+$ (x = 1-3) catalyst through a β-hydride transfer to the metal generates the trinuclear Mo_3S_4 cluster hydride. Dehydrogenation takes place through protonation by HCOOH to form Mo-H···HCOOH dihydrogen adducts, with regeneration of the Mo_3S_4 formate cluster. This proposal has been validated by DFT calculations.

5.1.2. Introduction

Major worldwide transformations are required to achieve the United Nations sustainable development goal on affordable and clean energy (SDG 7).[1-3] In this context, hydrogen has emerged as a promising option as a green energy carrier due to its straightforward availability from renewable energy and H_2O.[4] However, specifically storage and transportation of hydrogen remain critical issues regarding safety and practicability. To overcome these limitations, a variety of physical and

chemical hydrogen storage materials are currently under investigation.[5] Among them, formic acid (FA) is widely explored due to its chemical properties such as availability, low toxicity and its recyclability *via* CO_2 hydrogenation.[6]

In general, FA decomposition can proceed *via* decarboxylation giving H_2 and CO_2 or by decarbonylation giving H_2O and CO. In addition, FA can disproportionate to afford CH_3OH, H_2O and CO_2. For practical applications, formation of CO should be avoided because it poisons the catalysts in potential follow up fuel cell applications.[7] In the past decade, a variety of suitable homogeneous and heterogeneous catalysts for FA dehydrogenation have been developed.[6,8] Many of the highly selective catalysts are homogeneous organometallic complexes based on precious metals such as Ru,[9] Ir[10,11] or Rh.[12] In recent years, many efforts have been devoted to develop their earth-abundant counterparts and remarkable advances have been achieved, *e.g.*, using hydrido Fe-PN(H)P pincer complexes[13] while promising results were also obtained with Mn,[14] Co[15] or Cu[16]. In most cases, the structure of the ligand has a strong influence on the dehydrogenation activity due to metal-ligand cooperativity which causes stabilization of the active species or assists outer-sphere interactions involved in key determining mechanism steps.[17]

While molybdenum is one of the Nature's favorite metals for many biological transformations, when it comes to CO_2 hydrogenation or FA dehydrogenation, the number of reported Mo-based catalysts is still rare. In fact, only a few heterogeneous Mo-based catalysts (carbides, nitrides and/or sulfides) are known to catalyze the dehydrogenation of formic acid.[18-23] However, in these cases the chemoselectivity remains a key issue due to the generation of CO. As an example, utilizing MoS_2 nanoclusters deposited on graphene surfaces allowed for quantitative conversion of FA at 250 °C.[21] The major decomposition products are CO_2, H_2 and methyl formate (MF); therefore, in this case disproportionation competes with FA dehydrogenation. Simulation studies of the nanoclusters structure revealed the presence of Mo-edge atoms that the authors tentatively identified as the active sites

of the reaction. In 2021, Li and coworkers reported a CO-free FA dehydrogenation protocol using MoS_2 on graphene decorated on Ni foam (Ni/G/MoS_2).[23] Full conversion and 100% selectivity towards H_2 and CO_2 was achieved at 100 °C. Notably, the latter material has a sulfur terminated surface which has strong adsorption for the H sites and weak adsorption for the O sites of FA. According to the authors, this resulted in the high selectivity of their protocol.

Homogeneous catalytic systems for selective FA dehydrogenations using molybdenum are also limited to a few examples shown in Scheme 5.1.[24-26] Interestingly, the pincer (PN(H)P)MoH(OCOH)$(CO)_2$ compound (Beller and Junge,[25] Scheme 5.1), in addition to FA dehydrogenation, it also catalyzes its disproportionation to methanol while stoichiometric amounts of methanol are produced in the presence of the mononuclear Cp*Mo$(PMe_3)_2$(CO)H hydrido complex (Parkin,[24] Scheme 5.1). In contrast, the hydrido $[Mo_3S_4H_3(dmpe)_3]^+$ (dmpe = 1,2-(bis)dimethyl-phosphinoethane) (Llusar,[26] Scheme 5.1) cluster catalyst is selective towards H_2 production.

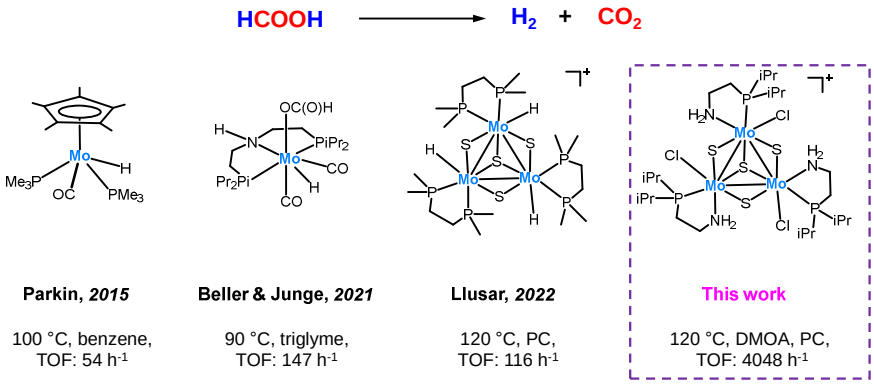

Scheme 5.1. Reported Mo-based catalysts active in the FA dehydrogenation.

The proposed dehydrogenation reaction mechanism for Cp*Mo$(PMe_3)_2$(CO)H and $[Mo_3S_4H_3(dmpe)_3]^+$ share common features. Both complexes interact with FA to form dihydride Mo-(H_2) species or dihydrogen Mo-H···HCOOH species, in the case of $[Mo_3S_4H_3(dmpe)_3]^+$, from which hydrogen is

released with the concomitant formation of formate-substituted derivatives that regenerates the hydrido catalysts through a β-hydride elimination accompanied by CO_2 release. As to (PN(H)P)MoH(OCOH)$(CO)_2$, formate decarboxylation through a β-hydride transfer to the metal generates dihydride Mo-(H_2) species. Selectivity in favor of either dehydrogenation or decarboxylation is determined in the next step. More specifically, dehydrogenation takes place through dihydrogen reductive elimination or *via* protonation by HCOOH, with regeneration of the (PN(H)P)MoH(OCOH)$(CO)_2$ metal hydride. While not mandatory, N-H proton-assisted dehydrogenation may also be operative in this last case. Disproportionation in the presence of mononuclear complexes Cp*Mo$(PMe_3)_2$(CO)H and (PN(H)P)MoH(OCOH)$(CO)_2$ results from a hydride transfer from the metal dihydride Mo-(H_2) species to an activated/protonated molecule of HCOOH. To date, the hydrido $[Mo_3S_4H_3(dmpe)_3]^+$ cluster is the most active and selective homogeneous Mo-based catalysts for FA dehydrogenation.

Herein, we report an efficient and selective homogeneous molybdenum catalyst for FA dehydrogenation using a trinuclear non-hydride metal cluster sulfide decorated with aminophosphine ligands. The optimal $[Mo_3S_4Cl_3(ed^ip_rp)_3]^+$ (ed^ip_rp = 2-(diisopropylphosphino)ethylamine) pre-catalyst operates in the presence of a base without fragmentation of the cluster showing an activity remarkably higher to that of known homogeneous molybdenum catalysts. The synthesis and crystal structure of this new complex is also presented. Finally, a tentative mechanism for this reaction is postulated based on stoichiometric and catalytic experiments, validated by theoretical studies.

5.1.3. Results and discussion

5.1.3.1. Synthesis and characterization of the catalyst

Motivated by the potential of molybdenum cluster sulfides as FA dehydrogenation catalysts, we undertook an exploratory study aimed to identify active cluster complexes. For that purpose, we tested several trinuclear Mo_3S_4 compounds,

represented in Table 5.1. Except for **4**$^{+}$, the synthesis and crystal structures of the rest of the compounds have been previously reported.[25,27-30] The catalytic tests were performed in a glass reactor connected to a manual burette (Figure SI5.5). Initial experiments were performed under base-free reaction conditions (120 ºC and propylene carbonate (PC) as solvent) employed for the catalytic hydrogen production from FA using the diphosphino $[Mo_3S_4H_3(dmpe)_3]^+$ (**2**$^{+}$) cluster.[26] As no gas evolution was observed using the Mo_3S_4 catalysts **3**$^{+}$ to **7**$^{+}$, catalytic tests were performed in the presence of Et_3N. In general, the proposed mechanism for FA dehydrogenation using bifunctional ligands proceeds *via* a formate intermediate, therefore, the base is important to start the catalytic cycle.[31]

Two aminophosphino trinuclear complexes (**3**$^{+}$ and **4**$^{+}$) differing in the nature of the group attached to the phosphorous atom and three imidazolyl amino cluster compounds (**5**$^{+}$-**7**$^{+}$) with the NH_2 moiety gradually substituted by methyl groups were investigated in our work.[29,30] Complex **1**, a typical precursor for the preparation of Mo_3S_4 complexes was also tested.[27] For comparative purposes, we have also included in our studies the diphosphino Mo_3S_4 hydrido cluster (**2**$^{+}$) and the pincer complex (PN(H)P)Mo(OCOH)$(CO)_2$ (**8**).[25,28] The results of catalyst screening are summarized in Table 5.1. Gas evolution/time diagrams are represented in Figure SI5.7.

In the case of the already reported diphosphino $[Mo_3S_4H_3(dmpe)_3]^+$ (**2**$^{+}$) catalyst, addition of Et_3N improved the catalytic activity (TOF 116 *vs.* 411 h^{-1}).[26] For the other Mo_3S_4 clusters (**3**$^{+}$-**7**$^{+}$), gas evolution started after addition of the HCOOH/Et_3N (5:2) mixture to the preheated solution of the catalysts. While similar TON were obtained for compounds **2**$^{+}$, **3**$^{+}$ and **4**$^{+}$ (Table 5.1, entries 2-4), the highest catalytic activity was achieved using compound **4**$^{+}$ (Table 5.1, entry 4). Therefore, replacing the phenyl group bound to the phosphorous atom of the aminophosphino ligand by isopropyl increased the catalytic activity of the Mo_3S_4 cluster complex.

Table 5.1. Catalyst screening for the FA dehydrogenation.[a]

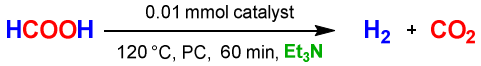

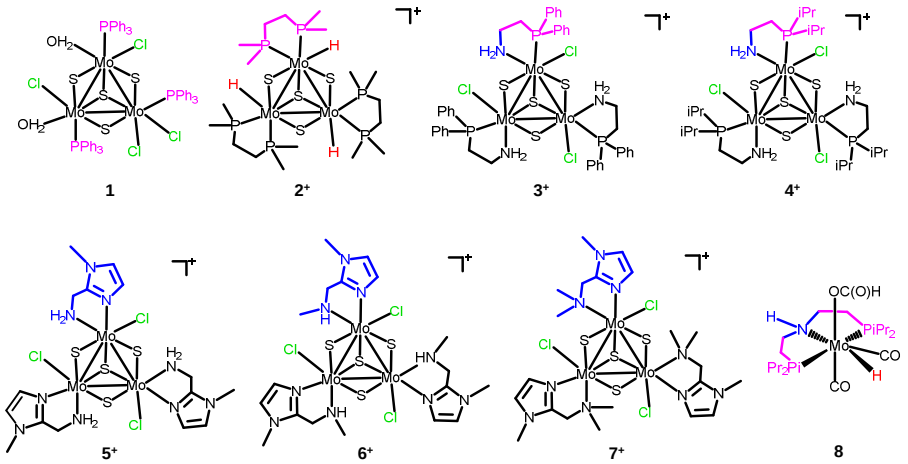

Entry	Catalyst	Conversion(%)[c]	TON[d]	TOF_{10min}[e]
1	1	25	25	55
2	2^+	>99	98	411
3	3^+	97.5	96	272
4	4^+	>99	98	589
5	5^+	85	84	117
6	6^+	10	10	18
7	7^+	4	4	18
8	8^+	2	2	18
9[b]	4^+	-	-	-

[a] Reaction conditions: HCOOH (1 mmol), Et_3N (0.4 mmol), Mo_3S_4 catalyst (0.01 mmol), PC (1.5 mL), T (120 °C), 60 min. [b] Same conditions as [a] without addition of a base. [c] Based on gas evolved. [d] TON values are calculated at the end of the reaction. [e] TOF is obtained for the most active 10 min period of the reaction. Gas evolution monitored with manual burettes, corrected by the blank volume and content of the gas phase analyzed by gas chromatography (GC). The CO content was below the detection limit (<10 ppm) (Figure SI5.6). Experiments were performed at least twice except entry 2.

As expected, no catalytic activity was found for **4**$^{+}$ in the absence of a base (Table 5.1, entry 9). Little gas evolution was observed for the cluster precursor **1** corroborating the crucial role of the ligand. The catalytic activity of the imidazolyl amino-containing clusters decreased in the order **5**$^{+}$ > **6**$^{+}$ > **7**$^{+}$ (Table 5.1, entries 5-7). Hence, we conclude that methylation of one hydrogen atom of the N-H moiety in **5**$^{+}$ leads to a significant decrease in the catalytic activity. In agreement with this observation, complete alkylation of the N-H moieties in **5**$^{+}$ drastically lowered the hydrogen yield. To obtain evidence about the cluster integrity during the catalytic protocol, ESI-MS was recorded after catalytic gas evolution in the presence of the **4**$^{+}$ cluster. Notably, no decomposition products could be observed, and the only peak registered corresponds to the **4**$^{+}$ complex supporting a cluster catalysis mechanism (Figure SI5.14). The catalytic activity of the mononuclear pincer Mo catalyst (**8**) reported as active by some of us for FA dehydrogenation and disproportionation was also tested under these conditions showing only a negligible activity. In all experiments, the possibility of FA disproportionation was also investigated but neither methanol nor methyl formate were detected by gas chromatography.

For the synthesis of the new cluster cation $[Mo_3S_4Cl_3(ed^ip_rp)_3]^+$ (**4**$^{+}$), we followed the procedure developed by one of our groups for the synthesis of other Mo_3S_4 derivatives.[30,32] The cluster precursor $Mo_3S_4Cl_4(PPh_3)_3(H_2O)_2$ was reacted with a slight excess of the aminophosphine ed^ip_rp ligand in EtOH at room temperature for 3 hours. The reaction proceeds with color changes from green to brown and back to green. The desired product was precipitated with pentane as the chloride salt, redissolved in methanol and precipitated with sodium tetraphenylborate as $[Mo_3S_4Cl_3(ed^ip_rp)_3]BPh_4$ (**4**(BPh_4)). The product identity was confirmed by ESI-MS on the basis of its m/z value of 1005.9 and its characteristic isotopic pattern (Figure SI5.4).

The structure of cation **4**$^{+}$ has been determined by single crystal X-ray diffraction as its chloride salt and solved in space group P-1. Figure 5.1 shows the

ORTEP view of **4**$^{+}$ together with the most relevant bond distances. The crystal structure contains two crystallographically independent cluster units, two chloride atoms and one dichloromethane molecule.

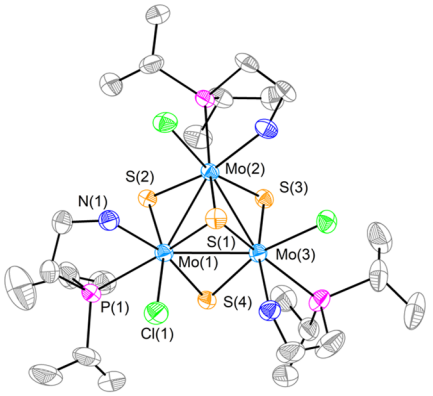

Figure 5.1. ORTEP representation of the $[Mo_3S_4Cl_3(ed^ip_rp)_3]^+$ (**4**$^{+}$) cation (ellipsoids at 50% probability) with the atom-numbering scheme. Hydrogen atoms have been omitted for clarity. Main bond distances: Mo-Mo = 2.760 [6] Å, Mo-(μ_3-S) = 2.346 [4] Å, Mo-(μ-S)$_{trans\text{-}NH_2}$ = 2.300 [5] Å, Mo-(μ-S)$_{trans\text{-}Cl}$ = 2.296 [6] Å, Mo-Cl = 2.510 [12] Å, Mo-N = 2.254 [7] Å, Mo-P = 2.576 [10] Å. Standard deviations for averaged values are given in square brackets. CCDC reference number 2261460.

The trinuclear Mo_3S_4 unit possesses an incomplete cubane-type arrangement with the molybdenum and sulfur atoms occupying adjacent vertices leaving a vacant metal position. The three metal atoms define an approximately equilateral triangle and the Mo-Mo bond distance of 2.760 [6] Å corresponds to a single metal-metal bond. Cluster **4**$^{+}$ shares main geometric features with other trinuclear cluster analogs.[29] Each metal atom in **4**$^{+}$ shows a pseudo-octahedral environment and its coordination sphere includes a phosphorous and a nitrogen atom from the ed^ip_rp ligand, a chlorine atom, one capping and two bridging sulfur atoms. A relevant feature for this compound is the specific coordination of the aminophosphino ligand in which the three phosphorous atoms are located *trans* to the capping sulfur atom as observed for other aminophosphino M_3S_4 (M = Mo, W) clusters.[29,33]

The solid-state structure of complex **4**$^{+}$ is preserved in solution as evidenced by the $^{31}P\{^1H\}$ NMR spectrum registered in CD_2Cl_2, which showed a single signal at 53.55 ppm attributed to the three equivalent phosphorous atoms from the

aminophosphine ligands which are located above the metal plane (Figure SI5.1). The cluster C_3 symmetry is evidenced by ^{1}H NMR spectroscopy where the aminophosphine signals demonstrate that all bidentate ligands are equivalent. In particular, the protons associated to the N-H moiety of the ligand appear at 2.80 and 3.29 ppm in agreement with two different hydrogen orientations. More details about ^{1}H NMR and ^{13}C{^{1}H} NMR spectra are given in the Section 5.2 Supporting Information (SI) (Figures SI5.2 and SI5.3).

5.1.3.2. Catalytic performance

At this point, different important reaction variables were varied such as FA concentration and catalyst loading, solvent, base and FA to base ratio employing $[Mo_3S_4Cl_3(ed^ipr_p)_3]BPh_4$ (**4**(BPh_4)) as catalyst. The influence of the FA concentration was evaluated keeping the amount of catalyst **4**$^+$ constant (Table 5.2: entries 1-3 and Figure SI5.8).

Table 5.2. Molybdenum-catalyzed dehydrogenation of formic acid: Influence of the formic acid concentration and catalyst loading.[a]

Entry	FA (mmol)	Cat. (μmol)	V_{PC} (mL)	$V_{H_2+CO_2}$ (mL)[c]	TON[d]	TOF_{10min} (h^{-1})[f]
1	1	10	1.5	48	98	1472[g]
2	5	10	1.5	281	574	791
3	10	10	1.5	408	834	288
4[b]	10	10	5	450	921	546
5[b]	10	5	5	305	1247[e]	368
6[b]	10	20	5	482	493	1251

[a] Reaction conditions: catalyst **4**$^+$ (0.01 mmol), PC (1.5 mL), T (120 °C). [b] HCOOH (10 mmol), Et_3N (4 mmol), catalyst **4**$^+$ (0.01 mmol), PC (5 mL), T (120 °C). [c] Gas evolution monitored with manual burettes, corrected by the blank volume and content of the gas phase analyzed by GC. [d] TON values are calculated at the end of the reaction. [e] TON value is calculated after system saturation (t = 240 min). [f] TOF values are calculated at the first 10 min of reaction. [g] TOF value is calculated after 4 min. All the experiments were performed at least twice, and average values are used in the table. (St. Dev. < 10%).

Increasing the amount of FA from 1 to 10 mmol (entries 1-3, Table 5.2) proportionally increased the TON. Interestingly, the diphosphino $[Mo_3S_4H_3(dmpe)_3]^+$ (**2**$^+$) losses efficiency at higher HCOOH loading that is at lower pH.[26] However, the TOF_{10min} numbers using **4**$^+$ decreased on going from 5 to 10 mmol of FA (Table 5.2: entries 2-3). This is likely due to pH changes over the course of the reaction. A variation of the FA concentration by increasing the solvent volume (Table 5.2: entries 3-4 and Figure SI5.9) resulted in a remarkable improvement of the catalytic activity. Next, the catalyst loading was investigated at constant FA concentration (Table 5.2: entries 4-6 and Figure SI5.10). A decrease in the catalyst loading by half decreases the catalytic activity; however, doubling the amount of pre-catalyst caused only a *ca.* 2-fold increase of the TOF. Then, we decided to continue our studies using a catalyst concentration of 0.01%, that is, the conditions of entry 4 in Table 5.2.

Previous studies demonstrated that the solvent has a decisive influence in this transformation as it can shift FA decomposition from dehydrogenation to disproportionation.[25] Hence, the effect of the solvent on the reaction was examined and the resulting gas evolution curves are represented in Figure 5.2a. Significant catalytic activity towards hydrogen evolution was observed in toluene although PC continues to be a better choice. In the case of THF, gas release was almost negligible. The reaction mixture was analysed to detect any potential products resulting from FA disproportionation but neither methyl formate nor methanol were detected.

Then, the influence of the temperature was investigated using PC as solvent (Figure 5.2b). As expected, decreasing the temperature resulted in slower gas evolution. Both gas evolution/time curves in Figure 5.2a - 5.2b show a slope change in the curve, that is an induction period, which is more visible for the systems with slower kinetics. In the early stage of the reaction, we also observed a color change from green to brown. These observations agree with **4**$^+$ being the pre-catalyst from which active species are formed after HCOOH/Et_3N addition. Incidentally, **4**$^+$ does not react with HCOOH in the absence of a base (Figures SI5.15-SI5.16).

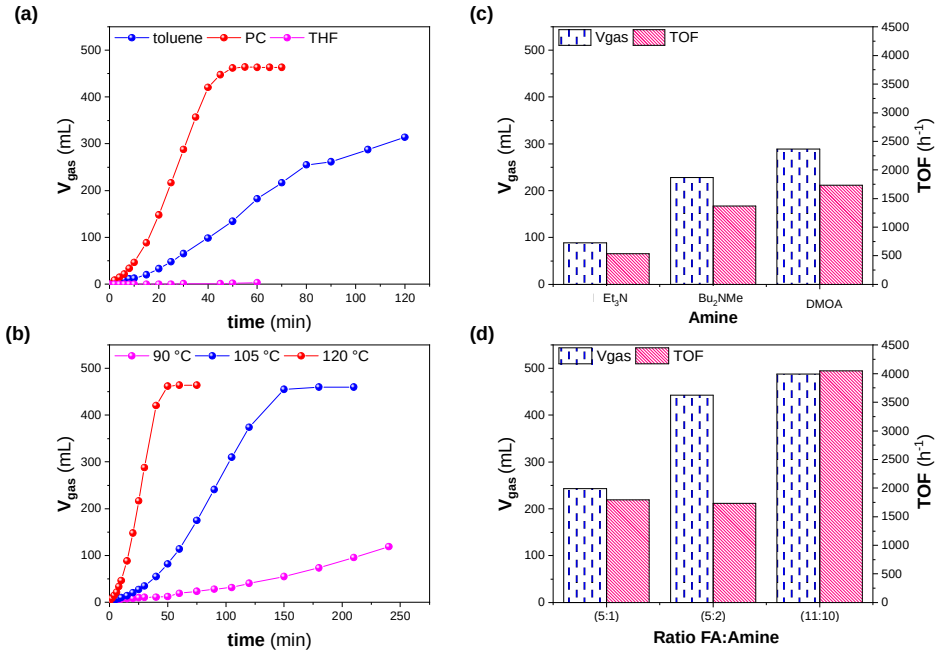

Figure 5.2. Molybdenum-catalyzed dehydrogenation of formic acid. Influence of (a) solvent (toluene, PC, THF), (b) temperature (90 °C, 105 °C, 120 °C), (c) base (Et_3N, Bu_2NMe, DMOA) and (d) ratio of FA:DMOA (5:1, 5:2, 11:10). TOF values are obtained for the first active 10 min period of the reaction. Standard conditions if not otherwise noted: **4**$^+$ was used as the catalyst, 10 mmol of FA, 4 mmol Et_3N, T = 120 °C, 5 mL PC.

In the next step, we investigated the influence of the base as well as the FA to base ratio and the results are summarized in Figures 5.2c-5.2d. The corresponding gas evolution/time curves are given in the Section 5.2 (Figures SI5.11-SI5.12). The use of N,N-dimethyloctylamine (DMOA) instead of Et_3N (Figure 5.2c) noticeably increased the performance achieving TOFs of *ca.* 2000 h^{-1}. Decrease of the FA to DMOA ratio (Figure 5.2d) to 11:10 resulted in a significant improvement of the catalytic activity reaching TOFs of 4048 h^{-1} (3743 h^{-1} after 15 min). On the other hand, a significant drop in the catalytic activity was found upon increasing the FA to DMOA ratio from 5:2 to 5:1 (TOF: 1736 *vs.* 374 h^{-1}) which demonstrates the crucial role of the base during the reaction.

Finally, recycling experiments were performed. After each run, as the base is expected to be recovered, only neat FA was added to the solution. The catalyst

system stayed active in the tested four runs; however, some loss of activity is observed after the second run as shown in Figure SI5.13. We assume that catalyst deactivation occurs through fragmentation of the trinuclear cluster catalyst, in agreement with the previously described diphosphino Mo_3S_4 cluster catalyst.[26] Hence, to further improve this class of catalysts to a practically applicable level, it is important to increase the stability of the cluster by respective ligand design.

5.1.3.3. Mechanistic insights

Previous studies have shown that aminophosphino $[M_3S_4X_3(aminophosphine)_3]^+$ (M = Mo, W) cluster complexes present distinctive features when compared to its diphosphine analogs such as the facile substitution of the halide ligands (X) by other halides or pseudohalides. Conversion occurs *via* the formation of two reaction intermediates associated to the mono and disubstituted trinuclear complexes.[34] Kinetic studies showed that the mechanism of substitution is strongly dependent on the nature of the leaving group. On the other hand, Collision Induced Dissociation (CID) experiments combined with the calculated energy requirements for the partial decoordination of the ligand are contrary to the general idea regarding the hemilabile character of the aminophosphine ligand.[29]

For FA dehydrogenation reactions it is generally accepted that the corresponding formate complex is the starting point or crucial intermediate of the catalytic cycle. Hence, the presence of base and pH are important factors for this transformation.[17,24,26,31] From the formate species, β-hydride elimination produces the respective hydride complex. To gain insight on the ligand substitution process, halide by formate, we investigated the stoichiometric reaction between **4**$^+$ and FA in presence of Et_3N using a FA:Et_3N (5:2) mixture. Milder reaction conditions (lower temperature) compared to those of the catalytic protocol were employed to prevent complications due to β-hydride elimination. The $^{31}P\{^1H\}$ NMR spectrum of the mixture after 10 minutes of reaction in acetonitrile-*d*$_3$ (CD_3CN) at 50 °C shows a series of signals with the typical pattern of a sequential substitution of the **4**$^+$ chlorine atoms by formate ligands, represented in Figure 5.3a.[26] It should be noted that the

loss of symmetry of the two resulting intermediates, the monosubstituted $[Mo_3S_4Cl_2(OCOOH)(ed^ip_rp)_3]^+$ (**M**) and disubstituted $[Mo_3S_4Cl(OCOOH)_2(ed^ip_rp)_3]^+$ (**D**), makes the three phosphorus atoms non-equivalent. For both cluster complexes, three signals of equal intensity are expected in the $^{31}P\{^1H\}$ NMR spectrum. The singlet observed at δ = 56.70 ppm has been tentatively assigned to the triple substituted $[Mo_3S_4(OCOOH)_3(ed^ip_rp)_3]^+$ product (**T**) which recovers the C_3 symmetry of its **4**$^+$ cluster precursor.

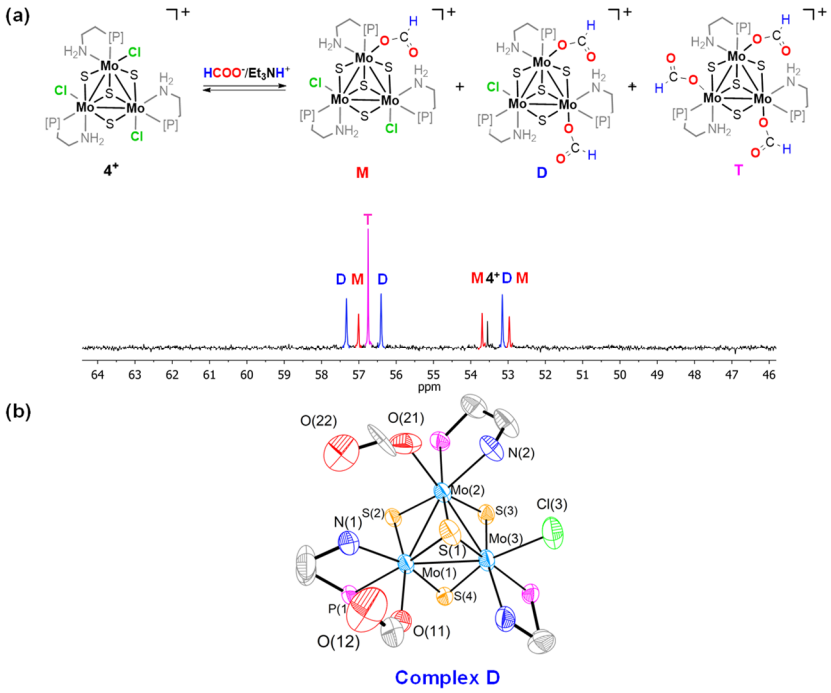

Figure 5.3. Reaction product between **4**$^+$ and 7.5 eq. of a FA/Et_3N (5:2) mixture at 50 ºC in CD_3CN. (a) $^{31}P\{^1H\}$ NMR (162 MHz, CD_3CN, 298 K) spectrum of the reaction mixture, recorded at room temperature. Signals have been tentatively assigned according to the shift in comparison with **4**$^+$ and the trisubstituted complex (**T**). (b) ORTEP representation of the $[Mo_3S_4Cl(OCOH)_2(ed^ip_rp)_3]^+$ cation (ellipsoids at 50% probability) with the atom-numbering scheme. Hydrogen atoms, isopropyl substituents, and the minor component of the disordered ed^ip_rp ligand have been omitted for clarity. Main bond distances: Mo-Mo = 2.760 [5] Å, Mo-(μ_3-S) = 2.357 [13] Å, Mo-(μ-S)$_{trans\text{-}NH_2}$ = 2.295 [12] Å, Mo-(μ-S)$_{trans\text{-}NH_2}$ = 2.292 Å, Mo-(μ-S)$_{trans\text{-}O}$= 2.288 [12] Å, Mo-N = 2.266 [4] Å, Mo-P = 2.572 [10] Å, Mo-O = 2.244 [5] Å, Mo-Cl = 2.512 [15] Å. Standard deviations for averaged values are given in square brackets. CCDC reference number 2261461.

To our delight, some crystals were formed overnight into the NMR tube by slow evaporation of the solvent. While the quality of most of these crystals was not suitable for single crystal X-ray diffraction experiments, finally we were able to select one crystal valid for that purpose. Figure 5.3b shows the ORTEP view of $[Mo_3S_4Cl(OCOH)_2(ed^ip_rp)_3]^+$ (**D**) together with the most relevant bond distances. The crystal structure is solved in space group P-1 and it contains one crystallographically independent cluster unit with formula $[Mo_3S_4Cl(OCOH)_2(ed^ip_rp)_3]^+$ resulting from the substitution of two of the chlorine atoms bound to molybdenum in **4**$^+$ by two formate ligands. Incidentally, one of the ed^ip_rp ligand is disordered over two positions (see 5.1.5. Experimental Section).

The $[Mo_3S_4Cl(OCOH)_2(ed^ip_rp)_3]^+$ cation shares common structural features with its chloride cluster precursor **4**$^+$. Inspection of the interatomic distances revealed the presence of (NH)-H···O(COH) hydrogen bonds with a N(1)-O(11) distance of 2.875 Å and a N(2)-O(21) distance of 2.787 Å. In addition, the terminal formate oxygen atoms O(12) and O(22) forms hydrogen contacts with the H(NH) moiety with a N(1)-O distance of 2.781 Å for O(12) and 2.805 Å for O(22). In order to prove whether or not the measured crystal was representative of the crystalline sample, we recorded the $^{31}P\{^1H\}$ NMR spectrum of the crystalline product after filtration (Figure SI5.17). The spectrum shows eight signals of similar intensity associated to **4**$^+$ and to the mono- (**M**), di- (**D**) and tri-substituted (**T**) formate cluster complexes. Therefore, the crystal structure composition of $[Mo_3S_4Cl(OCOH)_2(ed^ip_rp)_3]^+$ is not representative of the whole crystalline sample. Next, we registered the ESI-MS spectra of the sample at 10 and 20 V (Figures SI5.18-SI5.19). The spectrum at 10 V showed one broad signal which can be tentatively assigned to **4**$^+$ (m/z = 1006) and to the mono-substituted $[Mo_3S_4Cl_2(OCOOH)(ed^ip_rp)_3]^+$ (**M**) (m/z = 1016) complex based on their m/z values and isotopic patterns. Therefore, the di- and tri-substituted species suffer a transformation at the mass spectrometer towards **4**$^+$ (*vide infra*). At higher cone voltages (20 V), a new signal emerged identified as the hydrido $[Mo_3S_4Cl_2H(ed^ip_rp)_3]^+$

(m/z = 972) cluster cation, which suggests that $[Mo_3S_4Cl_2(OCOH)(ed^ip_rp)_3]^+$ (**M**) undergoes partially a β-hydride elimination at the mass spectrometer to form the corresponding hydrido species.

Based on the above results, we propose a tentative catalytic cycle for FA dehydrogenation (FAD), represented in Scheme 5.2, simplified to a single metal center. In our proposal, the cluster **4**$^+$ acts as pre-catalyst in agreement with the induction period observed in the catalytic reaction monitoring (Figure 5.2a-5.2b), as mentioned above. First, the terminal chlorine atoms of the **4**$^+$ cluster are substituted by $HCOO^-$ ligands to form the formate complex. Next β-hydride elimination followed by CO_2 release leads to the hydrido cluster. In the final step, protonation of the hydride results in the formation of dihydrogen species from which hydrogen is released and the active formate species are regenerated. Protonation of the Mo-H group in cuboidal diphosphino Mo_3S_4 clusters by HCOOH to form dihydrogen Mo-H···HCOOH species is well established.[26,35]

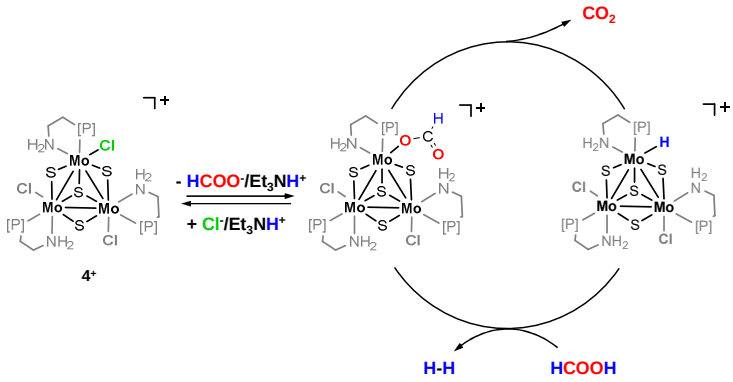

Scheme 5.2. Proposed catalytic cycle for the dehydrogenation of FA.

To obtain information about active species and reaction intermediates, the FAD reaction was monitored by ESI-MS spectrometry and $^{31}P\{^1H\}$ NMR spectroscopy, represented in Figure 5.4. For that purpose, milder reaction conditions (1 mmol of FA, 0.030 mmol of Et_3N and 0.010 mmol of the **4**$^+$ catalyst) were employed to facilitate sampling. At first glance, the reaction monitoring results may

seem contradictory. While ESI-MS only showed the presence of cluster $[Mo_3S_4Cl_3(ed^ip_rp)_3]^+$ (**4**$^+$) without any time evolution along the course of the reaction (Figure 5.4a); the $^{31}P\{^1H\}$ NMR spectrum evidenced the presence of several species in the reaction mixture (Figure 5.4b). Since aminophosphino Mo_3S_4 complexes can undergo transformations in the mass spectrometer, the utility of this technique for reaction monitoring is limited except to confirm the operation of a cluster catalysis mechanism. The $^{31}P\{^1H\}$ NMR spectra after 30 minutes of reaction (Figure 5.4b) within the 52 to 58 ppm range matches with the products obtained from the stoichiometric reaction between the **4**$^+$ cluster catalyst and formic acid in presence of Et_3N (Figure 5.3a), that is the mono-, di- and tri-substituted $[Mo_3S_4Cl_{3-x}(OCOH)_x(ed^ip_rp)_3]^+$ (x = 1,2 and 3) species (**M**, **D** and **T**) plus some unreacted **4**$^+$ cluster. In addition, an extra singlet signal appeared at δ = 64.16 ppm, marked with an **H**. Incidentally, this signal is also observed upon heating the reaction mixture formed by the mono-, di-, and tri-substituted $[Mo_3S_4Cl_{3-x}(OCOH)_x(ed^ip_rp)_3]^+$ (x = 1, 2 and 3) species (Figure SI5.20).

Because it is well known that formate complexes undergo β-hydride elimination to form hydrido species, we have tentatively assigned the singlet signal, labelled as **H**, to the hydrido $[Mo_3S_4H_3(ed^ip_rp)_3]^+$ cluster cation. Notably, we were unable to detect any signal of hydrido species by ^1H NMR spectroscopy. This is not surprising since previous NMR studies on the hydrido $[W_3S_4H_3(edpp)_3]^+$ (edpp = (2-aminoethyl)diphenylphosphine) cluster showed that one of the hydrogen atoms of the NH_2 aminophosphine group is rapidly exchanging with the hydride and as a consequence no hydride signal is seen by ^1H NMR spectroscopy.[36] Unfortunately, all attempts to synthesize and isolate this last postulated species failed.

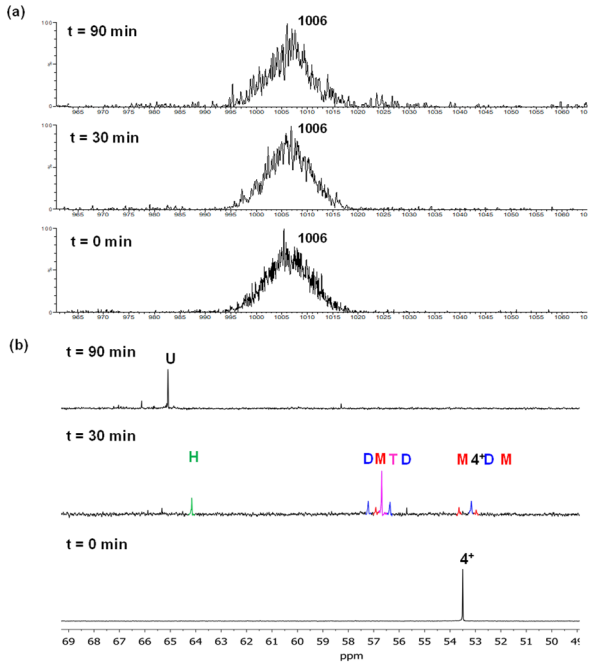

Figure 5.4. Monitoring of the catalytic reaction by (a) ESI-MS spectrometry and (b) $^{31}P\{^{1}H\}$ NMR (162 MHz, CD_3CN, 298 K) spectroscopy. Reaction conditions: HCOOH (1 mmol), Et_3N (0.03 mmol), catalyst **4**$^{+}$ (0.01 mmol), PC (1.5 mL), T (120 °C)

The $^{31}P\{^{1}H\}$ NMR spectrum at the end of the reaction when no FA is left (Figure 5.4b, 90 min) showed a unique signal at δ = 65.09 ppm labelled as **U**. This signal is also observed upon reacting the **4**$^{+}$ complex catalyst with 40 eq. of Et_3N at 50 °C (Figure SI5.21). Previous spectroscopic studies combined with theoretical calculations on the reactivity of the aminophosphino $[W_3S_4Br_3(edpp)_3]^+$ cluster towards Et_3N indicated that the amine acts as a base and abstracts one proton from the NH_2 group of the bidentate ligand while bromine dissociates.[36] Also, Collision Induced Fragmentation (CID) of the $[Mo_3S_4Cl_3(edpp)_3]^+$ (**3**$^{+}$) cluster catalyst occurred with HCl release to yield deprotonated $[Mo_3S_4(edpp\text{-}H)_3]^+$ species.[29] Based on these antecedents, we tentatively assigned the singlet signal at δ = 65.09 ppm to the $[Mo_3S_4(ed^ip_rp\text{-}H)_3]^+$ (**U**) unsaturated Mo=NH amido cluster. It is of interest to remark that the ESI-MS of this reaction mixture, **4**$^{+}$ and Et_3N, showed a sole peak (Figure SI5.22) attributed to the **4**$^{+}$ cluster catalyst. This fact gives further

support to the ability of these aminophosphine Mo_3S_4 clusters to react in the mass spectrometer and transform into the **4**$^{+}$ cluster precursor.

5.1.3.4. Computational studies

Once direct or indirect experimental evidence were obtained to support our mechanism proposal depicted in Scheme 5.2, that is formation of the cluster formate and the hydrido complex, we undertook a theoretical study based on the density functional theory (DFT) to validate our proposal (see 5.1.5.4. Computational Methods for more details). The calculated free energy profile (Figure 5.5) has been restricted to a single metal center, a common simplification in this kind of cluster complexes where substitution reactions occur with statistically controlled kinetics.[35]

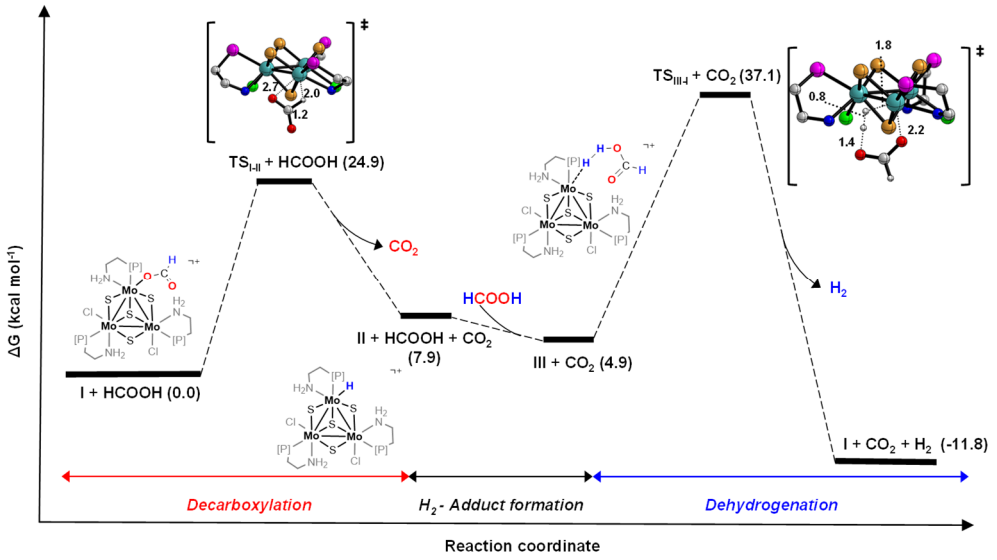

Figure 5.5. DFT calculated energy profile for FA dehydrogenation catalyzed by **4**$^{+}$. Free-energy values are given in kcal mol^{-1}, quoted relative to **I** + HCOOH at 393.15 K and the standard 1 atm pressure. For simplicity, only the skeleton of the ed^{i}p$_{r}$p ligands was drawn. Distances are given in Å. Color code: Mo (cyan), S (orange), P (pink), N (dark blue), O (red), C (grey), H (white).

First, complex **4**$^{+}$ exchanges a chlorine atom by a formate ligand generating the active species (**I**). The process is slightly exergonic (-0.76 kcal·mol^{-1}) in agreement with our experimental observation on the coexistence in the reaction mixture of the

formate substituted $[Mo_3S_4Cl_{3-x}(OCOH)_x(ed^ipr_p)_3]^+$ (x = 1,2,3) species and the **4**$^+$ chloride precursor under stoichiometric conditions. The proposed catalytic cycle (Scheme 5.2) starts with the active formate complex (**I**), considered from this moment on the reference of our cycle. The initial step of the catalytic process entails the liberation of CO_2 from the formate complex (**I**) *via* a β-hydride elimination (**TS$_{I-II}$**). Notice that high temperatures are needed to overcome the barrier (24.9 kcal·mol^{-1}) towards the formation of the hydride species (**II**). This result supports our assignment of the $^{31}P\{^1H\}$ NMR signal registered at δ = 64.16 ppm, labeled with an **H** in Figures 5.4b and SI5.20, only observed in the catalytic reaction mixture run at 120 °C or upon heating at 90 °C the $[Mo_3S_4Cl_{3-x}(OCOH)_x(ed^ipr_p)_3]^+$ (x = 0, 1, 2, and 3) reaction mixture prepared under stoichiometric conditions. In the second step, FA addition results in the formation of a dihydrogen Mo-H···HCOOH (**III**) adduct with a variation in the free energy of -3 kcal·mol^{-1}. The opposite tendency is observed for the formation of the diphosphino Mo_3S_4 dihydrogen adduct which is endergonic at 120 °C by *ca.* 3 kcal·mol^{-1}.[26,35] We attribute the higher stabilization energy in the case of **III** to the hydrogen bond formation between the carbonyl group of the FA and the NH protons of the ligand in the adjacent metal, with a N···O optimized distance of 2.941 Å. The beneficial role of ligands containing NH functionalities in stabilizing formic acid *via* hydrogen bond interactions has been well established in the literature.[31,37]

In the final step, the dihydrogen adduct (**III**) releases hydrogen through **TS$_{III-I}$** and regenerates the formate **I** active species. The calculated barrier for the H_2 release (32.2 kcal·mol^{-1}) indicates that dehydrogenation is the rate determining step. Hence, higher temperatures favour this last step of the catalytic cycle and we observe optimum TON upon increasing the reaction temperature to 120 °C. Similar energy barriers were calculated for the FA dehydrogenation using the diphosphino Mo_3S_4 cluster hydride.[26] Overall, FA dehydrogenation is an exergonic process with a relative energy of -11.8 kcal·mol^{-1} that leads to the regeneration of the catalytic active species.

5.1.4. Conclusions

In this work, we demonstrate that novel molybdenum catalysts are highly active and selective in formic acid dehydrogenation. Within a series of air-stable aminophosphino and imidazolyl amino Mo_3S_4 cuboidal clusters, $[Mo_3S_4Cl_3(ed^ip_rp)_3]^+$ (**4**$^+$, ed^ip_rp = (2-(diisopropylphosphino)ethylamine)) showed significantly improved performance (TOF = 4048 h^{-1}) compared to all other molybdenum compounds reported for this transformation up to date. In the crystal structure of **4**$^+$, the three phosphorous atoms of the ligand are located *trans* to the capping sulfur atoms. Complex **4**$^+$ acts as a pre-catalyst from which the active formate substituted species $[Mo_3S_4Cl_{3-x}(OCOH)_x(ed^ip_rp)_3]^+$ (x = 1, 2, 3) are generated.

These last species coexist with the **4**$^+$ cluster precursor along the catalytic protocol. The crystal structure of one of the substitution products $[Mo_3S_4Cl(OCOH)_2(ed^ip_rp)_3]^+$ shows hydrogen bonding between the formate hydrogen atoms and the aminophosphine NH_2 protons. A cluster catalysis mechanism is proposed based on stoichiometric and catalytic experiments and our proposal has been validated by DFT calculations. The catalytic cycle entails as the first step elimination of CO_2 starting from the active Mo_3S_4 cluster formate through an intermolecular mechanism without the need of a vacant coordination site. The resulting hydrido cluster interacts with FA to form dihydrogen Mo-H···HCOOH species from which hydrogen is released with the concomitant regeneration of the active formate Mo_3S_4 cluster. The overall process is highly selective with a CO content in the generated gas phase bellow 10 ppm.

5.1.5. Experimental section

5.1.5.1. General remarks

All reactions were carried out under inert atmosphere (nitrogen or argon) using standard Schlenck techniques. Reactants obtained from commercial sources were used as received. Solvents were degassed through three freeze-thaw cycles and stored

under argon or nitrogen. Elemental analyses were carried out on a EuroEA3000 Eurovector Analyzer. ^{1}H NMR spectra were obtained at Bruker Avance III HD 400 MHz or 300 MHz. $^{13}C\{^{1}H\}$ NMR spectra were obtained at 101 MHz .$^{31}P\{^{1}H\}$ NMR spectra were recorded at 121 MHz or 162 MHz. NMR chemical shifts are reported in ppm and were referenced to the solvents. $^{31}P\{^{1}H\}$ NMR chemical shifts are reported in ppm referenced to an external 85% solution of H_3PO_4. Abbreviations used in the reported NMR experiments: b, broad; s, singlet; d, doublet; t, triplet; m, multiplet. High resolution mass spectra spectra were registered in a QTOF Premier instrument equipped with an orthogonal Z-spray-electrospray interface (Waters, Manchester, UK) operated in the V-mode at a resolution of *ca.* 10 000 (FWHM). The drying and cone gas was nitrogen set to flow rates of 300 and 30 $L \cdot h^{-1}$, respectively. A capillary voltage of 3.5 kV was used in the positive scan mode and the cone voltage was set to Uc = 20 V. ESI-MS spectra were registered using a triple quadrupole mass spectrometer with an orthogonal Z-spray electrospray source (Waters, Manchester). The temperature of the source block was set to 100 °C, and the solvation temperature was set to 120 °C. A capillary voltage of 3.3 kV was used in the positive scan mode, and the cone voltage was set to Uc = 20 V. Sample solutions in CH_3CN were injected with a syringe pump directly connected to the ESI source at a flow rate of 10 $\mu L \cdot min^{-1}$. Chemical identification of the cluster species was carried out by comparing the experimental and theoretical isotopic pattern calculated from its elemental composition by using the MassLynx 4.1 program.[38] Gas content was determined by gas-phase GC. Presence of methyl formate or methanol in the reaction mixture were performed in the liquid phase(s) by GC using hexadecane as internal standard. GC measurements were carried out on an Agilent 6890A GC System equipped with a FID and a capillary column Agilent (HP-innowax, 30 m x 250 μm x 0.25 μm). Formic acid was quantified in the liquid phase by HPLC (Nucleodur C18 Pyramid 0.25m, 5 μm, UV (210 nm)) applying propionic acid as internal standard.

5.1.5.2. Catalyst preparation

All reactions were performed under a nitrogen atmosphere using standard Schlenck techniques. The trinuclear precursor $Mo_3S_4Cl_4(PPh_3)_3(H_2O)_2$ (**1**) was prepared according to the literature procedure.[27] Cluster salts $[Mo_3S_4H_3(dmpe)_3](BPh_4)$ ([**2**](BPh$_4$)), $[Mo_3S_4Cl_3(edpp)_3]BPh_4$ ([**3**](BPh$_4$)), $[Mo_3S_4Cl_3(ImNH_2)_3]BF_4$ ([**5**](BF$_4$)), $[Mo_3S_4Cl_3(ImNHMe)_3]BF_4$, ([**6**](BF$_4$)) and $[Mo_3S_4Cl_3(ImNMe_2)_3]BF_4$ ([**7**]BF$_4$) were obtained following previously reported synthetic methodologies.[28-30] Mononuclear molybdenum catalyst was provided by the group "Catalysis for Energy Technlogies" in LIKAT.

Synthesis of $[Mo_3S_4Cl_3(ed^ip_rp)_3](BPh_4)$ ([4](BPh$_4$)): A small excess of the diisopropylaminophosphine ligand (76 mg, 0.473 mmol) was added to a green suspension of the freshly prepared $[Mo_3S_4Cl_4(PPh_3)_3(H_2O)_2]$ cluster (200 mg, 0.147 mmol) in 40 mL of nitrogen flushed ethanol. This addition was accompanied by color changes (green → brown → green) and caused the complete solution of the solid. The reaction mixture was reacted for 3 hours at room temperature and then, the volume was reduced to ¼ of the initial volume in the vacuum line. Following, pentane was added until a precipitate appeared, and the mixture was kept in the fridge overnight to complete precipitation process. Next, the solid was separated by filtration, washed with hot hexane and counter anion exchange was carried out by redissolving the solid in the minimum amount of methanol and adding $NaBPh_4$. Then, the desired product was precipitated as a green solid into the methanolic solution. Again, the solid was separated by filtration and washed with methanol and diethyl ether, affording the air-stable product characterized as $[Mo_3S_4Cl_3(ed^ip_rp)_3](BPh_4)$ (110 mg, 68% yield).

^{1}H NMR (CD_2Cl_2, 400 MHz): δ = 1.17 (dd, J = 15.1 Hz and 7.4 Hz, 9H, CH_3, *H$_E$*), 1.26 (dd, J = 14.0 and 7.0 Hz, 9H, CH_3, *H$_E$*), 1.59-1.67 (m, 9H, CH_3, *H$_F$*), 1.70 (dd, J =15.5 and 7.0 Hz, 9H, CH_3, *H$_F$*), 2.32-2.49 (m, 6H, CH_2-N, *H$_B$*), 2.56 (m, 3H, CH-P, *H$_C$*), 2.74 (b, 3H, NH, *H$_A$*), 3.16 (dp, J = 9.2 and 7.1 Hz, 3H, CH, *H$_D$*); 3.32 (d, J = 11.3 Hz, 3H, NH, *H$_A$*), 3.37-3.50 (m, 3H, CH-P, *H$_C$*), 3.71 (h, J = 7.4 Hz, 3H, CH,

H$_D$), 6.87 (t, J = 6.6 Hz, 4H, CH, BPh_4^-), 7.03 (t, J = 7.4 Hz, 8H, CH, BPh_4^-), 7.29-7.34 (m, 8H, CH, BPh_4^-); $^{13}C\{^1H\}$ NMR (CD_3CN, 101 MHz): δ = 20.77 (s, CH_3, *C*$_E$), 21.39 (s, CH_3, *C*$_E$), 21.61 (s, CH_3, *C*$_F$), 21.96 (s, CH_3, *C*$_F$), 27.09 (d, CH_2, *C*$_B$), 27.47 (d, CH, *C*$_D$), 29.65 (d, CH, *C*$_D$), 46.57 (d, CH_2, *C*$_C$), 122.28 (s, CH, BPh_4^-), 126.19 (s, CH, BPh_4^-), 136.51 (s, CH, BPh_4^-); $^{31}P\{^1H\}$ NMR (162 MHz, CD_2Cl_2) δ = 53.55 (s, 3P) ppm; HR-MS (ESI/Q-TOF) *m*/*z* calcd. for $Mo_3S_4Cl_3C_{24}H_{60}N_3P_3^+$: 1005.9100 $[M]^+$; found: 1005.8958 $[M]^+$. Elemental analysis (%) calcd. for $Mo_3S_4Cl_3P_3N_3C_{48}H_{80}B$: C: 43.50; H: 6.08; N: 3.17; S: 9.68; found C: 43.95; H: 6.18; N: 3.32; S: 9.79.

5.1.5.3. X-ray data collection and structure refinement

Single crystals of $[Mo_3S_4Cl_3(ed^ipr^tp)_3]Cl$ [**4**]Cl cluster suitable for X-ray analysis were obtained by slow diffusion of pentane over a dichloromethane solution containing the cluster. Crystals of $[Mo_3S_4Cl(HCOO)_2(ed^ipr^tp)_3]BPh_4$ were grown by slow evaporation of a sample solution of the reaction mixture between **4**$^+$ and excess of FA:Et_3N (5:2) in CD_3CN. Diffraction data collection was performed at T = 200(14) K on an Agilent Supernova diffractometer equipped with an Atlas CCD detector. Mo-K_α radiation (λ = 0.71073 Å) was used for cluster **4**$^+$ and Cu-K_α radiation (λ = 1.54184 Å) in the case of $[Mo_3S_4Cl(OCOH)_2(ed^ipr^tp)_3]^+$. No instrument or crystal instabilities were observed during data collection. Absorption corrections based on the multi-scan method were applied.[39,40] The structures were solved by direct methods and refined by the full-matrix method based on F^2 with the program SHELXL-13 using the Olex2 software package.[41-43]

The structures of the complex salts [**4**]Cl·CH_2Cl_2 and $[Mo_3S_4Cl(OCOH)_2(ed^ipr^tp)_3]BPh_4 \cdot CH_3CN$ were refined in the triclinic P-1 space group. Graphics were performed with the Diamond visual crystal structure information system software.[44] Hydrogen atoms were refined in their geometrically calculated positions using a riding model, whereas those bond to disordered C atoms were not included in the model. The non-hydrogen atoms of the clusters and the counterions were refined anisotropically. In both cases, a solvent molecule was

found in the model. In the **4**$^{+}$ complex one of the chloride counter anions was found disordered over two positions with relative occupancies of 0.58 and 0.42. Also, one C atom of the isopropyl ligand was disordered over two positions, C44 and C45, with relative occupancies of 0.5. For $[Mo_3S_4Cl(OCOH)_2(ed^ip_rp)_3]^+$, also one P atom of one of the ed^ip_rp ligands was disordered over two positions P28A and P28B with a chemical occupancy of 0.15 and 0.85. Nor restrains neither constrains were employed during the refinement. One disordered molecule of acetonitrile was modeled using the solvent mask tool (21 electrons detected, 22 electrons assigned to the disordered CH_3CN; solvent r = 1.2; truncation = 1.2).

CCDC 2261460 and 2261461 contain the supplementary crystallographic data for this chapter. The data can be obtained free of charge from The Cambridge Crystallographic Data Centre via www.ccdc.cam.ac.uk/structures.

5.1.5.4. Catalytic activity test

General procedure for FA dehydrogenation: A 3-neck double wall reactor is attached to a condenser connected to a manual burettes system, illustrated in Figure SI5.5. The apparatus is purged 3 times and flushed with argon for 15 minutes. Solvent and the catalyst are added under an argon overpressure. The setup is heated to the desired temperature while being flushed with argon. Once the temperature is reached, the burette is closed to the atmosphere and the argon/vacuum line is closed. After letting the system equilibrates for 30-60 min, the mixture formic acid:amine is added into the reactor and the timer turns on. When the reaction is finished, a 5 mL degassed syringe was used to obtain a gas sample analyzed by gas chromatography.

5.1.5.5. Computational details

DFT calculations were run with Gaussian 09 (Revision D.01).[44] Geometry optimizations were carried out at the BP86/BS1 level,[45,46] where Mo and S atoms were described using the SDD relativistic ECP and associated basis set,[47] with added polarization functions for the latter (ζ = 0.503),[48] and the remaining atoms were described with the 6-31G(d,p) basis set.[49,50] Solvent effects (propylene carbonate, ε

= 64.0) were included self-consistently in these optimizations through the PCM method.[51,52] Temperature used was 120 ºC and atmospheric pressure. All stationary points were characterized at this level of theory by analytical frequency calculations as either minima (all positive eigenvalues) or transition states (one negative eigenvalue). Intrinsic reaction coordinate (IRC) calculations and subsequent geometry optimizations were used to confirm the minima linked by each transition state. In addition, single-point dispersion corrections were computed using Grimme's D3 parameter set and zero damping.[53] Thus, the free energies shown herein were obtained by adding the dispersion correction to the Gibbs energies computed at the BP86/BS1(PCM) level.

5.1.6. References

[1] D. Mellmann, P. Sponholz, H. Junge, M. Beller, *Chem. Soc. Rev.,* **2016**, *45*, 3954-3988.

[2] G. W. Huber, S. Iborra, A. Corma, *Chem. Rev.,* **2006**, *106*, 4044-4098.

[3] United Nations, "Sustainable Development Goals," can be found under https://sdgs.un.org/goals/goal7.

[4] S. J. Davis, N. S. Lewis, M. Shaner, S. Aggarwal, D. Arent, I. L. Azevedo, S. M. Benson, T. Bradley, J. Brouwer, Y.-M. Chiang, C. T. M. Clack, A. Cohen, S. Doig, J. Edmonds, P. Fennell, C. B. Field, B. Hannegan, B.-M. Hodge, M. I. Hoffert, E. Ingersoll, P. Jaramillo, K. S. Lackner, K. J. Mach, M. Mastrandrea, J. Ogden, P. F. Peterson, D. L. Sanchez, D. Sperling, J. Stagner, J. E. Trancik, C.-J. Yang, K. Caldeira, *Science.,* **2018**, *360*, eaas9793.

[5] P. Preuster, C. Papp, P. Wasserscheid, *Acc. Chem. Res.,* **2017**, *50*, 74-85.

[6] K. Sordakis, C. Tang, L. K. Vogt, H. Junge, P. J. Dyson, M. Beller, G. Laurenczy, *Chem. Rev.,* **2018**, *118*, 372-433.

[7] A. Kumar, S. Semwal, J. Choudhury, *ACS Catal.,* **2019**, *9*, 2164-2168.

[8] M. Younas, M. Rezakazemi, M. S. Arbab, J. Shah, W. U. Rehman, *Int. J. Hydrogen Energy,* **2022**, *47*, 11694-11724.

[9] S. Kar, M. Rauch, G. Leitus, Y. Ben-David, D. Milstein, *Nat. Catal.,* **2021**, *4*, 193-201.

[10] J. H. Barnard, C. Wang, N. G. Berry, J. Xiao, *Chem. Sci.,* **2013**, *4*, 1234-1244.

[11] A. Iturmendi, M. Iglesias, J. Munarriz, V. Polo, V. Passarelli, J. J. Pérez-Torrente, L. A. Oro, *Green Chem.,* **2018**, *20*, 4875-4879.

[12] P. Hermosilla, A. Urriolabeitia, M. Iglesias, V. Polo, M. A. Casado, *Inorg. Chem. Front.,* **2022**, *9*, 4538-4547.

[13] E. A. Bielinski, P. O. Lagaditis, Y. Zhang, B. Q. Mercado, C. Würtele, W. H. Bernskoetter, N. Hazari, S. Schneider, *J. Am. Chem. Soc.,* **2014**, *136*, 10234-10237.

[14] I. Dutta, N. A. Alobaid, F. L. Menicucci, P. Chakraborty, C. Guan, D. Han, K.-W. Huang, *Int. J. Hydrogen Energy,* **2023**, *48*, 26559-26567.

[15] N. Lentz, A. Aloisi, P. Thury, E. Nicolas, T. Cantat, *Organometallics,* **2021**, *40*, 565-569.

[16] N. Scotti, R. Psaro, N. Ravasio, F. Zaccheria, *RSC Adv.,* **2014**, *4*, 61514-61517.

[17] M. Iglesias, F. J. Fernández-Alvarez, *Catalysts,* **2021**, *11*, 1288.

[18] J. Cao, J. Wang, Y. Ma, X. Li, P. Xiaokaiti, X. Hao, A. Abudula, G. Guan, *J. Alloys Compd.,* **2018**, *735*, 1463-1471.

[19] J. Wang, X. Li, J. Zheng, J. Cao, X. Hao, Z. Wang, A. Abudula, G. Guan, *Energy Convers. Manag.,* **2018**, *164*, 122-131.

[20] Z. Yu, Y. Yang, S. Yang, J. Zheng, X. Hao, G. Wei, H. Bai, A. Abudula, G. Guan, *Appl. Catal. B Environ.,* **2022**, *313*, 121445.

[21] V. O. Koroteev, D. A. Bulushev, A. L. Chuvilin, A. V. Okotrub, L. G. Bulusheva, *ACS Catal.,* **2014**, *4*, 3950-3956.

[22] I. Kurnia, A. Yoshida, Y. A. Situmorang, Y. Kasai, A. Abudula, G. Guan, *ACS Sustain. Chem. Eng.,* **2019**, *7*, 8670c8677.

[23] X. Bai, S. Li, Y. Zhang, S. Zhu, L. Gao, R. Cong, W. Yu, S. Wang, B. Liang, Y. Li, *Green Chem.,* **2021**, *23*, 7630-7634.

[24] M. C. Neary, G. Parkin, *Chem. Sci.,* **2015**, *6*, 1859-1865.

[25] E. Alberico, T. Leischner, H. Junge, A. Kammer, R. Sang, J. Seifert, W. Baumann, A. Spannenberg, K. Junge, M. Beller, *Chem. Sci.,* **2021**, *12*, 13101-13119.

[26] E. Guillamón, I. Sorribes, V. S. Safont, A. G. Algarra, M. J. Fernández-Trujillo, E. Pedrajas, R. Llusar, M. G. Basallote, *Inorg. Chem.,* **2022**, *61*, 16730-16739.

[27] V. P. Fedin, M. N. Sokolov, Y. V. Mironov, B. A. Kolesov, S. V. Tkachev, V. Y. Fedorov, *Inorganica Chim. Acta* , **1990**, *167*, 39-45.

[28] A. G. Algarra, M. G. Basallote, M. J. Fernández-Trujillo, M. Feliz, E. Guillamón, R. Llusar, I. Sorribes, C. Vicent, *Inorg. Chem.,* **2010**, *49*, 5935-5942.

[29] T. F. Beltrán, V. S. Safont, R. Llusar, *Eur. J. Inorg. Chem.,* **2016**, 5171-5179.

[30] M. Gutiérrez-Blanco, E. Guillamón, V. S. Safont, A. G. Algarra, M. J. Fernández-Trujillo, K. Junge, M. G. Basallote, R. Llusar, M. Beller, *Inorg. Chem. Front.,* **2023**, *10*, 1786-1794.

[31] M. Iglesias, L. A. Oro, *Eur. J. Inorg. Chem.,* **2018**, 2125-2138.

[32] E. Pedrajas, I. Sorribes, K. Junge, M. Beller, R. Llusar, *ChemCatChem,* **2015**, *7*, 2675-2681.

[33] T. F. Beltrán, R. Llusar, *Polyhedron,* **2019**, *167*, 39-43.

[34] T. F. Beltrán, J. Á. Pino-Chamorro, M. J. Fernández-Trujillo, V. S. Safont, M. G. Basallote, R. Llusar, *Inorg. Chem.,* **2015**, *54*, 607-618.

[35] V. S. Safont, I. Sorribes, J. Andrés, R. Llusar, M. Oliva, M. R. Ryzhikov, *Phys. Chem. Chem. Phys.,* **2019**, *21*, 17221-17231.

[36] J. A. Pino-Chamorro, T. F. Beltrán, M. J. Fernández-Trujillo, M. G. Basallote, R. Llusar, A. G. Algarra, *Eur. J. Inorg. Chem.,* **2017**, 5006-5014.

[37] A. Luque, A. Iturmendi, L. Rubio-Pérez, J. Munárriz, V. Polo, V. Passarelli, M. Iglesias, L. A. Oro, *J. Organomet. Chem.,* **2020**, *916*, 121259.

[38] *MassLynx*, Waters Corporation, Milford, MA, **2005**.

[39] *CrysAlis*, version 171.36.24, Agilent Technologies, Santa Clara, CA, **2012**.

[40] R. C. Clark, J. S. Reid, *Acta Crystallogr. Sect. A,* **1995**, *51*, 887-897.

[41] O. V. Dolomanov, L. J. Bourhis, R. J. Gildea, J. A. K. Howard, H. Puschmann, *J. Appl. Crystallogr.,* **2009**, *42*, 339-341.

[42] L. J. Bourhis, O. V Dolomanov, R. J. Gildea, J. A. K. Howard, H. Puschmann, *Acta Cryst,* **2015**, *71*, 59-75.

[43] G. M. Sheldrick, *Acta Crystallogr. Sect. A Found. Crystallogr.,* **2008**, *64*, 112-122.

[44] Gaussian 09. Revision D.01; M. J. Frisch, G. W. Trucks, H. B. Schlegel, G. E. Scuseria, M. A. Robb, J. R. Cheeseman, G. Scalmani, V. Barone, B. Mennucci, G. A. Petersson, H. Nakatsuji, M. Caricato, X. Li. H. P. Hratchian, A. F. Izmaylov, J. Bloino, G. Zheng, J. L. Sonnenberg, M. Hada, M. Ehara, K. Toyota, R. Fukuda, J. Hasegawa, M. Ishida, T. Nakajima, Y. Honda, O. Kitao, H. Nakai, T. Vreven, J. A. Montgomery, Jr. J. E. Peralta, F. Ogliaro, M. Bearpark, J. J. Heyd, E. Brothers, K. N. Kudin, V. N. Staroverov, T. Keith, R. Kobayashi, J. Normand, K. Raghavachari, A. Rendell, J. C. Burant, S. S. Iyengar, J. Tomasi, M. Cossi, N. Rega, J. M. Millam, M. Klene, J. E. Knox, J. B. Cross, V. Bakken, C. Adamo, J. Jaramillo, R. Gomperts, R. E. Stratmann, O. Yazyev, A. J. Austin, R. Cammi, C. Pomelli, J. W. Ochterski, R. L. Martin, K. Morokuma, V. G. Zakrzewski, G. A. Voth, P. Salvador, J. J. Dannenberg, S. Dapprich, A. D. Daniels, O. Farkas, J. B. Foresman, J. V. Ortiz, J. Cioslowski, D. J. Fox, Gaussian. Inc.: Wallingford CT. **2013**.

[45] J. P. Perdew, *Phys. Rev. B.* **1986**, *33*, 8822-8824.

[46] A. D. Becke, *Phys. Rev. A.*, **1988**, *38,* 3098-3100.

[47] D. Andrae, U. Häussermann, M. Dolg, H. Stoll, H. Preuss, *Theor. Chim. Acta.,* **1990**, *77*, 123-141.

[48] A. Hollwarth, M. Böhme, S. Dapprich, A. W. Ehlers, A. Gobbi, V. Jonas, K. F. Köhler, R. Stegmann, A. Veldkamp, G. Frenking, *Chem. Phys. Lett.,* **1993**, *208*, 237-240.

[49] W. J. Hehre, R. Ditchfield, J. A. Pople, *J. Chem. Phys.,* **1972**, *56*, 2257-2261.

[50] P. C. Harihanan, J. A. Pople. *Theor. Chim. Acta.,* **1973**, *28,* 213-222.

[51] M. Cossi, G. Scalmani, N. Rega, V. Barone, *J. Chem. Phys.,* **2002**, *117*, 43-54.

[52] J. Tomasi, B. Mennucci, R. Cammi, *Chem. Rev.*, **2005**, *105*, 2999-3093.

[53] S. Grimme, J. Antony, S. Ehrlich, H. Krieg, *J. Chem. Phys.,* **2010**, *132*, 154104.

5.2. Supporting information

5.2.1. Catalyst characterization

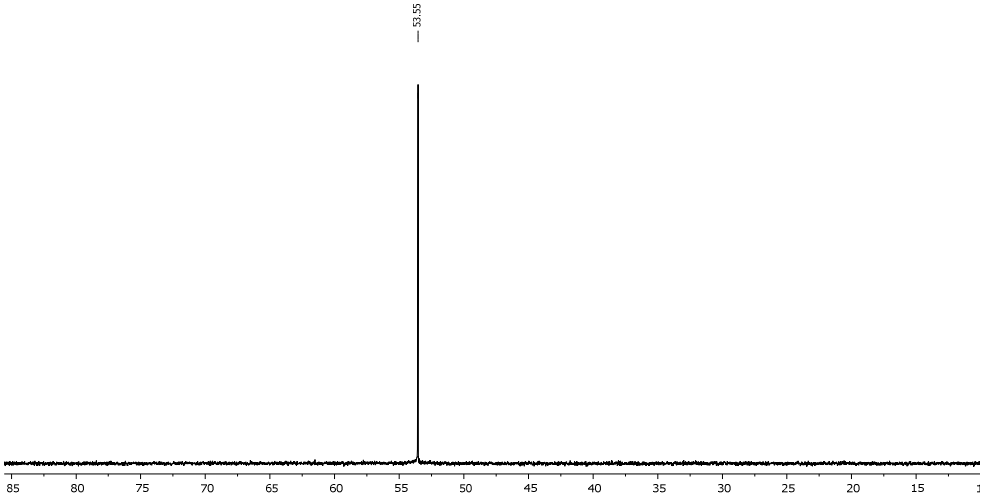

Figure SI5.1. $^{31}P\{^{1}H\}$ NMR (162 MHz, CD_2Cl_2, 298 K) spectrum of the $[Mo_3S_4Cl_3(ed^ipr^tp)_3]BPh_4$ complex.

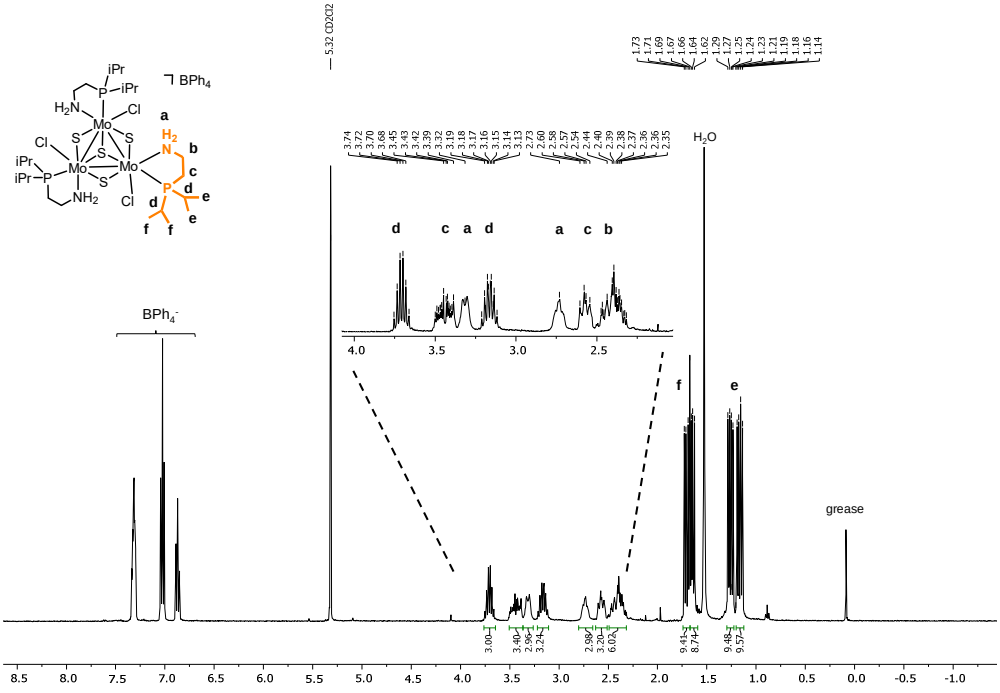

Figure SI5.2. ^{1}H NMR (400 MHz, CD_2Cl_2, 298 K) spectrum of the $[Mo_3S_4Cl_3(ed^ipr^tp)_3]BPh_4$ complex.

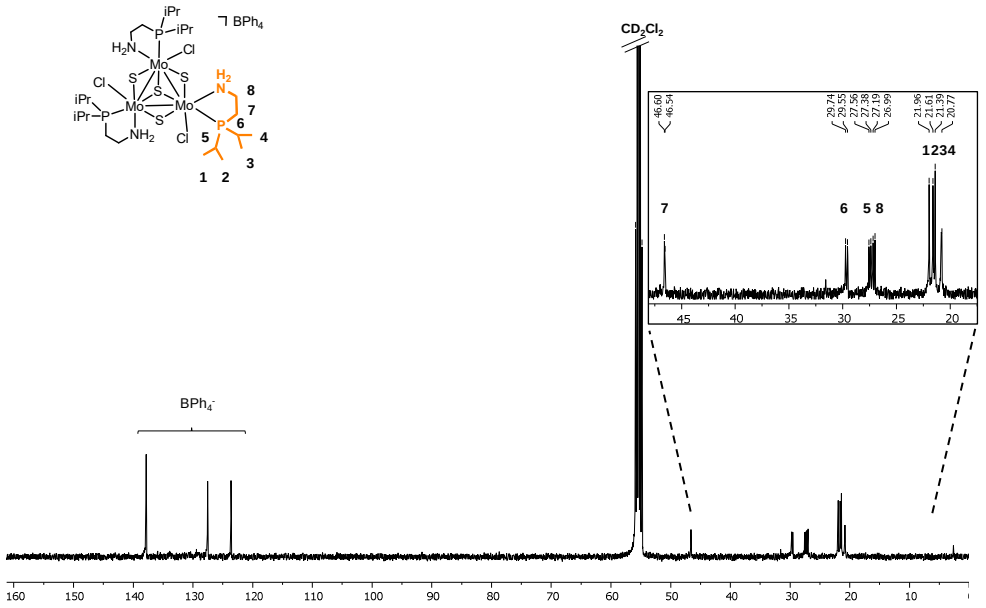

Figure SI5.3. $^{13}C\{^{1}H\}$ NMR (101 MHz, CD_2Cl_2, 298 K) spectrum of the $[Mo_3S_4Cl_3(ed^{i}p_{r}p)_3]BPh_4$ complex.

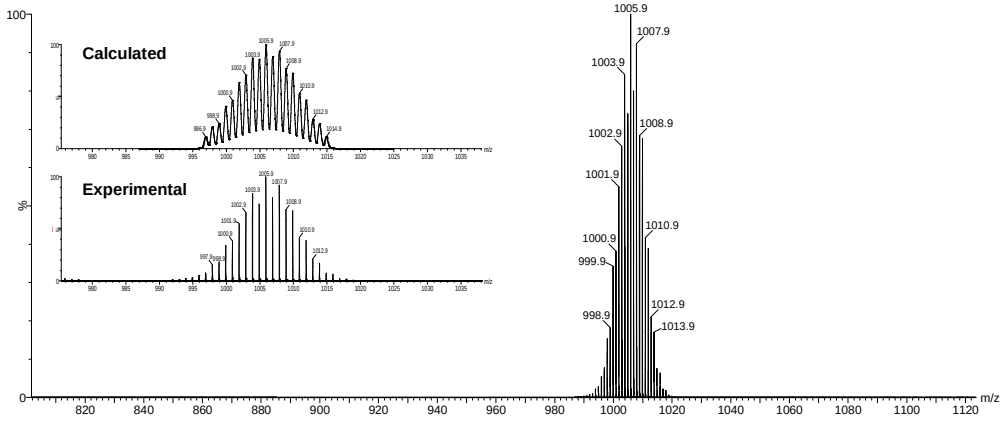

Figure SI5.4. HR-MS spectrum of the $[Mo_3S_4Cl_3(ed^{i}p_{r}p)_3]BPh_4$ complex recorded at 20 V.

5.2.2. Crystallographic data

Crystal data for $[Mo_3S_4Cl_3(ed^ip_rp)_3]_2Cl_2 \cdot CH_2Cl_2$: $C_{49}H_{119}Cl_{10}Mo_6N_6P_6S_8$, M = 2164.93, triclinic, space group P-1, a = 12.9349(6) Å, b = 15.9802(4) Å, c = 22.0560(7) Å, α = 77.986(3)°, β = 87.372(3)°, γ = 78.457(3)°, V = 4368.9(3) Å^3, T = 200(14) K, Z = 2, μ(Mo-K_α) = 1.476 mm^{-1}. Reflections collected/unique = 48677/17122 (R_{int} = 0.0638). Final refinement converged with R_1 = 0.0883 and ωR_2 = 0.1536 for all reflections, GOF = 1.047, max/min residual electron density 2.10/-1.17 e/Å^{-3}.

Crystal data for $[Mo_3S_4Cl(OCOH)_2(ed^ip_rp)_3]BPh_4 \cdot CH_3CN$: $C_{50}H_{82}BClMo_3N_3O_4P_3S_4$, M = 1340.65, triclinic, space group P-1, a = 14.4453(4) Å, b = 14.6827(3) Å, c = 17.4433(6) Å, α = 110.462(3)°, β = 104.417(3)°, γ = 106.362(3)°, V = 3067.37(17) Å^3, T = 200.1(2) K, Z = 2, μ(Cu-K_α) = 7.687 mm^{-1}. Reflections collected/unique = 44782/11827 (R_{int} = 0.0725). Final refinement converged with R_1 = 0.0627 and ωR_2 = 0.1467 for all reflections, GOF = 1.028, max/min residual electron density 1.22/-1.17 e/Å^{-3}.

5.2.3. Formic acid dehydrogenation set-up

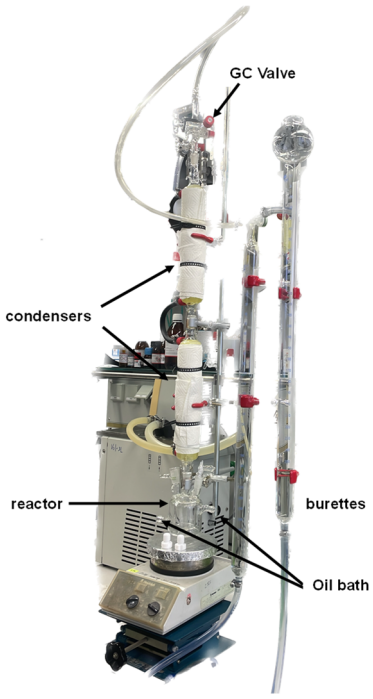

Figure SI5.5. Manual burette set up for the dehydrogenation of FA.

5.2.4. Calculation of TON and TOF

- Molar volume of H_2 and CO_2

Molar volumes can be easily calculated from the Van der Waals equation as follows:

$$V_{m_{H_2}(25\ °C)} = \frac{R \cdot T}{p} + b - \frac{a}{R \cdot T} = 24.48 \qquad \text{(SI5.1)}$$

R = 8.3145 $m^3 \cdot Pa \cdot mol^{-1} \cdot K^{-1}$

T = 273.15 + room temperature (°C) K

P = 101325 Pa

a = 24.9 x 10^{-3} $Pa \cdot m^6 \cdot mol^{-2}$

b = 26.7 x 10^{-6} $m^3 \cdot mol^{-1}$

$$V_{m_{CO_2}(25\,°C)} = \frac{R \cdot T}{p} + b - \frac{a}{R \cdot T} = 24.36 \quad \text{(SI5.2)}$$

R = 8.3145 $m^3 \cdot Pa \cdot mol^{-1} \cdot K^{-1}$

T = 273.15 + room temperature (°C) K

P = 101325 Pa

a = 36.5 x 10^{-2} $Pa \cdot m^6 \cdot mol^{-2}$

b = 42.7 x 10^{-6} $m^3 \cdot mol^{-1}$

- Turnover number (TON)

Gas evolution was corrected with the blank volume considering 1:1 ratio of H_2:CO_2 according to GC analysis (Section SI5.2.5). The blank volume corresponds to the gas evolution of the same reaction without catalyst. The turnover number (TON) is calculated with the following equation:

$$TON = \frac{\frac{Vobs - Vblank}{V_{m_{H_2}} + V_{m_{CO_2}}}}{n_{cat}} \quad \text{(SI5.3)}$$

V_{obs}: volume measured in the catalytic reaction.

V_{blank}: volume measured in the catalytic reaction without catalyst.

$V_{m_{H_2}}$25 °C and $V_{m_{CO_2}}$25 °C: molar volumes of H_2 and CO_2 respectively calculated with the Van Der Waals equation.

- Turnover frequency (TOF)

The turnover number frequency (TOF) was calculated with the experimental TON value.

$$TOF = \frac{TON}{time} \quad \text{(SI5.4)}$$

5.2.5. Typical GC Chromatogram

After the reaction has finished, the gas phase of all the experiments have been analysed by introducing a 10 mL glass syringe through the GC valve, depicted in Figure SI5.5. A typical gas chromatogram is shown in the following figure.

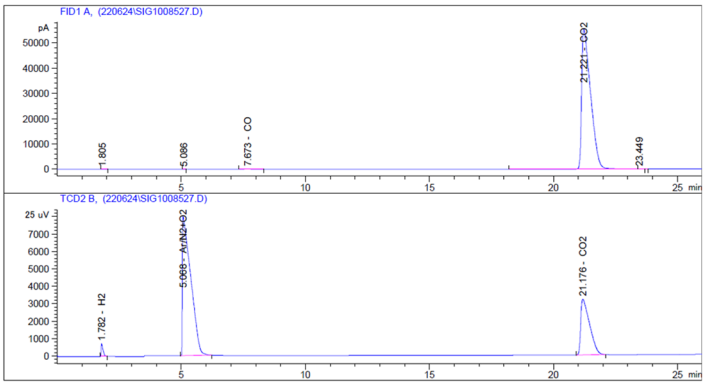


```
=====================================================================
          External Standard Report (Sample Amount is 0!)
=====================================================================

Sorted By             :      Signal
Calib. Data Modified  :      6/27/2022 3:39:33 PM
Multiplier            :      1.0000
Dilution              :      1.0000
Use Multiplier & Dilution Factor with ISTDs

Signal 1: FID1 A,

RetTime  Type     Area     Amt/Area    Amount   Grp   Name
 [min]          [pA*s]                [Vol. %]
-------|------|----------|----------|----------|--|------------------
  7.673 BB      743.79047 1.47840e-5 1.09962e-2    CO
 14.496            -          -          -         CH4
 21.221 BBAS   1.38069e6  1.41658e-5   19.55853    CO2

Totals :                               19.56952

Signal 2: TCD2 B,

RetTime  Type     Area     Amt/Area    Amount   Grp   Name
 [min]         [25 uV*s]              [Vol. %]
-------|------|----------|----------|----------|--|------------------
  1.782 BB     3703.50513 5.88799e-3   21.80619    H2
  5.068 BB S   1.86849e5  3.10131e-4   57.94779    Ar/N2+O2
  7.644            -          -          -         CO
 14.476            -          -          -         CH4
 21.176 BB     7.89177e4  2.44423e-4   19.28928    CO2

Totals :                               99.04326


2 Warnings or Errors :

Warning : Calibrated compound(s) not found
Warning : Elution order of calibrated compounds may have changed

=====================================================================
                        *** End of Report ***
```

Figure SI5.6. Spectra of the gas evolved from the formic acid decomposition reaction. Reaction conditions: HCOOH (10 mmol), HCOOH:Et_3N(5:2), $[Mo_3S_4Cl_3(ed^ipr p)_3]BPh_4$ (0.010 mmol), PC (1.5 mL), T (120 °C), time (4 h). (FID signals measured after methanizing CO and CO_2)

5.2.6. Gas evolution plots

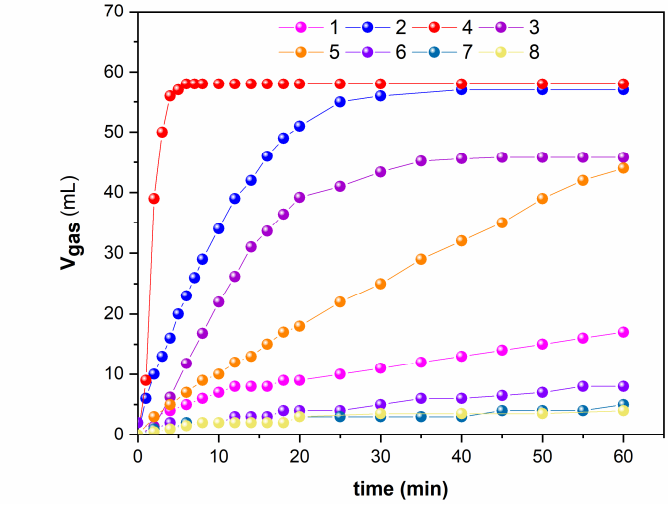

Figure SI5.7. Comparison of the catalytic activity of Mo_3S_4 catalysts. Reaction conditions: HCOOH (1 mmol), Et_3N (0.4 mmol), Mo_3S_4 catalyst (0.01 mmol), PC (1.5 mL), T (120 °C), time (60 min). Gas evolution monitored with manual burettes and content of the gas phase analyzed by GC.

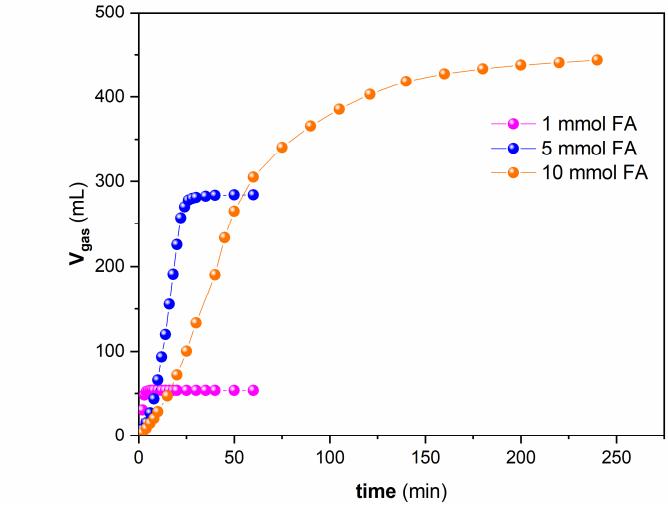

Figure SI5.8. Variation on the formic acid concentration. Reaction conditions: HCOOH (1, 5 and 10 mmol), Et_3N (0.4, 2 and 4 mmol), **4**$^+$ catalyst (0.01 mmol), PC (1.5 mL), T (120 °C), time (60 min). Gas evolution monitored with manual burettes and content of the gas phase analyzed by GC.

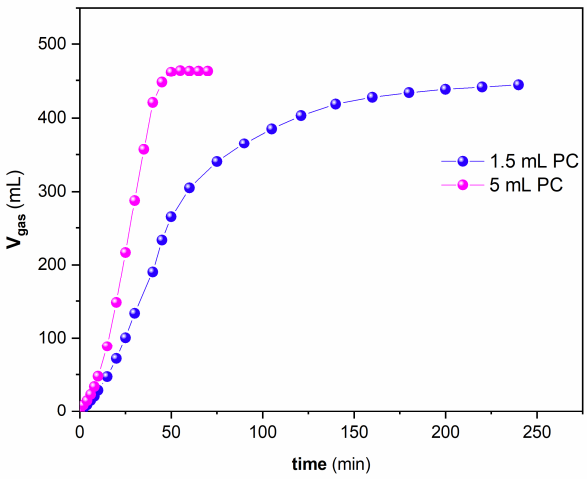

Figure SI5.9. Variation on the solvent volume. Reaction conditions: HCOOH (10 mmol), Et_3N (4 mmol), **4**$^+$ catalyst (0.01 mmol), PC (mL), T (120 °C), time (60 min). Gas evolution monitored with manual burettes and content of the gas phase analyzed by GC.

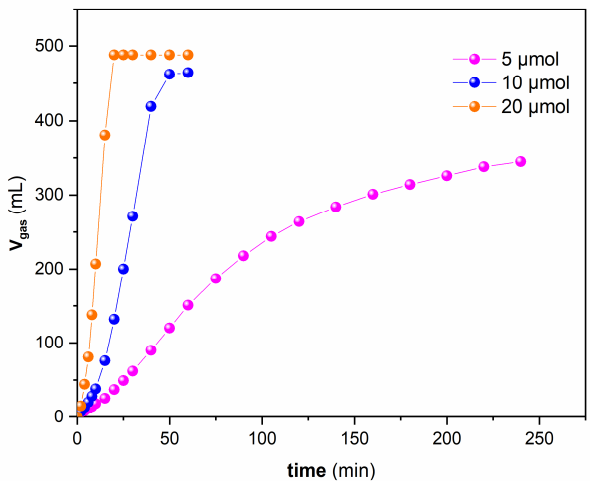

Figure SI5.10. Variation on the catalyst amount. Reaction conditions: HCOOH (10 mmol), Et_3N (4 mmol), **4**$^+$ catalyst (0.01 mmol), PC (5 mL), T (120 °C), time (60 min). Gas evolution monitored with manual burettes and content of the gas phase analyzed by GC.

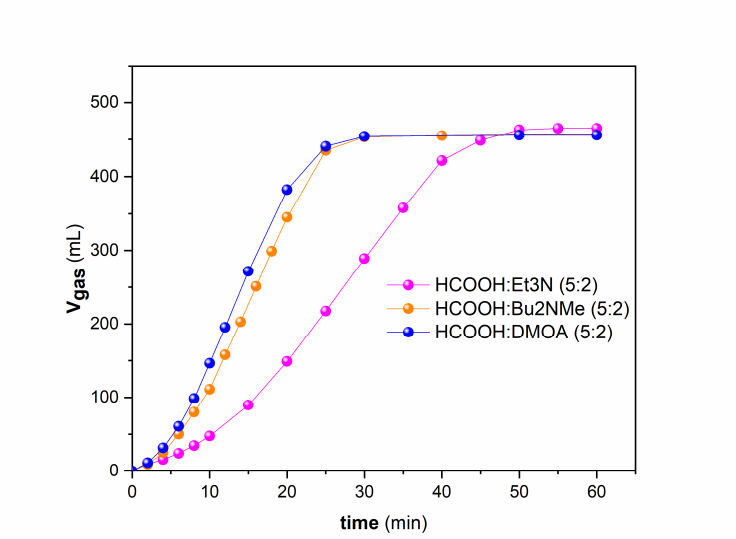

Figure SI5.11. Influence of the base. Reaction conditions: HCOOH (10 mmol), amine (4 mmol), **4**$^{+}$ catalyst (0.01 mmol), PC (5 mL), T (120 °C), time (60 min). Gas evolution monitored with manual burettes and content of the gas phase analyzed by GC.

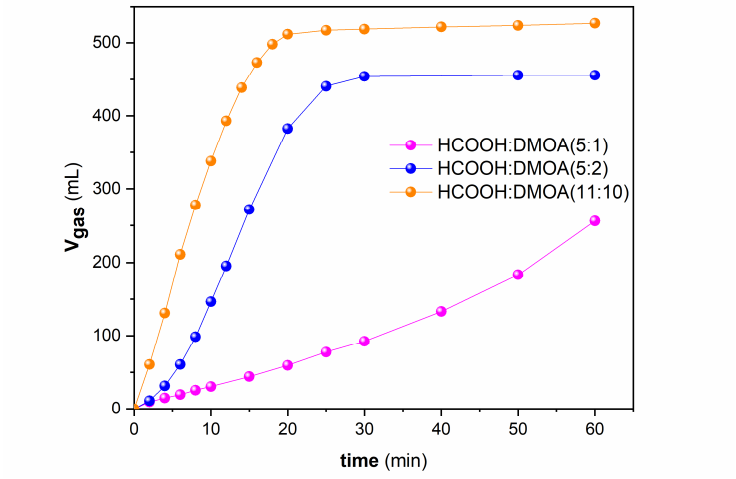

Figure SI5.12. Variation on the ratio FA:amine. Reaction conditions: HCOOH (10 mmol), DMOA (mmol), **4**$^{+}$ catalyst (0.01 mmol), PC (5 mL), T (120 °C), time (60 min). Gas evolution monitored with manual burettes and content of the gas phase analyzed by GC.

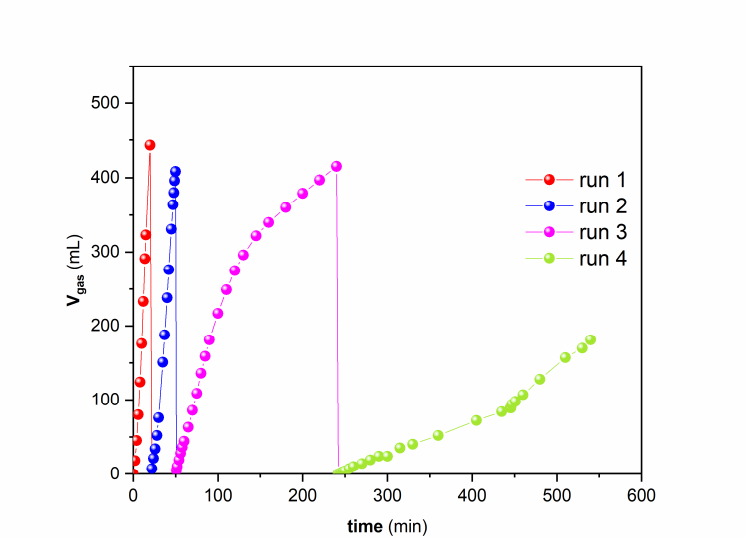

Figure SI5.13. Kinetic profile for the recycling experiments in the dehydrogenation of FA. Reaction conditions: HCOOH (10 mmol), DMOA (4 mmol), **4**$^{+}$ catalyst (0.01 mmol), T (120 ºC), PC (5 mL).

5.2.7. Cluster monitoring during catalysis

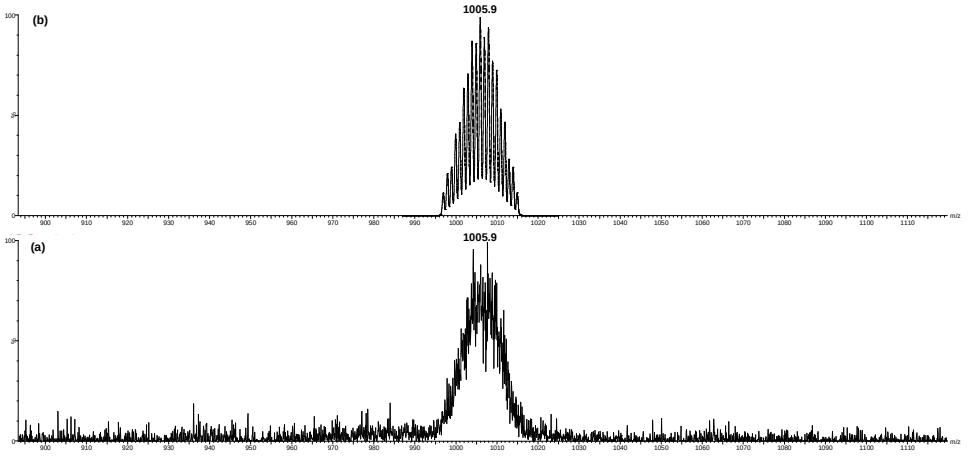

Figure SI5.14. ESI-MS spectra of complex **4**$^{+}$ in CH_3CN at 20 V after the catalytic reaction of FA dehydrogenation (a) compared with the simulated peak (b).

5.2.8. Mechanistic experiments

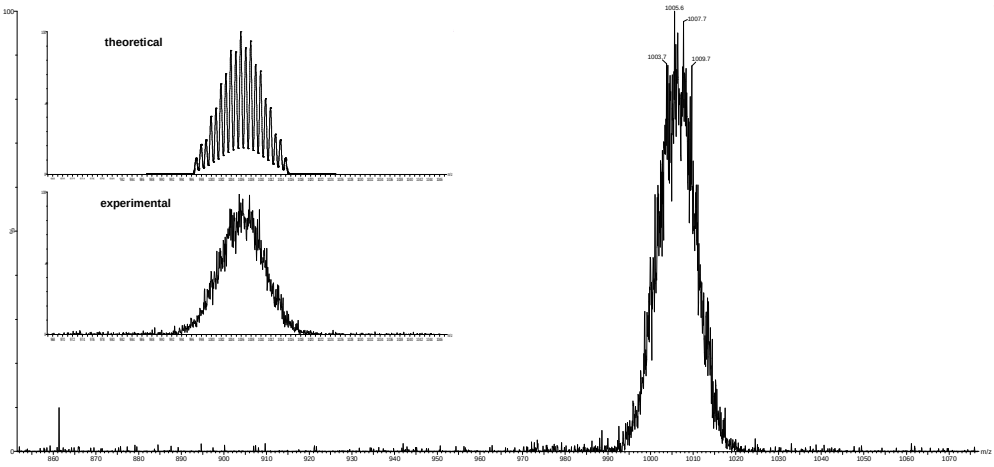

Figure SI5.15. ESI-MS spectra of complex **4**$^{+}$ after 24 h of the addition of an excess of FA (100 eq.) at 50 ºC in CD_3CN. The experiment was recorded at 20 V.

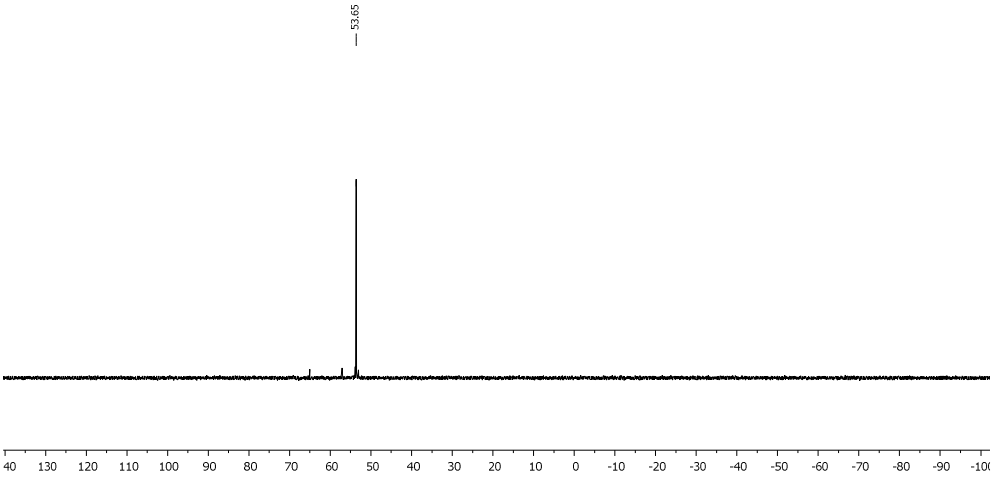

Figure SI5.16. $^{31}P\{^{1}H\}$ NMR (162 MHz, CD_3CN, 298 K) spectrum of complex **4**$^{+}$ after reaction with an excess of FA (100 eq.) at 50 ºC in CD_3CN. The spectrum was recorded at room temperature.

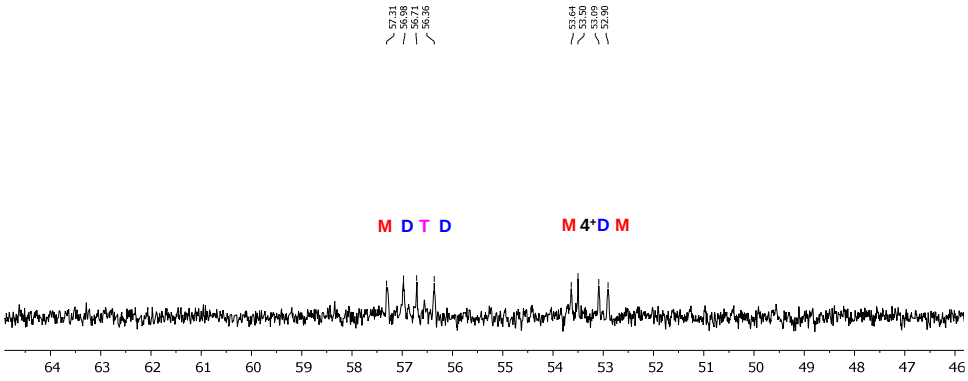

Figure SI5.17. $^{31}P\{^{1}H\}$ NMR (162 MHz, CD_3CN, 298 K) spectrum of the crystals obtained after reacting complex **4**$^{+}$ with a 7.5 eq. of a FA:Et_3N (5:2) mixture.

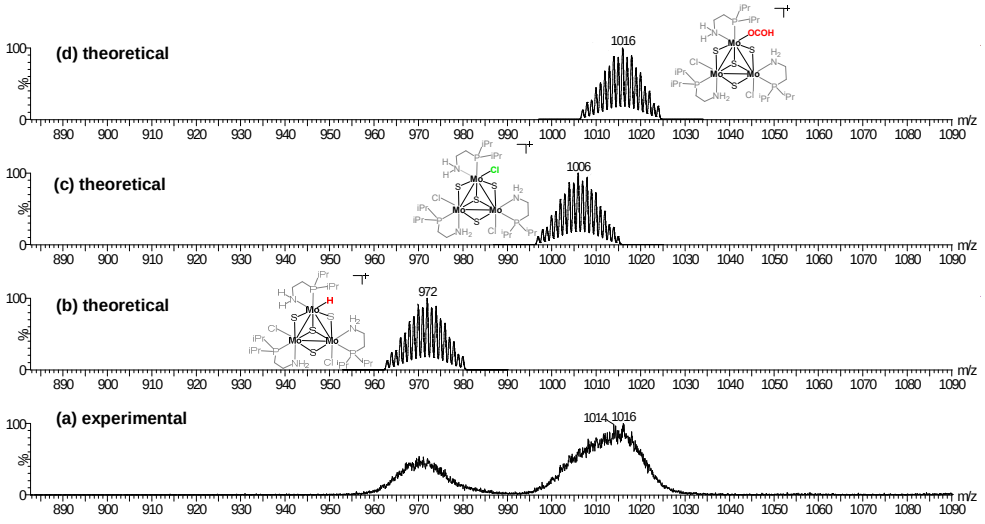

Figure SI5.18. ESI-MS spectra in CH_3CN at 10 V of the crystals obtained after reacting complex **4**$^{+}$ with a 7.5 eq. of a FA:Et_3N (5:2) mixture (a) compared with the simulated peak for $[Mo_3S_4Cl_2(OCOH)(ed^ipr p)_3]^+$(b) and $[Mo_3S_4Cl_3(ed^ipr p)_3]^+$(c).

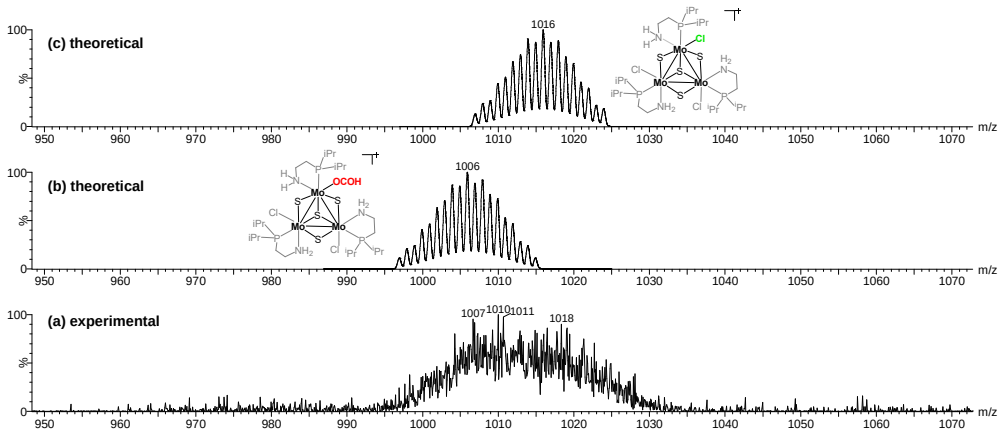

Figure SI5.19. ESI-MS spectra in CH_3CN at 20 V of the crystals obtained after reacting complex **4**$^+$ with a 7.5 eq. of a FA:Et_3N (5:2) mixture (a) compared with the simulated peak for $[Mo_3S_4Cl_2H(ed^ipr^tp)_3]^+$(b) $[Mo_3S_4Cl_3(ed^ipr^tp)_3]^+$(c) and $[Mo_3S_4Cl_2(OCOH)(ed^ipr^tp)_3]^+$(d).

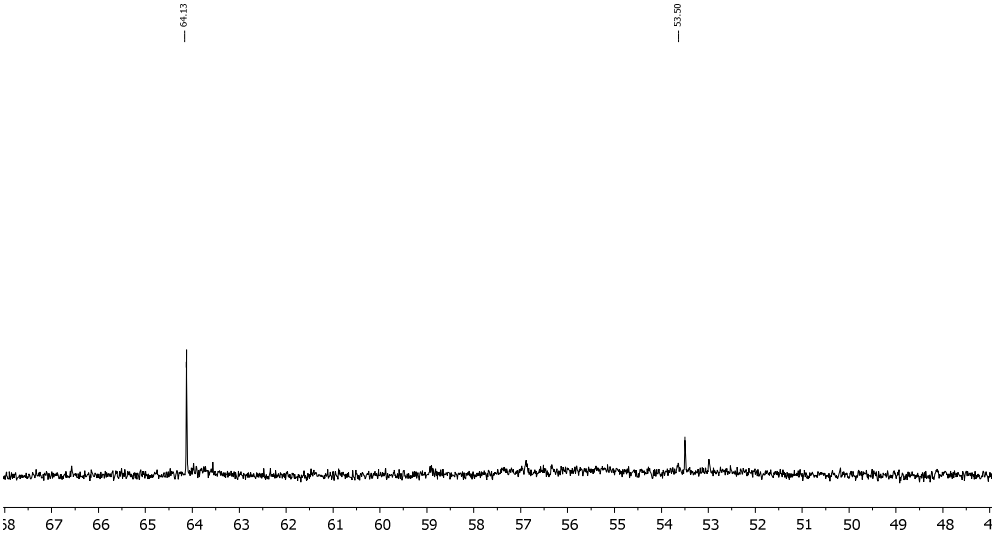

Figure SI5.20. $^{31}P\{^1H\}$ NMR (162 MHz, CD_3CN, 298 K) spectrum of complex **4**$^+$ after reacting with 7.5 eq. of a FA:Et_3N (5:2) mixture upon heating at 90 ºC overnight. Spectra was recorded at room temperature.

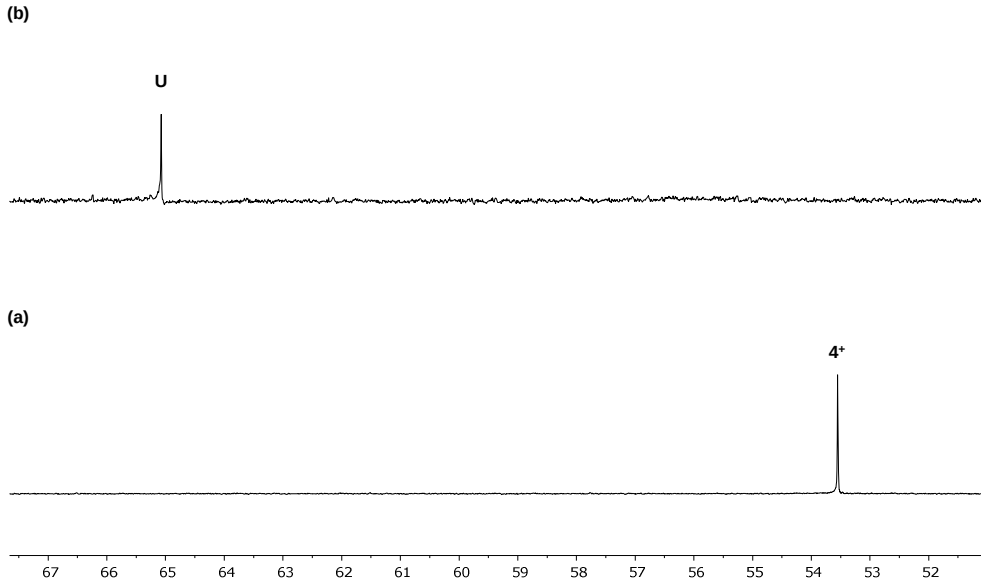

Figure SI5.21. $^{31}P\{^{1}H\}$ NMR (162 MHz, CD_3CN, 298 K) spectra of an acetonitrile-d_3 solution of **4**$^{+}$ (a) in the presence of 40 eq. of triethylamine (b). All experiments were performed at 50 ºC. Spectra were recorded at room temperature.

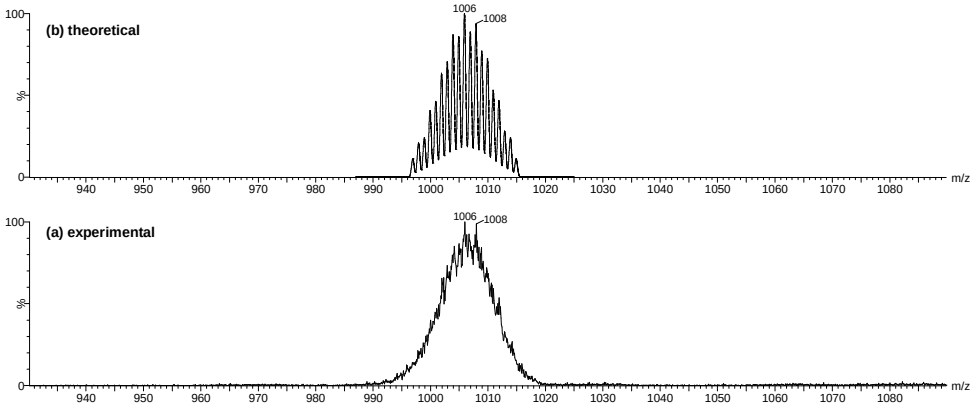

Figure SI5.22. ESI-MS spectra in CH_3CN at 20 V in acetonitrile-d_3 solution of **4**$^{+}$ in the presence of 40 eq. of triethylamine (a) compared with the theoretical (b).

5.2.9. Absolute energies of the computed species

Table SI5.1. BP86 Gibbs Free energies (G corr.) computed with BS1 and including solvent effects; Grimme's D3 dispersion correction. Free energies obtained as the sum of the two previous columns. All values are given in Hartrees/particle.

Species	E(BS1/PCM)	G (BS1/PCM)	D3 corr. (0)	G (BS2)
HCOOH	-189.7699	-189.7705	-0.0012	-189.7717
Et_3N	-292.4054	-292.2560	-0.0203	-292.2763
Et_3NH^+	-292.8677	-292.6989	-0.0237	-292.7226
$HCOO^-$	-189.2862	-189.2995	-0.0006	-189.3001
Cl^-	-460.3924	-460.4130	0.0000	-460.4130
H_2	-1.176599	-1.183072	-0.0001	-1.1832
CO_2	-188.5887	-188.6071	-0.0002	-188.6073
4^+	-3766.1555	-3765.4704	-0.2313	-3765.7017
I	-3495.0815	-3494.381	-0.2345	-3494.615
TSI-II	-3495.038	-3494.339	-0.2365	-3494.576
II	-3306.4671	-3305.7737	-0.2217	-3305.995
III (adduct)	-3496.2512	-3495.5370	-0.2349	-3496.2512
TSIII-I	-3491.9282	-3495.4761	0.2445	-3495.721

5.2.10. Cartesian coordinates of the DFT optimized species

Stationary point: HCOOH

	x	y	z
C	0.1291	0.4030	-0.0001
H	0.0837	1.5109	0.0002
O	1.1526	-0.2623	0.0000
O	-1.1287	-0.0943	0.0000
H	-1.0487	-1.0760	0.0001

Stationary point: Et_3N

	x	y	z
N	-0.0016	-0.0004	-0.7940
C	-1.4420	-0.1538	-0.6349
H	-1.9436	0.5567	-1.3260
H	-1.7013	-1.1681	-0.9960
C	-2.0571	0.0474	0.7713
H	-1.9060	1.0795	1.1304
H	-3.1469	-0.1345	0.7369
H	-1.6200	-0.6396	1.5146
C	0.8518	-1.1710	-0.6371
H	0.4848	-1.9611	-1.3262
H	1.8588	-0.8889	-1.0021
C	0.9902	-1.8021	0.7695
H	0.0232	-2.1911	1.1308
H	1.6966	-2.6517	0.7357
H	1.3639	-1.0766	1.5106
C	0.5861	1.3238	-0.6365
H	1.4501	1.4034	-1.3302
H	-0.1639	2.0556	-0.9950
C	1.0719	1.7556	0.7683
H	1.4544	2.7922	0.7343
H	0.2612	1.7153	1.5144
H	1.8945	1.1119	1.1233

Stationary point: Et_3NH^+

	x	y	z
N	-0.0013	0.0027	-0.9306
C	-1.3647	0.6159	-0.5793
H	-1.5249	1.4021	-1.3334
H	-2.1006	-0.1816	-0.7660
C	-1.5076	1.2027	0.8213
H	-0.8409	2.0638	0.9812
H	-2.5422	1.5726	0.9104
H	-1.3479	0.4668	1.6218
C	0.1476	-1.4861	-0.5827
H	-0.4542	-2.0151	-1.3378
H	1.2057	-1.7259	-0.7705
C	-0.2896	-1.9081	0.8161
H	-1.3682	-1.7599	0.9771
H	-0.0949	-2.9898	0.8995
H	0.2693	-1.4075	1.6190
C	1.2129	0.8755	-0.5792
H	1.9697	0.6249	-1.3388
H	0.8891	1.9124	-0.7583
C	1.8018	0.6986	0.8166
H	2.6440	1.4047	0.9005
H	1.0930	0.9301	1.6240
H	2.2102	-0.3119	0.9700
H	-0.0005	0.0050	-1.9616

Stationary point: Cl^-

	x	y	z
Cl	2.1644	0.1157	0.0000

Stationary point: $HCOO^-$

	x	y	z
C	-0.0001	0.3247	0.0001
H	-0.0006	1.4764	-0.0003
O	-1.1471	-0.2141	0.0000
O	1.1472	-0.2139	0.0000

Stationary point: H_2

	x	y	z
H	0.0000	0.0000	0.3755
H	0.0000	0.0000	-0.3755

Stationary point: CO_2

	x	y	z
C	0.0000	0.0000	0.0000
O	0.0000	0.0000	1.1814
O	0.0000	0.0000	-1.1814

Stationary point: 4^+

	x	y	z
Mo	0.9124	-1.3533	-0.5781
Mo	-1.5909	-0.0945	-0.6717
S	-1.1430	1.7151	0.7334
S	-0.9420	-1.8107	0.7607
S	1.9912	0.1178	0.8650
S	0.0849	-0.0155	-2.3696
Cl	-2.9291	1.3498	-2.3109
Cl	0.4227	-3.3050	-2.1497
Mo	0.7491	1.4470	-0.6024
Cl	2.7591	1.9240	-2.0980
N	-2.5859	-1.7260	-1.9460
H	-1.8418	-2.4021	-2.1977

H	-2.8805	-1.2699	-2.8206
C	-3.7456	-2.4488	-1.3397
H	-3.3460	-3.1070	-0.5504
H	-4.2281	-3.0900	-2.0985
N	2.8728	-1.4151	-1.7704
H	3.0739	-0.4389	-2.0563
H	2.6672	-1.9410	-2.6311
C	4.0681	-2.0020	-1.0948
H	4.3792	-1.2968	-0.3064
H	4.9015	-2.0917	-1.8142
N	-0.1112	3.1276	-1.9110
H	-1.0468	2.8064	-2.2226
H	0.4818	3.1737	-2.7512
C	-0.2190	4.4861	-1.2995
H	-0.5160	5.2222	-2.0676
H	-1.0220	4.4460	-0.5450
P	1.6531	3.5970	0.5775
P	2.2568	-3.2363	0.6455
P	-3.9263	-0.3007	0.4509
C	1.6288	-5.0146	0.9162
H	2.1338	-5.3134	1.8534
C	-5.0379	1.2299	0.4910
H	-4.7026	1.7549	-0.4223
C	3.4938	3.9386	0.9304
H	3.4579	4.5628	1.8424
C	3.7195	-3.3739	-0.5152
H	3.4199	-4.0547	-1.3288
H	4.5939	-3.8193	-0.0140
C	-4.7552	-1.4489	-0.7703
H	-5.1547	-0.8178	-1.5832
H	-5.6064	-1.9792	-0.3127
C	1.1184	4.8839	-0.6727
H	1.8971	4.9194	-1.4526
H	1.0547	5.8868	-0.2204
C	3.0011	-2.7767	2.3228
H	3.4230	-1.7695	2.1479
C	2.0563	-6.0076	-0.1816
H	1.6785	-7.0102	0.0864

H	1.6284	-5.7369	-1.1605
H	3.1508	-6.0845	-0.2799
C	0.1092	-5.0737	1.1562
H	-0.1737	-6.1089	1.4180
H	-0.2126	-4.4181	1.9811
H	-0.4447	-4.7829	0.2488
C	4.1379	-3.6993	2.8026
H	4.9786	-3.7471	2.0924
H	4.5359	-3.3089	3.7558
H	3.7895	-4.7286	2.9951
C	1.8908	-2.6540	3.3859
H	2.3179	-2.2582	4.3236
H	1.0839	-1.9742	3.0647
H	1.4438	-3.6365	3.6177
C	-4.0190	-1.2266	2.0988
H	-3.5596	-2.1976	1.8274
C	-5.4468	-1.4961	2.6128
H	-6.0981	-1.9609	1.8553
H	-5.3943	-2.1891	3.4710
H	-5.9310	-0.5714	2.9670
C	-3.1439	-0.5878	3.1971
H	-3.0695	-1.2835	4.0512
H	-2.1221	-0.3742	2.8431
H	-3.5811	0.3512	3.5719
C	-4.7502	2.1403	1.7008
H	-5.2642	3.1064	1.5531
H	-5.1331	1.7062	2.6391
H	-3.6748	2.3484	1.8255
C	-6.5475	0.9458	0.3483
H	-7.0772	1.9111	0.2607
H	-6.7879	0.3588	-0.5520
H	-6.9611	0.4204	1.2231
C	0.7996	4.1005	2.1890
H	-0.2744	3.9708	1.9602
C	4.2005	4.7571	-0.1672
H	3.7350	5.7432	-0.3231
H	5.2460	4.9316	0.1427
H	4.2186	4.2164	-1.1275

C	4.2781	2.6565	1.2624
H	5.3070	2.9294	1.5574
H	3.8278	2.0923	2.0948
H	4.3340	1.9906	0.3860
C	1.0294	5.5644	2.6099
H	2.0865	5.7698	2.8506
H	0.7048	6.2853	1.8430
H	0.4435	5.7698	3.5229
C	1.1711	3.1234	3.3225
H	0.5659	3.3472	4.2181
H	0.9869	2.0732	3.0406
H	2.2324	3.2228	3.6102

Stationary point: I

	x	y	z
Mo	-0.1352	1.6293	-0.5415
Mo	1.4155	-0.6948	-0.7035
S	0.2063	-2.0318	0.7716
S	1.7373	1.0974	0.7389
S	-1.7975	0.8758	0.8999
S	-0.1576	0.0664	-2.3495
Cl	1.8498	-2.5984	-2.3601
Cl	1.3388	3.0776	-2.0989
Mo	-1.3752	-0.9174	-0.5386
N	3.0390	0.2536	-2.0209
H	2.7016	1.2080	-2.2528
H	3.0546	-0.2806	-2.9006
C	4.4177	0.3310	-1.4526
H	4.4005	1.0884	-0.6512
H	5.1263	0.6772	-2.2259
N	-1.6945	2.7934	-1.7047
H	-2.3540	2.0992	-2.1364
H	-1.1769	3.2234	-2.4847
C	-2.4552	3.8509	-0.9817
H	-3.0961	3.3533	-0.2347
H	-3.1174	4.3858	-1.6866
N	-1.3844	-2.8755	-1.7570

H	-0.4243	-3.0195	-2.1216
H	-1.9902	-2.6917	-2.5674
C	-1.8545	-4.1074	-1.0593
H	-1.9320	-4.9434	-1.7774
H	-1.0886	-4.3763	-0.3125
P	-3.1145	-2.3830	0.7589
P	-0.2760	3.9053	0.7605
P	3.6045	-1.6551	0.3438
C	1.1837	5.0955	1.0499
H	0.9118	5.5904	2.0006
C	3.8456	-3.5303	0.3590
H	3.2986	-3.8144	-0.5591
C	-4.9123	-1.8193	1.0439
H	-5.1855	-2.3157	1.9935
C	-1.4823	4.8331	-0.3271
H	-0.8966	5.3400	-1.1120
H	-2.0207	5.6107	0.2379
C	4.8474	-1.0342	-0.9113
H	4.8708	-1.7724	-1.7320
H	5.8613	-0.9804	-0.4818
C	-3.2119	-3.8482	-0.4039
H	-3.9506	-3.5893	-1.1794
H	-3.5756	-4.7503	0.1138
C	-1.1272	3.8264	2.4499
H	-2.0319	3.2236	2.2452
C	1.3236	6.1910	-0.0248
H	2.1813	6.8340	0.2406
H	1.5214	5.7586	-1.0195
H	0.4353	6.8395	-0.0876
C	2.5207	4.3615	1.2598
H	3.2975	5.1008	1.5248
H	2.4750	3.6175	2.0710
H	2.8346	3.8457	0.3378
C	-1.5743	5.1877	3.0159
H	-2.2439	5.7368	2.3351
H	-2.1296	5.0177	3.9550
H	-0.7194	5.8410	3.2597
C	-0.2571	3.0566	3.4629

H	-0.8203	2.9136	4.4015
H	0.0346	2.0624	3.0852
H	0.6614	3.6155	3.7137
C	4.1695	-0.8980	1.9808
H	4.1942	0.1791	1.7227
C	5.5796	-1.3119	2.4453
H	6.3436	-1.1988	1.6594
H	5.8807	-0.6699	3.2919
H	5.6001	-2.3545	2.8021
C	3.1369	-1.0798	3.1125
H	3.4217	-0.4437	3.9688
H	2.1208	-0.7914	2.7976
H	3.1039	-2.1213	3.4698
C	3.1584	-4.2161	1.5566
H	3.1470	-5.3070	1.3865
H	3.7046	-4.0378	2.4979
H	2.1154	-3.8865	1.6907
C	5.3069	-4.0044	0.2139
H	5.3065	-5.1007	0.0788
H	5.8148	-3.5685	-0.6605
H	5.9101	-3.7839	1.1089
C	-2.5939	-3.1030	2.4251
H	-1.5791	-3.4955	2.2274
C	-5.9011	-2.3012	-0.0348
H	-5.9453	-3.3995	-0.1086
H	-6.9128	-1.9480	0.2316
H	-5.6548	-1.8906	-1.0276
C	-5.0205	-0.2980	1.2555
H	-6.0645	-0.0405	1.5076
H	-4.3780	0.0581	2.0767
H	-4.7409	0.2516	0.3421
C	-3.4739	-4.2634	2.9274
H	-4.5067	-3.9405	3.1443
H	-3.5180	-5.1047	2.2178
H	-3.0510	-4.6515	3.8707
C	-2.4796	-1.9846	3.4807
H	-2.0530	-2.3956	4.4119
H	-1.8291	-1.1614	3.1408

H	-3.4688	-1.5628	3.7307
O	-3.1799	-0.8554	-1.7056
C	-3.7219	-0.1196	-2.6361
H	-4.5673	-0.6381	-3.1449
O	-3.4225	1.0390	-2.9821

Stationary point: TS_{I-II}

	x	y	z
Mo	-0.8283	-1.3613	-0.6622
S	-2.1121	0.0338	0.6861
S	0.9098	-1.7628	0.8070
S	0.9460	1.6663	0.9377
S	0.0946	0.0609	-2.3641
Cl	-2.7670	-1.6373	-2.3334
Mo	-0.7892	1.4324	-0.6135
Cl	-0.0687	3.3916	-2.0713
N	-0.1068	-3.1436	-1.9044
H	0.8929	-2.9552	-2.1092
H	-0.6225	-3.1068	-2.7939
C	-0.2390	-4.5025	-1.3008
H	0.5166	-4.5819	-0.5015
H	-0.0071	-5.2737	-2.0568
N	2.7580	1.8810	-1.5036
H	2.0061	2.5784	-1.6662
C	3.8434	2.4826	-0.6725
H	3.3631	2.9852	0.1828
H	4.3816	3.2527	-1.2527
N	-2.6415	1.6676	-1.9431
H	-2.8904	0.7111	-2.2597
H	-2.3369	2.1881	-2.7774
C	-3.8394	2.3323	-1.3495
H	-4.6035	2.4962	-2.1299
H	-4.2640	1.6419	-0.6020
P	-2.0896	3.3779	0.5591
P	3.9030	0.0463	0.7229
P	-2.0671	-3.3543	0.4709
C	4.9854	-1.4918	0.5236

H	4.7185	-1.8252	-0.4958
C	-3.9574	-3.3084	0.5172
H	-4.1761	-2.6967	-0.3777
C	-1.3394	5.0856	0.9442
H	-1.8793	5.3880	1.8608
C	4.8167	1.3999	-0.1991
H	5.3148	0.9334	-1.0671
H	5.6071	1.8431	0.4295
C	-1.6514	-4.7069	-0.7500
H	-2.3871	-4.6360	-1.5698
H	-1.7523	-5.7058	-0.2958
C	-3.4333	3.6626	-0.7140
H	-3.0179	4.3323	-1.4856
H	-4.3062	4.1682	-0.2710
C	3.8982	0.6489	2.5152
H	3.5013	1.6760	2.3930
C	4.5736	-2.6177	1.4929
H	5.0936	-3.5478	1.2052
H	4.8613	-2.3868	2.5318
H	3.4895	-2.8155	1.4664
C	6.5061	-1.2371	0.5633
H	7.0250	-2.1771	0.3054
H	6.8304	-0.4747	-0.1623
H	6.8505	-0.9313	1.5629
C	5.2935	0.7500	3.1634
H	6.0265	1.2828	2.5367
H	5.2047	1.3079	4.1120
H	5.7017	-0.2447	3.4057
C	2.9183	-0.1251	3.4184
H	2.8456	0.3882	4.3931
H	1.9071	-0.1751	2.9836
H	3.2628	-1.1543	3.6098
C	-1.3736	-3.9802	2.1153
H	-0.3130	-4.1571	1.8480
C	-1.9743	-5.3109	2.6104
H	-1.9598	-6.1036	1.8452
H	-1.3822	-5.6727	3.4695
H	-3.0121	-5.1821	2.9586

C	-1.3988	-2.9117	3.2286
H	-0.7686	-3.2514	4.0690
H	-1.0085	-1.9404	2.8835
H	-2.4166	-2.7561	3.6202
C	-4.5103	-2.5708	1.7532
H	-5.5894	-2.3879	1.6071
H	-4.4016	-3.1734	2.6701
H	-4.0251	-1.5949	1.9175
C	-4.6423	-4.6796	0.3378
H	-5.7331	-4.5197	0.2707
H	-4.3300	-5.1953	-0.5837
H	-4.4588	-5.3530	1.1899
C	-3.0128	2.9455	2.1533
H	-3.4937	1.9776	1.9200
C	-1.6151	6.1498	-0.1346
H	-2.6917	6.3186	-0.2954
H	-1.1771	7.1079	0.1967
H	-1.1497	5.8801	-1.0964
C	0.1610	5.0077	1.2805
H	0.5149	6.0097	1.5821
H	0.3707	4.3144	2.1110
H	0.7457	4.6838	0.4041
C	-4.1138	3.9467	2.5532
H	-3.7088	4.9484	2.7782
H	-4.8938	4.0551	1.7829
H	-4.6079	3.5833	3.4713
C	-2.0140	2.7195	3.3064
H	-2.5519	2.3365	4.1908
H	-1.2306	1.9895	3.0417
H	-1.5218	3.6615	3.6054
Mo	1.6476	0.0189	-0.5483
O	2.5697	-2.2038	-1.7997
H	3.1319	1.6744	-2.4410
C	3.0643	-1.2881	-2.5247
H	3.0669	-0.2474	-1.9353
O	3.5595	-1.2154	-3.6492

Stationary point: II

	x	y	z
Mo	1.1530	-1.0786	-0.6476
Mo	-1.5385	-0.2746	-0.6426
S	-1.4164	1.6275	0.7173
S	-0.5371	-1.8335	0.7798
S	2.1104	0.6147	0.6672
S	0.0476	0.0910	-2.4148
Mo	0.5180	1.6426	-0.6669
N	-2.2462	-2.0811	-1.8807
H	-1.3959	-2.5878	-2.1884
H	-2.6879	-1.6947	-2.7264
C	-3.1800	-3.0320	-1.2091
H	-2.6025	-3.5672	-0.4364
H	-3.5459	-3.7815	-1.9337
N	3.0473	-0.9000	-1.9656
H	3.1005	0.0644	-2.3187
H	2.8691	-1.5012	-2.7824
C	4.3536	-1.2768	-1.3432
H	4.6035	-0.5000	-0.6022
H	5.1486	-1.2799	-2.1100
N	-0.7000	3.1278	-1.9604
H	-1.5971	2.6543	-2.1705
H	-0.2143	3.2371	-2.8586
C	-0.9590	4.4706	-1.3633
H	-1.4396	5.1336	-2.1051
H	-1.6688	4.3231	-0.5323
P	1.2323	3.8910	0.2791
P	2.8381	-2.6828	0.5471
P	-3.7583	-0.9190	0.5545
C	2.5207	-4.5258	0.9173
H	3.1420	-4.7099	1.8130
C	-5.1738	0.3356	0.5455
H	-4.9999	0.8296	-0.4287
C	3.0241	4.4863	0.2000
H	2.9460	5.5744	0.3879
C	4.2405	-2.6565	-0.6923

H	4.0039	-3.4085	-1.4632
H	5.1976	-2.9464	-0.2293
C	-4.3587	-2.2755	-0.5921
H	-4.9425	-1.7804	-1.3879
H	-5.0356	-2.9734	-0.0723
C	0.3485	5.0868	-0.8622
H	1.0200	5.3008	-1.7110
H	0.1534	6.0430	-0.3492
C	3.6054	-2.0430	2.1554
H	3.8899	-1.0046	1.9029
C	3.0034	-5.4820	-0.1904
H	2.7957	-6.5195	0.1260
H	2.4696	-5.3038	-1.1383
H	4.0871	-5.4055	-0.3726
C	1.0548	-4.8122	1.2904
H	0.9626	-5.8683	1.6012
H	0.6994	-4.1849	2.1236
H	0.3882	-4.6467	0.4285
C	4.8689	-2.7917	2.6181
H	5.6630	-2.8048	1.8547
H	5.2794	-2.2846	3.5091
H	4.6546	-3.8339	2.9105
C	2.5412	-1.9870	3.2693
H	2.9581	-1.4823	4.1582
H	1.6433	-1.4322	2.9493
H	2.2299	-2.9992	3.5810
C	-3.6177	-1.7468	2.2473
H	-2.9628	-2.6090	2.0129
C	-4.9366	-2.2934	2.8276
H	-5.4991	-2.9146	2.1120
H	-4.7082	-2.9258	3.7038
H	-5.5959	-1.4808	3.1749
C	-2.8794	-0.8671	3.2775
H	-2.6467	-1.4715	4.1718
H	-1.9328	-0.4680	2.8779
H	-3.4995	-0.0166	3.6051
C	-5.0357	1.4019	1.6503
H	-5.7628	2.2116	1.4614

H	-5.2589	0.9885	2.6482
H	-4.0294	1.8514	1.6744
C	-6.5937	-0.2680	0.5307
H	-7.3187	0.5483	0.3624
H	-6.7387	-1.0051	-0.2746
H	-6.8542	-0.7479	1.4869
C	0.5642	4.3933	1.9803
H	-0.5263	4.4072	1.7831
C	3.6544	4.2742	-1.1890
H	3.0636	4.7183	-2.0067
H	4.6517	4.7479	-1.2049
H	3.7796	3.2007	-1.4066
C	3.9118	3.8582	1.2919
H	4.9386	4.2528	1.1951
H	3.5630	4.0899	2.3099
H	3.9620	2.7614	1.1846
C	0.9932	5.8027	2.4351
H	2.0635	5.8399	2.6991
H	0.8000	6.5786	1.6761
H	0.4235	6.0803	3.3391
C	0.8179	3.3438	3.0804
H	0.2551	3.6254	3.9879
H	0.4870	2.3393	2.7712
H	1.8829	3.2849	3.3588
H	1.6296	2.3137	-1.8242
Cl	0.9093	-3.1278	-2.1692
Cl	-3.1901	0.8486	-2.2672

Stationary point: III (Mo-H···HCOOH adduct)

	x	y	z
Mo	-0.6647	1.4222	-0.4399
Mo	1.6024	-0.2233	-0.6934
S	1.0718	-1.9172	0.8345
S	1.3458	1.6160	0.7198
S	-1.9121	0.1776	1.1031
S	-0.2390	-0.1075	-2.2266
Mo	-0.9215	-1.3664	-0.3164
N	2.6626	1.1985	-2.1591
H	1.9926	1.9599	-2.3753
H	2.8020	0.6656	-3.0287
C	3.9614	1.7824	-1.7099
H	3.7340	2.5132	-0.9160
H	4.4393	2.3296	-2.5422
N	-2.6562	1.8966	-1.4894
H	-3.1113	1.0477	-1.8738
H	-2.3797	2.4548	-2.3104
C	-3.6719	2.6607	-0.7064
H	-4.0297	2.0031	0.1032
H	-4.5363	2.9042	-1.3498
N	-0.4141	-3.2266	-1.5959
H	0.5544	-3.0685	-1.9330
H	-1.0016	-3.2405	-2.4380
C	-0.5047	-4.5517	-0.9122
H	-0.3683	-5.3674	-1.6445
H	0.3290	-4.6034	-0.1926
P	-2.1267	-3.2322	0.9450
P	-1.5228	3.5386	0.8511
P	4.0585	-0.3127	0.1525
C	-0.5606	5.1778	1.0142
H	-0.9055	5.5716	1.9885
C	4.9555	-1.9797	0.1213
H	4.4601	-2.4616	-0.7419
C	-4.0016	-3.2285	1.1879
H	-4.2316	-4.2793	1.4504
C	-3.0469	3.9423	-0.1565

H	-2.7213	4.5806	-0.9945
H	-3.7810	4.5168	0.4307
C	4.8918	0.6799	-1.1980
H	5.1220	-0.0230	-2.0177
H	5.8460	1.1103	-0.8518
C	-1.8517	-4.6898	-0.2013
H	-2.6731	-4.6977	-0.9384
H	-1.9002	-5.6395	0.3570
C	-2.1675	3.2337	2.6039
H	-2.7984	2.3328	2.4887
C	-0.9147	6.2208	-0.0633
H	-0.3280	7.1366	0.1284
H	-0.6576	5.8615	-1.0733
H	-1.9791	6.5033	-0.0454
C	0.9626	4.9715	1.0996
H	1.4462	5.9459	1.2924
H	1.2498	4.2863	1.9128
H	1.3606	4.5685	0.1541
C	-3.0402	4.3642	3.1814
H	-3.9146	4.5950	2.5523
H	-3.4204	4.0521	4.1700
H	-2.4698	5.2967	3.3341
C	-1.0019	2.8845	3.5509
H	-1.4005	2.5922	4.5379
H	-0.3950	2.0482	3.1655
H	-0.3366	3.7513	3.7087
C	4.4741	0.6304	1.7370
H	4.1237	1.6494	1.4792
C	5.9759	0.7088	2.0751
H	6.5955	1.0300	1.2224
H	6.1241	1.4436	2.8860
H	6.3596	-0.2593	2.4364
C	3.6562	0.1515	2.9539
H	3.7986	0.8601	3.7886
H	2.5781	0.0977	2.7327
H	3.9866	-0.8405	3.3012
C	4.6731	-2.8330	1.3732
H	5.0498	-3.8570	1.2026

H	5.1901	-2.4383	2.2637
H	3.5961	-2.9049	1.5966
C	6.4677	-1.9055	-0.1755
H	6.8482	-2.9333	-0.3139
H	6.6965	-1.3461	-1.0962
H	7.0346	-1.4521	0.6524
C	-1.3706	-3.8437	2.5700
H	-0.3819	-4.2041	2.2226
C	-4.7620	-2.8724	-0.1020
H	-4.4766	-3.5018	-0.9603
H	-5.8433	-3.0168	0.0686
H	-4.5986	-1.8184	-0.3798
C	-4.4524	-2.3180	2.3470
H	-5.5528	-2.3561	2.4289
H	-4.0381	-2.6293	3.3181
H	-4.1652	-1.2676	2.1688
C	-2.1259	-5.0295	3.2024
H	-3.1015	-4.7203	3.6133
H	-2.2985	-5.8568	2.4946
H	-1.5295	-5.4324	4.0394
C	-1.1180	-2.7227	3.5977
H	-0.5168	-3.1248	4.4321
H	-0.5661	-1.8775	3.1560
H	-2.0572	-2.3353	4.0252
H	-2.3731	-1.7109	-1.2419
Cl	0.0382	3.2323	-2.1221
Cl	2.5436	-1.8987	-2.4060
O	-3.3609	-1.8654	-3.4819
H	-2.9192	-1.6848	-2.5839
C	-4.2204	-0.8741	-3.7443
H	-4.7566	-1.0617	-4.6953
O	-4.4094	0.1179	-3.0421

Stationary point: TS_{III-I}

	x	y	z
Mo	-0.8284	-1.3997	-0.5156
Mo	-0.8132	1.3964	-0.5716
Mo	1.7444	0.0116	-0.5238
S	0.8073	-1.5893	1.0843
S	-2.2736	0.0149	0.6057
S	0.1016	-0.0310	-2.2685
S	0.7920	1.6344	1.0540
P	-1.9731	-3.3939	0.7416
P	3.9045	0.0959	0.9194
P	-2.2873	3.2094	0.6087
H	2.2912	-1.7327	-0.7190
H	3.8417	-0.8885	-4.0216
C	3.2434	-1.0577	-3.1055
O	3.1538	-0.0626	-2.3003
O	2.7153	-2.1979	-2.9193
H	2.3132	-1.8958	-1.5971
C	5.3615	-1.0368	0.4644
H	6.0325	-0.9459	1.3382
C	3.9498	-0.1136	2.8084
H	4.0209	-1.2122	2.9261
C	4.1428	2.2745	-0.8083
H	4.7202	1.6867	-1.5362
H	4.3939	3.3399	-0.9592
C	4.4770	1.8493	0.6241
H	3.9380	2.4855	1.3496
H	5.5563	1.9664	0.8174
C	-1.7616	-3.6136	2.6264
H	-2.5923	-4.2919	2.8976
C	-3.8190	-3.8376	0.5509
H	-3.9797	-4.5330	1.3976
C	-0.7945	-4.5450	-1.5093
H	-1.7340	-4.4385	-2.0711
H	-0.2127	-5.3672	-1.9626
C	-1.0537	-4.8296	-0.0282
H	-0.0918	-4.9290	0.5021

H	-1.6027	-5.7771	0.1014
C	-2.8608	3.0030	2.4267
H	-2.9761	4.0494	2.7653
C	-1.8482	5.0625	0.6362
H	-2.5876	5.4642	1.3564
C	-3.4848	2.8591	-1.8938
H	-2.9412	3.7237	-2.3039
H	-4.4018	2.7184	-2.4934
C	-3.8448	3.0874	-0.4234
H	-4.4231	2.2300	-0.0409
H	-4.4708	3.9888	-0.3094
N	-2.5884	1.6737	-2.0483
N	2.6972	2.0589	-1.1150
N	-0.0459	-3.2564	-1.6587
H	-2.1667	1.7042	-2.9847
H	-3.1245	0.7917	-2.0127
H	2.5504	2.1626	-2.1271
H	2.1247	2.7919	-0.6747
H	0.0022	-3.0118	-2.6561
H	0.9254	-3.4107	-1.3592
Cl	-0.0329	3.2985	-2.0677
Cl	-2.6787	-1.7926	-2.2879
C	-2.0367	5.8307	-0.6837
H	-3.0670	5.7600	-1.0690
H	-1.3392	5.4829	-1.4602
H	-1.8367	6.9007	-0.4946
C	-0.4373	5.2743	1.2175
H	-0.3128	4.7977	2.2041
H	-0.2492	6.3551	1.3439
H	0.3304	4.8678	0.5387
C	-1.7988	2.3346	3.3190
H	-2.1451	2.3527	4.3678
H	-0.8262	2.8501	3.2760
H	-1.6358	1.2828	3.0291
C	-4.2319	2.3170	2.5846
H	-5.0374	2.8612	2.0662
H	-4.4894	2.2900	3.6583
H	-4.2175	1.2764	2.2198

C	4.9110	-2.5085	0.3754
H	4.2955	-2.8184	1.2372
H	5.8002	-3.1622	0.3497
H	4.3316	-2.7001	-0.5428
C	6.1652	-0.6123	-0.7775
H	6.5942	0.3976	-0.6741
H	5.5560	-0.6396	-1.6936
H	7.0082	-1.3125	-0.9132
C	5.2082	0.5321	3.4300
H	5.2792	0.2283	4.4886
H	5.1434	1.6330	3.4061
H	6.1492	0.2345	2.9404
C	2.6937	0.3706	3.5496
H	2.7941	0.1249	4.6220
H	1.7758	-0.1040	3.1704
H	2.5735	1.4642	3.4687
C	-4.1878	-4.5928	-0.7397
H	-3.6149	-5.5259	-0.8637
H	-4.0448	-3.9623	-1.6302
H	-5.2549	-4.8729	-0.6846
C	-4.7242	-2.6077	0.7516
H	-4.5407	-2.0996	1.7121
H	-5.7815	-2.9273	0.7405
H	-4.5732	-1.8769	-0.0596
C	-1.9601	-2.2861	3.3833
H	-1.9284	-2.4787	4.4703
H	-2.9274	-1.8100	3.1565
H	-1.1612	-1.5663	3.1373
C	-0.4462	-4.3007	3.0408
H	-0.3699	-5.3299	2.6550
H	-0.4113	-4.3599	4.1432
H	0.4393	-3.7328	2.7092

Chapter 6

Conclusions

"In the middle of difficulties lies opportunity."

Albert Einstein

The following concluding remarks can be drawn from the results presented in this PhD thesis:

i. Substitution of the outer ligands in the $Mo_3S_4Cl_4(PPh_3)_3(H_2O)_2$ precursor affords air-stable imidazolyl amino Mo_3S_4 clusters through simple synthetic procedures. All complexes have been fully characterized by elemental analysis, mass spectrometry, and nuclear magnetic resonance.

ii. The structure of the new complexes has been determined by single-crystal X-ray diffraction. The central Mo_3S_4 unit features a C_3 symmetry with the outer positions on each metal occupied by one chlorine and two nitrogen atoms. In all complexes, the amino group is located *trans* to the bridging sulfurs. This disposition is also preserved in solution.

iii. Complexes $[Mo_3S_4Cl_3(ImNH_2)_3]^+$, $[Mo_3S_4Cl_3(ImNHMe)_3]^+$ and $[Mo_3S_4Cl_3(ImNMe_2)_3]^+$ react with diphenylacetylene (dpa) to form the corresponding cycloaddition product under conditions of reversible equilibrium.

iv. The $[Mo_3S_4Cl_3(ImNH_2)_3]^+$ cluster is an efficient chemo- and stereoselective catalyst for the semihydrogenation of a series of dpa derivatives towards the (*Z*)-isomer.

v. Reaction monitoring *via* spectrometric techniques confirms the integrity of $[Mo_3S_4Cl_3(ImNH_2)_3]^+$ during the catalytic reaction thus a cluster catalysis mechanism is proposed. Control experiments suggest the participation of the sulfur bridges in the catalytic cycle.

vi. A mechanism for the (*Z*)-selective semihydrogenation of dpa has been proposed in which H_2 activation occurs at the sulfur bridges and generates a bis(hydrosulfido) $[Mo_2^{III}Mo^{IV}(\mu_3\text{-}S)(\mu\text{-}S\text{-}H)_2(\mu\text{-}S)]^{4+}$ intermediate. Then, semihydrogenation of the dpa by the bis(hydrosulfido) species occurs in a two-step process to render the (*Z*)-stilbene. Analysis of the transferred hydrogens as a hydride, proton, or hydrogen atom confirms that the process

falls within a hydrogen atom transfer category by the $[Mo_3^{IV}(\mu_3\text{-}S)(\mu\text{-}S\text{-}H)_2(\mu\text{-}S)]^{4+}$cluster.

vii. Catalytic experiments using deuterated methanol agree with the formation of acidic hydrosulfido ligands acting as the active sites. Exchange of the S-H protons by deuterium the vinylic dpa positions to afford (*Z*)-d_2-stilbene.

viii. The catalytic activity of a series of Mo_3S_4 cluster derivatives (diphosphine, aminophosphine, diamine, etc), including the new imidazolyl amino complexes, have been tested in formic acid dehydrogenation (FAD). The best performance is achieved with the aminophosphine cluster complex $[Mo_3S_4Cl_3(ed^ipr_fp)_3]^+$.

ix. The FAD process is highly selective towards CO_2 and H_2 with a CO content below 10 ppm.

x. Spectroscopic and spectrometric techniques confirm the integrity of $[Mo_3S_4Cl_3(ed^ipr_fp)_3]^+$ cluster cation throughout the reaction. Mechanistic investigations based on stoichiometric and catalytic experiments suggest that the $[Mo_3S_4Cl_{3-x}(OCOH)_x(ed^ipr_fp)_3]^+$(x = 1-3) formate complexes act as the active species in the FAD process.

xi. The above proposal has been validated by DFT calculations. The first step entails CO_2 elimination from $[Mo_3S_4Cl_{3-x}(OCOH)_x(ed^ipr_fp)_3]^+$(x = 1-3) with the concomitant formation of a hydride intermediate. Next, a dihydrogen Mo-H···HCOOH species is generated from which H_2 is released and the formate Mo_3S_4 cluster is recovered.